Fractional Order Controllers for Complex Valued Systems and System with Multiple Nonlinearities

A thesis submitted

in partial fulfillment for the award of the degree of

Doctor of Philosophy

by

P. Sathishkumar

Department of Avionics

Indian Institute of Space Science and Technology

Thiruvananthapuram, India

November 2019

Certificate

This is to certify that the thesis titled ***Fractional Order Controllers for Complex Valued Systems and System with Multiple Nonlinearities*** submitted by **P. Sathishkumar**, to the Indian Institute of Space Science and Technology, Thiruvananthapuram, in partial fulfillment for the award of the degree of **Doctor of Philosophy** is a bonafide record of the original work carried out by him under my supervision. The contents of this thesis, in full or in parts, have not been submitted to any other Institute or University for the award of any degree or diploma.

Name of the Supervisor
Dr. N. Selvaganesan
Associate Professor,
Department of Avionics,
IIST.

Name of the Department Head
Dr. B. S. Manoj
Professor and Head,
Department of Avionics,
IIST.

Place: Thiruvananthapuram
Date: November 2019

Declaration

I declare that this thesis titled ***Fractional Order Controllers for Complex Valued Systems and System with Multiple Nonlinearities*** submitted in partial fulfillment for the award of the degree of **Doctor of Philosophy** is a record of the original work carried out by me under the supervision of **Dr. N. Selvaganesan**, and has not formed the basis for the award of any degree, diploma, associateship, fellowship, or other titles in this or any other Institution or University of higher learning. In keeping with the ethical practice in reporting scientific information, due acknowledgments have been made wherever the findings of others have been cited.

Place: Thiruvananthapuram
Date: November 2019

P. Sathishkumar
(SC15D025)

This thesis is dedicated to my naina, amma, manaivi and magal (Thulashika)

Acknowledgements

The work presented in this thesis would not have been possible without my close association with many people. I take this opportunity to extend my sincere gratitude and appreciation to all those who made this Ph.D thesis possible.

First and foremost, I would like to extend my sincere gratitude to my research supervisor ***Dr. N. Selvaganesan*** for introducing me to this exciting field of fractional control theory and for his dedicated help, guidance, advice, inspiration, encouragement and continuous support and patience throughout my Ph.D. His continuous motivation has changed a lot in me as a person in this society. During our course of interaction for the last four years, I have learnt a lot from him, including how to solve a problem, managing skills, keeping oneself happy, balancing family and career. His technical and editorial advice is very important for the completion of this thesis. I am really happy to be associated with a mentor like him.

I gratefully acknowledge doctoral committee chairman, ***Dr. B. S. Manoj***, Professor, IIST and extend my sincere thanks to the other members of my doctoral committee ***Dr. Indra Narayan Kar***, Professor, IIT Delhi, ***Dr. Gopal jee***, VSSC, ***Dr. M. S. Harsha Simha***, Assistant Professor, IIST and ***Dr. E. Natarajan***, Associate Professor, IIST for their periodic assessments of my research work.

I further take this opportunity to thank ***Shri. M. V. Dhekane***, Prof. Satish Dhawan Professor, IIST and ***Dr. Sam Zachariah***, Adjunct Professor, IIST for their kind technical support and assistance. I also extend my thanks to ***Dr. Gigy J. Alex***, Assistant Professor, IIST for her assistance in writing my thesis.

I am also thankful to my institute, especially **Department of Avionics**, for picking me up as a doctoral student and providing me an excellent research environment. I would like to express my sincere gratitude to our present Director **Dr. V. K. Dadhwal** and our former director ***Dr. K. S. Dasgupta*** as well for their encouragement and continuous support.

I wish to thank my father ***(Shri. V. Perumal)***, my mother ***(Smt. P. Jaya)***, my brother ***(Shri. P. Sundarajan)***, my in-law family members, other relatives and all my friends for their unconditional love and support. Last but not least, a heartfelt thanks goes out to my dear wife ***(Smt. Ramani Sathishkumar)***, who stood by me through all the thicks and thins.

-P. Sathishkumar

Abstract

Fractional Calculus (FC) is a branch of mathematics which generalises classical integer-order calculus to handle integrals and derivatives of *arbitrary* orders. Recently, the FC has received attention in various science and engineering fields including control theory. In control theory, one deals with the modelling, design and analysis of Fractional Order (FO) systems and controllers, whose dynamics are governed by FO differential equations. In this thesis, unified tuning expressions of Fractional Order Controllers (FOCs) for the proposed universal plant structure to meet Wang et al specifications are derived. Further, this work is extended to tune the parameters of the Complex Coefficient Integer Order Controllers (CCIOCs) and Complex Coefficient Fractional Complex Order Controllers (CCFCOCs) for such universal plant. This thesis also investigates the limit cycle prediction using various methods and its suppression using FOCs for system with multiple nonlinearities.

The thesis start with the proposal of defining plant model having complex coefficients and complex order derivatives plus dead time as a universal plant structure. Then, unified tuning expressions of FOCs such as PI^{α}, $[PI]^{\alpha}$, PD^{β}, $[PD]^{\beta}$ and $K_c\left(\frac{s}{\omega_{gc}}\right)^{\alpha+j\beta}$ are derived to meet the desired gain crossover frequency, phase margin and Isodamping property (Wang et al specifications) for the proposed universal plant structure using its positive frequency (ω^{+}) information. Two different case studies are simulated to demonstrate the controller tuning for the proposed structure. Performing the tuning of controllers by considering ω^{+} information is applicable only for Integer Order (IO)/FO plants containing real coefficients which have an even symmetrical magnitude and odd symmetrical phase behaviour in frequency response.

In general, plant with complex coefficients provides unsymmetrical magnitude and phase behaviour in its frequency response. Hence, tuning of controllers for universal plants by considering only its ω^{+} information alone is not adequate. This type of tuning reduces stability margins and deteriorates its time response. Therefore, tuning of controllers for universal plants require both ω^{+} and negative frequency (ω^{-}) information which in turn demands complex coefficient controllers.

To address this problem, Complex Coefficient Integer Order Controllers (CCIOCs) and Complex Coefficient Fractional Complex Order Controllers (CCFCOCs) are proposed. Unified tuning expressions are derived for CCIOCs by considering both ω^{+} and ω^{-} information of such universal plant. In case of CCFCOCs, the controller parameters are

obtained through optimization technique due to its difficulty in solving by analytical approach. Numerical simulations are performed for few case studies to demonstrate the proposed CCIOCs and CCFCOCs. The results are compared with real coefficient Integer Order Controllers (IOCs) and FOCs tuned only in ω^+.

Then, the focus is on the prediction of limit cycle using graphical approaches and its suppression using FOCs for system containing multiple nonlinearities. In practical systems having separable hard nonlinearities, sustained oscillation is detected at the steady state response due to the presence of stable limit cycles. An optimization problem is proposed to tune IOCs/FOCs parameters for system with multiple nonlinearities to suppress the limit cycle magnitude in addition to meet the desired closed loop specifications. To extend the applicability of the existing Nyquist plot for predicting this limit cycle, an Input Dependent Nyquist Plot (IDNP) is proposed in this work. A servo system with backlash and relay nonlinearities is considered as a case study for limit cycle prediction with obtained FOCs using an IDNP. The predicted limit cycle information is compared with optimization results, Input Dependent Root Locus (IDRL) and are validated through closed loop simulations. It is found that FOCs have remarkably eliminated the limit cycle oscillation in comparison to IO PD controller at steady state of the closed loop response. Further, the robustness of the designed controllers are tested under system parameter uncertainty, disturbance and measurement noise conditions.

Contents

List of Figures

List of Tables

Abbreviations

CCFCOCs	Complex Coefficient Fractional Complex Order Controllers
CCIOCs	Complex Coefficient Integer Order Controllers
CCPD	Complex Coefficient Proportional Derivative
CCPI	Complex Coefficient Proportional Integral
CCPID	Complex Coefficient Proportional Integral Derivative
CFE	Continued Fraction Expansion
CRONE	Commande Robuste dOrdre Non-Entier
DF	Describing Function
FC	Fractional Calculus
FCOCs	Fractional Complex Order Controllers
FO	Fractional Order
FOCs	Fractional Order Controllers
FOPDT	First Order Plus Dead Time
FO-PID	Fractional Order-Proportional Integral Derivative
GM	Gain Margin
IAE	Integral Absolute Error
IDNP	Input Dependent Nyquist Plot
IDRL	Input Dependent Root Locus
IO	Integer Order
IOCs	Integer Order Controllers
ISE	Integral Square Error
ITAE	Integral Time Absolute Error
LTI	Linear Time Invariant
OLTF	Open Loop Transfer Function
ORA	Oustaloup Recursive Approximation
PM	Phase Margin
PSE	Power Series Expansion

QFT	Quantitative Feedback Theory
TF	Transfer Function

Nomenclature

J^n	$n-$fold Integration
$\mathbb{R}^+, \mathbb{R}_{>0}$	Set of Positive Real Numbers
J^α_{RL}	Riemann-Liouville Fractional Integral
$\Gamma(\alpha)$	Gamma Function
D^n	n^{th} Order Derivative
D^α_{RL}	Riemann-Liouville Fractional Derivative
$\mathbb{N}$	Set of Natural Numbers
D^α_C	Caputo Fractional Derivative
D^α_{GL}	Grunwald-Letnikov derivative
J^α_{GL}	Grunwald-Letnikov Integral
$\mathbb{R}$	Set of Real Numbers
$\mathcal{L}\{\cdot\}$	Laplace Transform
$f^{(k)}(t)$	k^{th} Derivative of $f(t)$
$\mathbb{Z}$	Set of Integer Numbers
$\mathbb{C}$	Set of Complex Numbers
$F_{CRONE}(s)$	CRONE Approximation of $F(s)$
dB	decibels
$F_{Matsuda}(s)$	Matsuda Approximation of $F(s)$
$F_{HighCFE}(s)$	High-CFE Approximation of $F(s)$
$F_{LowCFE}(s)$	Low-CFE Approximation of $F(s)$
$F_{Oustaloup}(s)$	Oustaloup Approximation of $F(s)$
$F_{GenOustaloup}(s)$	Generalized Oustaloup Approximation of $F(s)$
$F_{ModOustaloup}(s)$	Modified Oustaloup Approximation of $F(s)$
$F_{GenModOustaloup}(s)$	Generalized Modified Oustaloup Approximation of $F(s)$
$F_{Chareff}(s)$	Chareff Approximation of $F(s)$
$N(\cdot)$	Describing Function for Nonlinearity
$\mathbb{R}_{\geq 0}$	Set of Non-negative Real Numbers

$\mathbb{R}_{\neq 0}$	Set of Real Numbers Except 0
$G(s, X)$	System Transfer Function with Nonlinearity
$C(s)$	Controller Transfer function
$N_b(X)$	Describing Function for Backlash Nonlinearity
$N_r(X_1)$	Describing Function for Relay Nonlinearity
ϕ_m	Phase margin
ω_{gc}	Gain Crossover frequency
ω^+	Positive frequency
ω^-	Negative frequency
ψ	Slope of the phase of the universal plant at ω_{gc}
S	Sensitivity Transfer Function
T	Complementary Sensitivity Transfer function
ω_{BW}	Bandwidth
M_S	Maximum absolute value of Sensitivity function
M_T	Maximum absolute value of Complementary Sensitivity function

Chapter 1

Introduction

Classical calculus deals with integer-order differentiation and n-fold integration. Its generalisation to handle integrals and derivatives of arbitrary orders (say for instance, the derivative of 0.5^{th} order) leads to a branch in mathematics widely known as Fractional Calculus (FC) [1]. In FC, the word fractional is a misnomer, since the order can be real or complex. In control theory, FC finds applications in modelling, design and analysis of Fractional Order (FO) systems and controllers, whose dynamics are governed by FO differential equations.

This thesis mainly investigate the tuning of Fractional Order Controllers (FOCs) for the proposed universal plant structure. The plant structure has complex coefficients and complex order derivatives plus dead time. Then, unified tuning expressions of FOCs such as PI^{α}, $[PI]^{\alpha}$, PD^{β}, $[PD]^{\beta}$ and $K_c\left(\frac{s}{\omega_{gc}}\right)^{\alpha+j\beta}$ are derived to meet Wang et al specifications using its positive frequency (ω^{+}) information. Further, tuning of parameters of the Complex Coefficient Integer Order Controllers (CCIOCs) and Complex Coefficient Fractional Complex Order Controllers (CCFCOCs) for such universal plant using its ω^{+} and negative frequency (ω^{-}) information are presented. This work also deals limit cycle prediction using various methods and its suppression using FOCs for system with multiple nonlinearities.

1.1 Literature Survey and Motivation

The thought of FC came into light instantly after the classical calculus is proposed. Its first appearance is originated in a letter written by Leibnitz to L'Hospital in 1695 [2]. For more than 300 years, this concept is mainly grown as a pure theoretical area of mathematics that generalises the integer order calculus to arbitrary orders [1], [3], [4], [5]. During this period, outstanding contributions are made by very famous mathematicians and some

of the notable names are L. Euler, J. L. Lagrange, P. S. Laplace, J. B. J. Fourier, J. Liouville, N. H. Abel, B. Riemann, A. K. Grunwald, A. V. Letnikov, J. Hadamard, G. H. Hardy, etc [6], [7], [8]. These works led to better understanding about the prospects of FC in characterising the memory and hereditary properties of various materials and processes. On the other side, the conventional calculus revealed the restricted potential in these regards [9], [10], [11], [12], [13].

Last few decades observed many advancements in the computer technology and also the progress of numerical methods for finding solutions of fractional-order differential equations. This stimulated the researchers to find the applications of FC in different science and engineering fields [4], [14], [15], [16]. The fields include viscoelasticity [17], [18], capacitor theory [19], control theory [20], [21], [22], fractals [23], [24], oscillators [25], [26], polymer physics and rheology [27], [28], bioengineering [29], [30], multipoles and electromagnetic theory [31], [32], electrochemistry [33], signals and systems [34], and many more [35], [36], [37], [38], [39].

In control theory, the FC is applied in two ways: 1) System modelling, 2) Controller design [40], [41], [42], [43], [44]. In the latter application, one designs FOCs whose dynamics are governed by fractional-order differential equations [45], [46], [47], [48], [13].

The continuous domain Transfer Function (TF) of a FOC has irrational form structure, which is a ratio of polynomials having arbitrary powers (also known as *pseudo-polynomials* [49]). For the rational approximation of such TFs, several methods have been proposed in the literature. A survey of these methods is found in [50], [51]. Some of the popular methods include Carlson [52], Charef [53], Matsuda [54], Crone [45], Continued Fraction Expansion (CFE) [55], [51], Oustaloup [56], etc.

The selection of a particular method for rational approximation depends on factors such as allowable order of the resultant TF, degree of accuracy in the desired frequency range, time-domain behaviour, etc. Considering such factors together, it is difficult to claim one of these methods as the best one [45]. However, among them, the Oustaloup method [56] is used popularly to obtain a reasonably good rational fit for the given fractional-order TF within the specified frequency range [57]. A modified version of Oustaloup method provides better approximation at lower and upper frequency ends, though at the cost of increased order [57], [58].

Several methods are proposed in the literature for the discretisation of fractional-order TF as well. The methods include direct discretisation using Al-Alaoui operator via CFE [59], direct recursive discretisation with Tustin operator, discretisation using backward-difference operator via Power Series Expansion (PSE) [60], discretisation algorithm based on the

quadrature formula [61], an approach based on B-splines function [62], etc.

The irrational form TF of FOCs enables them to possess better abilities over their integer-order counterparts in meeting stringent loop shaping requirements. The FOCs such as PI^{α}, $[PI]^{\alpha}$, PD^{β}, $[PD]^{\beta}$, $PI^{\alpha}D^{\beta}$ [63], [58], [64] are superclass of their integer counterparts (i.e. PI, PD, PID). Therefore, one expects them to perform better owing to the design flexibility offered by their additional parameters [21], [60], [65]. For instance, the $PI^{\alpha}D^{\beta}$ controller has additional tuning parameters α, β than the PID, which makes it better [66].

Design of FOCs has received a considerable attention in the literature from both academic and industrial point of view [45], [67], [68]. In [69], [70], the design of $PI^{\alpha}D^{\beta}$ has been presented to meet five design specifications (*Monje et al specifications*) by *numerically* solving a constrained optimization problem. The solution in this case is possible with $PI^{\alpha}D^{\beta}$ controller due to its five parameters unlike the conventional PID which has only three parameters. The above work is further extended in [71] to develop *analytical* rules for $PI^{\alpha}D^{\beta}$ controllers meeting Monje et al specifications. For this purpose, the change in the numerically obtained controller parameters due to variations in the plant parameters is translated into tuning rules by means of least square fitting.

Another interesting work in [72] discusses the superiority of $PI^{\alpha}D^{\beta}$ over PID for controlling fractional-order systems in order to meet desired stability margins. The work in [73] constructs tuning rules for $PI^{\alpha}D^{\beta}$ to minimize the Integral Absolute Error (IAE) with a constraint on the maximum sensitivity. In [74], it has been shown that under the given optimization condition of minimizing performance indices such as Integral Time Absolute Error (ITAE) and Integral Square Error (ISE), the best $PI^{\alpha}D^{\beta}$ controller outperforms the best PID controller. The work in [75] presents the superiority of $PI^{\alpha}D^{\beta}$ over conventional PID in minimizing IAE and ISE for the cart-servo laboratory set-up.

In the existing fractional control literature, a large number of works are devoted to the tuning of three-parameter FOCs such as PI^{α}, $[PI]^{\alpha}$, PD^{β} and $[PD]^{\beta}$. To achieve the system stability and robustness, these three-parameter FOCs are tuned to meet the Wang et al specifications: (i) gain crossover frequency, (ii) phase margin and (iii) Isodamping condition [76], [77], [78], [79], [80], [81], [82], [82], [83], [84], [85], [86]. Gain crossover frequency and phase margin are selected to have a control over settling time and overshoot of the closed loop time response respectively. The Isodamping condition ensures constant overshoot towards variation in system gain. These advantages are utilised in the following research works to tune the three-parameter controllers for various engineering applications.

The design of PI^{α} and $[PI]^{\alpha}$ controllers for robust velocity servo plant has been pre-

sented in [76]. The work in [77] considers First Order Plus Dead Time (FOPDT) systems and designs PI^{α} and $[PI]^{\alpha}$ controllers. The design of PI^{α} and $[PI]^{\alpha}$ controllers for a class of fractional-order systems which can accurately model many real systems in bioengineering (e.g. Cole-Cole model [29]) is discussed in [78]. The paper also discusses the design for fractional horsepower dynamometer. Design of PI^{α} controllers for the class of plants studied in [87] has been discussed in [79].

Design of PD^{β} for a class of typical second-order plants is discussed in [80]. Design of PD^{β} controller for the position control of dynamometer is presented in [81]. In [82], PD^{β} controller is designed systematically for the generalized fractional capacitor membrane model. The $[PD]^{\beta}$ controller design is proposed for robust motion control systems in [83] and for the FC model of membrane charging in [84].

Fractional Complex Order Controller (FCOC) is designed for a DC motor [85] to meet the desired specifications. Recently, authors proposed a method to obtain a robust FOC to control a pump in [88] and for an unstable linear active bearing system in [89]. The controller design is carried out by following Bode's ideal transfer function as the reference function to have desired phase margin and robust to gain parameter variation. It is interesting to observe in these works that the tuning expressions of the controllers meeting Wang et al specifications have been derived by considering a particular plant TF. If one desires to tune them for some other plant TF, the exercise of deriving the corresponding expressions needs to be carried out again, which is tedious and work intensive.

Hence, a generalized plant structure with real coefficients and fractional order derivatives is introduced in [90], [91], [92], [93]. A unified tuning expressions are also derived for such a generalised plant structure which suit for any type of Integer Order (IO)/Fractional Order (FO) plants. In these papers, controller parameter expressions for fractional structures PI^{α}, PD^{β}, $[PI]^{\alpha}$ and $[PD]^{\beta}$ are obtained which are ready-to-use for any plant TF of integer or fractional-order with real coefficients. All these tuning techniques are limited to integer and fractional order derivative models with real coefficients.

In general, physical systems of IO/FO with real coefficients are considered for system design and analysis. Very few literature present physical systems with complex coefficients and are reported in: (i) design of asymmetric bandpass and band rejection filters [94], (ii) whirling shaft, vibrational systems and filters [95], (iii) modelling of three-phase electrical systems [96], [97], (iv) representation of Coriolis force in mechanics [98] and (v) algorithms for mobile radio communications [99].

Control theory is mainly developed for physical systems with real coefficients. Very few works are reported on complex coefficient systems in control literature. Some of

them are: Routh-Hurwitz test for various complex coefficient polynomials are discussed in [100], [101], [102], [103], [104], [105]. Kharitonov's stability criterion for complex coefficient interval systems is presented in [106] and it is also used in [107], [108], [109], [110]. Nyquist stability criterion for three phase system with complex coefficient model is addressed in [96]. In [111], complex root locus is proposed and it is used to analyse the current control of a three-phase rectifier in the dq reference frame.

On the other hand, controller design for system with complex coefficients are reported in the following: In [112], state feedback controller is designed for rotational disk vibration system with minimum energy and better transient response. In [113], [114], complex coefficient frequency domain stability analysis for cross coupled anti-symmetrical system is studied and it is extended to magnetically suspended flywheel rotor system. In [115], [116], controller design for doubly fed induction machine is presented by employing complex root locus and Hurwitz test techniques respectively. In [117], ABC frame based complex coefficient controllers and filters are proposed to eliminate the current harmonics in order to improve the current quality of the three-phase grid connected inverter. In [118], authors proposed to design a controller for cavity field control and Cartesian feedback linearisation of RF amplifiers which have complex coefficients. In [119], complex coefficient filters are introduced in the design of sliding mode disturbance observer to eliminate the higher harmonics which in turn improves the estimation of disturbance without chattering.

Modelling and control of physical plant with complex order derivatives is one of the emerging fields in control theory. At first, complex order derivative is introduced in [120] and later in [121], [122], complex valued Maxwell model (complex coefficients and complex order derivatives) is presented to describe the mechanical properties of the viscoelastic devices. This model predicts the transient and steady state response close to the experimental results in comparison to real valued Maxwell model. Such viscoelastic characteristic is widely seen in space applications such as crew module in space flight, end effectors in robotic arm and viscoelastic dampers in seismic mitigation. Complex state space representation, model decomposition and stability condition for commensurate type complex fractional order systems are studied in [123]. In [124], frequency response for fractional complex order derivative models are presented. In [125], complex derivative orders are used to detect multiple faults in machines. Recently, existence and uniqueness of complex solutions for fractional complex order differential equations are discussed in [126].

Motivated from the above works, a universal plant structure is proposed by incorporating complex coefficients and complex order derivatives plus dead time as a plant model. In this thesis, unified controller parameter tuning expressions of FOCs: PI^{α}, $[PI]^{\alpha}$, PD^{β},

$[PD]^{\beta}$ and Fractional Complex Order Controller (FCOC): $K_c \left(\frac{s}{\omega_{gc}}\right)^{\alpha+j\beta}$ for universal plant structure to meet Wang et al specifications are derived. Here, the FOCs/FCOC parameters are obtained by utilising the positive frequency (ω^+) information only. It is noted that the sensitivity and complementary sensitivity functions have very high peak values in negative frequency (ω^-) which in turn reduces its stability margins and equivalent time domain performance. The reduced performance is due to the negligence of ω^- information in the controller design. Hence for complex valued plants, real valued Integer Order Controllers (IOCs)/Fractional Order Controllers (FOCs) are not suitable to meet the desired performance.

To improve the performance, controller has to be tuned by considering ω^- information also for complex valued plants. In general, IO/FO plants with real coefficients have even symmetrical magnitude and odd symmetrical phase behaviour in frequency response. Whereas, complex valued systems have unsymmetrical magnitude and phase behaviour in frequency response. Hence, controller should be complex valued and tuning is performed by including both ω^+ and ω^- information. This motivates to introduce complex coefficients in the existing real valued IOCs structure to satisfy the required specifications in ω^+ and ω^-. To show the superiority of FOCs, Complex Coefficient Fractional Complex Order Controllers (CCFCOC) are also proposed for universal plant to meet the Wang et al specifications in ω^+ and ω^-.

In engineering systems having separable nonlinearities, sustained oscillation is observed in the system output response at steady state [127]. The sustained oscillation is due to the presence of stable limit cycles. To study such systems, Describing Function (DF) analysis is adopted as a tool under the assumption that linear part of the system provides very good low pass filtering effect [128]. Analysis of system containing more than one nonlinearity is very challenging. In [129], single composite DF is derived for systems having nonlinearities in cascade and error caused by this composite DF is evaluated. In [130], [131], [132], [133], [134], DF for nonlinearities such as friction, static and dynamic backlash are obtained using fractional calculus.

In control theory and practice, graphical approaches such as Nyquist plot and root locus are used to predict the limit cycle behaviour for system with single nonlinearity. In [135], limit cycle condition is derived for any number of parallel nonlinear elements separated by linear components possessing strong low pass filter characteristics. However, it fails to provide the limit cycle stability information. Limit cycle prediction for nonlinear dynamical systems such as system with nonlinear friction and dynamic backlash using DF analysis is done in [136]. DF based limit cycle prediction for fractional order (FO) nonlinear systems

is presented in [137], [138], [139]. Accuracy of digital rational approximations of FO operators to predict the limit cycle using DF method is presented for a system with fractional order proportional integral derivative controller and plant subject to backlash in [140]. Prediction of limit cycle behaviour using DF contradicted with the time domain results for the system with relay feedback loop is investigated in [141]. This is due to insufficient filtering of higher order harmonics in the loop and hence by inserting an additional low pass filter in the loop, limit cycle prediction using DF is matched with the time domain results.

In [142], a method is presented to control system having backlash and saturation nonlinearities for accurate predictions of limit cycle details and system parameter values to eliminate oscillations. Stability analysis of systems with multiple nonlinearities using input dependent root locus (IDRL) in concurrence with DF is shown in [143] and its dynamics are displayed using pole-zero configuration. In [144], [145], limit cycle stability for the systems having multiple nonlinearities (both memory and memoryless) in a single feedback loop systems is determined through graphical approach under the assumption that the input to nonlinear element is a sinusoidal function of time. In [146], range of the hydroelectric system parameters for the stable limit cycle existence is well studied. Robust stability analysis of Luré systems with multiple nonlinearities [147] through Popov-Lyapunov approach is presented with the bounded range for individual system parameter uncertainty.

Controller design for sampled data system having single nonlinearity using quantitative feedback theory (QFT) technique is described in [148] and the applicability of QFT in case of multiple nonlinearities is unexplored. In [149], limit cycle characteristics and existence are detailed for a high performance hydraulic actuator and limit cycle is quenched by using linear controller. Sliding mode controller for stabilizing uncertain nonlinear systems with multiple inputs containing sector nonlinearities and deadzones is presented in [150]. In [151], sliding mode controller is tuned by using predicted limit cycle details for a FO system with relay nonlinearity. In [152], [153], [154] effective use of DF for the synthesis of controllers to meet the desired limit cycle details is studied. DF based tuning of IOCs and FOCs to suppress the limit cycle magnitude by proposing an optimization problem is adddressed [155], [156], [93] in addition to meet the desired specifications for system with single nonlinearity. Few researchers [157], [158] also suggested a FOCs with an anti-windup feature for plants with input saturation nonlinearity.

In [159], authors detailed the DF based stability analysis for systems with multiple nonlinearities in both graphical and analytical approach under various input conditions. In [159], [128], it is inferred that limit cycle prediction is done for the system with nonlinearity using Nyquist plot whose linear part of the system is of the form $G(s)$ (independent

of limit cycle magnitude (X) and frequency (ω)). On the other hand, limit cycle prediction for system of the form $G(s, X)$ (dependent of X and ω) with nonlinearity using Nyquist plot is limited.

This motivate to propose an Input Dependent Nyquist Plot (IDNP) to predict the limit cycle details. Controller design for systems with multiple nonlinearities using DF analysis is also not explored in the existing literature. Hence, an optimization problem is proposed to tune the FOC parameters for suppressing the limit cycle oscillation.

1.2 Research Contribution

The research contributions of the thesis are summarized as follows:

(i) FOCs for complex valued systems

- Plant model with complex coefficients and complex order derivatives plus dead time is proposed as a universal plant structure.
- Unified tuning expressions of $FOCs$ and $FCOC$ parameters are derived for universal plant structure to meet Wang et al specifications.
- Unified tuning expressions of the proposed CCIOCs parameter are derived for universal plant to meet the Wang et al specifications in ω^+ and ω^-.
- CCFCOCs structures are also proposed for universal plant structure and parameters are tuned using optimization technique.
- The detailed time domain analysis and frequency domain analysis (sensitivity and complementary sensitivity) are carried out for the chosen cases to validate the obtained $FOCs$, $FCOC$, $CCIOCs$ and $CCFCOCs$.

(ii) FOCs for system with multiple nonlinearities.

- IDNP is proposed to predict the limit cycle details for system with multiple nonlinearities.
- An optimization problem with stability and robustness constraints is proposed to obtain the controller parameters of FOCs for system with multiple nonlinearities to suppress the limit cycle magnitude in addition to meet the desired closed loop performance.

- The predicted limit cycle details are compared with the existing IDRL and optimization results. The predicted limit cycle information is further validated through closed loop simulation and the robustness of the controller is verified by introducing parameter uncertainty, disturbance and measurement noise.

1.3 Organisation of Thesis

- Chapter 2 discusses the preliminaries of FC and its extension to propose TF containing complex coefficients with complex order derivatives plus dead time as universal plant structure. It also gives introduction about FOC, $FCOC$, $CCIOCs$ and $CCFCOCs$.

- In chapter 3, a universal plant structure is proposed which accommodates any IO/FO plant TF. For such a plant, the tuning expressions are derived for PI^{α}, $[PI]^{\alpha}$, PD^{β}, $[PD]^{\beta}$ and $K_c \left(\frac{s}{\omega_{gc}}\right)^{\alpha+j\beta}$ to satisfy the Wang et al specifications. With the help of numerical examples, the usefulness of the deduced expressions are demonstrated.

- Chapter 4 presents the unified tuning expressions of CCIOCs for the proposed universal structure to satisfy the constraints both in ω^{+} and ω^{-}. This work is also extended to propose CCFCOCs structure and tune its parameters using optimization technique. Numerical examples are illustrated to show the superiority of the complex coefficient controllers over real coefficient controllers.

- In chapter 5, IDNP is proposed to predict the limit cycle details for system with multiple nonlinearities. Servo system with backlash and relay nonlinearities is considered as a case study to predict the observed limit cycle using the proposed IDNP. A constrained optimization problem is formulated to suppress the observed limit cycle using IOCs and FOCs in addition to meet the desired closed loop specifications. Furthermore, its graphical interpretation is presented which is useful to compare the designed controllers in terms of limit cycle suppression. From the simulation results, the superiority of FOCs over IOCs is claimed.

- Chapter 6 provides the conclusion and future direction of this research work.

Chapter 2

Preliminaries of Fractional Calculus

2.1 Introduction

Similar to the generalisation of integer exponents into fractional exponents, the idea of Fractional Calculus (FC) can be perceived as a natural outgrowth of conventional Integer Order (IO) calculus. In case of an integer exponent (say) $x^3 = 1 \cdot x \cdot x \cdot x$, its physical meaning can be interpreted as the multiplication of 1 three times by x. In case of fractional exponent $x^{5.23}$, this interpretation is not possible since one cannot conceive the meaning of multiplying one 5.23 number of times by x. But still, the term $x^{5.23}$ exists and has definite value for the given x which is verifiable by infinite series expansion.

In the same way, the meaning of derivatives and integrals of arbitrary orders is arguably impossible to grasp [160] unlike their IO counterparts. Nevertheless, they still exist as long as one sticks to the mathematical world alone. Their formulations emerge quite naturally by extending the notions of IO calculus to arbitrary orders. It is important to note that such extension can lead to orders which are real or even complex.

Let us consider an infinite sequence of n-fold integrals and n^{th} order derivatives, which is presented as follows:

$$\ldots, \int_a^t d\tau_2 \int_a^{\tau_2} f(\tau_1) d\tau_1, \int_a^t f(\tau_1) d\tau_1, f(t), \frac{df(t)}{dt}, \frac{d^2 f(t)}{dt^2}, \ldots \tag{2.1}$$

The sequence (2.1) can be made continuous by considering the derivatives and integrals of arbitrary real orders.

In this chapter, we discuss the basics of such FC operations and their applications to the control theory in terms of development of Fractional-Order Controllers (FOCs).

2.2 Definitions in Fractional Calculus

The following definitions are used to describe the fractional derivative and integration operation:

1. Riemann-Liouville Fractional Integral [160]

   This definition is derived directly from the traditional expression of repeated integration. For this purpose, it starts with the following Cauchy's formula for evaluating n^{th} integration (J^n) of the function $f(t)$:

$$J^n f(t) = \frac{1}{(n-1)!} \int_a^t (t-\tau)^{n-1} f(\tau) d\tau \tag{2.2}$$

   The subscripts a and t denote the two limits (or terminals [35]) related to the operation. Since (2.2) contains factorial, it cannot be used for non-integer n. By replacing the factorial by its analytical expansion i.e. gamma function in order to generalize (2.2) for all $\alpha \in \mathbb{R}^+$, we obtain Riemann-Liouville fractional integral J^α_{RL} as follows:

$$J^\alpha_{RL} f(t) = \frac{1}{\Gamma(\alpha)} \int_a^t (t-\tau)^{\alpha-1} f(\tau) d\tau \tag{2.3}$$

   where, the gamma function $\Gamma(\alpha)$ is defined by the integral

$$\Gamma(\alpha) = \int_0^\infty e^{-t} t^{\alpha-1} dt \tag{2.4}$$

   Properties

   (a) Integration of order, $\alpha = 0$

$$J^0_{RL} f(t) = f(t) \tag{2.5}$$

   (b) Repeated Integration

$$J^\alpha_{RL} J^\beta_{RL} f(t) = J^{\alpha+\beta}_{RL} f(t) \tag{2.6}$$

   where, $\alpha, \beta \in \mathbb{R}^+$.

(c) Convolution

Let the $\phi_\alpha(t)$ be defined as:

$$\phi_\alpha(t) = \frac{t^{\alpha-1}}{\Gamma(\alpha)} \tag{2.7}$$

Then, (2.3) can be expressed as the following convolution:

$$J^\alpha_{RL} f(t) = \phi_\alpha(t) * f(t) \tag{2.8}$$

2. Riemann-Liouville Fractional Derivative [10]

The fractional derivative D^α_{RL} is expressed as:

$$D^\alpha_{RL} := D^n D^{\alpha-n} = D^n J^{n-\alpha}_{RL} \tag{2.9}$$

where, D denotes derivative operation and $(n-1) < \alpha \leq n; (n \in \mathbb{N})$.

Therefore, from (2.3) and (2.9), the Riemann-Liouville fractional derivative is obtained as follows:

$$D^\alpha_{RL} f(t) = \frac{d^n}{dt^n} \left[\frac{1}{\Gamma(n-\alpha)} \int_a^t \frac{f(\tau)}{(t-\tau)^{\alpha-n+1}} d\tau \right] \tag{2.10}$$

3. Caputo Fractional Derivative [22]

The fractional derivative D^α_C is expressed as:

$$D^\alpha_C := D^{\alpha-n} D^n = J^{n-\alpha}_{RL} D^n \tag{2.11}$$

Therefore, from (2.3) and (2.11), the Caputo fractional derivative is obtained as follows:

$$D^\alpha_C f(t) = J^{n-\alpha}_{RL} f^n(t) = \frac{1}{\Gamma(n-\alpha)} \int_a^t \frac{f^n(\tau)}{(t-\tau)^{\alpha-n+1}} d\tau \tag{2.12}$$

4. Grunwald-Letnikov Derivative [74]

We have the following fundamental definition of n^{th} order derivative ($n \in \mathbb{N}$):

$$D^n f(t) = \lim_{h \to 0} \frac{1}{h^n} \sum_{k=0}^{n} (-1)^k \binom{n}{k} f(t - kh) \tag{2.13}$$

where,

$$\binom{n}{k} = \frac{n!}{(n-k)!k!} = \frac{\Gamma(n+1)}{\Gamma(n-k+1)\Gamma(k+1)}$$

The generalization of (2.13) to α^{th} order ($\alpha \in \mathbb{R}^+$) leads to the following Grunwald-Letnikov derivative (D^{α}_{GL}):

$$D^{\alpha}_{GL} f(t) = \lim_{h \to 0} \frac{1}{h^{\alpha}} \sum_{k=0}^{\left[\frac{t-a}{h}\right]} (-1)^k \binom{\alpha}{k} f(t - kh) \tag{2.14}$$

where,

$$\binom{\alpha}{k} = \frac{\Gamma(\alpha+1)}{\Gamma(\alpha-k+1)\Gamma(k+1)}$$

In (2.14), $f(t)$ is defined over $[a, t]$. Also, $\left[\frac{t-a}{h}\right]$ truncates $\left(\frac{t-a}{h}\right)$ to integer.

5. Grunwald-Letnikov Integral [160]

   Generalization of (2.13) to $(-\alpha)^{th}$ order ($\alpha \in \mathbb{R}^+$) leads to the following Grunwald-Letnikov integral (J^{α}_{GL}):

$$J^{\alpha}_{GL} f(t) = D^{-\alpha} f(t) = \lim_{h \to 0} \frac{1}{h^{-\alpha}} \sum_{k=0}^{\left[\frac{t-a}{h}\right]} (-1)^k \binom{-\alpha}{k} f(t - kh) \tag{2.15}$$

   Using the identity $\binom{-\alpha}{k} = (-1)^k \frac{\Gamma(\alpha+k)}{\Gamma(\alpha)k!}$, we rewrite (2.15) as follows:

$$J^{\alpha}_{GL} f(t) = \lim_{h \to 0} h^{\alpha} \sum_{k=0}^{\left[\frac{t-a}{h}\right]} \frac{\Gamma(\alpha+k)}{\Gamma(\alpha)k!} f(t - kh) \tag{2.16}$$

6. Miller-Ross Sequential Fractional Derivative [10]

   It is defined as follows:

$$D^{\alpha} f(t) = D^{\alpha_1} D^{\alpha_2} \dots D^{\alpha_n} f(t) \tag{2.17}$$

   where,

$$\alpha = \sum_{k=1}^{n} \alpha_k, 0 < \alpha_k \leq 1 \tag{2.18}$$

   This definition is useful for obtaining fractional derivative of any arbitrary order. The derivative operator D^{α} can be Riemann-Liouville or Caputo.

7. Oldham and Spanier [39]

$$\frac{d^q f(\beta x)}{dx^q} = \beta^q \frac{d^q f(\beta x)}{d(\beta x)^q} \tag{2.19}$$

   This makes it suitable for the study of scaling and scale invariance. There is connection between local-scaling, box-dimension of an irregular function and order of Local Fractional Derivative.

8. Kolwankar and Gangal [39]

   Local fractional derivative is defined by Kolwankar and Gangal to explain the behavior of *continuous but nowhere differentiable* function. For $0 < q < 1$, the local fractional derivative at point $x = y$, for $f : [0, 1] \to \mathbb{R}$ is:

$$D^q f(y) = \lim_{x \to y} \frac{d^q (f(x) - f(y))}{d(x - y)^q} \tag{2.20}$$

Some Important Observations

1. By virtue of its form, the definition (2.14) is utilized for the numerical evaluation of fractional derivatives. On the other hand, Riemann-Liouville (2.10) and Caputo (2.12) definitions are useful in finding the fractional derivatives analytically [160].

2. Grunwald-Letnikov derivative given in (2.14) can also be expressed as follows [10]:

$$D^{\alpha}_{GL}f(t) = \sum_{k=0}^{m} \frac{f^{(k)}(a)(t-a)^{-\alpha+k}}{\Gamma(-\alpha+k+1)} + \frac{1}{\Gamma(-\alpha+m+1)} \int_{a}^{t} (t-\tau)^{m-\alpha} f^{(m+1)}(\tau) d\tau \tag{2.21}$$

This is true under the assumption that the derivatives $f^{(k)}(t), (k = 1, 2, \ldots, m+1)$ are continuous in the closed interval $[a, t]$ and m is an integer number satisfying the condition $m > \alpha - 1$. The smallest possible value for m is obtained by the inequality $m \leq \alpha < m + 1$.

For the above assumptions, Riemann-Liouville fractional derivative given in (2.10) can also be expressed as follows:

$$D^{\alpha}_{RL}f(t) = \sum_{k=0}^{m} \frac{f^{(k)}(a)(t-a)^{-\alpha+k}}{\Gamma(-\alpha+k+1)} + \frac{1}{\Gamma(-\alpha+m+1)} \int_{a}^{t} (t-\tau)^{m-\alpha} f^{(m+1)}(\tau) d\tau \tag{2.22}$$

Therefore, from (2.21) and (2.22), the Grunwald-Letnikov derivative definition (2.14) is equivalent to the Riemann-Liouville derivative definition (2.10) under the above discussed assumptions.

3. On substituting $n = m + 1$, Riemann-Lioville derivative definition (2.22) can be rewritten as:

$$\begin{aligned} D^{\alpha}_{RL}f(t) &= \sum_{k=0}^{n-1} \frac{f^{(k)}(a)(t-a)^{-\alpha+k}}{\Gamma(-\alpha+k+1)} + \frac{1}{\Gamma(-\alpha+n)} \int_{a}^{t} (t-\tau)^{n-1-\alpha} f^{(n)}(\tau) d\tau \\ &= \frac{1}{\Gamma(n-\alpha)} \int_{a}^{t} \frac{f^{(n)}(\tau)}{(t-\tau)^{\alpha-n+1}} d\tau + \sum_{k=0}^{n-1} \frac{f^{(k)}(a)(t-a)^{-\alpha+k}}{\Gamma(-\alpha+k+1)} \end{aligned} \tag{2.23}$$

Therefore, using (2.7), (2.12), and (2.23), we get:

$$D^{\alpha}_{RL}f(t) = D^{\alpha}_{C}f(t) + \sum_{k=0}^{n-1} \phi_{k-\alpha+1}(t-a) f^{(k)}(a) \tag{2.24}$$

The equation (2.24) represents the relationship between Riemann-Lioville and Caputo derivatives.

4. With $a = 0$, Caputo's derivative (2.12) of a constant is 0 whereas the Riemann-Lioville derivative of a constant is unbounded at $t = 0$. However, if one considers the lower terminal a as $-\infty$ in the Riemann-Lioville derivative definition (2.10), the derivative of a constant is 0.

5. Short Memory Principle [10]: It follows from the coefficients in the Grunwald-Letnikov definition (2.14) that for $t >> a$, the role of the *history* of the behavior of the function $f(t)$ near the lower terminal a can be neglected. This leads to the following *short memory principle* which takes into account the behavior of $f(t)$ only in the recent past, i.e. in the interval $[t-L, t]$ instead of $[a, t]$; where, L is the memory length:

$$D^{\alpha}_{GL} f(t) := {}_{a}D^{\alpha}_{t} \approx {}_{t-L}D^{\alpha}_{t}, \qquad (t < a + L) \tag{2.25}$$

Thus, according to (2.25), the Grunwald-Letnikov fractional derivative with the fixed lower terminal a is approximated by the one with moving lower terminal $t - L$. Due to this, the number of addends in the approximated derivative definition never exceeds $[L/h]$. This simplification, however, leads to some inaccuracy due to loss in information.

2.3 Laplace Transform of Fractional Derivatives

Laplace transform of the function $f(t)$ is a function $F(s)$ of the complex variable s. The $F(s)$ is obtained as:

$$F(s) = \mathcal{L}\{f(t)\} = \int_{0}^{\infty} e^{-st} f(t) dt \tag{2.26}$$

The Laplace transform of fractional derivatives (with the lower terminal $a = 0$) are as follows [10]:

1. Laplace Transform of Riemann-Liouville Derivative

$$\mathcal{L}\{D^{\alpha}_{RL} f(t)\} = s^{\alpha} F(s) - \sum_{k=0}^{n-1} s^{k} D^{(\alpha-k-1)}_{RL} f(0) \tag{2.27}$$

where, $F(s) = \mathcal{L}\{f(t)\}$ and $(n-1) \leq \alpha < n$.

2. Laplace Transform of Caputo Derivative

$$\mathcal{L}\{D_C^{\alpha} f(t)\} = s^{\alpha} F(s) - \sum_{k=0}^{n-1} s^{\alpha-k-1} f^{(k)}(0) \tag{2.28}$$

where, $(n-1) \leq \alpha < n$.

3. Laplace Transform of Grunwald-Letnikov Derivative (2.21) with $a = 0$

$$\mathcal{L}\{D_{GL}^{\alpha} f(t)\} = s^{\alpha} F(s) \tag{2.29}$$

As seen from (2.27), for calculating Laplace transform of Riemann-Liouville derivative one requires initial conditions $D_{RL}^{(\alpha-k-1)} f(0)$, which are fractional derivatives. On the other hand, the Laplace transform of Caputo derivative (2.28) requires initial conditions $f^{(k)}(0)$, which are IO derivatives. Since such initial conditions can be easily interpreted from physical data and observations, Caputo derivative is a more practical definition than Riemann-Liouville derivative.

2.4 Fractional Order Transfer Functions

Fractional Order (FO) differential/integral equation are composed of FO derivatives/integrals. A system of such equations describes the dynamics of FO processes.

Consider a Linear Time Invariant (LTI) FO system which is governed by the following FO ordinary differential equation:

$$\begin{aligned} a_n D^{\alpha_n} y(t) + a_{n-1} D^{\alpha_{n-1}} y(t) + ... + a_0 D^{\alpha_0} y(t) = \\ b_m D^{\beta_m} u(t) + b_{m-1} D^{\beta_{m-1}} u(t) + ... + b_0 D^{\beta_0} u(t) \end{aligned} \tag{2.30}$$

where, $y(t)$ and $u(t)$ denote output and input signals, respectively.

Also, $a_i, \alpha_i (i = 0, 1, \ldots, n), b_k, \beta_k (k = 0, 1, \ldots, m) \in \mathbb{R}$; $n, m \in \mathbb{N}$.

In (2.30), Caputo's derivative definition (2.12) is preferred (with $a = 0$) as it allows consideration of conventional initial conditions.

The Laplace transform of (2.30) assuming zero initial conditions results into the following Transfer Function (TF):

$$\frac{Y(s)}{U(s)} = \frac{b_m s^{\beta_m} + b_{m-1} s^{\beta_{m-1}} + ... + b_0 s^{\beta_0}}{a_n s^{\alpha_n} + a_{n-1} s^{\alpha_{n-1}} + ... + a_0 s^{\alpha_0}} \tag{2.31}$$

where, $Y(s) = \mathcal{L}\{y(t)\}, U(s) = \mathcal{L}\{u(t)\}$

The TF of the form (2.31) represents either a *commensurate* or a *non-commensurate* order system. It is a *commensurate* order system, if there exists a greatest common divisor $q \in \mathbb{R}$ such that $\alpha_i = qe_i, \beta_k = qf_k; e_i, f_k \in \mathbb{Z}$. In such case, q is the commensurate order, which can be rational or irrational.

The discussions on the stability of FO LTI systems and the analytical solutions of FO ordinary differential equations have been provided in APPENDIX A.

2.5 Continuous Domain Approximation Methods

The fractional-order TFs have irrational form, which is the ratio of pseudo-polynomials, i.e. polynomials of arbitrary orders. From their approximation using rational functions, several methods have been proposed in the literature, which are as follows:

1. Carlson [52]

   The Carlson rational approximation of the fractional-order term $H(s) = [G(s)]^\alpha$ is obtained recursively as follows:

   $$H_i(s) = H_{i-1}(s)\frac{(v-1)(H_{i-1}(s))^v + (v+1)G(s)}{(v+1)(H_{i-1}(s))^v + (v-1)G(s)} \tag{2.32}$$

   where, $i \in \mathbb{N}$; $H_0(s) = 1$; $\alpha = \frac{1}{v}$. $G(s)$ is a rational function of complex variable s. The approximation (2.32) is applicable only if $v \in \mathbb{N}$. In other words, α can only assume values $1, \frac{1}{2}, \frac{1}{3}, \frac{1}{4}$, etc.

2. CRONE [44]

   (CRONE is the (French) acronym of *Commande Robuste dOrdre Non-Entier*)

   For $F(s) = s^\alpha$ $(0 < \alpha \leq 1)$, its CRONE approximation is given as follows:

   $$F_{CRONE}(s) = C_0 \prod_{n=1}^{N} \frac{1 + \frac{s}{\omega_{zn}}}{1 + \frac{s}{\omega_{pn}}} \tag{2.33}$$

   where,

$$k = \left(\frac{\omega_h}{\omega_l}\right)^{\frac{|\alpha|}{N}}, \eta = \left(\frac{\omega_h}{\omega_l}\right)^{\frac{1-|\alpha|}{N}}, \omega_{z1} = \omega_l\sqrt{\eta}$$
$$\omega_{pn} = \omega_{zn}k \qquad n = 1, 2, ..., N$$
$$\omega_{z(n+1)} = \omega_{pn}\eta \qquad n = 1, 2, ..., (N-1)$$

N is order of approximation. $[\omega_l, \omega_h]$ is the frequency range of interest. C_0 is such that $F_{CRONE}(s)$ magnitude of 0 decibels (dB) at $\omega = 1$ rad/s.

3. Matsuda [54]

   For the Matsuda approximation of $F(s) = s^\alpha$, its gain ($|F(j\omega)|$) is found at several frequencies. The number of frequencies determines the order of approximation. Let the frequencies chosen be $\omega_0, \omega_1, \omega_2, ..., \omega_N$. Then, the Matsuda approximation $F_{Matsuda}(s)$ is obtained as follows:

$$F_{Matsuda}(s) = \beta_0 + \frac{s - \omega_0}{\beta_1 + \frac{s-\omega_1}{\beta_2 + \frac{s-\omega_2}{\beta_3 + ...}}} \tag{2.34}$$

   where,

$$\beta_0 = d_0(\omega_0), \beta_k = \frac{\omega_k - \omega_{k-1}}{d_{k-1}(\omega_k) - d_{k-1}(\omega_{k-1})}$$
$$d_0(\omega) = |\omega^\alpha|, d_k(\omega) = \frac{\omega - \omega_{k-1}}{d_{k-1}(\omega) - d_{k-1}(\omega_{k-1})}$$
$$k = 1, 2, ...N$$

4. Continued Fraction Expansion (CFE) [55]

   Let us consider the approximation of $F(s) = s^\alpha$. There are following two categories of this method:

   (a) High CFE ($F_{HighCFE}(s)$)

   This is a good approximation for higher frequencies ($\omega > \lambda; \lambda > 0$), which is obtained as follows:

$$F_{HighCFE}(s) = \lambda^\alpha \left[0; \frac{1}{1}; \frac{-\alpha\frac{s}{\lambda}}{1}; \left\{\frac{\frac{i(i+\alpha)}{(2i-1)2i}\frac{s}{\lambda}}{1}, \frac{\frac{i(i-\alpha)}{(2i+1)2i}\frac{s}{\lambda}}{1}\right\}_{i=1}^{n}\right] \tag{2.35}$$

   where, n decides the order of approximation.

$\left[\frac{p_0}{q_0}; \frac{p_1}{q_1}; \frac{p_2}{q_2}; \frac{p_3}{q_3}...\right]$ implies the term $\frac{p_0}{q_0} + \frac{p_1}{q_1+\frac{p_2}{q_2+\frac{p_3}{q_3+...}}}$.

(b) Low CFE ($F_{LowCFE}(s)$)

This is a good approximation for lower frequencies $(\omega < \lambda; \lambda > 0)$, which is obtained as follows:

$$F_{LowCFE}(s) = \lambda^{\alpha} \left[0; \frac{1}{1}; \frac{\alpha\frac{\lambda}{s}}{1}; \left\{ \frac{\frac{i(i-\alpha)}{(2i-1)2i}\frac{\lambda}{s}}{1}, \frac{\frac{i(i+\alpha)}{(2i+1)2i}\frac{\lambda}{s}}{1} \right\}_{i=1}^{n}\right] \tag{2.36}$$

5. Oustaloup [56]

The Oustaloup approximation $F_{Oustaloup}(s)$ of $F(s) = s^{\alpha}$ assuming that the expected fitting range $[\omega_b, \omega_h]$ is obtained as follows:

$$F_{Oustaloup}(s) = K \prod_{k=-N}^{N} \frac{s + z_k}{s + p_k} \tag{2.37}$$

where,

$$z_k = \omega_b \left(\frac{\omega_h}{\omega_b}\right)^{\frac{k+N+\frac{1}{2}(1-\alpha)}{2N+1}}$$
$$p_k = \omega_b \left(\frac{\omega_h}{\omega_b}\right)^{\frac{k+N+\frac{1}{2}(1+\alpha)}{2N+1}}$$
$$K = \omega_h^{\alpha}$$

In this method, order of approximation is $(2N + 1)$, which is an odd number $(N = 1, 2, \dots)$ The following generalized Oustaloup method can be used to obtain the approximation $F_{GenOustaloup}(s)$ having order, $N = 1, 2, \dots$

$$F_{GenOustaloup}(s) = K \prod_{k=1}^{N} \frac{s + z_k}{s + p_k} \tag{2.38}$$

where,

$$z_k = \omega_b \left(\frac{\omega_h}{\omega_b}\right)^{\frac{2k-1-\alpha}{2N}}$$
$$p_k = \omega_b \left(\frac{\omega_h}{\omega_b}\right)^{\frac{2k-1+\alpha}{2N}}$$
$$K = \omega_h^{\alpha}$$

6. Modified Oustaloup [74]

This method provides a better approximation than Oustaloup method with respect to both low frequency and high frequency at the cost of increase in the order of approximation. The modified Oustaloup approximation $F_{ModOustaloup}(s)$ of $F(s) = s^{\alpha}$ is obtained as follows:

$$F_{ModOustaloup}(s) = \left(\frac{d\omega_h}{b}\right)^{\alpha} \frac{ds^2 + b\omega_h s}{d(1-\alpha)s^2 + b\omega_h s + d\alpha} \prod_{k=-N}^{N} \frac{s + z_k}{s + p_k} \tag{2.39}$$

where,

$$z_k = \left(\frac{d\omega_h}{b}\right)^{\frac{\alpha-2k}{2N+1}}, p_k = \left(\frac{b\omega_h}{d}\right)^{\frac{\alpha+2k}{2N+1}}$$

In above method, order of approximation is $(2N+1)$, which is an odd number $(N = 1, 2, \dots)$. The following generalized modified Oustaloup method can be used to obtain the approximation $F_{GenModOustaloup}(s)$ having order, $N = 1, 2, \dots$

$$F_{GenModOustaloup}(s) = \left(\frac{d\omega_h}{b}\right)^{\alpha} \frac{ds^2 + b\omega_h s}{d(1-\alpha)s^2 + b\omega_h s + d\alpha} \prod_{k=1}^{N} \frac{s + z_k}{s + p_k} \tag{2.40}$$

$$z_k = \omega_b \left(\frac{\omega_h}{\omega_b}\right)^{\frac{2k-1-\alpha}{2N}}$$
$$p_k = \omega_b \left(\frac{\omega_h}{\omega_b}\right)^{\frac{2k-1+\alpha}{2N}}$$

7. Chareff [53]

The Chareff approximation $F_{Chareff}(s)$ of the irrational TF of the form $F(s) = \frac{1}{(1+\frac{s}{pT})^{\alpha}}$ is obtained as follows:

$$F_{Chareff}(s) = \frac{\prod_{i=0}^{N-1} \left(1 + \frac{s}{z_i}\right)}{\prod_{i=0}^{N} \left(1 + \frac{s}{p_i}\right)} \tag{2.41}$$

where, the coefficients are computed for obtaining a maximum deviation of y in dB from the original magnitude response in the frequency domain as follows:

$$p_i = p_0(ab)^i, z_i = ap_0(ab)^i, p_0 = pT\sqrt{b}, a = 10^{\frac{y}{10(1-\alpha)}}, b = 10^{\frac{y}{10\alpha}}$$

The above approximation methods are illustrated with the help of a numerical example as follows:

Example 2.1. *Let us consider the rational approximation of $F(s) = s^{0.5}$. The numerical details considered for each method are presented in Table 2.1. The magnitude and phase Bode plots of $s^{0.5}$ (i.e. Original) and its rational approximations obtained using different methods are shown in Fig. 2.1 and Fig. 2.2 respectively. The Chareff method is not considered as the TF under consideration is not in the suitable form, i.e. $\frac{1}{(1+\frac{s}{pT})^\alpha}$.*

Table 2.1: Numerical details for different rational approximation methods

Method	**Parameters**
Carlson	$i = 2$
CRONE	$N = 3, \omega_l = 0.01, \omega_h = 100$
Matsuda	$[\omega_0, \omega_1, \ldots, \omega_n]$ = 15 logarithmically spaced points between $[0.1, 10]$
High CFE	$\lambda = 1, n = 4$
Low CFE	$\lambda = 1, n = 4$
Oustaloup	$N = 2, \omega_b = 0.01, \omega_h = 100$
Modified Oustaloup	$N = 2, b = 10, d = 9, \omega_b = 0.01, \omega_h = 100$

The Oustaloup approximation obtained using (2.37) *with $N = 2$ is same as the one obtained using* (2.38) *for $N = 5$. This is because the order of approximation in the formal case is $2N + 1$ and is N in the latter one. The above is true for the modified Oustaloup approximation as well when obtained using* (2.39) *and* (2.40) .

Although we have different methods for the rational approximation, it is difficult to claim one of them as the best method [71]. The relative merits of each method depend on the differentiation order, on whether one is more interested in an accurate frequency behavior or in accurate time responses, on how large admissible TFs may be, etc. However, the Oustaloup method is used in many occasions to obtain reasonably good rational fit for the given fractional-order TF within the specified frequency range [57].

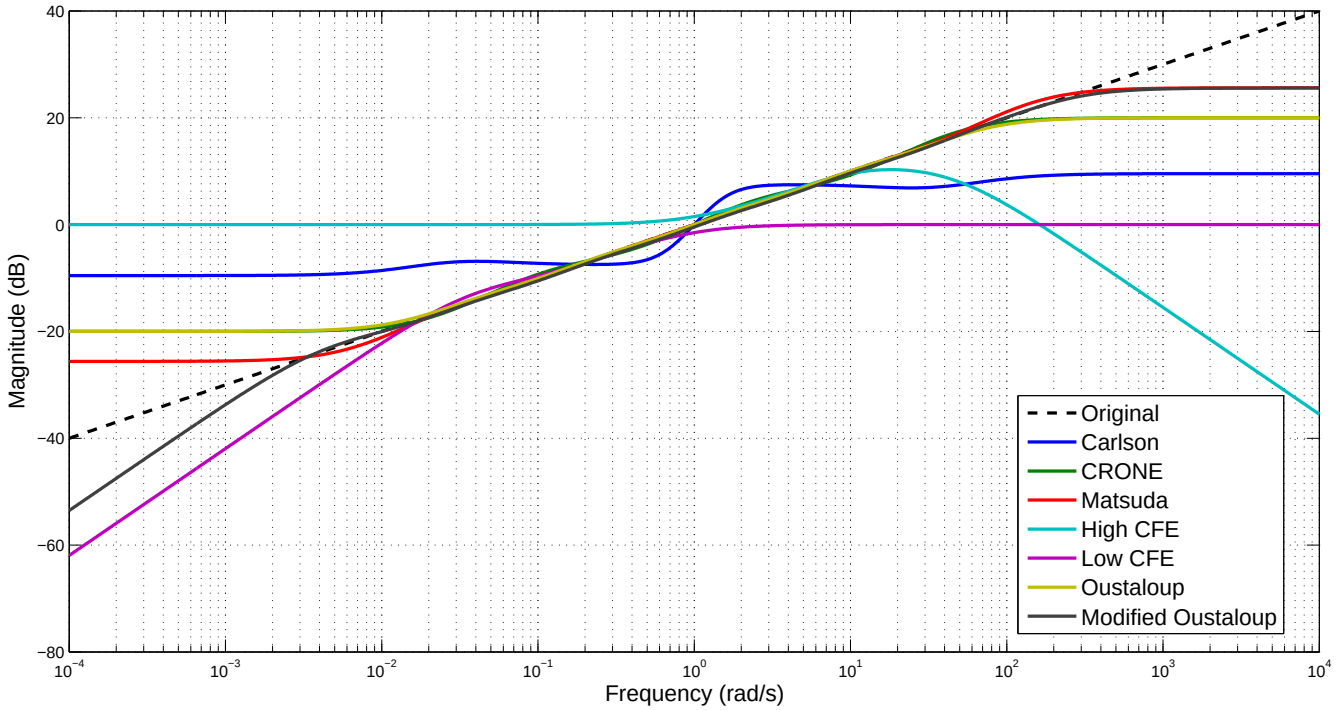

Figure 2.1: Magnitude Bode Plots for $s^{0.5}$

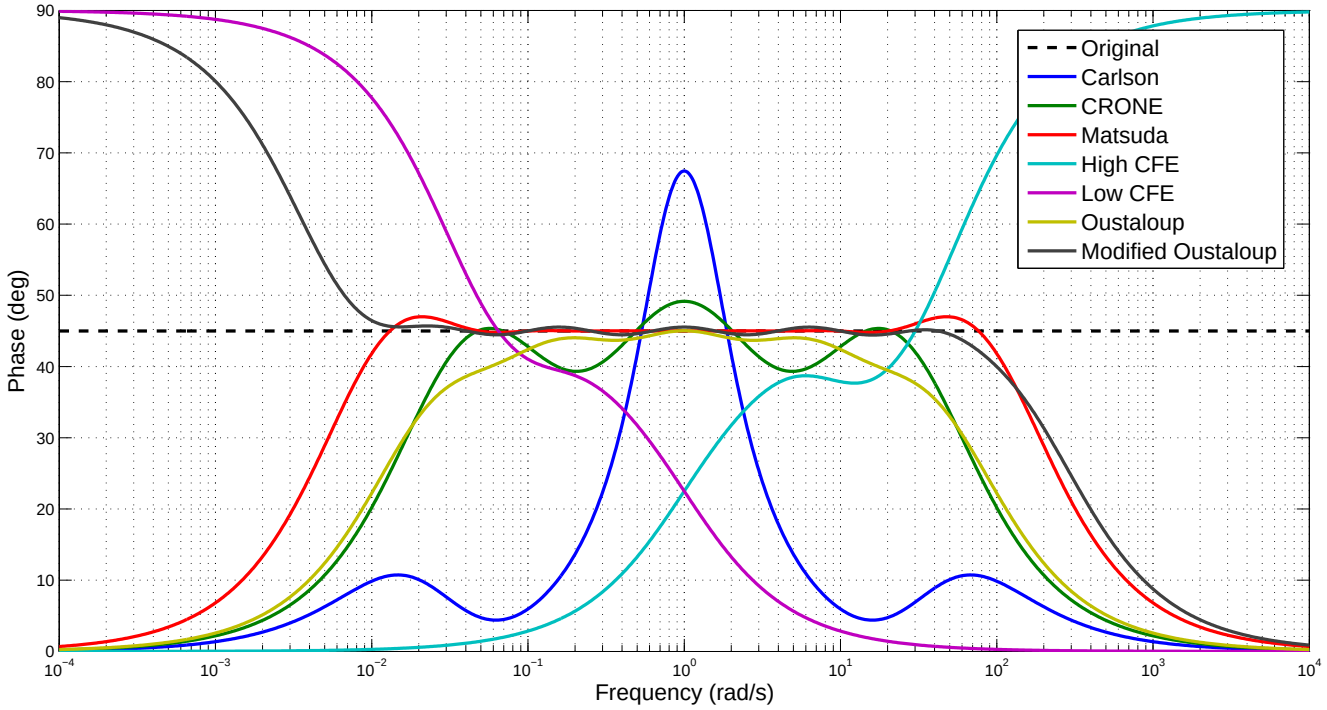

Figure 2.2: Phase Bode Plots for $s^{0.5}$

2.6 Complex Order Derivatives

The order of the derivatives need not be real alone, it can be complex in nature. Hence, the complex order derivative can be written as $F(s) = s^z$; where, $z \in \mathbb{C}$; $z = \alpha + j\beta$. Depending on the sign of α and β, different frequency responses can be realised. The frequency response of $F(s) = s^{\alpha+j\beta}$ is given by:

$$\begin{aligned} F(j\omega) &= (j\omega)^{\alpha+j\beta} \\ &= \omega^{\alpha}(j)^{\alpha+j\beta}\omega^{j\beta} \\ &= \omega^{\alpha}(e^{j\frac{\pi\alpha}{2}})(e^{-\frac{\pi\beta}{2}})\omega^{j\beta} \\ &= \omega^{\alpha}(e^{j\frac{\pi\alpha}{2}})(e^{-\frac{\pi\beta}{2}})(e^{j\beta\ln(\omega)}) \\ &= \omega^{\alpha}(e^{-\frac{\pi\beta}{2}})(e^{j\frac{\pi\alpha}{2}})(e^{j\beta\ln(\omega)}) \\ F(j\omega) &= \omega^{\alpha}e^{-\frac{\pi\beta}{2}}e^{j(\beta\ln(\omega)+\frac{\pi\alpha}{2})} \end{aligned} \tag{2.42}$$

The magnitude of $F(j\omega)$ in decibels (dB) is given by:

$$\begin{aligned} |F(j\omega)|_{dB} &= 20log_{10}(|F(j\omega)|) \\ &= 20\alpha log_{10}(\omega) + 20log_{10}(e^{-\frac{\pi\beta}{2}}) \end{aligned} \tag{2.43}$$

The phase of $F(j\omega)$ in radians is given by:

$$\begin{aligned} \angle F(j\omega) &= \frac{\pi\alpha}{2} + \beta\ln(\omega) \\ &= \frac{\pi\alpha}{2} + \beta\ln(10)log_{10}(\omega) \end{aligned} \tag{2.44}$$

From (2.43) and (2.44), it is observed that both magnitude and phase of $F(j\omega)$ are linear with $log_{10}(\omega)$ and it is seen in Fig. 2.3. It is also noted that the sign of α determines the slope of the magnitude plot and the sign of β determines the slope of the phase plot.

2.7 Integer Order Approximations of Complex Order Derivatives

Among all the methods mentioned in section 2.5, the most widely used and often the best performing one is CRONE approximation (2.33).

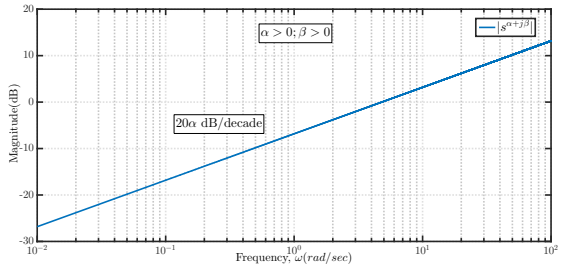

(a) Magnitude plot for $\alpha > 0$ and $\beta > 0$

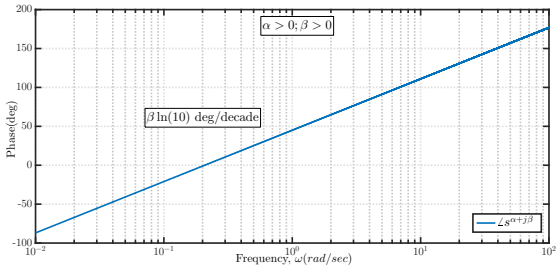

(b) Phase plot for $\alpha > 0$ and $\beta > 0$

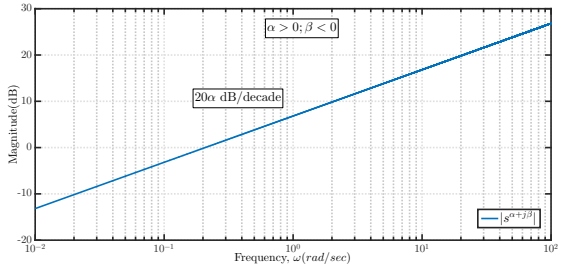

(c) Magnitude plot for $\alpha > 0$ and $\beta < 0$

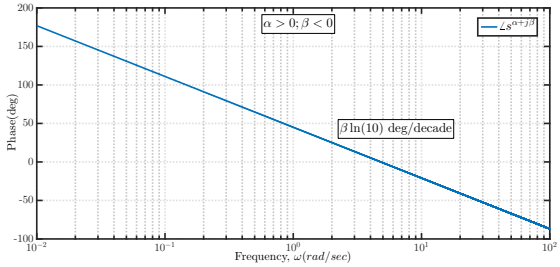

(d) Phase plot for $\alpha > 0$ and $\beta < 0$

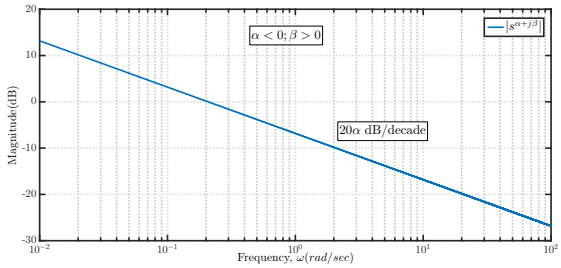

(e) Magnitude plot for $\alpha < 0$ and $\beta > 0$

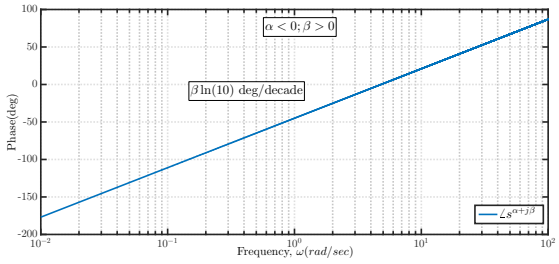

(f) Phase plot for $\alpha < 0$ and $\beta > 0$

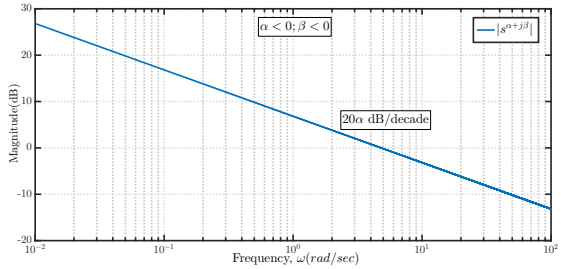

(g) Magnitude plot for $\alpha < 0$ and $\beta < 0$

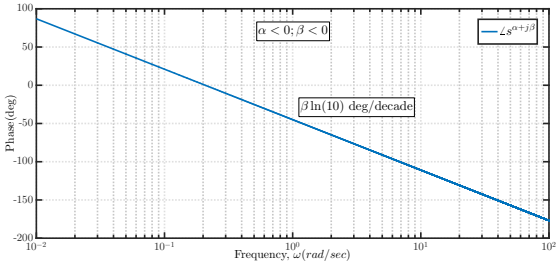

(h) Phase plot for $\alpha < 0$ and $\beta < 0$

Figure 2.3: Bode frequency responses of $s^{\alpha+j\beta}$

Example 2.2. *As an example, consider the complex order derivative* $F(s) = s^{0.5+j0.5}$ *and its CRONE approximation is performed using* (2.33) *over a band of frequency* $(0.01$ *to* $100\,rad/sec)$ *of order* $N = 10$ *is given as:*

$$F_{CRONE}(s) = \frac{\begin{array}{r}(0.9902 + j0.009)s^{10} + (80.45 - j18.05)s^9 + (1759 - j851.7)s^8 \\ +(1.286 * 10^4 - j1.043 * 10^4)s^7 + (3.285 * 10^4 - j4.239 * 10^4)s^6 \\ +(2.826 * 10^4 - j6.177 * 10^4)s^5 + (6684 - j3.317 * 10^4)s^4 - (207.1 + j6589)s^3 \\ - (127 + j474.2)s^2 - (6.172 + j11.52)s - (0.06546 + j0.0743)\end{array}}{\begin{array}{r}-(0.06682 + j0.0744)s^{10} - (6.344 + j11.57)s^9 - (132.8 + j477.6)s^8 \\ -(273 + j6652)s^7 + (6428 - j3.356 * 10^4)s^6 + (2.794 * 10^4 - j6.265 * 10^4)s^5 \\ +(3.277 * 10^4 - j4.312 * 10^4)s^4 + (1.289 * 10^4 - j1.065 * 10^4)s^3 \\ + (1768 - j877.1)s^2 + (81.06 - j19)s + (1 - j1.11 * 10^{-16})\end{array}} \tag{2.45}$$

The approximated form of $s^{\alpha+j\beta}$ *is a complex coefficient integer order TF. Hence, it is necessary to draw the frequency response of* $F(s)$ *both in positive frequency* (ω^+) *and negative frequency* (ω^-)*. Fig. 2.4a and Fig. 2.4b show the magnitude and phase plots of exact and CRONE approximated form of* $s^{0.5+j0.5}$ *respectively for both in* ω^+ *and* ω^- *frequencies.*

2.8 Complex Valued Transfer Function: Universal Plant Structure

A universal plant structure $G(s)$ in (2.46) is proposed, which can accommodate any known class of IO/FO/Fractional Complex Order (FCO) with real and / or complex coefficient plant TFs:

$$\begin{aligned} G(s) &= K\frac{\left((a_0 + jb_0)s^{\alpha_0+j\beta_0} + (a_1 + jb_1)s^{\alpha_1+j\beta_1} + \cdots + (a_m + jb_m)s^{\alpha_m+j\beta_m}\right)}{\left((c_0 + jd_0)s^{\gamma_0+j\delta_0} + (c_1 + jd_1)s^{\gamma_1+j\delta_1} + \cdots + (c_n + jd_n)s^{\gamma_n+j\delta_n}\right)}e^{-Ls} \\ &= K\frac{\sum_{i=0}^{m}(a_i + jb_i)s^{\alpha_i+j\beta_i}}{\sum_{k=0}^{n}(c_k + jd_k)s^{\gamma_k+j\delta_k}}e^{-Ls} \end{aligned} \tag{2.46}$$

where, $K, a_i, b_i, \alpha_i, \beta_i, c_k, d_k, \gamma_k, \delta_k$ and L are real constants. L represents time delay or dead time of the plant. The structure (2.46) can represent any given IO/FO/FCO plant TF with appropriate choice of its parameters.

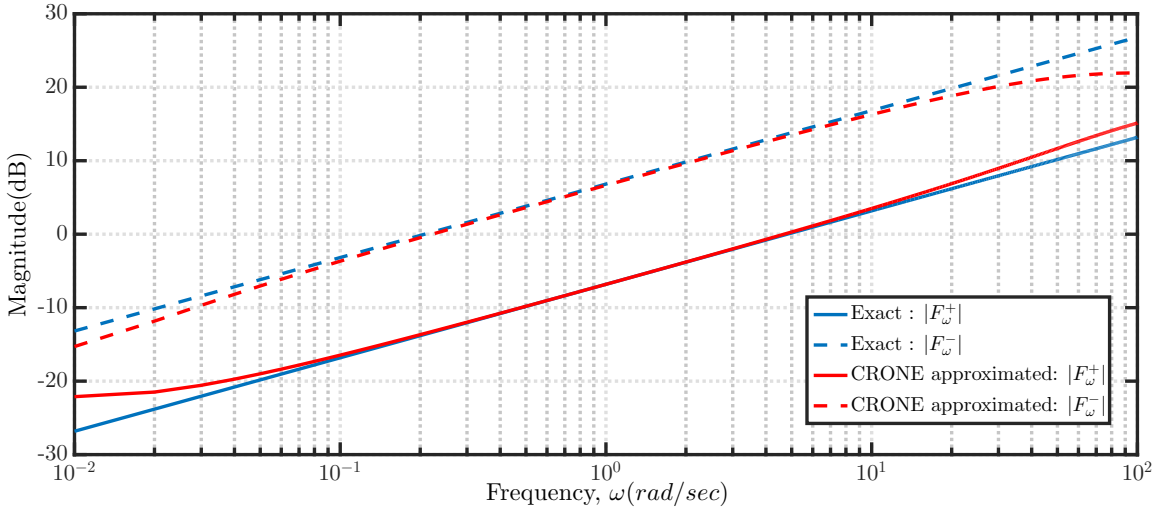

(a) Magnitude Bode Plots for $s^{0.5+j0.5}$

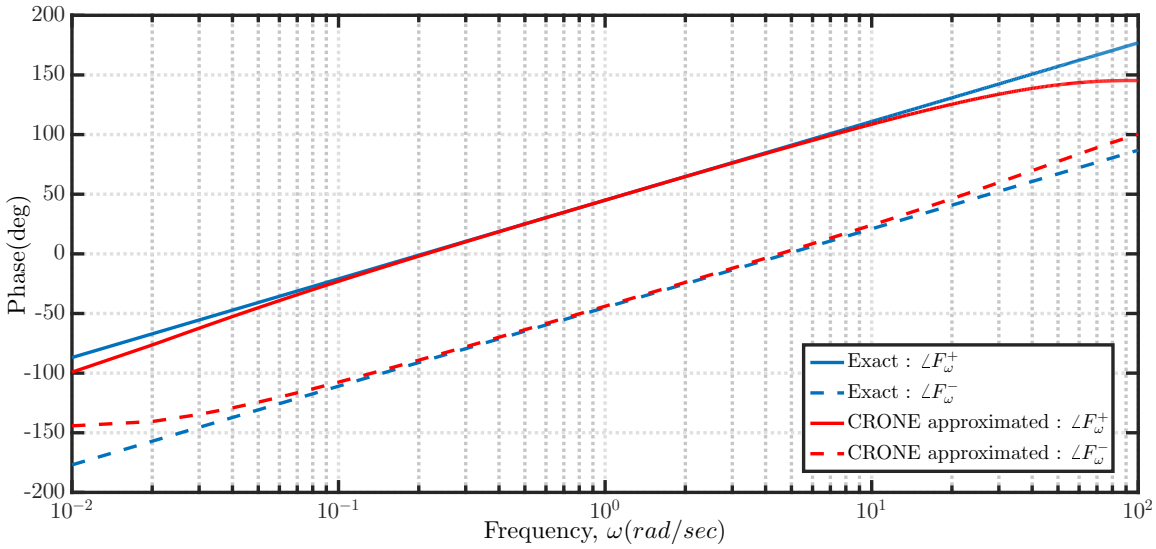

(b) Phase Bode Plots for $s^{0.5+j0.5}$

Figure 2.4: Exact and approximated frequency responses of $s^{0.5+j0.5}$

2.9 Positive and Negative Frequency Analysis of Universal Plant Structure

Transfer functions with real coefficients and IO/FO have an even symmetrical magnitude and odd symmetrical phase behaviour in frequency response. The frequency response for (i) IO/FO plants containing complex coefficients and (ii) fractional complex order plants containing real/complex coefficients have unsymmetrical magnitude and phase behaviour. Hence, the proposed universal structure in (2.46) has unsymmetrical magnitude and phase

behaviour. To illustrate let us consider the transfer function:

$$G(s) = \frac{(1+j)s^{0.2+j0.3}}{(2+j3)s^{2.2+j0.8} + js^{j0.2} + 3}$$

The ω^+ response of G(s) is given as:

$$G(j\omega) = \frac{(1+j)(j\omega)^{0.2+j0.3}}{(2+j3)(j\omega)^{2.2+j0.8} + j(j\omega)^{j0.2} + 3}$$

The ω^- response of G(s) is given as:

$$G(-j\omega) = \frac{(1+j)(-j\omega)^{0.2+j0.3}}{(2+j3)(-j\omega)^{2.2+j0.8} + j(-j\omega)^{j0.2} + 3}$$

The magnitude and phase plots of $G(j\omega)$ and $G(-j\omega)$ are shown in Fig. 2.5a and Fig. 2.5b respectively. It is evident that the frequency response of complex valued systems have unsymmetrical magnitude and phase behaviour.

2.10 Fractional Order Controllers

Fractional Order Controllers (FOCs) are the ones which possess dynamics that are governed by FC. Some of the popular LTI FOCs ($C(s)$) are as follows:

1. Fractional order proportional integral controller

   It is of two types,

   (a) PI^α

   $$C(s) = K_p + \frac{K_i}{s^\alpha} \tag{2.47}$$

   The other form of PI^α is:

   $$C(s) = K_1\left(1 + \frac{K_2}{s^\alpha}\right) \tag{2.48}$$

   (2.47) and (2.48) are related as: $K_p = K_1$, $K_i = K_1K_2$. Both these forms of PI^α controller are used in this thesis.

   (b) $[PI]^\alpha$

   $$C(s) = \left(K_p + \frac{K_i}{s}\right)^\alpha \tag{2.49}$$

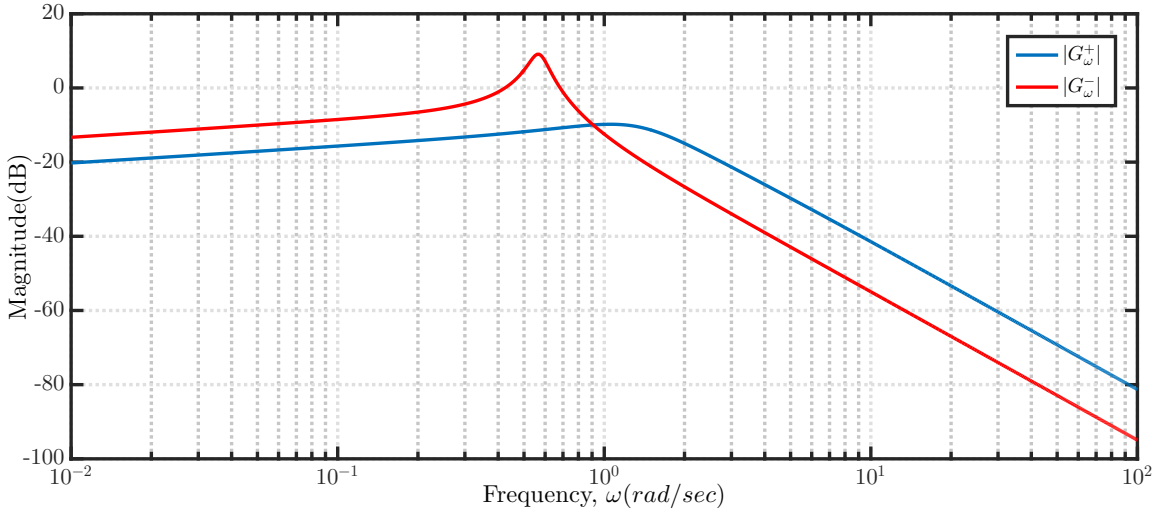

(a) Magnitude Bode Plots

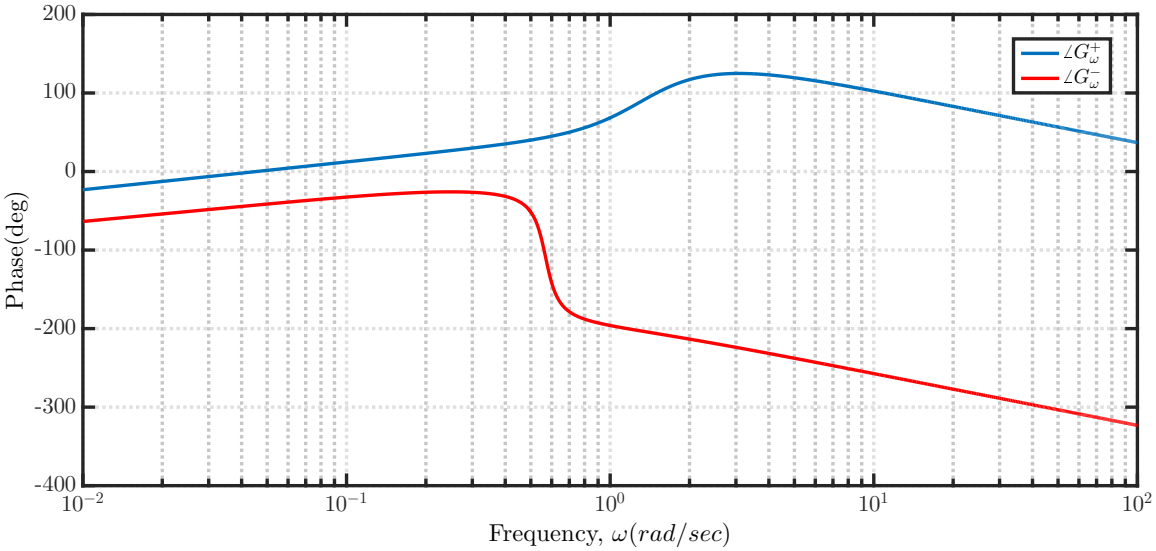

(b) Phase Bode Plots

Figure 2.5: ω^+ and ω^- frequency responses of complex valued TF

The other form of $[PI]^\alpha$ is:

$$C(s) = K_1 \left(1 + \frac{K_2}{s}\right)^\alpha \tag{2.50}$$

(2.49) and (2.50) are related as: $K_p = K_1^{\frac{1}{\alpha}}$, $K_i = K_1^{\frac{1}{\alpha}} K_2$. Both these forms of $[PI]^\alpha$ controller are used in this thesis.

Where, $\alpha > 0; K_p, K_i, \in \mathbb{R}$.

For $\alpha = 1$, (2.47) and (2.49) represent integer PI controller, $C(s) = K_p + \frac{K_i}{s}$.

2. Fractional order proportional derivative controller

   It is of two types,

   (a) PD^β

   $$C(s) = K_p + K_d s^\beta \tag{2.51}$$

   The other form of PD^β is:

   $$C(s) = K_1(1 + K_2 s^\beta) \tag{2.52}$$

   (2.51) and (2.52) are related as : $K_p = K_1$, $K_i = K_1 K_2$. Both these forms of PD^β controller are used in this thesis.

   (b) $[PD]^\beta$

   $$C(s) = (K_p + K_d s)^\beta \tag{2.53}$$

   The other form of $[PD]^\beta$ is:

   $$C(s) = K_1(1 + K_2 s)^\beta \tag{2.54}$$

   (2.53) and (2.54) are related as: $K_p = K_1^{\frac{1}{\beta}}$, $K_i = K_1^{\frac{1}{\beta}} K_2$. Both these forms of $[PD]^\beta$ controller are used in this thesis.

   where, $\beta > 0$; $K_p, K_d \in \mathbb{R}$.

   For $\beta = 1$, (2.51) and (2.53) represent integer PD controller, $C(s) = K_p + K_d s$.

3. Fractional order proportional integral derivative controller

   (a) $PI^\alpha D^\beta$

   $$C(s) = K_p + \frac{K_i}{s^\alpha} + K_d s^\beta \tag{2.55}$$

   The other form of $PI^\alpha D^\beta$ is:

   $$C(s) = K_1 \left(1 + \frac{K_2}{s^\alpha} + K_3 s^\beta\right) \tag{2.56}$$

   (2.55) and (2.56) are related as: $K_p = K_1$, $K_i = K_1 K_2$ and $K_d = K_1 K_3$. Both these forms of $PI^\alpha D^\beta$ controller are used in this thesis.

where, $\alpha > 0, \beta > 0; K_p, K_i, K_d \in \mathbb{R}$.

For $\alpha = 1$ and $\beta = 1$, (2.55) represents integer PID controller, $C(s) = K_p + \frac{K_i}{s} + K_d s$.

4. Fractional Complex Order Controller $(FCOC)$: Three parameter third generation robust CRONE controller handling complex order derivatives is given as [85]:

$$C(s) = K_c \left(\frac{s}{\omega_{gc}} \right)^{\alpha + j\beta} \tag{2.57}$$

where, $\alpha, \beta, K_c, \in \mathbb{R}$. ω_{gc} is the gain crossover frequency and $\alpha + j\beta$ is the complex order of the derivative.

2.11 Complex Coefficient Controllers

Complex Coefficient Integer Order Controllers (CCIOCs) and Complex Coefficient Fractional Complex Order Controllers (CCFCOCs) are proposed in this thesis and are as follows:

1. Complex Coefficient Integer Order Controllers

   (a) Complex Coefficient Proportional Integral (CCPI) controller

   $$C(s) = (K_{pr} + jK_{pi}) + \frac{(K_{ir} + jK_{ii})}{s} \tag{2.58}$$

   where, $K_{pr}, K_{pi}, K_{ir}, K_{ii} \in \mathbb{R}$.

   (b) Complex Coefficient Proportional Derivative (CCPD) controller

   $$C(s) = (K_{pr} + jK_{pi}) + (K_{dr} + jK_{di})s \tag{2.59}$$

   where, $K_{pr}, K_{pi}, K_{dr}, K_{di} \in \mathbb{R}$.

   (c) Complex Coefficient Proportional Integral Derivative (CCPID) controller

   $$C(s) = (K_{pr} + jK_{pi}) + \frac{(K_{ir} + jK_{ii})}{s} + (K_{dr} + jK_{di})s \tag{2.60}$$

   where, $K_{pr}, K_{pi}, K_{ir}, K_{ii}, K_{dr}, K_{di} \in \mathbb{R}$.

2. Complex Coefficient Fractional Complex Order Controllers (CCFCOCs)

   (a) Complex Coefficient Fractional Complex Order PD^{γ} or PI^{γ} controller like structure:

$$C(s) = (K_{1r} + jK_{1i}) + \frac{(K_{2r} + jK_{2i})}{s^{\gamma_r + j\gamma_i}} \tag{2.61}$$

   (b) Complex Coefficient Fractional Complex Order $[PI]^{\alpha}$ controller like structure:

$$C(s) = \left[(K_{1r} + jK_{1i}) + \frac{(K_{2r} + jK_{2i})}{s}\right]^{\alpha_r + j\alpha_i} \tag{2.62}$$

   (c) Complex Coefficient Fractional Complex Order $[PD]^{\beta}$ controller like structure:

$$C(s) = \left[(K_{1r} + jK_{1i}) + (K_{2r} + jK_{2i})s\right]^{\beta_r + j\beta_i} \tag{2.63}$$

   (d) Complex Coefficient Fractional Complex Order $PI^{\alpha}D^{\beta}$ controller like structure:

$$C(s) = (K_{1r} + jK_{1i}) + \frac{(K_{2r} + jK_{2i})}{s^{\alpha_r + j\alpha_i}} + (K_{3r} + jK_{3i})s^{\beta_r + j\beta_i} \tag{2.64}$$

   where, $K_{1r}, K_{1i}, K_{2r}, K_{2i}, K_{3r}, K_{3i}, \gamma_r, \gamma_i, \alpha_r, \alpha_i, \beta_r, \beta_i \in \mathbb{R}$.

In this thesis, unified controller parameter expressions are obtained for FOCs defined in (2.48), (2.50), (2.52), (2.54) and (2.57) to meet Wang et al specifications in chapter 3. In chapter 4, unified controller parameter expressions are obtained for CCIOCs defined in (2.58), (2.59) and (2.60) to meet Wang et al specifications in ω^+ and ω^- for the universal plant structure. This work is also extended by tuning the CCFCOCs defined in (2.61), (2.62) and (2.63) through optimization technique. In chapter 5, FOCs such as (2.47), (2.49), (2.51), (2.53) and (2.55) are tuned to investigate their limit cycle performance for system with multiple nonlinearities.

2.12 Summary

This chapter covers the preliminaries related to FC and FOCs. The various definitions in FC and their properties are discussed. The chapter further presents continuous domain approximation methods which are useful for rationalizing the FO TFs, and it concludes by providing the TF details of FOCs, FCOC, CCIOCs and CCFCOCs.

Chapter 3

Fractional Controller Tuning Expressions for a Universal Plant Structure

3.1 Introduction

In general, researchers use numerous methods to tune Integer Order (IO) and Frational Order Controllers (FOCs) for the given generalized plant structure. This structure deals with IO/Fractional Order (FO) plant plus dead time with real coefficients. In specific, the existing literature widely concentrate on the tuning of three parameter FOCs such as PI^{α}, $[PI]^{\alpha}$, PD^{β}, $[PD]^{\beta}$ and Fractional Complex Order Controller (FCOC) like $K_c\left(\frac{s}{\omega_{gc}}\right)^{\alpha+j\beta}$ to meet Wang et al specifications [76]. Few other literature works which provide such controller tuning expressions for a class of Transfer Functions (TFs) like position and velocity servo system are seen in [80], [83], [81], [85]. On the other hand, some works are reported for First Order Plus Dead Time (FOPDT) process in [77], [78] and for a class of FO plants in [84]. In [90], [91], [92], [93], these controller tuning expressions are unified for any class of real valued IO/FO plants with dead time. Instead of restricting only to real valued IO/FO plants, if one obtains the controller tuning expressions to a complex valued TFs (accommodating all class of TFs), it will greatly reduce the effort required to tune the controllers for such systems. In this chapter, such unified controller tuning expressions are obtained to meet Wang et al specifications for the proposed universal plant structure.

The closed loop schematic of the proposed universal plant structure with controller to meet the required Wang et al specifications are specified in section 3.2. The universal plant structure is proposed and described in section 3.3. A unified FOCs and FCOC parameter expressions are derived in section 3.4. To demonstrate the obtained controller tuning for the defined structure, two different case studies are simulated to meet the desired Wang et

al specifications in section 3.5.

3.2 Generalised Closed Loop Schematic Representation

Let us consider the closed loop control schematic diagram of the universal plant $G(s)$ with controller $C(s)$ as shown in Fig. 3.1.

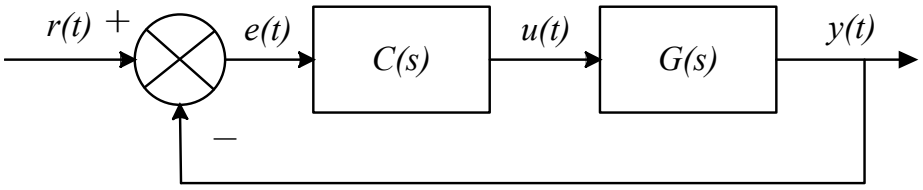

Figure 3.1: Closed loop schematic diagram of universal plant with controller

To obtain the controller parameter expressions, the following Wang et al specifications are considered:

1. Gain Crossover Frequency (ω_{gc}):

$$|G_{\omega_{gc}}||C(j\omega_{gc})| = 1 \tag{3.1}$$

2. Phase Margin (ϕ_m):

$$\angle G_{\omega_{gc}} + \angle C(j\omega_{gc}) + \pi = \phi_m \tag{3.2}$$

3. Robustness to gain variations (i.e. phase flatness at ω_{gc} or Isodamping condition): This condition ensures constant phase margin irrespective of plant gain variations.

$$\begin{aligned}
\left.\frac{d\angle[G(j\omega)C(j\omega)]}{d\omega}\right|_{\omega=\omega_{gc}} &= 0 \\
\left.\frac{d[\angle G(j\omega) + \angle C(j\omega)]}{d\omega}\right|_{\omega=\omega_{gc}} &= 0 \\
\left.\frac{d\angle G(j\omega)}{d\omega}\right|_{\omega=\omega_{gc}} + \left.\frac{d\angle C(j\omega)}{d\omega}\right|_{\omega=\omega_{gc}} &= 0 \\
\psi + \left.\frac{d\angle C(j\omega)}{d\omega}\right|_{\omega=\omega_{gc}} &= 0
\end{aligned} \tag{3.3}$$

$|G_{\omega_{gc}}|$, $\angle G_{\omega_{gc}}$ and ψ are the magnitude, phase and slope of the phase at ω_{gc} of the universal plant $G(s)$. $|C(j\omega_{gc})|$, $\angle C(j\omega_{gc})$ and $\frac{d\angle C(j\omega)}{d\omega}\Big|_{\omega=\omega_{gc}}$ are the magnitude, phase and slope of the phase at ω_{gc} of the controller $C(s)$.

3.3 Universal Plant Structure

To obtain the unified tuning expressions for the controller $C(s)$ in Fig. 3.1, we propose a universal plant structure $G(s)$ in (3.4), which can accommodate any known class of IO/FO/Fractional Complex Order (FCO) with real and/or complex coefficient plant TF:

$$\boxed{\begin{aligned} G(s) &= K\frac{\left((a_0+jb_0)s^{\alpha_0+j\beta_0}+(a_1+jb_1)s^{\alpha_1+j\beta_1}+\cdots+(a_m+jb_m)s^{\alpha_m+j\beta_m}\right)}{\left((c_0+jd_0)s^{\gamma_0+j\delta_0}+(c_1+jd_1)s^{\gamma_1+j\delta_1}+\cdots+(c_n+jd_n)s^{\gamma_n+j\delta_n}\right)}e^{-Ls} \\ &= K\frac{\sum_{i=0}^{m}(a_i+jb_i)s^{\alpha_i+j\beta_i}}{\sum_{k=0}^{n}(c_k+jd_k)s^{\gamma_k+j\delta_k}}e^{-Ls} \end{aligned}} \tag{3.4}$$

where, $K, a_i, b_i, \alpha_i, \beta_i, c_k, d_k, \gamma_k, \delta_k$ and L are real constants. L represents time delay or dead time of the plant. The structure (3.4) can represent any given IO/FO/FCO plant TF with appropriate choice of its parameters. The frequency response function of (3.4) is given as:

$$G(s)\Big|_{s=j\omega} = K\frac{\sum_{i=0}^{m}(a_i+jb_i)(j\omega)^{\alpha_i+j\beta_i}}{\sum_{k=0}^{n}(c_k+jd_k)(j\omega)^{\gamma_k+j\delta_k}}e^{-jL\omega} \tag{3.5}$$

$$G(j\omega) = K\frac{\sum_{i=0}^{m}(a_i+jb_i)(\omega)^{\alpha_i}e^{\frac{-\pi\beta_i}{2}}e^{j(\beta_i ln(\omega)+\frac{\pi\alpha_i}{2})}}{\sum_{k=0}^{n}(c_k+jd_k)(\omega)^{\gamma_k}e^{\frac{-\pi\delta_k}{2}}e^{j(\delta_k ln(\omega)+\frac{\pi\gamma_k}{2})}}e^{-jL\omega}$$

$$G(j\omega) = K\left[\frac{P_1+jQ_1}{P_2+jQ_2}\right]e^{-jL\omega} \tag{3.6}$$

where,

$$P_1 = \sum_{i=0}^{m}\omega^{\alpha_i}e^{\frac{-\pi\beta_i}{2}}\left[a_i\cos\Big(\beta_i ln(\omega)+\frac{\pi\alpha_i}{2}\Big)-b_i\sin\Big(\beta_i ln(\omega)+\frac{\pi\alpha_i}{2}\Big)\right]$$

$$Q_1 = \sum_{i=0}^{m} \omega^{\alpha_i} e^{\frac{-\pi\beta_i}{2}} \left[a_i \sin\Big(\beta_i ln(\omega) + \frac{\pi\alpha_i}{2}\Big) + b_i \cos\Big(\beta_i ln(\omega) + \frac{\pi\alpha_i}{2}\Big) \right]$$

$$P_2 = \sum_{k=0}^{n} \omega^{\gamma_k} e^{\frac{-\pi\delta_k}{2}} \left[c_k \cos\Big(\delta_k ln(\omega) + \frac{\pi\gamma_k}{2}\Big) - d_k \sin\Big(\delta_k ln(\omega) + \frac{\pi\gamma_k}{2}\Big) \right]$$

$$Q_2 = \sum_{k=0}^{n} \omega^{\gamma_k} e^{\frac{-\pi\delta_k}{2}} \left[c_k \sin\Big(\delta_k ln(\omega) + \frac{\pi\gamma_k}{2}\Big) + d_k \cos\Big(\delta_k ln(\omega) + \frac{\pi\gamma_k}{2}\Big) \right]$$

Then the unified expressions for magnitude, phase and slope of the phase at ω_{gc} of the universal plant $G(s)$ are obtained in (3.7), (3.8) and (3.9) respectively and are given as:

$$|G_{\omega_{gc}}| = K \left[\sqrt{\frac{P_1^2 + Q_1^2}{P_2^2 + Q_2^2}} \right] \Bigg|_{\omega=\omega_{gc}} \tag{3.7}$$

$$\angle G_{\omega_{gc}} = \left[\tan^{-1}\left(\frac{Q_1}{P_1}\right) - \tan^{-1}\left(\frac{Q_2}{P_2}\right) - L\omega \right] \Bigg|_{\omega=\omega_{gc}} \tag{3.8}$$

$$\psi = \left[\left(\frac{P_1 \frac{dQ_1}{d\omega} - Q_1 \frac{dP_1}{d\omega}}{P_1^2 + Q_1^2} \right) - \left(\frac{P_2 \frac{dQ_2}{d\omega} - Q_2 \frac{dP_2}{d\omega}}{P_2^2 + Q_2^2} \right) - L \right] \Bigg|_{\omega=\omega_{gc}} \tag{3.9}$$

where,

$$\frac{dP_1}{d\omega} = \sum_{i=0}^{m} \omega^{\alpha_i} e^{\frac{-\pi\beta_i}{2}} \left[\left(\frac{a_i\alpha_i - b_i\beta_i}{\omega} \right) \cos\Big(\beta_i ln(\omega) + \frac{\pi\alpha_i}{2}\Big) - \left(\frac{a_i\beta_i + b_i\alpha_i}{\omega} \right) \sin\Big(\beta_i ln(\omega) + \frac{\pi\alpha_i}{2}\Big) \right]$$

$$\frac{dQ_1}{d\omega} = \sum_{i=0}^{m} \omega^{\alpha_i} e^{\frac{-\pi\beta_i}{2}} \left[\left(\frac{a_i\beta_i + b_i\alpha_i}{\omega} \right) \cos\Big(\beta_i ln(\omega) + \frac{\pi\alpha_i}{2}\Big) + \left(\frac{a_i\alpha_i - b_i\beta_i}{\omega} \right) \sin\Big(\beta_i ln(\omega) + \frac{\pi\alpha_i}{2}\Big) \right]$$

$$\frac{dP_2}{d\omega} = \sum_{k=0}^{n} \omega^{\gamma_k} e^{\frac{-\pi\delta_k}{2}} \left[\left(\frac{c_k\gamma_k - d_k\delta_k}{\omega} \right) \cos\Big(\delta_k ln(\omega) + \frac{\pi\gamma_k}{2}\Big) - \left(\frac{c_k\delta_k + d_k\gamma_k}{\omega} \right) \sin\Big(\delta_k ln(\omega) + \frac{\pi\gamma_k}{2}\Big) \right]$$

$$\frac{dQ_2}{d\omega} = \sum_{k=0}^{n} \omega^{\gamma_k} e^{\frac{-\pi\delta_k}{2}} \left[\left(\frac{c_k\delta_k + d_k\gamma_k}{\omega} \right) \cos\left(\delta_k ln(\omega) + \frac{\pi\gamma_k}{2} \right) + \left(\frac{c_k\gamma_k - d_k\delta_k}{\omega} \right) \sin\left(\delta_k ln(\omega) + \frac{\pi\gamma_k}{2} \right) \right]$$

Remark 3.1. *It is further possible to replace the delay term by its generalised form* $e^{-Ls^{\zeta}}$ *in* (3.4)*;* $\zeta \in \mathbb{C}$ *i.e.* $\zeta = \zeta_r + j\zeta_i$*. However, there is no physical meaning of such term exists in the present literature. Therefore, only the conventional exponential term* e^{-Ls}*;* $L \in \mathbb{R}$ *is considered in* (3.4)*.*

3.4 Fractional Order Controllers and their Unified Tuning Expressions

In this section, unified tuning expressions of three parameter FOCs and FCOC parameters are obtained for the given universal system to meet the desired specifications (3.1), (3.2) and (3.3).

3.4.1 Tuning Expressions for FOCs

The unified tuning expressions for three parameter FOCs such as PI^{α}, $[PI]^{\alpha}$, PD^{β}, $[PD]^{\beta}$ are derived so as to meet Wang et al specifications. The controller structures have been described in (2.48), (2.50), (2.52) and (2.54) of Section 2.10.

3.4.1.1 Tuning Expressions for PI^{α} and PD^{β} Controllers

In general, PI^{α} and PD^{β} controllers given in (2.48) and (2.52) respectively are combined using the following general expression:

$$C(s) = K_1(1 + K_2 s^{\gamma}) \tag{3.10}$$

The frequency response of (3.10) is

$$C(j\omega) = K_1 \left[\left(1 + K_2\omega^{\gamma} \cos\left(\frac{\pi\gamma}{2} \right) \right)^2 + \left(K_2\omega^{\gamma} \sin\left(\frac{\pi\gamma}{2} \right) \right)^2 \right]^{\frac{1}{2}} e^{j\tan^{-1}\left[\frac{K_2\omega^{\gamma}\sin\left(\frac{\pi\gamma}{2}\right)}{1+K_2\omega^{\gamma}\cos\left(\frac{\pi\gamma}{2}\right)} \right]} \tag{3.11}$$

The magnitude and phase of $C(j\omega)$ and slope of $\angle C(j\omega)$ at desired ω_{gc} are as follows:

$$|C(j\omega_{gc})| = K_1\left[\left(1 + K_2\omega_{gc}^{\gamma}\cos\left(\frac{\pi\gamma}{2}\right)\right)^2 + \left(K_2\omega_{gc}^{\gamma}\sin\left(\frac{\pi\gamma}{2}\right)\right)^2\right]^{\frac{1}{2}} \tag{3.12}$$

$$\angle C(j\omega_{gc}) = \tan^{-1}\left[\frac{K_2\omega_{gc}^{\gamma}\sin\left(\frac{\pi\gamma}{2}\right)}{1 + K_2\omega_{gc}^{\gamma}\cos\left(\frac{\pi\gamma}{2}\right)}\right] \tag{3.13}$$

$$\left.\frac{d\angle C(j\omega)}{d\omega}\right|_{\omega=\omega_{gc}} = \frac{\gamma\omega_{gc}^{-1}\left(\frac{K_2\omega_{gc}^{\gamma}\sin\left(\frac{\pi\gamma}{2}\right)}{1+K_2\omega_{gc}^{\gamma}\cos\left(\frac{\pi\gamma}{2}\right)}\right)}{\left(1 + \left[\frac{K_2\omega_{gc}^{\gamma}\sin\left(\frac{\pi\gamma}{2}\right)}{1+K_2\omega_{gc}^{\gamma}\cos\left(\frac{\pi\gamma}{2}\right)}\right]^2\right)} \times \left(\frac{1}{1 + K_2\omega_{gc}^{\gamma}\cos\left(\frac{\pi\gamma}{2}\right)}\right) \tag{3.14}$$

Using (3.8) and (3.13), specification (3.2) becomes

$$\angle G_{\omega_{gc}} + \tan^{-1}\left[\frac{K_2\omega_{gc}^{\gamma}\sin\left(\frac{\pi\gamma}{2}\right)}{1 + K_2\omega_{gc}^{\gamma}\cos\left(\frac{\pi\gamma}{2}\right)}\right] + \pi = \phi_m$$

this implies,

$$K_2 = \frac{{\omega_{gc}}^{-\gamma}\tan A}{\sin\left(\frac{\pi\gamma}{2}\right) - \cos\left(\frac{\pi\gamma}{2}\right)\tan A} \tag{3.15}$$

Using (3.9) and (3.14), specification (3.3) becomes

$$\psi + \frac{\gamma\omega_{gc}^{-1}\left(\frac{K_2\omega_{gc}^{\gamma}\sin\left(\frac{\pi\gamma}{2}\right)}{1+K_2\omega_{gc}^{\gamma}\cos\left(\frac{\pi\gamma}{2}\right)}\right)}{\left(1 + \left[\frac{K_2\omega_{gc}^{\gamma}\sin\left(\frac{\pi\gamma}{2}\right)}{1+K_2\omega_{gc}^{\gamma}\cos\left(\frac{\pi\gamma}{2}\right)}\right]^2\right)} \times \left(\frac{1}{1 + K_2\omega_{gc}^{\gamma}\cos\left(\frac{\pi\gamma}{2}\right)}\right) = 0$$

$$\frac{-\gamma\tan A}{\psi\omega_{gc}(1+\tan^2 A)} = 1 + K_2\omega_{gc}^{\gamma}\cos\left(\frac{\pi\gamma}{2}\right)$$

this implies,

$$K_2 = \frac{H\gamma - 1}{\omega_{gc}^{\gamma}\cos\left(\frac{\pi\gamma}{2}\right)} \tag{3.16}$$

Using (3.7) and (3.12), specification (3.1) becomes

$$|G_{\omega_{gc}}|K_1\left[\left(1 + K_2\omega_{gc}^{\gamma}\cos\left(\frac{\pi\gamma}{2}\right)\right)^2 + \left(K_2\omega_{gc}^{\gamma}\sin\left(\frac{\pi\gamma}{2}\right)\right)^2\right]^{\frac{1}{2}} = 1$$

this implies,

$$K_1 = \frac{1}{H\gamma|G_{\omega_{gc}}|\sqrt{1+\tan^2 A}} \tag{3.17}$$

where,

$$A = \phi_m - \pi - \angle G_{\omega_{gc}}$$
$$H = \frac{-\tan A}{\psi\omega_{gc}(1+\tan^2 A)}$$

By solving (3.15) and (3.16), K_2 and γ are obtained. K_1 is obtained by substituting γ in (3.17).

- Case 1: $\gamma < 0$
  By considering $\alpha = -\gamma$, PI^α controller defined in (2.48) is obtained and it is given as

  $$C(s) = K_1\left(1 + \frac{K_2}{s^\alpha}\right) \tag{3.18}$$

  Then, the controller parameters for PI^α given in (2.47) are: $K_p = K_1$ and $K_i = K_1K_2$.

- Case 2: $\gamma > 0$
  By considering $\beta = \gamma$, PD^β controller defined in (2.52) is obtained and it is given as

  $$C(s) = K_1(1 + K_2 s^\beta) \tag{3.19}$$

  Then, the controller parameters for PD^β given in (2.51) are: $K_p = K_1$ and $K_d = K_1K_2$.

3.4.1.2 Tuning Expressions for $[\boldsymbol{PI}]^{\boldsymbol{\alpha}}$

To obtain the unified tuning expressions for $[PI]^\alpha$ controller, the structure described in (2.50) is considered and it is given as:

$$C(s) = K_1\left(1 + \frac{K_2}{s}\right)^\alpha \tag{3.20}$$

The frequency response of (3.20) is

$$C(j\omega) = K_1 \left(\sqrt{1 + \left(\frac{K_2}{\omega} \right)^2} \right)^{\alpha} e^{j\alpha \tan^{-1}\left(\frac{-K_2}{\omega}\right)} \tag{3.21}$$

The magnitude and phase of $C(j\omega)$ and slope of $\angle C(j\omega)$ at desired ω_{gc} are as follows:

$$|C(j\omega_{gc})| = K_1 \left(\sqrt{1 + \left(\frac{K_2}{\omega_{gc}} \right)^2} \right)^{\alpha} \tag{3.22}$$

$$\angle C(j\omega_{gc}) = \alpha \tan^{-1} \left(\frac{-K_2}{\omega_{gc}} \right) \tag{3.23}$$

$$\left. \frac{d\angle C(j\omega)}{d\omega} \right|_{\omega=\omega_{gc}} = \frac{\alpha}{1 + \left(-\frac{K_2}{\omega_{gc}} \right)^2} \left(\frac{K_2}{\omega_{gc}^2} \right) \tag{3.24}$$

Using (3.8) and (3.23), specification (3.2) becomes

$$\angle G_{\omega_{gc}} + \alpha \tan^{-1} \left(\frac{-K_2}{\omega_{gc}} \right) + \pi = \phi_m$$

this implies,

$$K_2 = -\omega_{gc} \tan \left(\frac{A}{\alpha} \right) \tag{3.25}$$

Using (3.9) and (3.24), specification (3.3) becomes

$$\psi + \frac{\alpha}{1 + \left(\frac{-K_2}{\omega_{gc}} \right)^2} \left(\frac{K_2}{\omega_{gc}^2} \right) = 0$$

this implies,

$$K_2 = \frac{-\omega_{gc}^2 \psi \left(1 + \tan^2 \left(\frac{A}{\alpha} \right) \right)}{\alpha} \tag{3.26}$$

Using (3.7) and (3.22), specification (3.1) becomes

$$|G_{\omega_{gc}}| K_1 \left(\sqrt{1 + \left(\frac{K_2}{\omega_{gc}} \right)^2} \right)^{\alpha} = 1$$

this implies,

$$K_1 = \frac{1}{|G_{\omega_{gc}}| \left(\sqrt{1+\tan^2\left(\frac{A}{\alpha}\right)}\right)^{\alpha}} \tag{3.27}$$

By solving (3.25) and (3.26), K_2 and α are obtained. K_1 is obtained by substituting α in (3.27).

Then the controller parameters for $[PI]^{\alpha}$ given in (2.49) are: $K_p = K_1^{\frac{1}{\alpha}}$ and $K_i = K_1^{\frac{1}{\alpha}} K_2$.

3.4.1.3 Tuning Expressions for $[PD]^{\beta}$

To obtain the unified tuning expressions for $[PD]^{\beta}$ controller, the structure described in (2.54) is considered and it is given as:

$$C(s) = K_1(1 + K_2 s)^{\beta} \tag{3.28}$$

The frequency response of (3.28) is

$$\begin{aligned} C(j\omega) &= K_1 \left(1 + jK_2\omega\right)^{\beta} \\ C(j\omega) &= K_1 \left(\sqrt{1+(K_2\omega)^2}\right)^{\beta} e^{j\beta \tan^{-1}(K_2\omega)} \end{aligned} \tag{3.29}$$

The magnitude and phase of $C(j\omega)$ and slope of $\angle C(j\omega)$ at desired ω_{gc} are as follows:

$$|C(j\omega_{gc})| = K_1 \left(\sqrt{1+(K_2\omega_{gc})^2}\right)^{\beta} \tag{3.30}$$

$$\angle C(j\omega_{gc}) = \beta \tan^{-1}(K_2\omega_{gc}) \tag{3.31}$$

$$\left.\frac{d\angle C(j\omega)}{d\omega}\right|_{\omega=\omega_{gc}} = \frac{\beta K_2}{1+(K_2\omega_{gc})^2} \tag{3.32}$$

Using (3.8) and (3.31), specification (3.2) becomes

$$\angle G_{\omega_{gc}} + \beta \tan^{-1}(K_2\omega_{gc}) + \pi = \phi_m$$

this implies,

$$K_2 = \frac{\tan\left(\frac{A}{\beta}\right)}{\omega_{gc}} \tag{3.33}$$

Using (3.9) and (3.32), specification (3.3) becomes

$$\psi + \frac{\beta K_2}{1 + (K_2 \omega_{gc})^2} = 0$$

this implies,

$$K_2 = \frac{-\psi \left(1 + \tan^2 \left(\frac{A}{\beta}\right)\right)}{\beta} \tag{3.34}$$

Using (3.7) and (3.30), specification (3.1) becomes

$$|G_{\omega_{gc}}| K_1 \left(\sqrt{1 + (K_2 \omega_{gc})^2}\right)^{\beta} = 1$$

this implies,

$$K_1 = \frac{1}{|G_{\omega_{gc}}| \left(\sqrt{1 + \tan^2 \left(\frac{A}{\beta}\right)}\right)^{\beta}} \tag{3.35}$$

By solving (3.33) and (3.34), K_2 and β are obtained. K_1 is obtained by substituting β in (3.35).

Then the controller parameters for $[PD]^{\beta}$ given in (2.53) are: $K_p = K_1^{\frac{1}{\beta}}$ and $K_d = K_1^{\frac{1}{\beta}} K_2$.

3.4.2 Tuning Expressions for $FCOC$

The three parameter $FCOC$ like structure described in (2.57) is considered and it is given as:

$$C(s) = K_c \left(\frac{s}{\omega_{gc}}\right)^{\alpha + j\beta} \tag{3.36}$$

The frequency response of (3.36) is

$$\begin{aligned} C(j\omega) &= K_c \left(\frac{j\omega}{\omega_{gc}}\right)^{\alpha + j\beta} \\ C(j\omega) &= K_c \left(\frac{\omega}{\omega_{gc}}\right)^{\alpha} \left(e^{\frac{-\pi\beta}{2}}\right) e^{j\left[\beta ln\left(\frac{\omega}{\omega_{gc}}\right) + \frac{\pi\alpha}{2}\right]} \end{aligned} \tag{3.37}$$

The magnitude and phase of $C(j\omega)$ and slope of $\angle C(j\omega)$ at desired ω_{gc} are as follows:

$$|C(j\omega_{gc})| = K_c e^{\frac{-\pi\beta}{2}} \tag{3.38}$$

$$\angle C(j\omega_{gc}) = \frac{\pi\alpha}{2} \tag{3.39}$$

$$\left.\frac{d\angle C(j\omega)}{d\omega}\right|_{\omega=\omega_{gc}} = \frac{\beta}{\omega_{gc}} \tag{3.40}$$

Using (3.8) and (3.39), specification (3.2) becomes

$$\angle G_{\omega_{gc}} + \frac{\pi\alpha}{2} + \pi = \phi_m$$

this implies,

$$\alpha = \frac{2A}{\pi} \tag{3.41}$$

Using (3.9) and (3.40), specification (3.3) becomes

$$\psi + \frac{\beta}{\omega_{gc}} = 0$$

this implies,

$$\beta = -\omega_{gc}\psi \tag{3.42}$$

Using (3.7) and (3.38), specification (3.1) becomes

$$|G_{\omega_{gc}}|K_c e^{\frac{-\pi\beta}{2}} = 1$$

this implies,

$$K_c = \frac{1}{|G_{\omega_{gc}}|e^{\frac{\pi\psi\omega_{gc}}{2}}} \tag{3.43}$$

From (3.41), (3.42) and (3.43) the controller parameters α, β and K_c are obtained to meet the desired specifications.

Remark 3.2. *It is important to note that though the Wang et al specifications ensure the required positive phase margin at a given gain crossover frequency, they do not guarantee closed loop stability in general. If there occur multiple gain crossover frequencies, such restrictive specifications cannot ensure all the phase margins to be positive. Hence, the generalized derivations presented in this section are useful only for those plants which lead to closed loop stability. Therefore, closed loop stability should be checked after designing the controller for Wang et al specifications.*

3.5 Results and Discussions

To validate the proposed unified fractional controller parameter expressions derived in Section 3.4, two different case studies are considered. The plant and its desired specifications are given in Table 3.1.

Table 3.1: Plant and its specifications

Case	Plant and specifications
I	Plant: $\frac{e^{-0.3s}}{0.04s^{1.8+0.6j}+1.04s^{0.8+0.3j}+1}$ specifications: $\omega_{gc} = 0.5\, rad/sec, \phi_m = 57^\circ$
II	Plant: $\frac{3+4j}{(0.8+0.2j)s^{1.9+0.4j}+(0.5+0.3j)s^{0.8+0.2j}}$ specifications: $\omega_{gc} = 5\, rad/sec, \phi_m = 60^\circ$

Table 3.2: Tuning results of $FOCs$ and $FCOC$

Case	Plant parameters	Controller	Controller parameters	Controller effort $J = \int_0^\infty \|u(t)\|^2 dt$
I	$K = 1, L = 0.3, a_0 = 1,$ $b_0 = 0, c_0 = 0.04, d_0 = 0,$ $c_1 = 1.04, d_1 = 0, c_2 = 1,$ $d_2 = 0, \alpha_0 = 0, \beta_0 = 0,$ $\gamma_0 = 1.8, \delta_0 = 0.6, \gamma_1 = 0.8,$ $\delta_1 = 0.3, \gamma_2 = 0, \delta_2 = 0$	PI^α	$K_1 = 0.3785$ $K_2 = 1.4567$ $\alpha = 1.28$	53.981
		$[PI]^\alpha$	$K_1 = 0.2369$ $K_2 = 1.5926$ $\alpha = 1.3640$	54.225
		$FCOC$	$K_c = 2.2641$ $\alpha = -1.0998$ $\beta = 0.39012$	73.193
II	$K = 1, L = 0, a_0 = 3,$ $b_0 = 4, c_0 = 0.8, d_0 = 0.2,$ $c_1 = 0.5, d_1 = 0.3, \alpha_0 = 0,$ $\beta_0 = 0, \gamma_0 = 1.9, \delta_0 = 0.4,$ $\gamma_1 = 0.8, \delta_1 = 0.2,$	PD^β	$K_1 = 1.5735$ $K_2 = 0.1313$ $\beta = 1.0807$	148.104
		$[PD]^\beta$	$K_1 = 1.5508$ $K_2 = 0.1044$ $\beta = 1.4260$	25676.274
		$FCOC$	$K_c = 4.6155$ $\alpha = 0.4367$ $\beta = 0.5850$	13.680

The cases I and II fit in the universal plant structure $G(s)$ by selecting the appropriate

parameters. By using the derived unified controller expressions, various FOC and $FCOC$ parameters for the given case studies are simulated in MATLAB [161] and the results are given in Table 3.2. It is found that PD^{β} and $[PD]^{\beta}$ controllers for case I, PI^{α} and $[PI]^{\alpha}$ controllers for case II doesn't exist and hence not listed in Table 3.2.

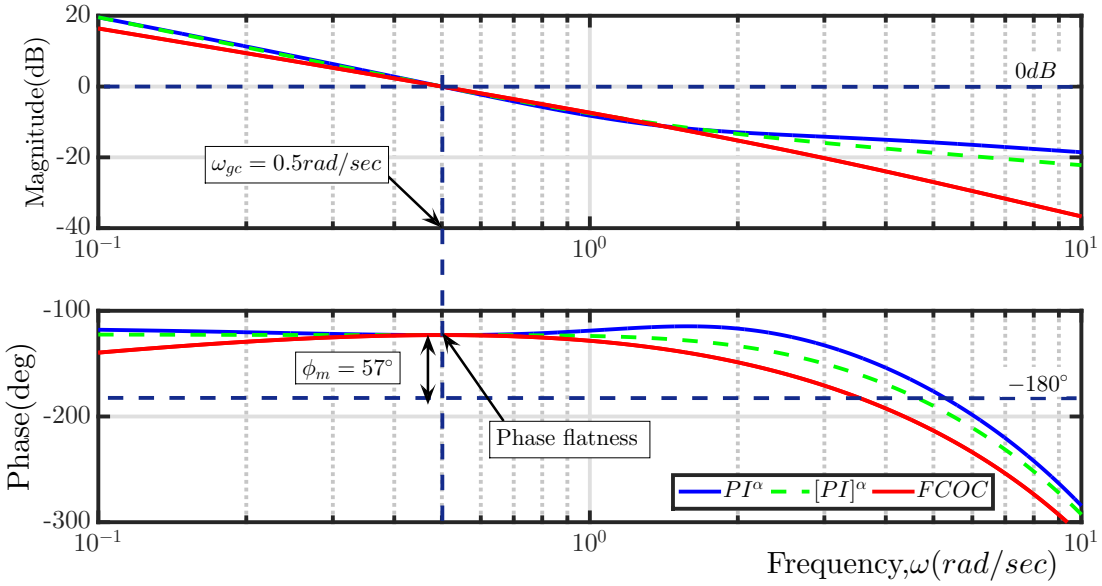

Figure 3.2: Open loop frequency responses of case I with listed controllers

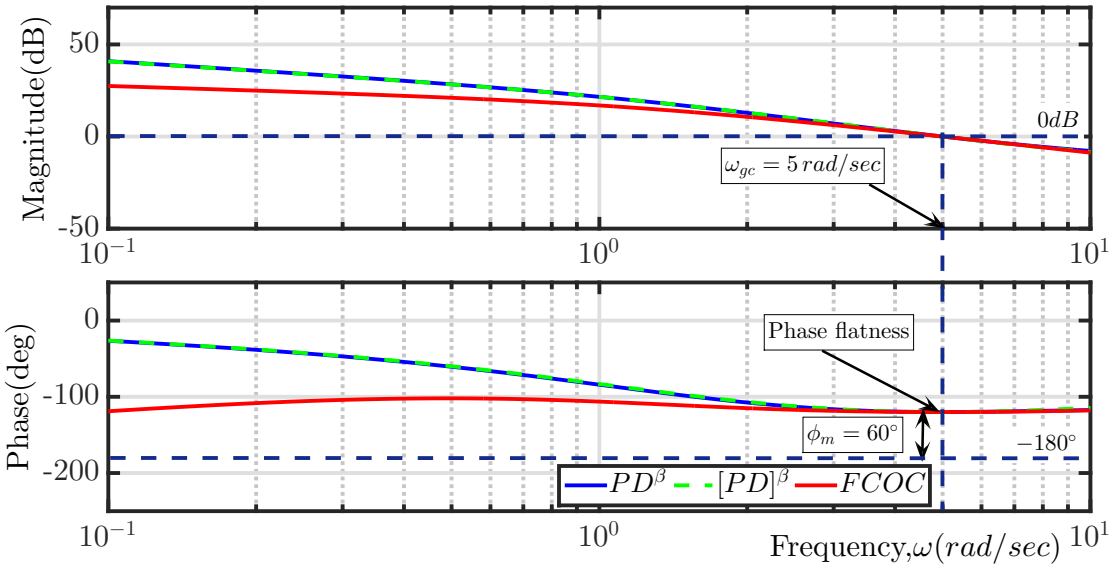

Figure 3.3: Open loop frequency responses of case II with listed controllers

Open loop frequency responses of the case I and case II with all the listed controllers are plotted as in Fig. 3.2 and Fig. 3.3 respectively. It is seen from the figures that the desired gain crossover frequency, phase margin and Isodamping conditions are met by the designed controllers. The Isodamping condition leads to the flatness of the phase response around the gain crossover frequency.

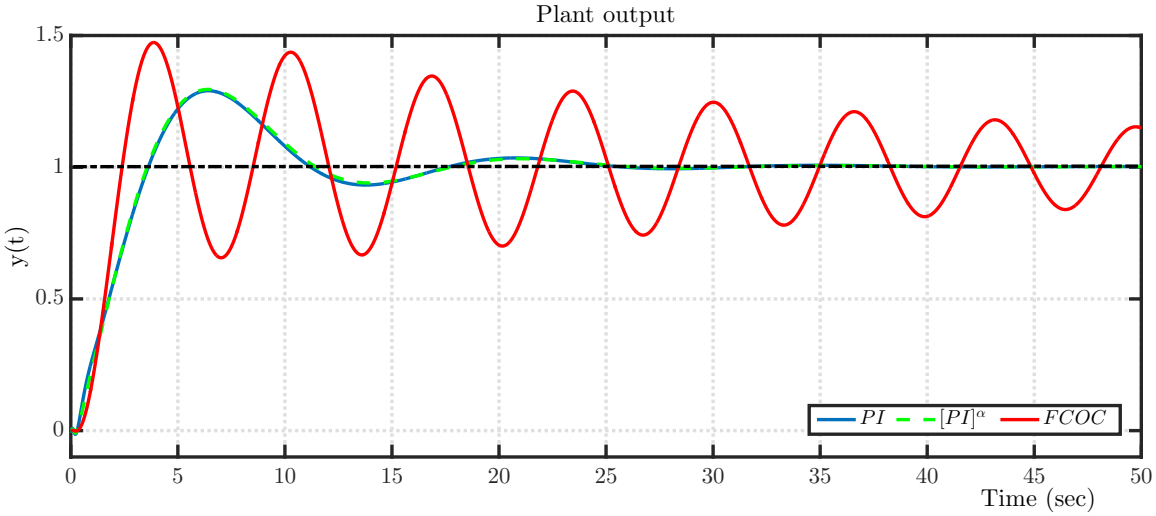

Figure 3.4: Plant output responses of case I with listed controllers

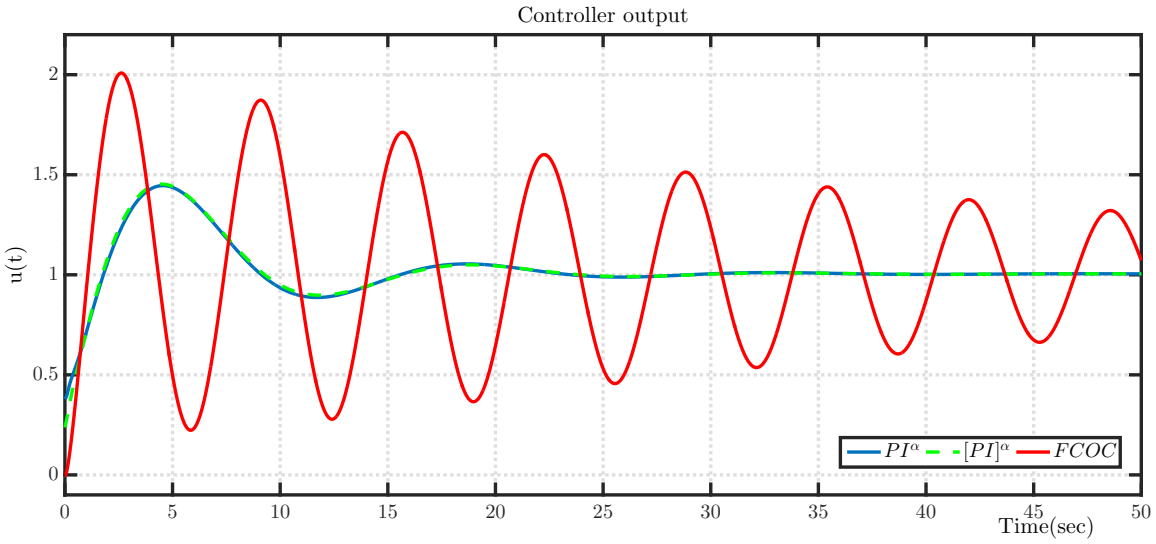

Figure 3.5: Controller output responses of case I with listed controllers

For time domain simulation PI^{α}, PD^{β} and $FCOC$ are approximated to IO by using Oustaloup Recursive Algorithm (ORA) [56], [45]. ORA approximation with order (N) 5 is

used over the frequency band $[0.001to1,000]rad/sec$. While $[PI]^{\alpha}$ and $[PD]^{\beta}$ are realized by the impulse response invariant discretisation method [162] in time domain which is used in [84]. Since $G(s)$ is a complex valued function, both real and imaginary responses exist in time domain. The real part of the closed loop unit step response (y(t)) for case I and case II are shown in Fig. 3.4 and Fig. 3.6 respectively. The real part of the controller output (u(t)) for case I and case II are shown in Fig. 3.5 and Fig. 3.7 respectively.

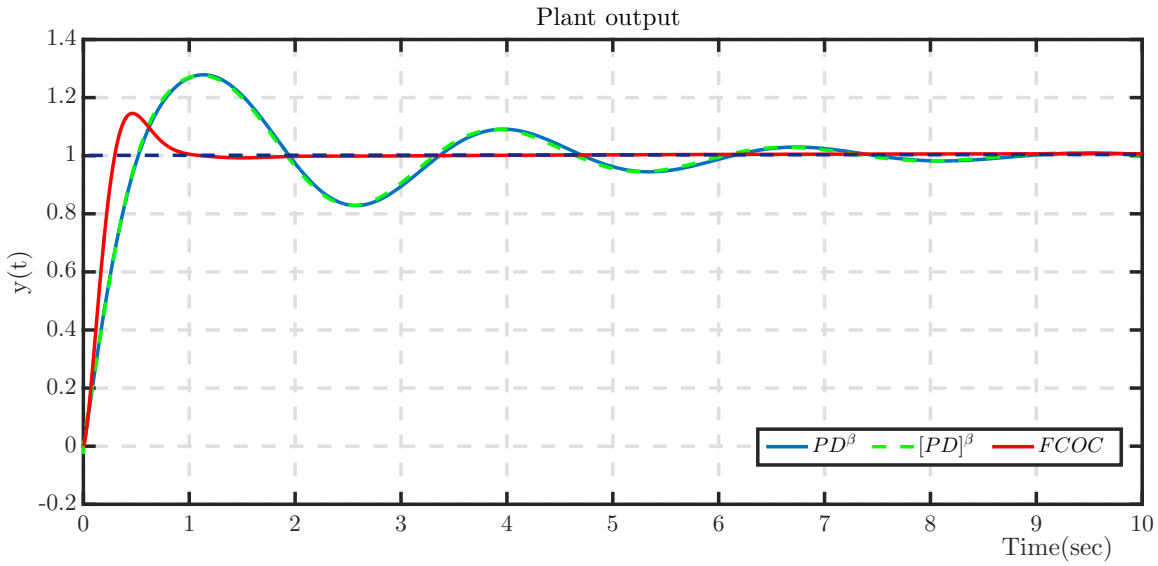

Figure 3.6: Plant output responses of case II with listed controllers

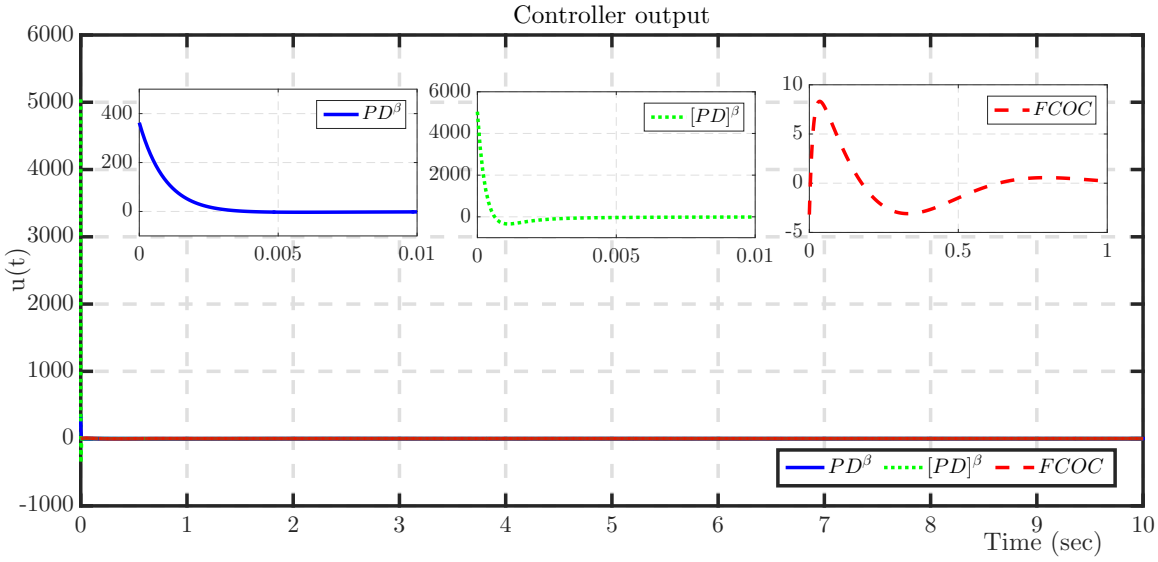

Figure 3.7: Controller output responses of case II with listed controllers

To analyse the controller performance, controller effort is selected as a performance index and shown in Table 3.2. For case I, it is observed that $FCOC$ has more control effort in comparison to PI^{α} and $[PI]^{\alpha}$ controllers. In case II, $FCOC$ has less control effort in comparison to PD^{β} and $[PD]^{\beta}$ controllers.

Stability and robustness to parameter variations of the cases I and II can be interpreted from the sensitivity (S) and complementary sensitivity (T) functions. These functions are related as $S + T = 1$ and are given as:

$$S(j\omega) = \frac{1}{1 + G(j\omega)C(j\omega)}; T(j\omega) = \frac{G(j\omega)C(j\omega)}{1 + G(j\omega)C(j\omega)}$$

Since the universal plant $G(s)$ is a complex valued function, the frequency response is not conjugate symmetric. Hence, the magnitude ratio plots $|S(j\omega)|$ and $|T(j\omega)|$ for case I and case II are drawn for both positive frequency (ω^{+}) and negative frequency (ω^{-}) [118] as shown in Fig. 3.8 and Fig. 3.9 respectively.

The peak value of the plots $|S(jw)|$ and $|T(jw)|$ are the maximum sensitivities M_S and M_T respectively which give a measure of robustness. M_S is referred as largest amplification of the load disturbances and M_T is referred as resonant peak. M_S also provides an assured Gain Margin (GM) and Phase Margin (PM) which determine the stability criteria [163].

$$M_S = \max_{\omega} |S(j\omega)|; M_T = \max_{\omega} |T(j\omega)|$$
$$GM \geq \frac{M_S}{M_S - 1}; PM \geq 2\sin^{-1}\left(\frac{1}{2M_S}\right)$$

M_S and M_T should be in the range of 1.2 to 2.0 and 1 to 1.5 respectively for a good measure of robustness. M_S, M_T, Bandwidth (ω_{BW}) and assured stability margins $(GM$ and $PM)$ are obtained from Fig. 3.8 and Fig. 3.9 for case I and case II respectively. The obtained values are listed in Table 3.3 for ω^{+} and ω^{-}.

From ω^{+} and ω^{-} analysis, it is observed that M_S obtained for PI^{α}, $[PI]^{\alpha}$ are lesser in comparison to $FCOC$ for case I. This assures lesser GM and PM for $FCOC$ and it is evident from the oscillatory behaviour as seen in Fig. 3.4. However for case II, M_S obtained for $FCOC$ is lesser in comparison to PD^{β} and $[PD]^{\beta}$. This assures more GM and PM for $FCOC$ as clearly indicated by more damped response in Fig. 3.6.

It is also inferred that $FCOC$ has larger ω_{BW} and M_T than PI^{α} and $[PI]^{\alpha}$ for case I. This is reflected as lesser rise time and more overshoot for $FCOC$ as shown in Fig. 3.4. Similarly for case II, it is observed that $FCOC$ has larger ω_{BW} and lesser M_T than PD^{β} and $[PD]^{\beta}$. This is reflected as lesser rise time and overshoot for $FCOC$ as shown in Fig. 3.6. This shows, the superiority of the fractional controllers is plant specific and

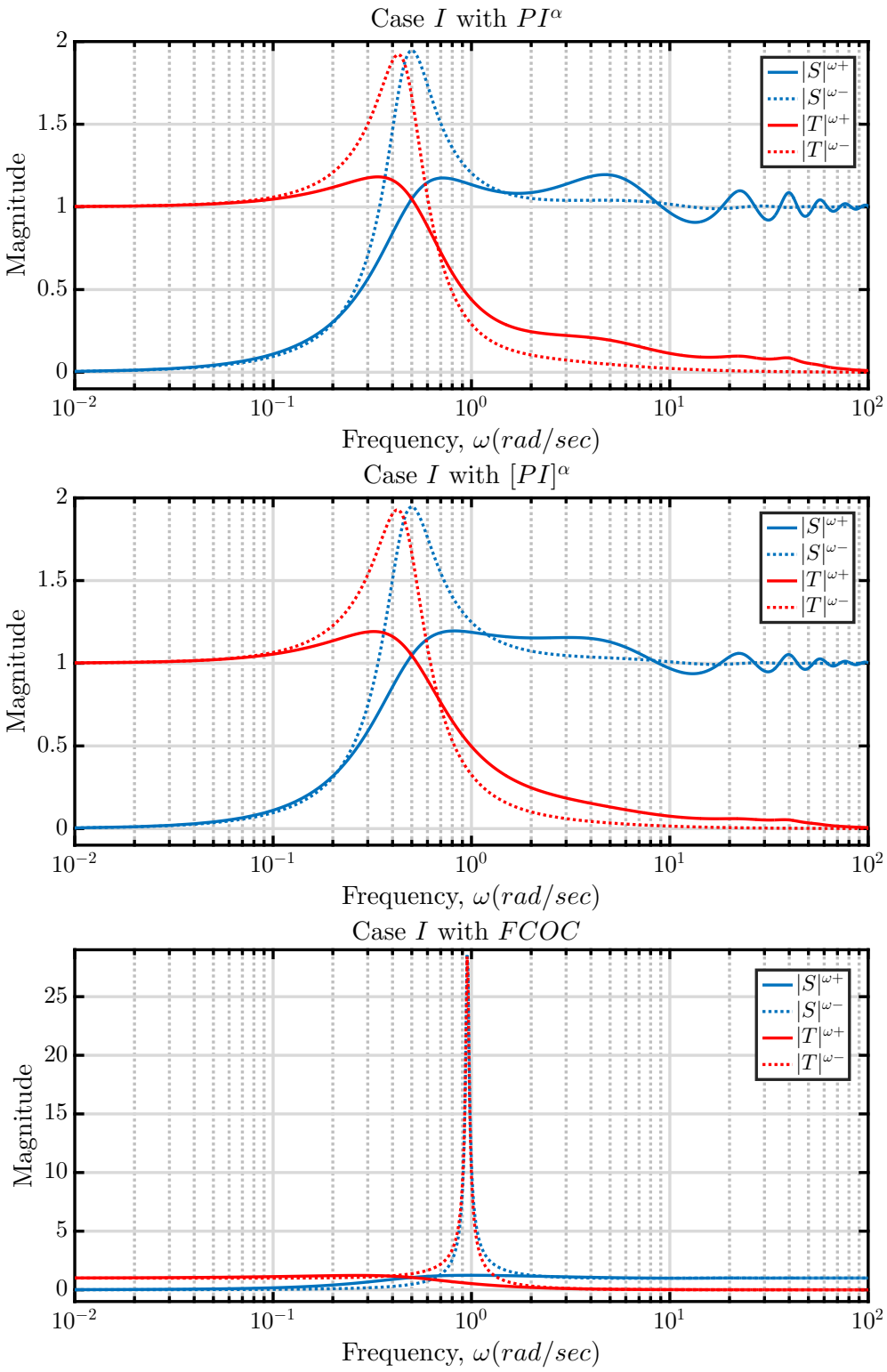

Figure 3.8: $|S(j\omega)|$ and $|T(j\omega)|$ plots of case I in ω^{+} and ω^{-} frequencies

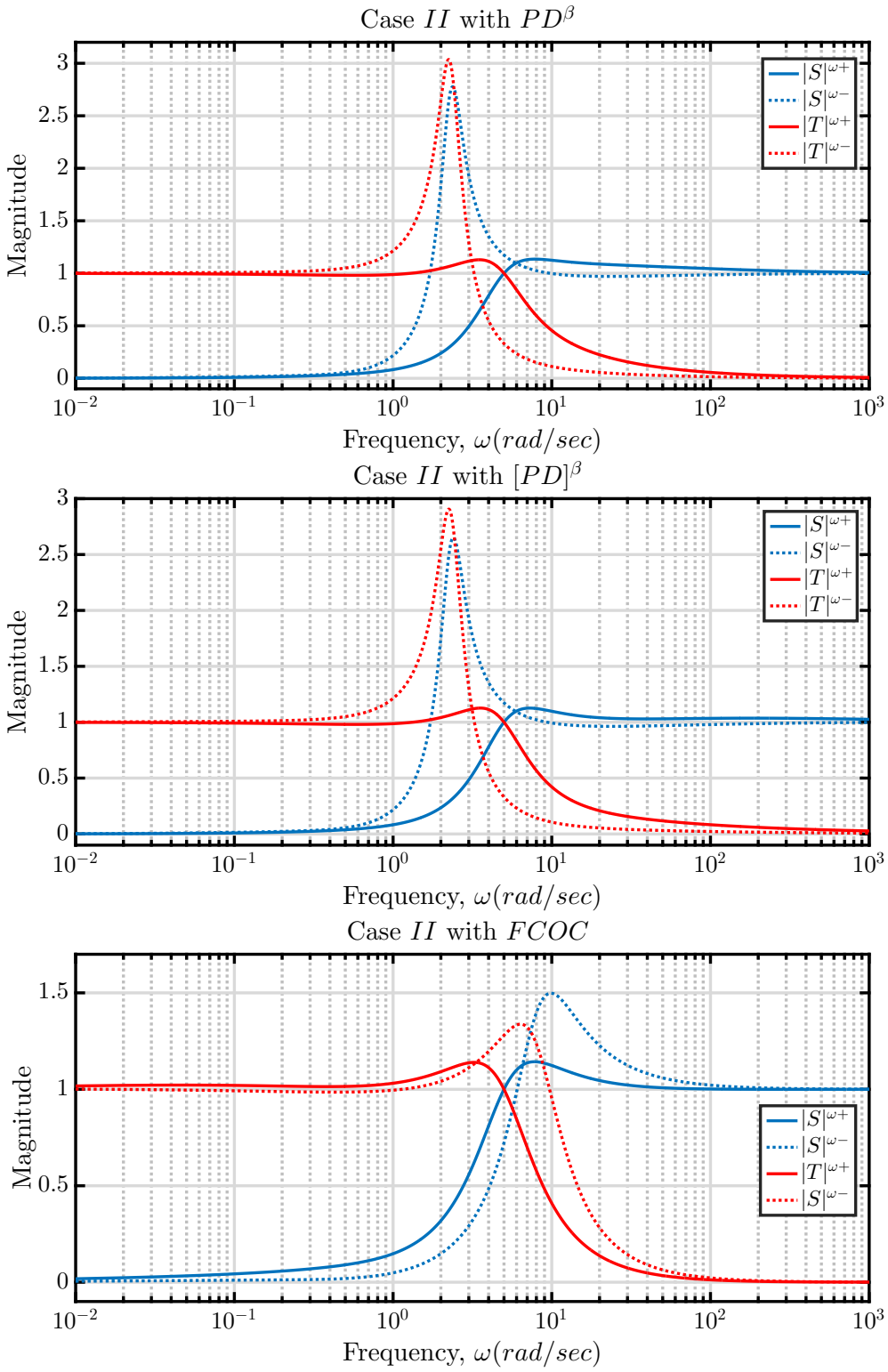

Figure 3.9: $|S(j\omega)|$ and $|T(j\omega)|$ plots of case II in ω^{+} and ω^{-} frequencies

Table 3.3: Observations from $|S(j\omega)|$ and $|T(j\omega)|$ plots

Case	Controller	Observations from positive frequency (ω^+) analysis	Observations from negative frequency (ω^-) analysis
I	PI^α	$M_S = 1.1951; M_T = 1.1816;$ $GM \geq 15.7425dB; PM \geq 49.4636^\circ$ $\omega_{BW} = 0.7135\, rad/sec$	$M_S = 1.9461; M_T = 1.9214;$ $GM \geq 6.2644dB; PM \geq 29.7748^\circ$ $\omega_{BW} = 0.6933\, rad/sec$
	$[PI]^\alpha$	$M_S = 1.1957; M_T = 1.1919;$ $GM \geq 15.7214dB; PM \geq 49.4385^\circ$ $\omega_{BW} = 0.7471\, rad/sec$	$M_S = 1.9461; M_T = 1.9274;$ $GM \geq 6.2646dB; PM \geq 29.7753^\circ$ $\omega_{BW} = 0.7113\, rad/sec$
	$FCOC$	$M_S = 1.2384; M_T = 1.2259;$ $GM \geq 14.3103dB; PM \geq 47.6241^\circ$ $\omega_{BW} = 0.7841\, rad/sec$	$M_S = 28.6365; M_T = 28.4114;$ $GM \geq 0.3087dB; PM \geq 2.0009^\circ$ $\omega_{BW} = 1.5115\, rad/sec$
II	PD^β	$M_S = 1.1349; M_T = 1.1290;$ $GM \geq 18.4962dB; PM \geq 52.2778^\circ$ $\omega_{BW} = 6.9699\, rad/sec$	$M_S = 2.7770; M_T = 3.0362;$ $GM \geq 3.8778dB; PM \geq 20.7453^\circ$ $\omega_{BW} = 3.6345\, rad/sec$
	$[PD]^\beta$	$M_S = 1.1261; M_T = 1.1264;$ $GM \geq 19.0147dB; PM \geq 52.7180^\circ$ $\omega_{BW} = 6.8180\, rad/sec$	$M_S = 2.6514; M_T = 2.9064;$ $GM \geq 4.1124dB; PM \geq 21.7394^\circ$ $\omega_{BW} = 3.6536\, rad/sec$
	$FCOC$	$M_S = 1.1429; M_T = 1.1396;$ $GM \geq 18.0594dB; PM \geq 51.8868^\circ$ $\omega_{BW} = 6.9390\, rad/sec$	$M_S = 1.4982; M_T = 1.3377;$ $GM \geq 9.5637dB; PM \geq 38.9921^\circ$ $\omega_{BW} = 11.9852\, rad/sec$

hence the selection of the controller is based on the computation of M_S and M_T in ω^+ and ω^- analysis.

3.6 Summary

In this chapter, a modification is suggested in the existing generalized plant structure by introducing complex coefficients and complex order derivatives. A unified expressions are derived for PI^α, $[PI]^\alpha$, PD^β, $[PD]^\beta$ and $K_c\left(\frac{s}{\omega_{gc}}\right)^{\alpha+j\beta}$ controller parameters for the proposed plant structure to meet the given specifications. Simulations are carried out for two different plants to validate the obtained unified expressions. Although, the work in this chapter focuses only on Wang et al specifications for developing the unified tuning expressions, one may also select any other set of three specifications and adopt the similar approach to obtain corresponding unified expressions.

Chapter 4

Complex Valued Controllers for Complex Valued Plants

4.1 Introduction

In the previous chapter, unified controller tuning expressions are obtained to meet Wang et al specifications for the complex valued universal plant structure. These controllers are tuned by considering only the positive frequency (ω^+) information of the plant. Performing the tuning of controllers by considering ω^+ information is applicable only for Integer Order (IO)/Fractional Order (FO) plants containing real coefficients which have an even symmetrical magnitude and odd symmetrical phase behaviour in frequency response. The frequency response for (i) IO/FO plants containing complex coefficients and (ii) fractional complex order plants containing real/complex coefficients have unsymmetrical magnitude and phase behaviour. Tuning of controllers for such plants by considering its ω^+ response alone, produces reduced stability margins and in turn deteriorates its time response. Hence, tuning of controllers for such plants require both ω^+ and negative frequency (ω^-)information to have better system response and improved stability margins, which in turn demands complex coefficient controllers. To address this problem, Complex Coefficient Integer Order Controllers (CCIOCs) such as CCPI/CCPD/CCPID controllers and Complex Coefficient Fractional Complex Order Controllers (CCFCOCs) are proposed in this chapter to meet Wang et al specifications both in ω^+ andω^- responses of the universal plant structure.

The closed loop schematic of universal plant structure with required Wang et al specifications both in ω^+ and ω^- are specified in section 4.2. The description of the proposed universal plant structure in ω^+ and ω^- is presented in section 4.3. A unified tuning expressions of CCIOCs and real coefficient Integer Order Controllers (IOCs) are derived in

section 4.4 for the universal plant structure. An optimization problem is also proposed to tune CCFCOCs in section 4.5. Numerical simulations are performed for different case studies with the proposed CCIOCs and CCFCOCs in section 4.6.

4.2 Generalized Closed Loop Schematic Representation

The closed loop representation of the universal plant $G(s)$ with controller $C(s)$ is shown in Fig. 4.1.

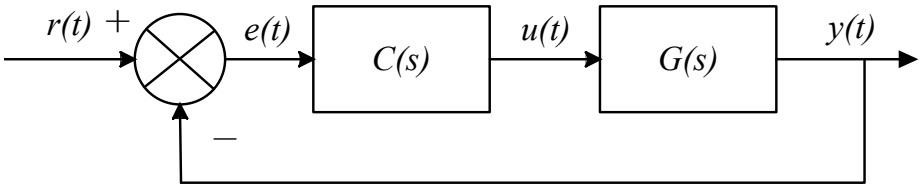

Figure 4.1: Closed loop representation of universal plant with controller

To obtain the controller expressions, the following Wang et al specifications are considered in both ω^+ and ω^-:

Positive frequency (ω^+):

(i) Gain cross over frequency (ω_{gc}):

$$|G^+_{\omega_{gc}}||C^+_{\omega_{gc}}| = 1 \tag{4.1}$$

(ii) Phase margin (ϕ_m):

$$\angle G^+_{\omega_{gc}} + \angle C^+_{\omega_{gc}} + \pi = \phi_m \tag{4.2}$$

(iii) Phase flatness (Isodamping) at ω_{gc}:

$$\begin{aligned} \left.\frac{d\angle[G_{\omega^+}C_{\omega^+}]}{d\omega}\right|_{\omega=\omega_{gc}} &= 0 \\ \left.\frac{d\angle G_{\omega^+}}{d\omega}\right|_{\omega=\omega_{gc}} + \left.\frac{d\angle C_{\omega^+}}{d\omega}\right|_{\omega=\omega_{gc}} &= 0 \\ \psi^+_{\omega_{gc}} + \left.\frac{d\angle C_{\omega^+}}{d\omega}\right|_{\omega=\omega_{gc}} &= 0 \end{aligned} \tag{4.3}$$

Negative frequency (ω^-)**:**

(i) Gain cross over frequency (ω_{gc}):

$$|G^-_{\omega_{gc}}||C^-_{\omega_{gc}}| = 1 \tag{4.4}$$

(ii) Phase margin (ϕ_m):

$$\angle G^-_{\omega_{gc}} + \angle C^-_{\omega_{gc}} - \pi = -\phi_m \tag{4.5}$$

(iii) Phase flatness (Isodamping) at ω_{gc}:

$$\begin{aligned} \left.\frac{d\angle[G_{\omega^-}C_{\omega^-}]}{d\omega}\right|_{\omega=\omega_{gc}} &= 0 \\ \psi^-_{\omega_{gc}} + \left.\frac{d\angle C_{\omega^-}}{d\omega}\right|_{\omega=\omega_{gc}} &= 0 \end{aligned} \tag{4.6}$$

$[|G^+_{\omega_{gc}}|,\ \angle G^+_{\omega_{gc}}$ and $\psi^+_{\omega_{gc}}]$ and $[|G^-_{\omega_{gc}}|,\ \angle G^-_{\omega_{gc}}$ and $\psi^-_{\omega_{gc}}]$ are the magnitude, phase and slope of the phase at ω_{gc} in ω^+ and ω^- response of the universal plant $G(s)$ proposed in section 4.3 respectively. $\left[|C^+_{\omega_{gc}}|, \angle C^+_{\omega_{gc}} \text{ and } \left.\frac{d\angle C_{\omega^+}}{d\omega}\right|_{\omega=\omega_{gc}}\right]$ and $\left[|C^-_{\omega_{gc}}|, \angle C^-_{\omega_{gc}} \text{ and } \left.\frac{d\angle C_{\omega^-}}{d\omega}\right|_{\omega=\omega_{gc}}\right]$ are the magnitude, phase and slope of the phase at ω_{gc} in ω^+ and ω^- responses of the controller $C(s)$ respectively.

4.3 Frequency Response of a Universal Plant

The structure of $G(s)$ as given in (3.4) is considered:

$$G(s) = K\frac{\sum_{i=0}^{m}(a_i + jb_i)s^{\alpha_i+j\beta_i}}{\sum_{k=0}^{n}(c_k + jd_k)s^{\gamma_k+j\delta_k}}e^{-Ls} \tag{4.7}$$

The ω^+ response function (G_{ω^+}) of (4.7) is given as:

$$G(s)\Big|_{s=j\omega} = K\frac{\sum_{i=0}^{m}(a_i+jb_i)(j\omega)^{\alpha_i+j\beta_i}}{\sum_{k=0}^{n}(c_k+jd_k)(j\omega)^{\gamma_k+j\delta_k}}e^{-jL\omega} \tag{4.8}$$

$$\begin{aligned} G_{\omega^+} &= K\frac{\sum_{i=0}^{m}(a_i+jb_i)(\omega)^{\alpha_i}e^{\frac{-\pi\beta_i}{2}}e^{j(\beta_i ln(\omega)+\frac{\pi\alpha_i}{2})}}{\sum_{k=0}^{n}(c_k+jd_k)(\omega)^{\gamma_k}e^{\frac{-\pi\delta_k}{2}}e^{j(\delta_k ln(\omega)+\frac{\pi\gamma_k}{2})}}e^{-jL\omega} \\ &= K\left[\frac{P_{\omega^+}+jQ_{\omega^+}}{R_{\omega^+}+jS_{\omega^+}}\right]e^{-jL\omega} \end{aligned} \tag{4.9}$$

where,

$$\begin{aligned} P_{\omega^+} &= \sum_{i=0}^{m}\omega^{\alpha_i}e^{\frac{-\pi\beta_i}{2}}\left[a_i\cos\left(\beta_i ln(\omega)+\frac{\pi\alpha_i}{2}\right)-b_i\sin\left(\beta_i ln(\omega)+\frac{\pi\alpha_i}{2}\right)\right] \\ Q_{\omega^+} &= \sum_{i=0}^{m}\omega^{\alpha_i}e^{\frac{-\pi\beta_i}{2}}\left[a_i\sin\left(\beta_i ln(\omega)+\frac{\pi\alpha_i}{2}\right)+b_i\cos\left(\beta_i ln(\omega)+\frac{\pi\alpha_i}{2}\right)\right] \\ R_{\omega^+} &= \sum_{k=0}^{n}\omega^{\gamma_k}e^{\frac{-\pi\delta_k}{2}}\left[c_k\cos\left(\delta_k ln(\omega)+\frac{\pi\gamma_k}{2}\right)-d_k\sin\left(\delta_k ln(\omega)+\frac{\pi\gamma_k}{2}\right)\right] \\ S_{\omega^+} &= \sum_{k=0}^{n}\omega^{\gamma_k}e^{\frac{-\pi\delta_k}{2}}\left[c_k\sin\left(\delta_k ln(\omega)+\frac{\pi\gamma_k}{2}\right)+d_k\cos\left(\delta_k ln(\omega)+\frac{\pi\gamma_k}{2}\right)\right] \end{aligned}$$

Therefore,

$$|G^+_{\omega_{gc}}| = K\left[\sqrt{\frac{P^2_{\omega^+}+Q^2_{\omega^+}}{R^2_{\omega^+}+S^2_{\omega^+}}}\right]\Big|_{\omega=\omega_{gc}} \tag{4.10}$$

$$\angle G^+_{\omega_{gc}} = \left[\tan^{-1}\left(\frac{Q_{\omega^+}}{P_{\omega^+}}\right)-\tan^{-1}\left(\frac{S_{\omega^+}}{R_{\omega^+}}\right)-L\omega\right]\Big|_{\omega=\omega_{gc}} \tag{4.11}$$

$$\psi^+_{\omega_{gc}} = \left[\left(\frac{P_{\omega^+}\frac{dQ_{\omega^+}}{d\omega}-Q_{\omega^+}\frac{dP_{\omega^+}}{d\omega}}{P^2_{\omega^+}+Q^2_{\omega^+}}\right)-\left(\frac{R_{\omega^+}\frac{dS_{\omega^+}}{d\omega}-S_{\omega^+}\frac{dR_{\omega^+}}{d\omega}}{R^2_{\omega^+}+S^2_{\omega^+}}\right)-L\right]\Big|_{\omega=\omega_{gc}} \tag{4.12}$$

where,

$$\begin{aligned} \frac{dP_{\omega^+}}{d\omega} = \sum_{i=0}^{m}\omega^{\alpha_i}e^{\frac{-\pi\beta_i}{2}}\Bigg[&\left(\frac{a_i\alpha_i-b_i\beta_i}{\omega}\right)\cos\Big(\beta_i ln(\omega)+\frac{\pi\alpha_i}{2}\Big) \\ &-\left(\frac{a_i\beta_i+b_i\alpha_i}{\omega}\right)\sin\Big(\beta_i ln(\omega)+\frac{\pi\alpha_i}{2}\Big)\Bigg] \end{aligned}$$

$$\frac{dQ_{\omega^+}}{d\omega} = \sum_{i=0}^{m} \omega^{\alpha_i} e^{\frac{-\pi\beta_i}{2}} \Bigg[\left(\frac{a_i\beta_i + b_i\alpha_i}{\omega} \right) \cos\Big(\beta_i ln(\omega) + \frac{\pi\alpha_i}{2} \Big) + \left(\frac{a_i\alpha_i - b_i\beta_i}{\omega} \right) \sin\Big(\beta_i ln(\omega) + \frac{\pi\alpha_i}{2} \Big) \Bigg]$$

$$\frac{dR_{\omega^+}}{d\omega} = \sum_{k=0}^{n} \omega^{\gamma_k} e^{\frac{-\pi\delta_k}{2}} \Bigg[\left(\frac{c_k\gamma_k - d_k\delta_k}{\omega} \right) \cos\Big(\delta_k ln(\omega) + \frac{\pi\gamma_k}{2} \Big) - \left(\frac{c_k\delta_k + d_k\gamma_k}{\omega} \right) \sin\Big(\delta_k ln(\omega) + \frac{\pi\gamma_k}{2} \Big) \Bigg]$$

$$\frac{dS_{\omega^+}}{d\omega} = \sum_{k=0}^{n} \omega^{\gamma_k} e^{\frac{-\pi\delta_k}{2}} \Bigg[\left(\frac{c_k\delta_k + d_k\gamma_k}{\omega} \right) \cos\Big(\delta_k ln(\omega) + \frac{\pi\gamma_k}{2} \Big) + \left(\frac{c_k\gamma_k - d_k\delta_k}{\omega} \right) \sin\Big(\delta_k ln(\omega) + \frac{\pi\gamma_k}{2} \Big) \Bigg]$$

Similarly, the ω^- response function (G_{ω^-}) of (4.7) is given as:

$$G(s)\Big|_{s=-j\omega} = K \frac{\sum_{i=0}^{m} (a_i + jb_i)(-j\omega)^{\alpha_i + j\beta_i}}{\sum_{k=0}^{n} (c_k + jd_k)(-j\omega)^{\gamma_k + j\delta_k}} e^{jL\omega} \tag{4.13}$$

$$G_{\omega^-} = K \left[\frac{P_{\omega^-} + jQ_{\omega^-}}{R_{\omega^-} + jS_{\omega^-}} \right] e^{jL\omega} \tag{4.14}$$

where,

$$P_{\omega^-} = \sum_{i=0}^{m} \omega^{\alpha_i} e^{\frac{\pi\beta_i}{2}} \left[a_i \cos\Big(\beta_i ln(\omega) - \frac{\pi\alpha_i}{2} \Big) - b_i \sin\Big(\beta_i ln(\omega) - \frac{\pi\alpha_i}{2} \Big) \right]$$

$$Q_{\omega^-} = \sum_{i=0}^{m} \omega^{\alpha_i} e^{\frac{\pi\beta_i}{2}} \left[a_i \sin\Big(\beta_i ln(\omega) - \frac{\pi\alpha_i}{2} \Big) + b_i \cos\Big(\beta_i ln(\omega) - \frac{\pi\alpha_i}{2} \Big) \right]$$

$$R_{\omega^-} = \sum_{k=0}^{n} \omega^{\gamma_k} e^{\frac{\pi\delta_k}{2}} \left[c_k \cos\Big(\delta_k ln(\omega) - \frac{\pi\gamma_k}{2} \Big) - d_k \sin\Big(\delta_k ln(\omega) - \frac{\pi\gamma_k}{2} \Big) \right]$$

$$S_{\omega^-} = \sum_{k=0}^{n} \omega^{\gamma_k} e^{\frac{\pi\delta_k}{2}} \left[c_k \sin\Big(\delta_k ln(\omega) - \frac{\pi\gamma_k}{2} \Big) + d_k \cos\Big(\delta_k ln(\omega) - \frac{\pi\gamma_k}{2} \Big) \right]$$

Therefore,

$$|G^{-}_{\omega_{gc}}| = K\left[\sqrt{\frac{P^2_{\omega^-}+Q^2_{\omega^-}}{R^2_{\omega^-}+S^2_{\omega^-}}}\right]\Bigg|_{\omega=\omega_{gc}} \tag{4.15}$$

$$\angle G^{-}_{\omega_{gc}} = \left[\tan^{-1}\left(\frac{Q_{\omega^-}}{P_{\omega^-}}\right) - \tan^{-1}\left(\frac{S_{\omega^-}}{R_{\omega^-}}\right) + L\omega\right]\Bigg|_{\omega=\omega_{gc}} \tag{4.16}$$

$$\psi^{-}_{\omega_{gc}} = \left[\left(\frac{P_{\omega^-}\frac{dQ_{\omega^-}}{d\omega} - Q_{\omega^-}\frac{dP_{\omega^-}}{d\omega}}{P^2_{\omega^-}+Q^2_{\omega^-}}\right) - \left(\frac{R_{\omega^-}\frac{dS_{\omega^-}}{d\omega} - S_{\omega^-}\frac{dR_{\omega^-}}{d\omega}}{R^2_{\omega^-}+S^2_{\omega^-}}\right) + L\right]\Bigg|_{\omega=\omega_{gc}} \tag{4.17}$$

where,

$$\frac{dP_{\omega^-}}{d\omega} = \sum_{i=0}^{m}\omega^{\alpha_i}e^{\frac{\pi\beta_i}{2}}\left[\left(\frac{a_i\alpha_i - b_i\beta_i}{\omega}\right)\cos\left(\beta_i ln(\omega) - \frac{\pi\alpha_i}{2}\right) - \left(\frac{a_i\beta_i + b_i\alpha_i}{\omega}\right)\sin\left(\beta_i ln(\omega) - \frac{\pi\alpha_i}{2}\right)\right]$$

$$\frac{dQ_{\omega^-}}{d\omega} = \sum_{i=0}^{m}\omega^{\alpha_i}e^{\frac{\pi\beta_i}{2}}\left[\left(\frac{a_i\beta_i + b_i\alpha_i}{\omega}\right)\cos\left(\beta_i ln(\omega) - \frac{\pi\alpha_i}{2}\right) + \left(\frac{a_i\alpha_i - b_i\beta_i}{\omega}\right)\sin\left(\beta_i ln(\omega) - \frac{\pi\alpha_i}{2}\right)\right]$$

$$\frac{dR_{\omega^-}}{d\omega} = \sum_{k=0}^{n}\omega^{\gamma_k}e^{\frac{\pi\delta_k}{2}}\left[\left(\frac{c_k\gamma_k - d_k\delta_k}{\omega}\right)\cos\left(\delta_k ln(\omega) - \frac{\pi\gamma_k}{2}\right) - \left(\frac{c_k\delta_k + d_k\gamma_k}{\omega}\right)\sin\left(\delta_k ln(\omega) - \frac{\pi\gamma_k}{2}\right)\right]$$

$$\frac{dS_{\omega^-}}{d\omega} = \sum_{k=0}^{n}\omega^{\gamma_k}e^{\frac{\pi\delta_k}{2}}\left[\left(\frac{c_k\delta_k + d_k\gamma_k}{\omega}\right)\cos\left(\delta_k ln(\omega) - \frac{\pi\gamma_k}{2}\right) + \left(\frac{c_k\gamma_k - d_k\delta_k}{\omega}\right)\sin\left(\delta_k ln(\omega) - \frac{\pi\gamma_k}{2}\right)\right]$$

Unified controller parameter expressions are obtained for $C(s)$ of the following real and complex coefficient IOCs to meet Wang et al specifications [86], [81], [85], [91] in both ω^+ and ω^-.

- Real coefficient integer order $PI/PD/PID$ controllers
- Complex coefficient integer order $PI/PD/PID$ controllers

4.4 Tuning of Complex and Real Coefficient $IOCs$

4.4.1 Unified Tuning Expressions for Complex Coefficient $IOCs$

In this subsection, unified complex valued integer order $PI/PD/PID$ controller parameter expressions are obtained for the given $G(s)$ to meet the required specifications (4.1), (4.2) and (4.3) in ω^+ and also (4.4), (4.5) and (4.6) in ω^-.

4.4.1.1 Tuning Expressions for Complex Coefficient PI (CCPI)

The $CCPI$ controller structure given in (2.58) is:

$$C(s) = (K_{pr} + jK_{pi}) + \frac{(K_{ir} + jK_{ii})}{s} \tag{4.18}$$

The ω^+ and ω^- responses (C_{ω^+} and C_{ω^-}) are given by

$$C_{\omega^+} = (K_{pr} + jK_{pi}) + \frac{(K_{ir} + jK_{ii})}{j\omega} \tag{4.19}$$

$$C_{\omega^-} = (K_{pr} + jK_{pi}) + \frac{(K_{ir} + jK_{ii})}{-j\omega} \tag{4.20}$$

The magnitude and phase of C_{ω^+} and C_{ω^-} at desired ω_{gc} are as follows:

$$|C^+_{\omega_{gc}}| = \sqrt{\left(K_{pr} + \frac{K_{ii}}{\omega_{gc}}\right)^2 + \left(K_{pi} - \frac{K_{ir}}{\omega_{gc}}\right)^2} \tag{4.21}$$

$$\angle C^+_{\omega_{gc}} = \tan^{-1}\left(\frac{K_{pi} - \frac{K_{ir}}{\omega_{gc}}}{K_{pr} + \frac{K_{ii}}{\omega_{gc}}}\right) \tag{4.22}$$

$$|C^-_{\omega_{gc}}| = \sqrt{\left(K_{pr} - \frac{K_{ii}}{\omega_{gc}}\right)^2 + \left(K_{pi} + \frac{K_{ir}}{\omega_{gc}}\right)^2} \tag{4.23}$$

$$\angle C^-_{\omega_{gc}} = \tan^{-1}\left(\frac{K_{pi} + \frac{K_{ir}}{\omega_{gc}}}{K_{pr} - \frac{K_{ii}}{\omega_{gc}}}\right) \tag{4.24}$$

Using (4.11) and (4.22), specification (4.2) becomes

$$\angle G^+_{\omega_{gc}} + \tan^{-1}\left(\frac{K_{pi} - \frac{K_{ir}}{\omega_{gc}}}{K_{pr} + \frac{K_{ii}}{\omega_{gc}}}\right) + \pi = \phi_m$$

this implies,

$$\left(\frac{K_{pi} - \frac{K_{ir}}{\omega_{gc}}}{K_{pr} + \frac{K_{ii}}{\omega_{gc}}}\right) = \tan A^+ \tag{4.25}$$

Using (4.16) and (4.24), specification (4.5) becomes

$$\angle G^{-}_{\omega_{gc}} + \tan^{-1}\left(\frac{K_{pi} + \frac{K_{ir}}{\omega_{gc}}}{K_{pr} - \frac{K_{ii}}{\omega_{gc}}}\right) - \pi = -\phi_m$$

this implies,

$$\left(\frac{K_{pi} + \frac{K_{ir}}{\omega_{gc}}}{K_{pr} - \frac{K_{ii}}{\omega_{gc}}}\right) = \tan A^{-} \tag{4.26}$$

Using (4.10) and (4.21), specification (4.1) becomes

$$|G^{+}_{\omega_{gc}}|\sqrt{\left(K_{pr} + \frac{K_{ii}}{\omega_{gc}}\right)^2 + \left(K_{pi} - \frac{K_{ir}}{\omega_{gc}}\right)^2} = 1$$

this implies,

$$K_{pr} + \frac{K_{ii}}{\omega_{gc}} = \frac{1}{|G^{+}_{\omega_{gc}}|\sqrt{1 + \tan^2 A^{+}}} = M^{+} \tag{4.27}$$

Using (4.15) and (4.23), specification (4.4) becomes

$$|G^{-}_{\omega_{gc}}|\sqrt{\left(K_{pr} - \frac{K_{ii}}{\omega_{gc}}\right)^2 + \left(K_{pi} + \frac{K_{ir}}{\omega_{gc}}\right)^2} = 1$$

this implies,

$$K_{pr} - \frac{K_{ii}}{\omega_{gc}} = \frac{1}{|G^{-}_{\omega_{gc}}|\sqrt{1 + \tan^2 A^{-}}} = M^{-} \tag{4.28}$$

Solving (4.27) and (4.28),

$$K_{pr} = \frac{M^{+} + M^{-}}{2} \tag{4.29}$$

$$K_{ii} = \frac{\omega_{gc}(M^{+} - M^{-})}{2} \tag{4.30}$$

Substituting (4.29) and (4.30) in (4.25) and (4.26), implies

$$K_{pi} = \frac{M^{+}\tan A^{+} + M^{-}\tan A^{-}}{2} \tag{4.31}$$

$$K_{ir} = \frac{\omega_{gc}(M^{-}\tan A^{-} - M^{+}\tan A^{+})}{2} \tag{4.32}$$

where,

$$A^+ = \phi_m - \pi - \angle G^+_{\omega_{gc}}$$
$$A^- = -\phi_m + \pi - \angle G^-_{\omega_{gc}}$$

Equations (4.29), (4.30), (4.31) and (4.32) are the controller parameters of $CCPI$ which satisfy the specifications (4.1) and (4.2) in ω^+ and also (4.4) and (4.5) in ω^-.

4.4.1.2 Tuning Expressions for Complex Coefficient PD (CCPD)

The $CCPD$ controller structure given in (2.59) is :

$$C(s) = (K_{pr} + jK_{pi}) + (K_{dr} + jK_{di})s \tag{4.33}$$

The ω^+ and ω^- responses (C_{ω^+} and C_{ω^-}) are given by

$$C_{\omega^+} = (K_{pr} + jK_{pi}) + (K_{dr} + jK_{di})(j\omega) \tag{4.34}$$
$$C_{\omega^-} = (K_{pr} + jK_{pi}) + (K_{dr} + jK_{di})(-j\omega) \tag{4.35}$$

The magnitude and phase of C_{ω^+} and C_{ω^-} at desired ω_{gc} are as follows:

$$|C^+_{\omega_{gc}}| = \sqrt{(K_{pr} - K_{di}\omega_{gc})^2 + (K_{pi} + K_{dr}\omega_{gc})^2} \tag{4.36}$$
$$\angle C^+_{\omega_{gc}} = \tan^{-1}\left(\frac{K_{pi} + K_{dr}\omega_{gc}}{K_{pr} - K_{di}\omega_{gc}}\right) \tag{4.37}$$
$$|C^-_{\omega_{gc}}| = \sqrt{(K_{pr} + K_{di}\omega_{gc})^2 + (K_{pi} - K_{dr}\omega_{gc})^2} \tag{4.38}$$
$$\angle C^-_{\omega_{gc}} = \tan^{-1}\left(\frac{K_{pi} - K_{dr}\omega_{gc}}{K_{pr} + K_{di}\omega_{gc}}\right) \tag{4.39}$$

Using (4.11) and (4.37), specification (4.2) becomes

$$\angle G^+_{\omega_{gc}} + \tan^{-1}\left(\frac{K_{pi} + K_{dr}\omega_{gc}}{K_{pr} - K_{di}\omega_{gc}}\right) + \pi = \phi_m$$

this implies,

$$\left(\frac{K_{pi} + K_{dr}\omega_{gc}}{K_{pr} - K_{di}\omega_{gc}}\right) = \tan A^+ \tag{4.40}$$

Using (4.16) and (4.39), specification (4.5) becomes

$$\angle G^-_{\omega_{gc}} + \tan^{-1}\left(\frac{K_{pi} - K_{dr}\omega_{gc}}{K_{pr} + K_{di}\omega_{gc}}\right) - \pi = -\phi_m$$

this implies,

$$\left(\frac{K_{pi} - K_{dr}\omega_{gc}}{K_{pr} + K_{di}\omega_{gc}}\right) = \tan A^{-} \tag{4.41}$$

Using (4.10) and (4.36), specification (4.1) becomes

$$|G^{+}_{\omega_{gc}}|\sqrt{(K_{pr} - K_{di}\omega_{gc})^2 + (K_{pi} + K_{dr}\omega_{gc})^2} = 1$$

this implies,

$$K_{pr} - K_{di}\omega_{gc} = \frac{1}{|G^{+}_{\omega_{gc}}|\sqrt{1 + \tan^2 A^{+}}} = M^{+} \tag{4.42}$$

Using (4.15) and (4.38), specification (4.4) becomes

$$|G^{-}_{\omega_{gc}}|\sqrt{(K_{pr} + K_{di}\omega_{gc})^2 + (K_{pi} - K_{dr}\omega_{gc})^2} = 1$$

this implies,

$$K_{pr} + K_{di}\omega_{gc} = \frac{1}{|G^{-}_{\omega_{gc}}|\sqrt{1 + \tan^2 A^{-}}} = M^{-} \tag{4.43}$$

Solving (4.42) and (4.43),

$$K_{pr} = \frac{M^{+} + M^{-}}{2} \tag{4.44}$$

$$K_{di} = \frac{M^{-} - M^{+}}{2\omega_{gc}} \tag{4.45}$$

Substituting (4.44) and (4.45) in (4.40) and (4.41),

$$K_{pi} = \frac{M^{+}\tan A^{+} + M^{-}\tan A^{-}}{2} \tag{4.46}$$

$$K_{dr} = \frac{M^{+}\tan A^{+} - M^{-}\tan A^{-}}{2\omega_{gc}} \tag{4.47}$$

Equations (4.44), (4.45), (4.46) and (4.47) are the controller parameters of $CCPD$ which satisfy the specifications (4.1) and (4.2) in ω^{+} and also (4.4) and (4.5) in ω^{-}.

4.4.1.3 Tuning Expressions for Complex Coefficient PID (CCPID)

The $CCPID$ controller structure given in (2.60) is:

$$C(s) = (K_{pr} + jK_{pi}) + \frac{(K_{ir} + jK_{ii})}{s} + (K_{dr} + jK_{di})s \tag{4.48}$$

The ω^+ and ω^- responses (C_{ω^+} and C_{ω^-}) are given by

$$C_{\omega^+} = (K_{pr} + jK_{pi}) + \frac{(K_{ir} + jK_{ii})}{j\omega} + (K_{dr} + jK_{di})(j\omega) \tag{4.49}$$

$$C_{\omega^-} = (K_{pr} + jK_{pi}) + \frac{(K_{ir} + jK_{ii})}{-j\omega} + (K_{dr} + jK_{di})(-j\omega) \tag{4.50}$$

The magnitude and phase of C_{ω^+} and C_{ω^-} at desired ω_{gc} are as follows:

$$|C^+_{\omega_{gc}}| = \left[\left(K_{pr} + \frac{K_{ii}}{\omega_{gc}} - K_{di}\omega_{gc} \right)^2 + \left(K_{pi} - \frac{K_{ir}}{\omega_{gc}} + K_{dr}\omega_{gc} \right)^2 \right]^{\frac{1}{2}} \tag{4.51}$$

$$\angle C^+_{\omega_{gc}} = \tan^{-1} \left(\frac{K_{pi} - \frac{K_{ir}}{\omega_{gc}} + K_{dr}\omega_{gc}}{K_{pr} + \frac{K_{ii}}{\omega_{gc}} - K_{di}\omega_{gc}} \right) \tag{4.52}$$

$$|C^-_{\omega_{gc}}| = \left[\left(K_{pr} - \frac{K_{ii}}{\omega_{gc}} + K_{di}\omega_{gc} \right)^2 + \left(K_{pi} + \frac{K_{ir}}{\omega_{gc}} - K_{dr}\omega_{gc} \right)^2 \right]^{\frac{1}{2}} \tag{4.53}$$

$$\angle C^-_{\omega_{gc}} = \tan^{-1} \left(\frac{K_{pi} + \frac{K_{ir}}{\omega_{gc}} - K_{dr}\omega_{gc}}{K_{pr} - \frac{K_{ii}}{\omega_{gc}} + K_{di}\omega_{gc}} \right) \tag{4.54}$$

Using (4.11) and (4.52), specification (4.2) becomes

$$\angle G^+_{\omega_{gc}} + \tan^{-1} \left(\frac{K_{pi} - \frac{K_{ir}}{\omega_{gc}} + K_{dr}\omega_{gc}}{K_{pr} + \frac{K_{ii}}{\omega_{gc}} - K_{di}\omega_{gc}} \right) + \pi = \phi_m$$

this implies,

$$\frac{K_{pi} - \frac{K_{ir}}{\omega_{gc}} + K_{dr}\omega_{gc}}{K_{pr} + \frac{K_{ii}}{\omega_{gc}} - K_{di}\omega_{gc}} = \tan A^+ \tag{4.55}$$

Using (4.16) and (4.54), specification (4.5) becomes

$$\angle G^-_{\omega_{gc}} + \tan^{-1} \left(\frac{K_{pi} + \frac{K_{ir}}{\omega_{gc}} - K_{dr}\omega_{gc}}{K_{pr} - \frac{K_{ii}}{\omega_{gc}} + K_{di}\omega_{gc}} \right) - \pi = -\phi_m$$

this implies,

$$\frac{K_{pi} + \frac{K_{ir}}{\omega_{gc}} - K_{dr}\omega_{gc}}{K_{pr} - \frac{K_{ii}}{\omega_{gc}} + K_{di}\omega_{gc}} = \tan A^- \tag{4.56}$$

Using (4.10) and (4.51), specification (4.1) becomes

$$|G^{+}_{\omega_{gc}}|\left[\left(K_{pr}+\frac{K_{ii}}{\omega_{gc}}-K_{di}\omega_{gc}\right)^2+\left(K_{pi}-\frac{K_{ir}}{\omega_{gc}}+K_{dr}\omega_{gc}\right)^2\right]^{\frac{1}{2}}=1$$

this implies,

$$K_{pr}+\frac{K_{ii}}{\omega_{gc}}-K_{di}\omega_{gc}=\frac{1}{|G^{+}_{\omega_{gc}}|\sqrt{1+\tan^2 A^{+}}}=M^{+} \tag{4.57}$$

Using (4.15) and (4.53), specification (4.4) becomes

$$|G^{-}_{\omega_{gc}}|\left[\left(K_{pr}-\frac{K_{ii}}{\omega_{gc}}+K_{di}\omega_{gc}\right)^2+\left(K_{pi}+\frac{K_{ir}}{\omega_{gc}}-K_{dr}\omega_{gc}\right)^2\right]^{\frac{1}{2}}=1$$

this implies,

$$K_{pr}-\frac{K_{ii}}{\omega_{gc}}+K_{di}\omega_{gc}=\frac{1}{|G^{-}_{\omega_{gc}}|\sqrt{1+\tan^2 A^{-}}}=M^{-} \tag{4.58}$$

From (4.57) and (4.58),

$$K_{pr}=\frac{M^{+}+M^{-}}{2} \tag{4.59}$$

$$\frac{K_{ii}}{\omega_{gc}}-K_{di}\omega_{gc}=\frac{M^{+}-M^{-}}{2} \tag{4.60}$$

Substituting (4.57) in (4.55) and (4.58) in (4.56),

$$K_{pi}-\frac{K_{ir}}{\omega_{gc}}+K_{dr}\omega_{gc}=M^{+}\tan A^{+} \tag{4.61}$$

$$K_{pi}+\frac{K_{ir}}{\omega_{gc}}-K_{dr}\omega_{gc}=M^{-}\tan A^{-} \tag{4.62}$$

From (4.61) and (4.62),

$$K_{pi}=\frac{M^{+}\tan A^{+}+M^{-}\tan A^{-}}{2} \tag{4.63}$$

$$\frac{K_{ir}}{\omega_{gc}}-K_{dr}\omega_{gc}=\frac{M^{-}\tan A^{-}-M^{+}\tan A^{+}}{2} \tag{4.64}$$

Then, the slope of $\angle C_{\omega^{+}}$ and $\angle C_{\omega^{-}}$ at desired ω_{gc} are obtained as:

$$\left.\frac{d\angle C_{\omega^{+}}}{d\omega}\right|_{\omega=\omega_{gc}}=\frac{\left(\frac{K_{ir}}{\omega_{gc}^2}+K_{dr}\right)-\tan A^{+}\left(-\frac{K_{ii}}{\omega_{gc}^2}-K_{di}\right)}{M^{+}(1+\tan^2 A^{+})} \tag{4.65}$$

$$\left.\frac{d\angle C_{\omega^{-}}}{d\omega}\right|_{\omega=\omega_{gc}}=\frac{\left(\frac{-K_{ir}}{\omega_{gc}^2}-K_{dr}\right)-\tan A^{-}\left(\frac{K_{ii}}{\omega_{gc}^2}+K_{di}\right)}{M^{-}(1+\tan^2 A^{-})} \tag{4.66}$$

Using (4.12) and (4.65), specification (4.3) becomes

$$\psi^{+}_{\omega_{gc}} + \frac{\left(\frac{K_{ir}}{\omega_{gc}} + K_{dr}\omega_{gc}\right) - \tan A^{+}\left(-\frac{K_{ii}}{\omega_{gc}} - K_{di}\omega_{gc}\right)}{\omega_{gc}M^{+}(1+\tan^2 A^{+})} = 0 \tag{4.67}$$

Eliminating K_{dr} and K_{di} in (4.67) using (4.60) and (4.64),

$$\frac{2K_{ir}}{\omega_{gc}} - \frac{M^{-}(\tan A^{-} - \tan A^{+})}{2} + \frac{2K_{ii}}{\omega_{gc}}\tan A^{+} = -\psi^{+}_{\omega_{gc}}\omega_{gc}M^{+}(1+\tan^2 A^{+}) \tag{4.68}$$

this implies,

$$K_{ir} + K_{ii}\tan A^{+} = H_1 \tag{4.69}$$

where,

$$H_1 = \frac{\omega_{gc}[-2\psi^{+}_{\omega_{gc}}\omega_{gc}M^{+}(1+\tan^2 A^{+}) + M^{-}(\tan A^{-} - \tan A^{+})]}{4}$$

Using (4.17) and (4.66), specification (4.6) becomes

$$\psi^{-}_{\omega_{gc}} + \frac{\left(\frac{-K_{ir}}{\omega_{gc}} - K_{dr}\omega_{gc}\right) - \tan A^{-}\left(\frac{K_{ii}}{\omega_{gc}} + K_{di}\omega_{gc}\right)}{\omega_{gc}M^{-}(1+\tan^2 A^{-})} = 0 \tag{4.70}$$

Eliminating K_{dr} and K_{di} in (4.70) using (4.60) and (4.64),

$$\frac{-2K_{ir}}{\omega_{gc}} + \frac{M^{+}(\tan A^{-} - \tan A^{+})}{2} - \frac{2K_{ii}}{\omega_{gc}}\tan A^{-} = -\psi^{-}_{\omega_{gc}}\omega_{gc}M^{-}(1+\tan^2 A^{-}) \tag{4.71}$$

this implies,

$$-K_{ir} - K_{ii}\tan A^{-} = H_2 \tag{4.72}$$

where,

$$H_2 = \frac{\omega_{gc}[-2\psi^{-}_{\omega_{gc}}\omega_{gc}M^{-}(1+\tan^2 A^{-}) + M^{+}(\tan A^{+} - \tan A^{-})]}{4}$$

Solving (4.69) and (4.72),

$$K_{ii} = \frac{H_1 + H_2}{\tan A^{+} - \tan A^{-}} \tag{4.73}$$

$$K_{ir} = \frac{-(H_1\tan A^{-} + H_2\tan A^{+})}{\tan A^{+} - \tan A^{-}} \tag{4.74}$$

Substituting (4.73) in (4.60) and (4.74) in (4.64), we get

$$K_{di} = \left(\frac{H_1 + H_2}{\omega_{gc}^2(\tan A^+ - \tan A^-)}\right) - \left(\frac{M^+ - M^-}{2\omega_{gc}}\right) \tag{4.75}$$

$$K_{dr} = \left(\frac{-H_1 \tan A^- - H_2 \tan A^+}{\omega_{gc}^2(\tan A^+ - \tan A^-)}\right) + \left(\frac{M^+ \tan A^+ - M^- \tan A^-}{2\omega_{gc}}\right) \tag{4.76}$$

Equations (4.59), (4.63), (4.73), (4.74), (4.75) and (4.76) are the controller parameters of $CCPID$ which satisfy the specifications (4.1), (4.2) and (4.3) in ω^+ and also satisfy (4.4), (4.5) and (4.6) in ω^-.

4.4.2 Unified Tuning Expressions for Real coefficient $IOCs$

The unified tuning expressions of the real coefficient IO $PI/PD/PID$ controllers for the universal plant $G(s)$ are obtained by considering only the ω^+ response of $G(s)$.

4.4.2.1 Tuning Expressions for PI Controller

Similar to the procedure adopted for $CCPI$ controller, the tuning expressions for PI controller are obtained by using the ω^+ response and are given below:

$$K_i = -K_p \omega_{gc} \tan\big(A^+\big) \tag{4.77}$$

$$K_p = \frac{1}{|G^+_{\omega_{gc}}|\sqrt{1 + \tan^2 A^+}} \tag{4.78}$$

where,

$$A^+ = \phi_m - \pi - \angle G^+_{\omega_{gc}}$$

Equations (4.77) and (4.78) are the controller parameters of PI which satisfy the specifications (4.1) and (4.2) in ω^+ only. The detailed derivation is given in APPENDIX B.1

4.4.2.2 Tuning Expressions for PD Controller

Similar to the procedure adopted for $CCPD$ controller, the tuning expressions for PD controller are obtained by using the ω^+ response and are given below:

$$K_d = \frac{K_1 \tan A^+}{\omega_{gc}} \tag{4.79}$$

$$K_p = \frac{1}{|G^+_{\omega_{gc}}|\sqrt{1+\tan^2 A^+}} \tag{4.80}$$

where,

$$A^+ = \phi_m - \pi - \angle G^+_{\omega_{gc}} \tag{4.81}$$

Equations (4.79) and (4.80) are the controller parameters of PD which satisfy the specifications (4.1) and (4.2) in ω^+ only. The detailed derivation is provided in APPENDIX B.2

4.4.2.3 Tuning Expressions for PID Controller

Similar to the procedure adopted for $CCPID$ controller, the tuning expressions for PID controller are obtained by using the ω^+ response and are given below:

$$K_p = \frac{1}{|G^+_{\omega_{gc}}|\sqrt{1+\tan^2 A^+}} \tag{4.82}$$

$$K_i = \frac{K_p\omega_{gc}}{2}\left(-\psi^+_{\omega_{gc}}\omega_{gc}(1+\tan^2 A^+) - \tan A^+\right) \tag{4.83}$$

$$K_d = \frac{K_p}{2\omega_{gc}}\left(\tan A^+ - \psi^+_{\omega_{gc}}\omega_{gc}(1+\tan^2 A^+)\right) \tag{4.84}$$

Substituting K_1 in (4.83) and (4.84), K_i and K_d are obtained respectively. Equations (4.82), (4.83) and (4.84) are the controller parameters of PID which satisfy the specifications (4.1), (4.2) and (4.3) in ω^+ only. The detailed derivation is provided in APPENDIX B.3

4.5 Tuning of Complex Coefficient $FCOCs$

Further to show the superiority of the fractional controllers, this work is extended to tune the proposed CCFCOCs defined in (2.61), (2.62) and (2.63) to meet the Wang et al specifications (4.1), (4.2) and (4.3) in ω^+ and (4.4), (4.5) and (4.6) in ω^-. Obtaining a unified expressions of CCFCOC parameters are tedious and hence, an optimization technique is used.

The following constrained optimization problem is proposed to tune the controller parameters by minimising the controller effort of the closed loop system shown in Fig. 4.1.

$$\underset{\text{(Controller Parameters)}}{\text{Minimize}} \quad J = \int_0^\infty |u(t)|^2 dt$$

subject to:

1. **Positive frequency (ω^+):**

   (i) Gain cross over frequency (ω_{gc}) :

   $$|G^+_{\omega_{gc}}||C^+_{\omega_{gc}}| = 1 \tag{4.85}$$

   (ii) Phase margin (ϕ_m) :

   $$\angle G^+_{\omega_{gc}} + \angle C^+_{\omega_{gc}} + \pi = \phi_m \tag{4.86}$$

   (iii) Phase flatness (Isodamping) at ω_{gc} :

   $$\left.\frac{d\angle[G_{\omega^+}C_{\omega^+}]}{d\omega}\right|_{\omega=\omega_{gc}} = 0 \tag{4.87}$$

2. **Negative frequency (ω^-):**

   (a) Gain cross over frequency (ω_{gc}) :

   $$|G^-_{\omega_{gc}}||C^-_{\omega_{gc}}| = 1 \tag{4.88}$$

   (b) Phase margin (ϕ_m) :

   $$\angle G^-_{\omega_{gc}} + \angle C^-_{\omega_{gc}} - \pi = -\phi_m \tag{4.89}$$

   (c) Phase flatness (Isodamping) at ω_{gc} :

   $$\left.\frac{d\angle[G_{\omega^-}C_{\omega^-}]}{d\omega}\right|_{\omega=\omega_{gc}} = 0 \tag{4.90}$$

4.6 Results and Discussions

In general, Complex Coefficient Transfer Functions (CCTF) are represented as two input two output system [118]. The illustration of realising the CCTF and its usage for simulating the case studies are discussed in the following section.

4.6.1 Case studies for CCIOCs

Three different case studies are selected to demonstrate the advantages of the proposed unified complex valued IOCs.

In order to represent the universal plant defined in (4.7), first its complex order derivatives has to be approximated using Oustaloup Recursive Algorithm (ORA) [45] to obtain its equivalent CCTF form. Then the obtained CCTF of plant is written as:

$$G(s) = G_r(s) + jG_i(s)$$

Similarly, the complex coefficient IOCs defined in (4.18), (4.33) and (4.48) are represented as:

$$C(s) = C_r(s) + jC_i(s)$$

$$\text{where, } C_r(s) = \frac{C(s) + C^*(s)}{2} \text{ and } C_i(s) = \frac{C(s) - C^*(s)}{2j}$$

Here, $C^*(s)$ is the conjugated form of $C(s)$. The action of complex coefficient IOCs on the error signal $e(t) = e_r(t) + je_i(t)$ giving $u(t) = u_r(t) + ju_i(t)$ and the action of CCTF on the signal $u(t) = u_r(t) + ju_i(t)$ giving $y(t) = y_r(t) + jy_i(t)$ are illustrated in the Fig. 4.2.

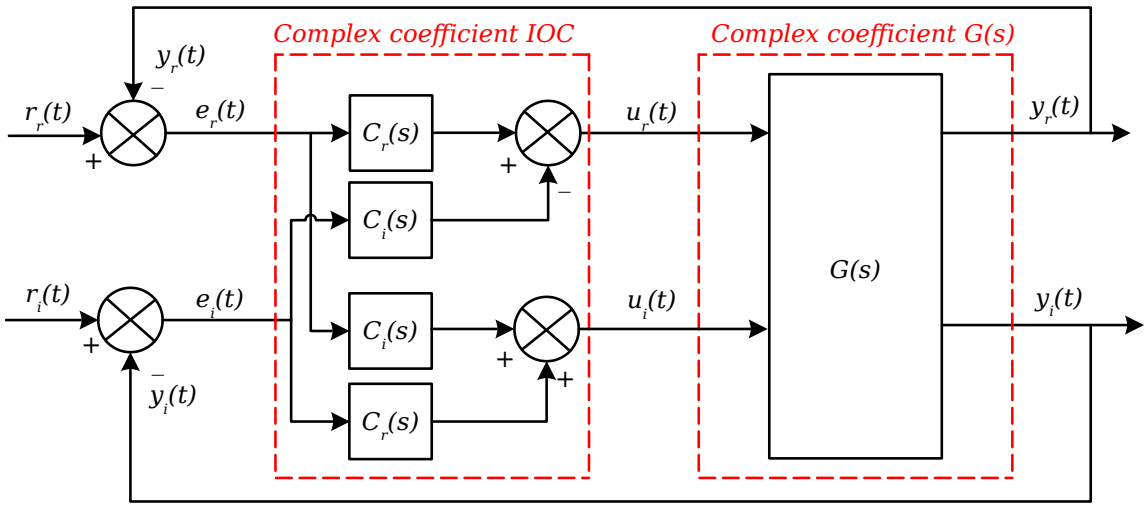

Figure 4.2: CCTF representation in closed loop

The plant and its required specifications are shown in Table 4.1; where, case I and case

II are chosen from Chapter 3.

Table 4.1: Plant and its specifications

Case	Plant and specifications
I	Plant: $\frac{e^{-0.3s}}{0.04s^{1.8+0.6j}+1.04s^{0.8+0.3j}+1}$ specifications: $\omega_{gc} = 0.5\, rad/sec, \phi_m = 57^\circ$
II	Plant: $\frac{3+4j}{(0.8+0.2j)s^{1.9+0.4j}+(0.5+0.3j)s^{0.8+0.2j}}$ specifications: $\omega_{gc} = 5\, rad/sec, \phi_m = 60^\circ$
III	Plant: $\frac{3+4j}{(0.8+0.2j)s^{1.1+0.2j}+(0.5+0.3j)}$ specifications: $\omega_{gc} = 5\, rad/sec, \phi_m = 60^\circ$

The derived real and complex valued IOC parameter expressions are used to obtain the controller parameters for these case studies and are listed in Table 4.2.

Fig. 4.3, Fig. 4.5 and Fig. 4.7 show the ω^+ and ω^- Bode magnitude responses of case I, case II and case III with the stable controllers in the Table 4.2 respectively. Fig. 4.3 and Fig. 4.7 also presents the zoomed responses near ω_{gc}. Fig. 4.4, Fig. 4.6 and Fig. 4.8 show the ω^+ and ω^- Bode phase responses of case I, case II and case III with the stable controllers in the Table 4.2 respectively.

It is clearly seen that magnitude and phase responses for plant with real valued IOCs satisfy the required specifications in ω^+ but not in ω^-. This is due to the unsymmetrical behaviour of the plant not getting compensated by the real valued IOCs having symmetrical behaviour. Hence, it necessitates to design a complex valued IOCs to satisfy the constraints simultaneously in both ω^+ and ω^-.

For simulation, unit step reference input $r(t) = r_r(t) + jr_i(t) = 1 + j0$ is applied to the closed loop shown in Fig. 4.2. To obtain the unit step response of the universal plant with obtained controllers, ORA is carried out for the approximation of the fractional order terms in the plant structure. Frequency band of $[0.001$ to $1,000]$ rad/s with order (N) 5 is selected for approximation. Even though the tuned controllers for each case study satisfy the required specifications, stability of the closed loop system is not guaranteed. Hence for further discussion, only stable controllers for different case studies are considered.

Sensitivity (S) and complementary sensitivity (T) functions [163] are used to study the stability and the robustness to parameter uncertainty of the case I, case II and case III. S

Table 4.2: Tuning results of real and complex valued IOCs

Plant parameters	Controller	Controller parameters	Controller effort ($J = \int_0^\infty \|u(t)\|^2 dt$)
Case:I $K = 1, L = 0.3, a_0 = 1,$ $b_0 = 0, c_0 = 0.04, d_0 = 0,$ $c_1 = 1.04, d_1 = 0, c_2 = 1,$ $d_2 = 0, \alpha_0 = 0, \beta_0 = 0,$ $\gamma_0 = 1.8, \delta_0 = 0.6, \gamma_1 = 0.8,$ $\delta_1 = 0.3, \gamma_2 = 0, \delta_2 = 0$	PI	$K_p = -0.1916; K_i = 0.6059$	22.026
	$CCPI$	$K_{pr} = 0.1146; K_{pi} = 0.0783$ $K_{ir} = 0.6450; K_{ii} = -0.1531$	21.412
	PD	$K_p = -0.1916; K_d = -2.4234$	does not exist
	$CCPD$	$K_{pr} = 0.1146; K_{pi} = 0.0783$ $K_{dr} = -2.580; K_{di} = 0.6124$	
	PID	$K_p = -0.1916; K_i = -0.4631;$ $K_d = -4.2757$	
	$CCPID$	$K_{pr} = 0.1146; K_{pi} = 0.0783$ $K_{ir} = 2.1217; K_{ii} = -0.4822$ $K_{dr} = 5.9067; K_{di} = -1.3164$	
Case:II $K = 1, L = 0, a_0 = 3,$ $b_0 = 4, c_0 = 0.8, d_0 = 0.2,$ $c_1 = 0.5, d_1 = 0.3, \alpha_0 = 0,$ $\beta_0 = 0, \gamma_0 = 1.9, \delta_0 = 0.4,$ $\gamma_1 = 0.8, \delta_1 = 0.2,$	PI	$K_p = 1.4249; K_i = -5.8325$	does not exist
	$CCPI$	$K_{pr} = 2.8899; K_{pi} = -1.8493$ $K_{ir} = -15.0791; K_{ii} = -7.3249$	
	PD	$K_p = 1.4249; K_d = 0.2333$	64.671
	$CCPD$	$K_{pr} = 2.8899; K_{pi} = -1.8493$ $K_{dr} = 0.6032; K_{di} = 0.2930$	524.575
	PID	$K_p = 1.4249; K_i = 0.5641;$ $K_d = 0.2559$	does not exist
	$CCPID$	$K_{pr} = 2.8899; K_{pi} = -1.8493$ $K_{ir} = -8.6711; K_{ii} = 1.9710$ $K_{dr} = 0.2563; K_{di} = 0.3718$	
Case:III $K = 1, L = 0, a_0 = 3,$ $b_0 = 4, c_0 = 0.8, d_0 = 0.2,$ $c_1 = 0.5, d_1 = 0.3, \alpha_0 = 0,$ $\beta_0 = 0, \gamma_0 = 1.1, \delta_0 = 0.2,$ $\gamma_1 = 0, \delta_1 = 0,$	PI	$K_p = 0.4365; K_i = 2.7086$	0.945
	$CCPI$	$K_{pr} = 0.8734; K_{pi} = -0.2091$ $K_{ir} = 1.6633; K_{ii} = -2.1842$	0.2725
	PD	$K_p = 0.4365; K_d = -0.1083$	23.868
	$CCPD$	$K_{pr} = 0.8734; K_{pi} = -0.2091$ $K_{dr} = -0.0665; K_{di} = 0.0874$	12.631
	PID	$K_p = 0.4365; K_i = 2.4214;$ $K_d = -0.0115$	1.011
	$CCPID$	$K_{pr} = 0.8734; K_{pi} = -0.2091$ $K_{ir} = 0.5896; K_{ii} = -2.1471$ $K_{dr} = -0.0429; K_{di} = 0.0015$	2.822

and T functions are given as :

$$S(j\omega) = \frac{1}{1 + G(j\omega)C(j\omega)}; T(j\omega) = \frac{G(j\omega)C(j\omega)}{1 + G(j\omega)C(j\omega)}$$

$$M_S = \max_{\omega} |S(j\omega)|; M_T = \max_{\omega} |T(j\omega)|$$
$$GM \geq \frac{M_S}{M_S - 1}; PM \geq 2\sin^{-1}\left(\frac{1}{2M_S}\right)$$

where, M_S and M_T are the maximum sensitivities of $|S(jw)|$ and $|T(jw)|$ plots respectively. M_S provides the maximum amplification factor of the load disturbances and

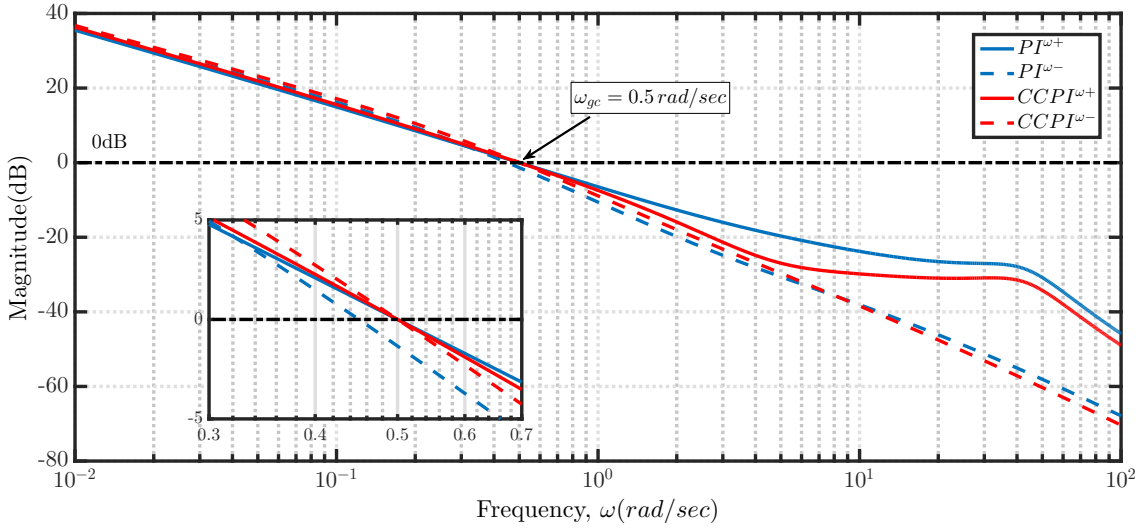

Figure 4.3: Open loop magnitude responses of case I with PI and $CCPI$ in ω^+ and ω^-

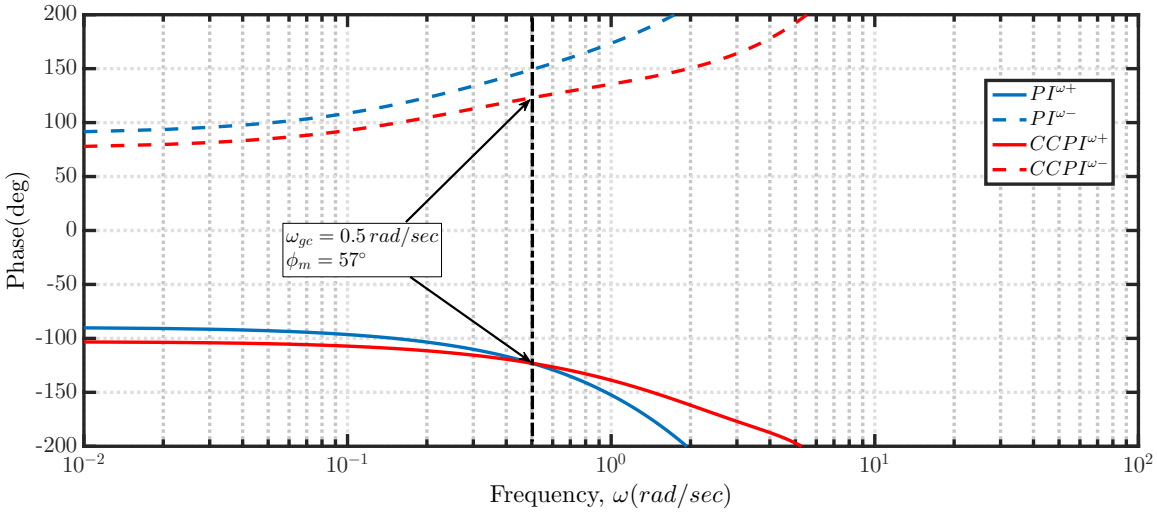

Figure 4.4: Open loop phase responses of case I with PI and $CCPI$ in ω^+ and ω^-

M_T describes the resonant peak. Assured Gain Margin (GM) and Phase Margin (PM) are computed from M_S which defines the stability margins [163]. For a good measure of robustness, M_S and M_T should lie in the range of 1.2 to 2.0 and 1 to 1.5 respectively.

$|S(j\omega)|$ and $|T(j\omega)|$ plots for real valued IOCs are shown in Fig. 4.9 for case I, Fig. 4.13 for case II, Fig. 4.17, Fig. 4.21 and Fig. 4.25 for case III. Similarly, $|S(j\omega)|$ and $|T(j\omega)|$ plots for complex valued IOCs are shown in Fig. 4.10 for case I, Fig. 4.14 for case II, Fig. 4.18, Fig. 4.22 and Fig. 4.26 for case III. M_S, M_T, Bandwidth (ω_{BW}) and guaranteed stability margins $(GM$ and $PM)$ are obtained from $|S(j\omega)|$ and $|T(j\omega)|$ plots

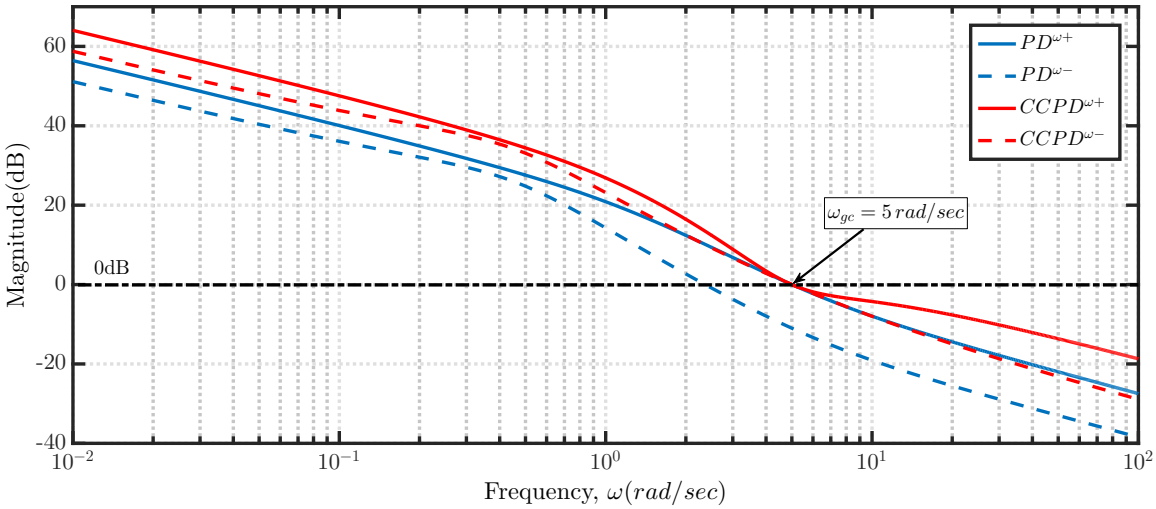

Figure 4.5: Open loop magnitude responses of case II with PD and $CCPD$ in ω^+ and ω^-

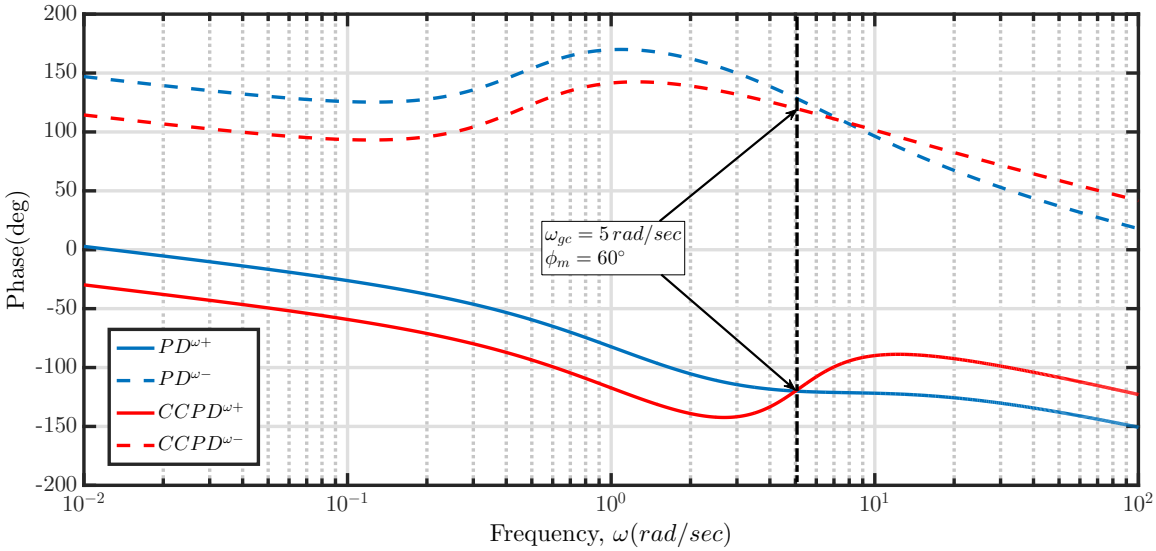

Figure 4.6: Open loop phase responses of case II with PD and $CCPD$ in ω^+ and ω^-

for plant with real and complex valued IOCs of all three cases. These values are computed for both ω^+ and ω^- and are listed in Table 4.3.

Since $G(s)$ is a complex valued function, both real and imaginary responses exist in time domain. The real part of the closed loop unit step responses are shown in Fig. 4.11 for case I, Fig. 4.15 for case II and Fig. 4.19, Fig. 4.23 and Fig. 4.27 for case III respectively.

The real part of the controller output responses are shown in Fig. 4.12 for case I, Fig.

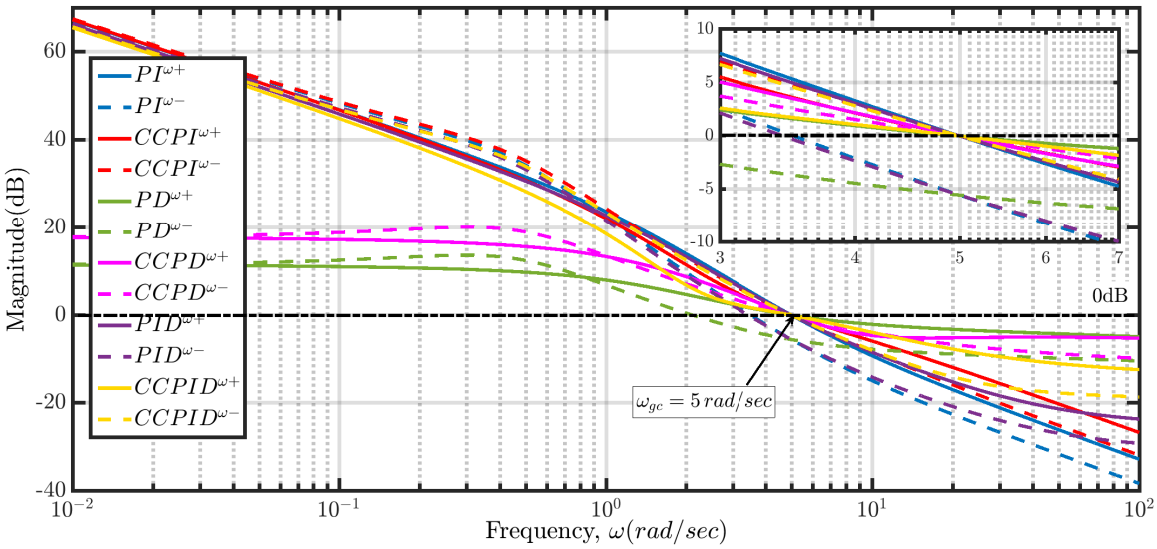

Figure 4.7: Open loop magnitude responses of case III with all controllers in ω^+ and ω^-

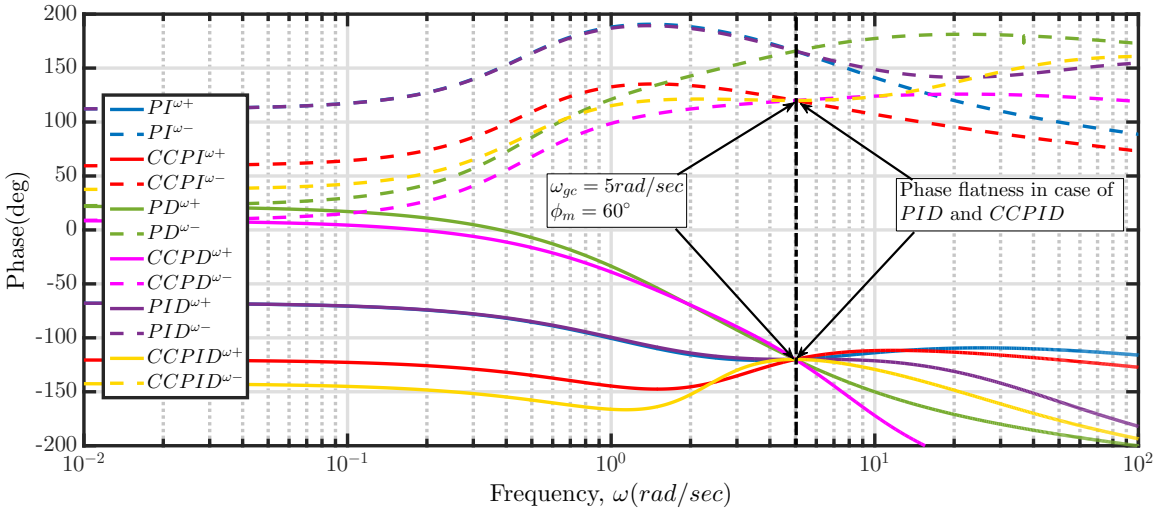

Figure 4.8: Open loop phase responses of case III with all controllers in ω^+ and ω^-

4.16 for case II and Fig. 4.20, Fig. 4.24 and Fig. 4.28 for case III respectively.

For case I, it is observed that both M_S and M_T obtained for $CCPI$ are lesser in comparison to PI from ω^+ and ω^- analysis. This assures increased GM and PM for $CCPI$ which is seen as a reduced overshoot in Fig. 4.11. It is also observed that $CCPI$ has larger ω_{BW} than PI which is reflected as lesser rise time in Fig. 4.11.

Similar trend is observed for $CCPD$ in comparison to PD of case II, $CCPI$ in comparison to PI of case III and $CCPID$ in comparison to PID of case III except $CCPD$ in comparison to PD of case III. In case III, $CCPD$ controller assures better stability

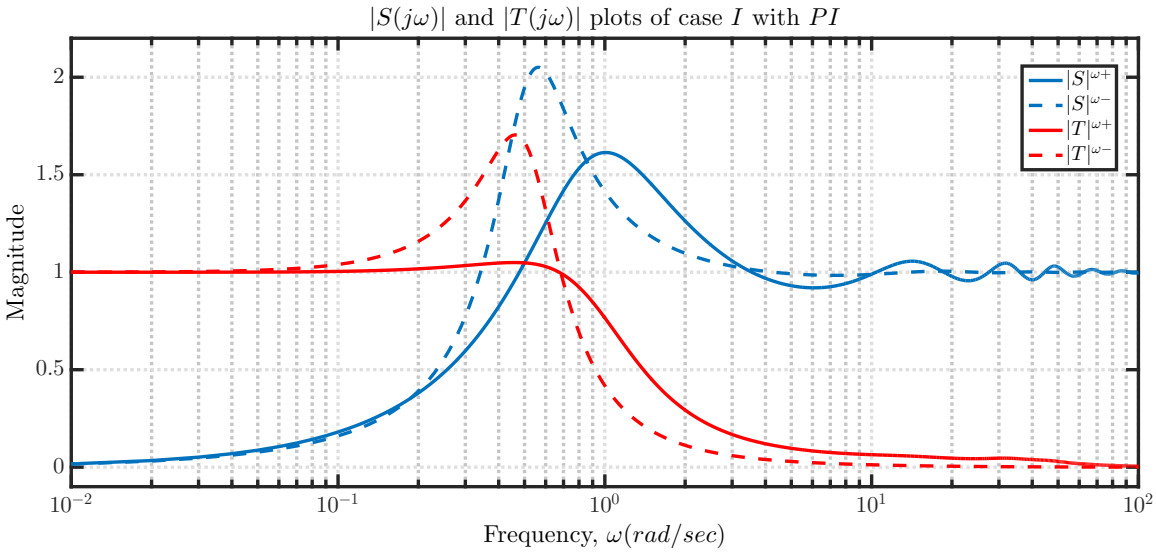

Figure 4.9: Sensitivity plots of case I with PI in ω^+ and ω^-

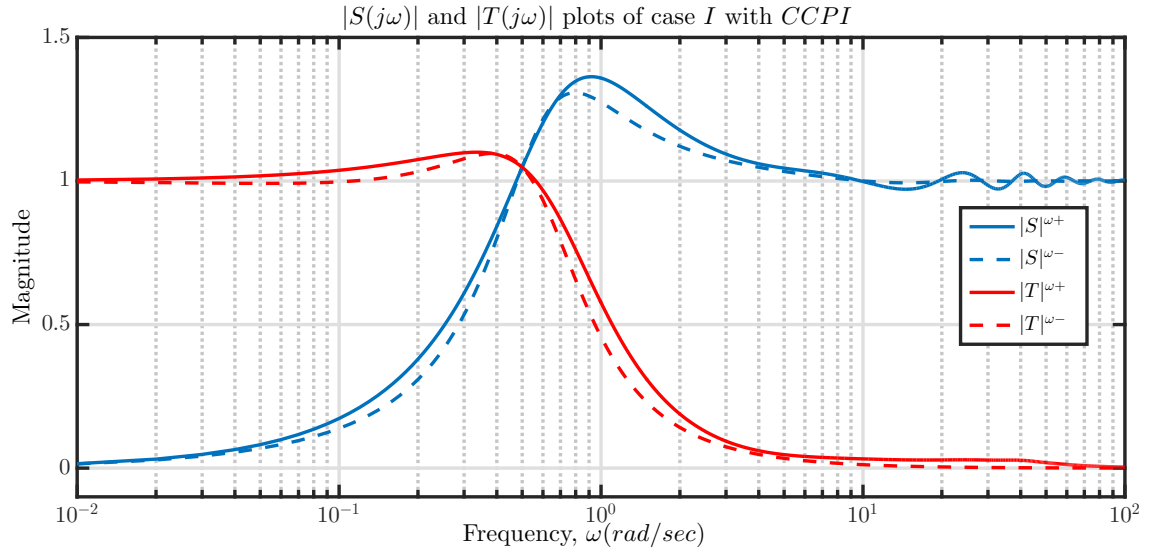

Figure 4.10: Sensitivity plots of case I with $CCPI$ in ω^+ and ω^-

margins and provides lesser bandwidth than PD. However, $CCPD$ and PD introduce error at steady state and hence, deteriorates the tracking performance.

Controller effort is computed for all cases with stable controllers as shown in Table 4.2. Since, tuning of real valued IOCs are performed by considering only ω^+ and whereas complex valued IOCs are tuned by considering both ω^+ and ω^-, the comparison of controller efforts for various controllers are not performed.

From the above analysis, it is observed that $CCPI$, $CCPD$ and $CCPID$ simultane-

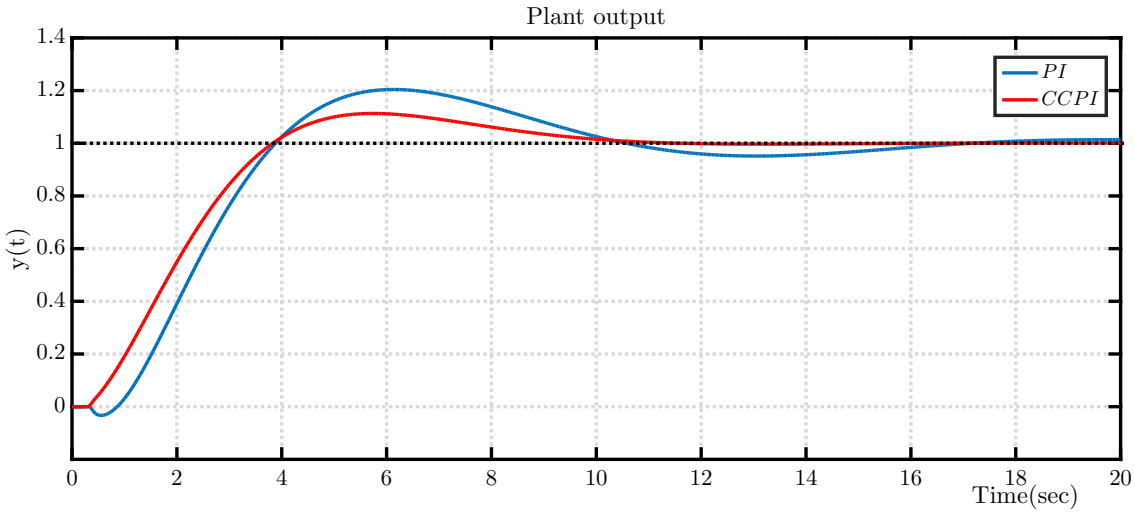

Figure 4.11: Plant output responses of case I with PI and $CCPI$

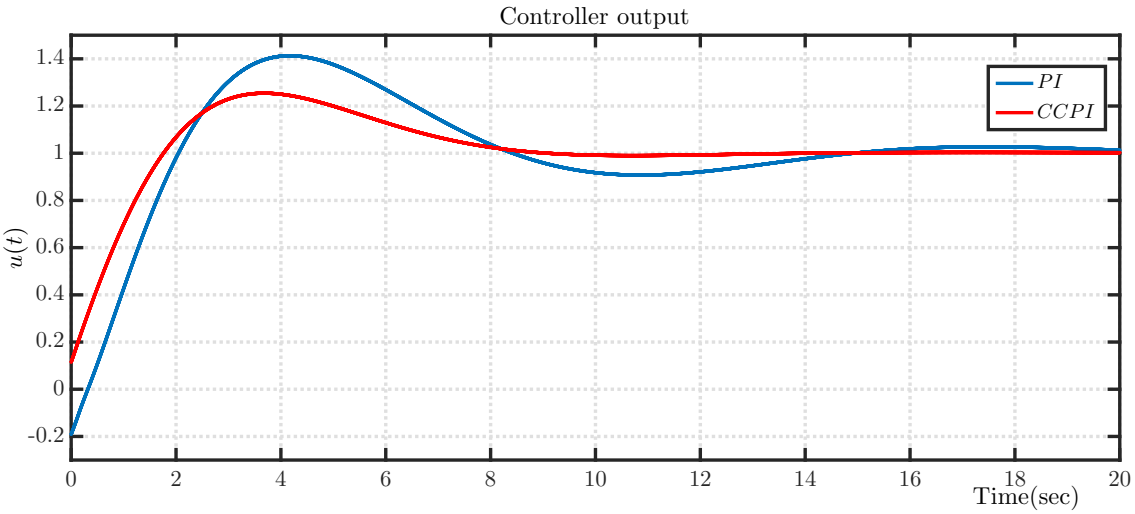

Figure 4.12: Controller output responses of case I with PI and $CCPI$

ously satisfy the required specifications in ω^+ and ω^-. It also provides improved stability margins and time response than real valued IOCs. Hence, only complex valued IOCs have to be selected for complex valued plants.

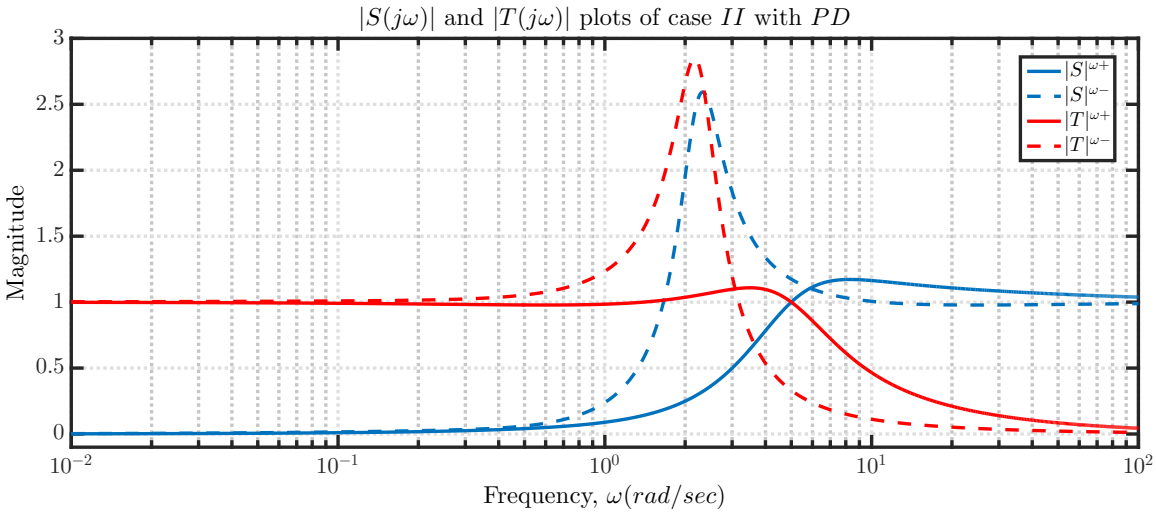

Figure 4.13: Sensitivity plots of case II with PD in ω^+ and ω^-

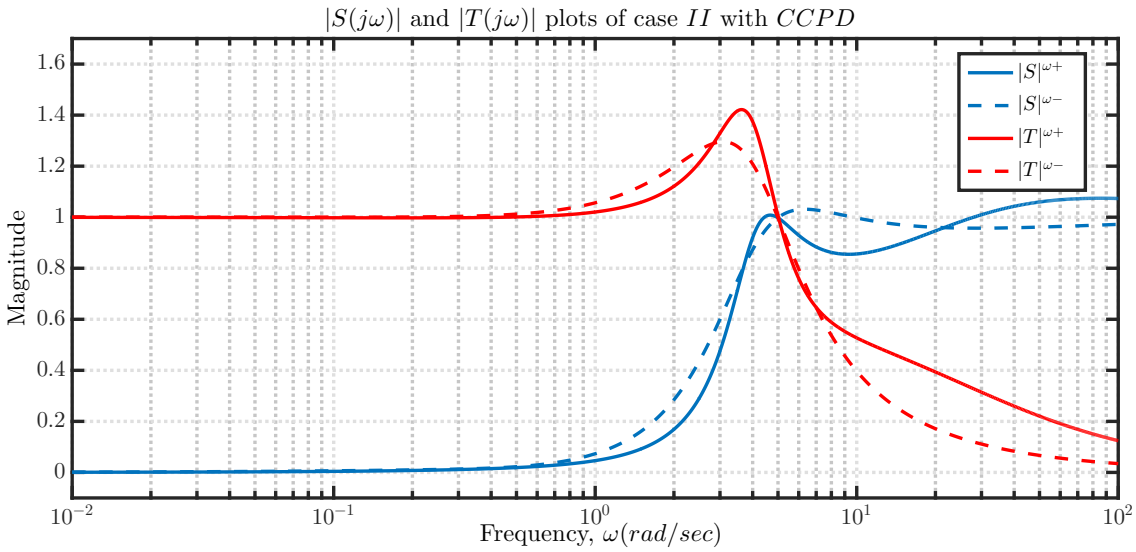

Figure 4.14: Sensitivity plots of case II with $CCPD$ in ω^+ and ω^-

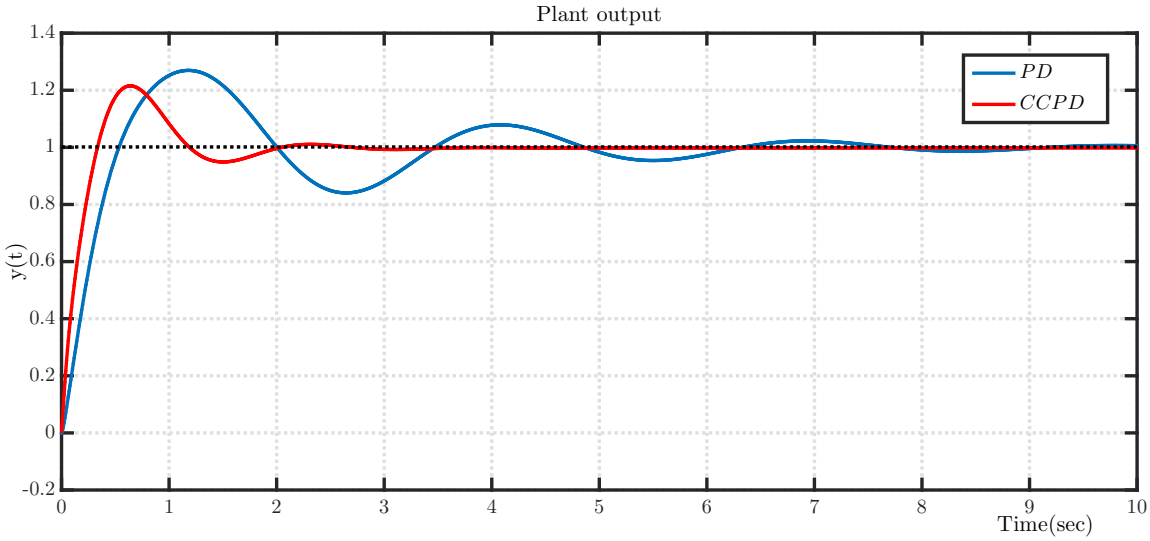

Figure 4.15: Plant output responses of case II with PD and $CCPD$

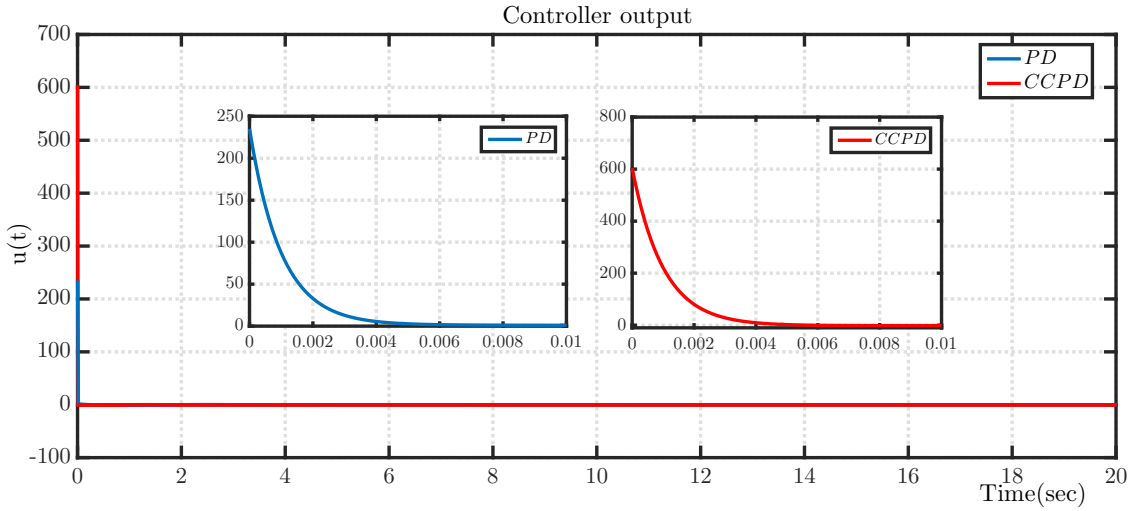

Figure 4.16: Controller output responses of case II with PD and $CCPD$

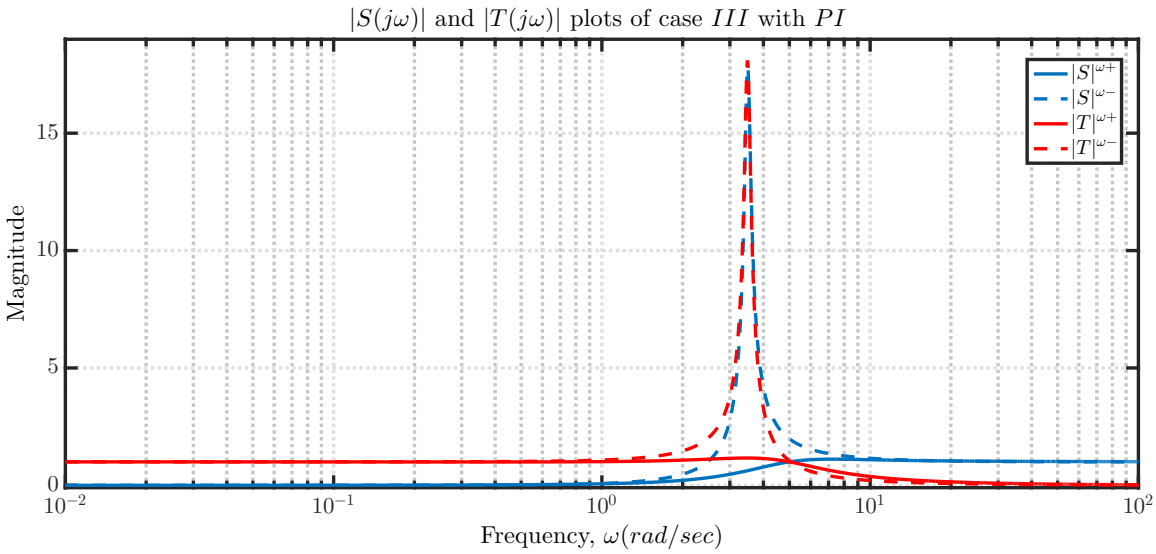

Figure 4.17: Sensitivity plots of case III with PI in ω^+ and ω^-

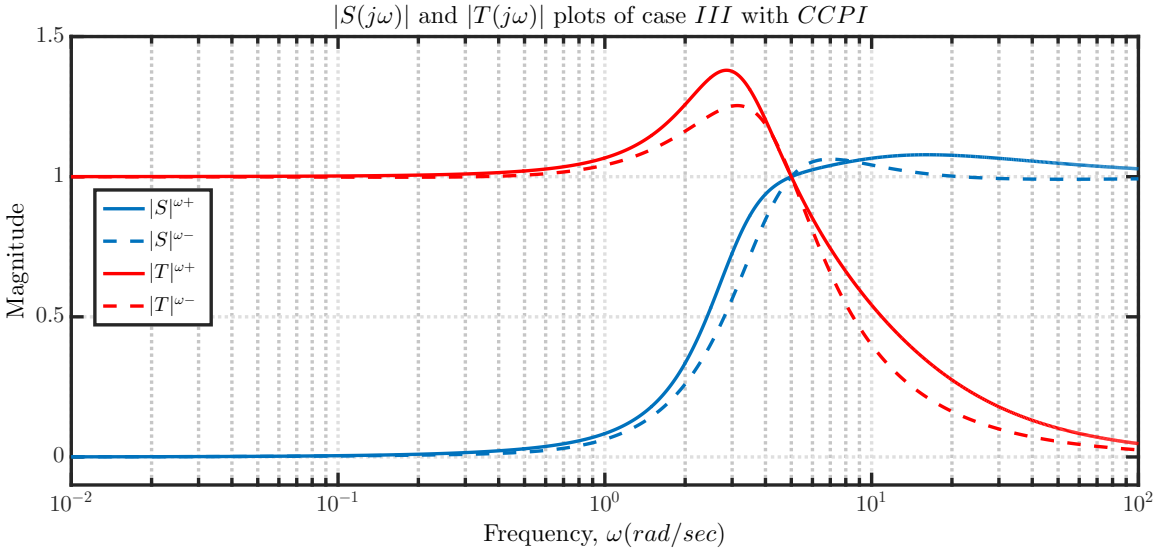

Figure 4.18: Sensitivity plots of case III with $CCPI$ in ω^+ and ω^-

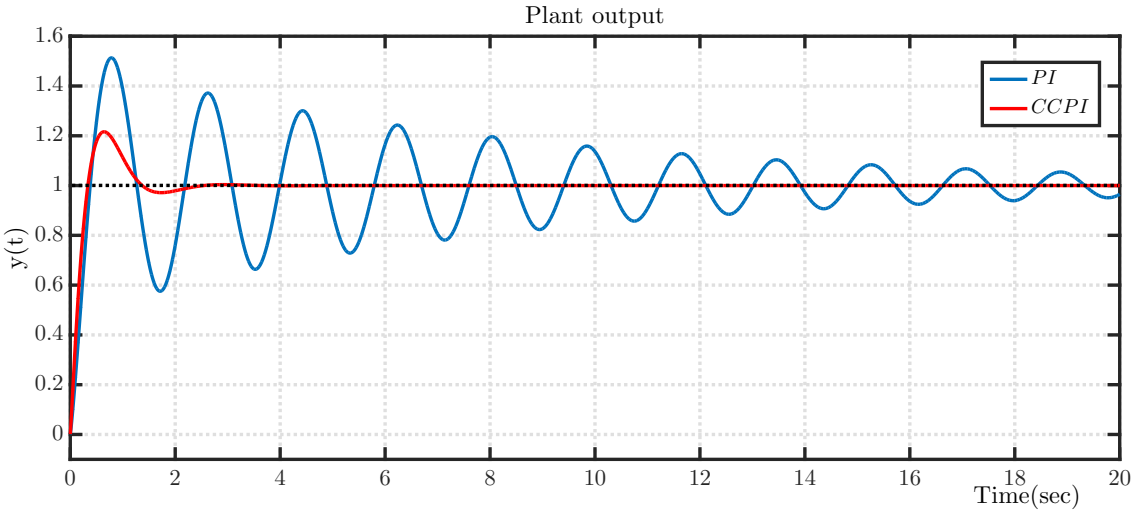

Figure 4.19: Plant output responses of case III with PI and $CCPI$

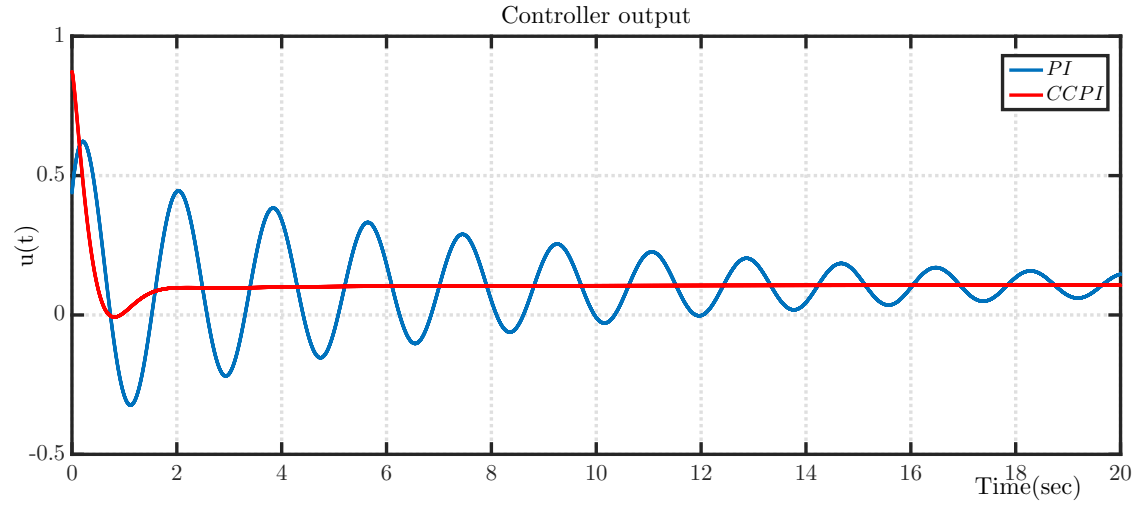

Figure 4.20: Controller output responses of case III with PI and $CCPI$

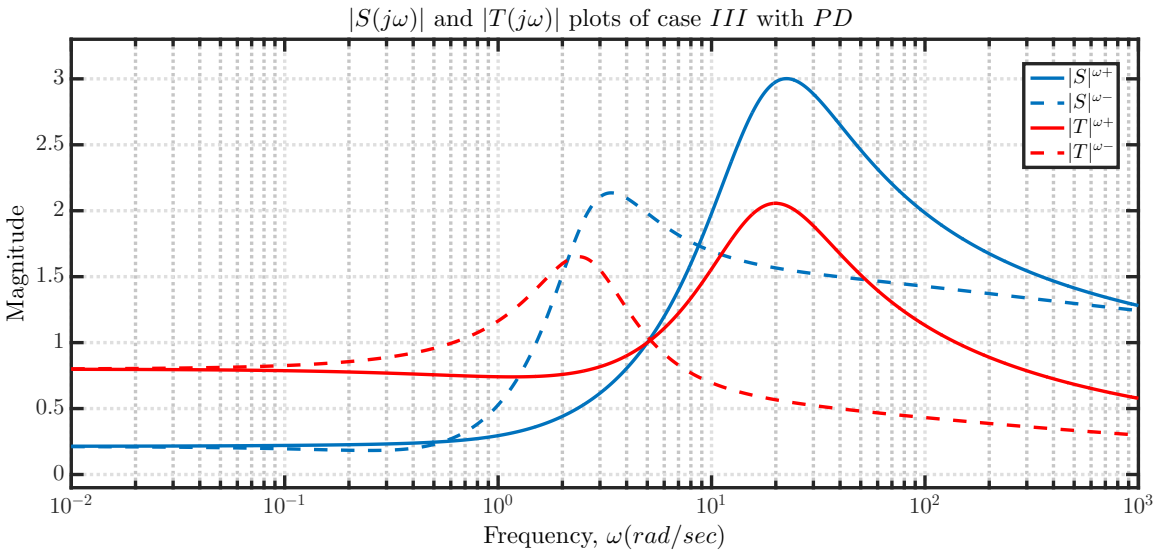

Figure 4.21: Sensitivity plots of case III with PD in ω^+ and ω^-

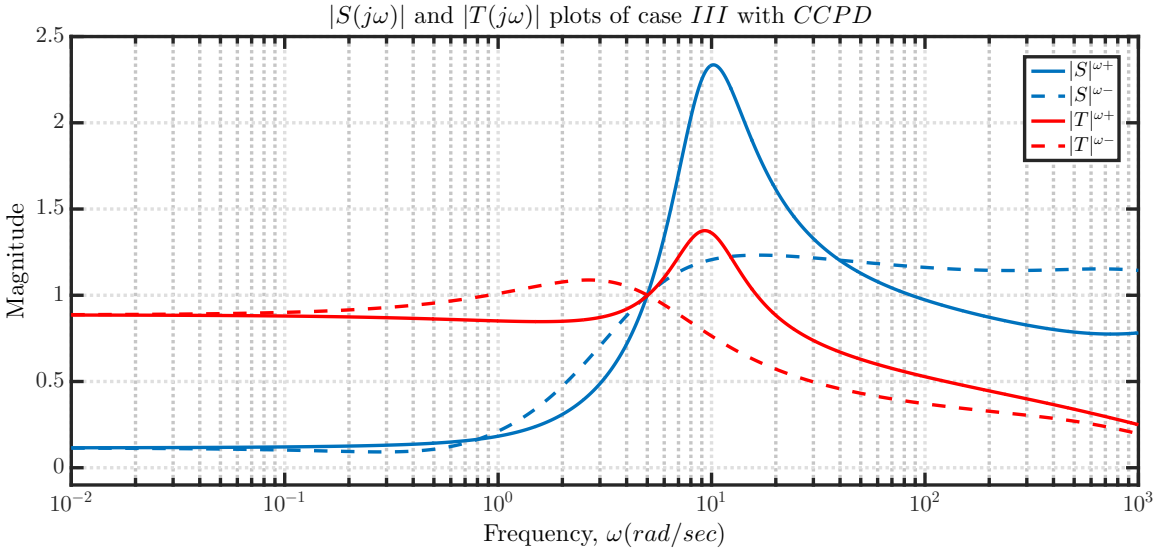

Figure 4.22: Sensitivity plots of case III with $CCPD$ in ω^+ and ω^-

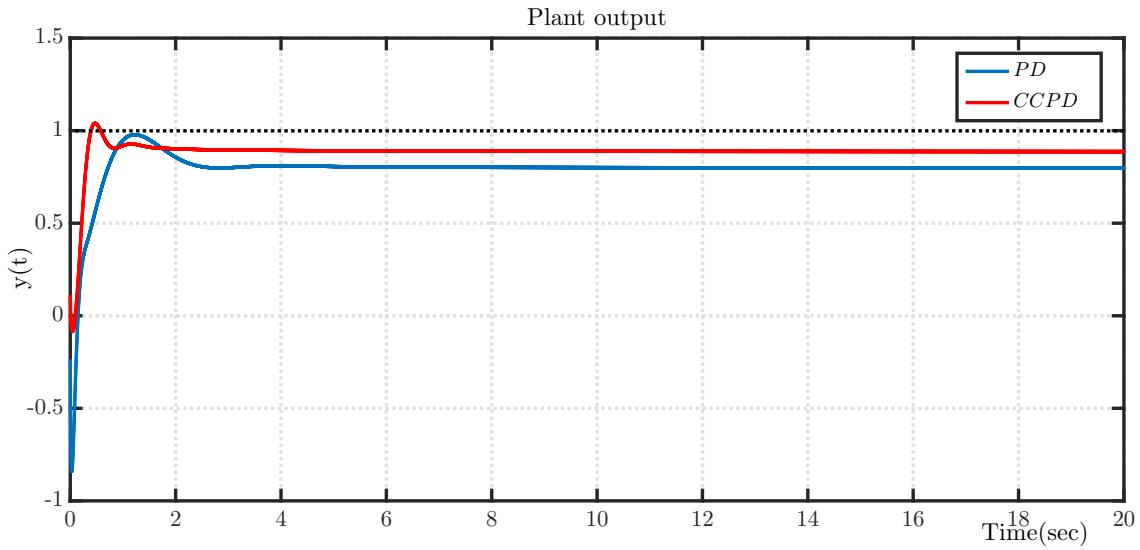

Figure 4.23: Plant output responses of case III with PD and $CCPD$

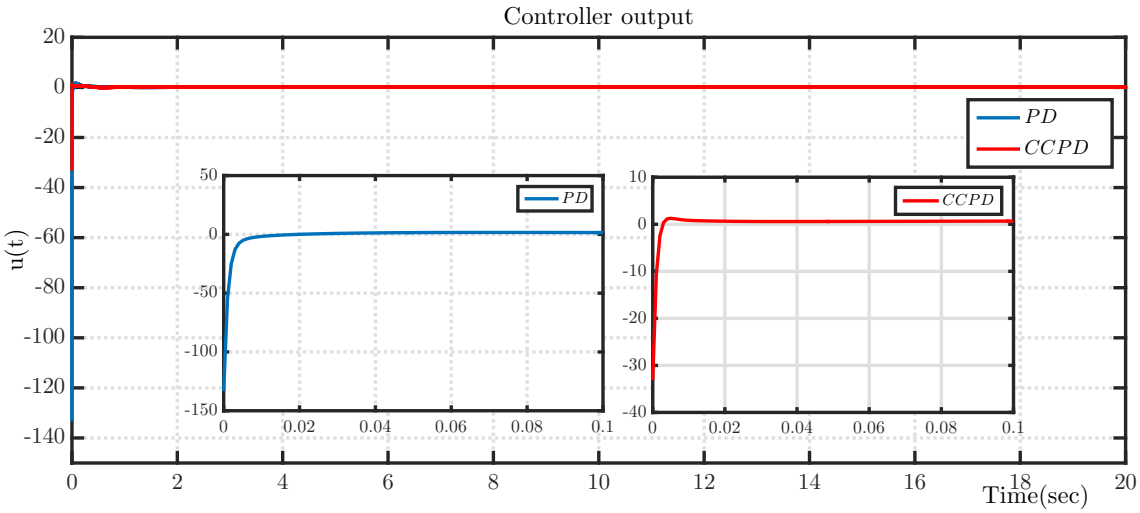

Figure 4.24: Controller output responses of case III with PD and $CCPD$

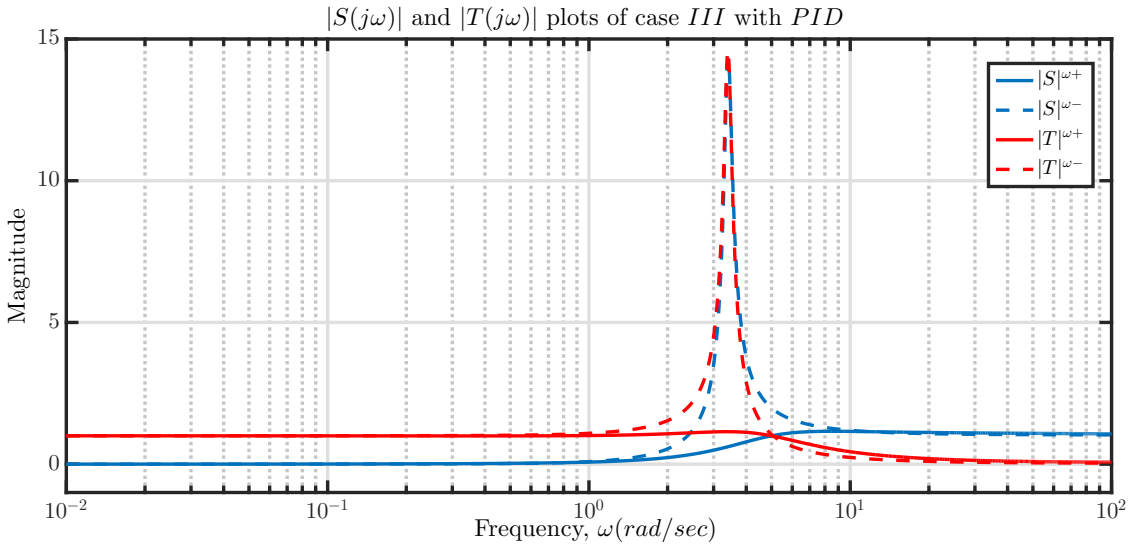

Figure 4.25: Sensitivity plots of case III with PID in ω^+ and ω^-

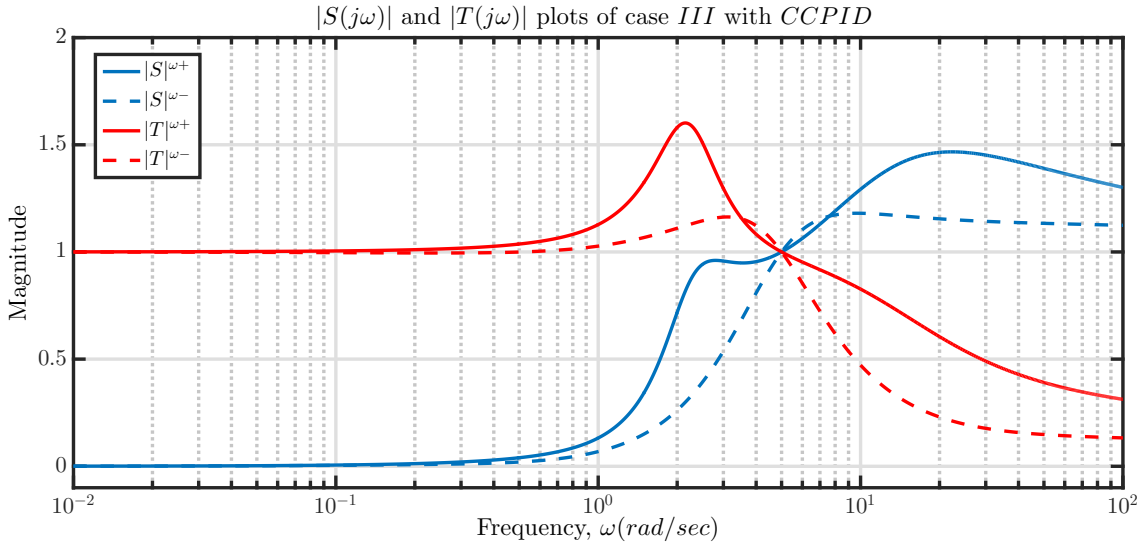

Figure 4.26: Sensitivity plots of case III with $CCPID$ in ω^+ and ω^-

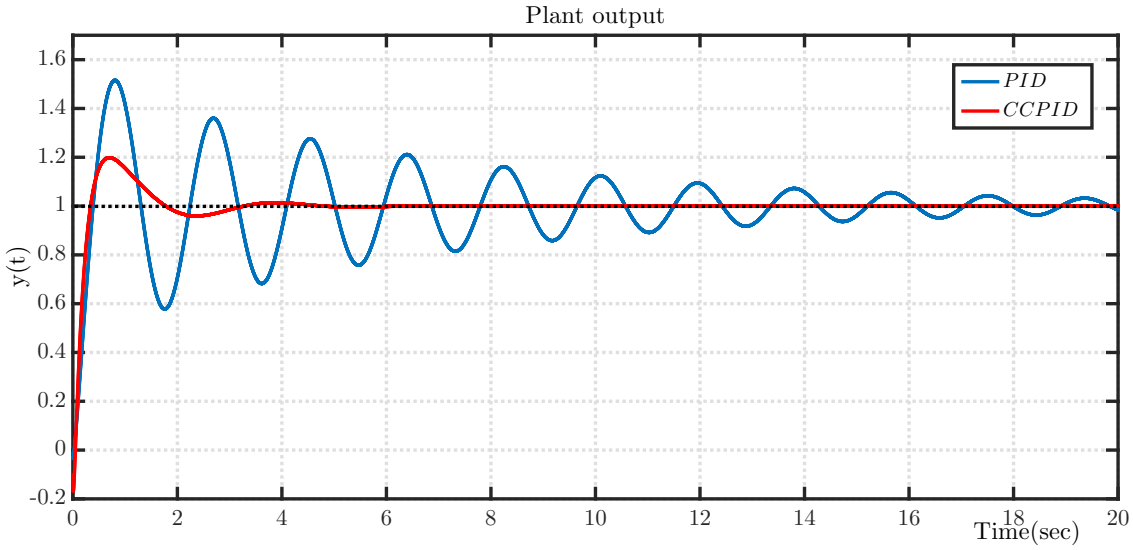

Figure 4.27: Plant output responses of case III with PID and $CCPID$

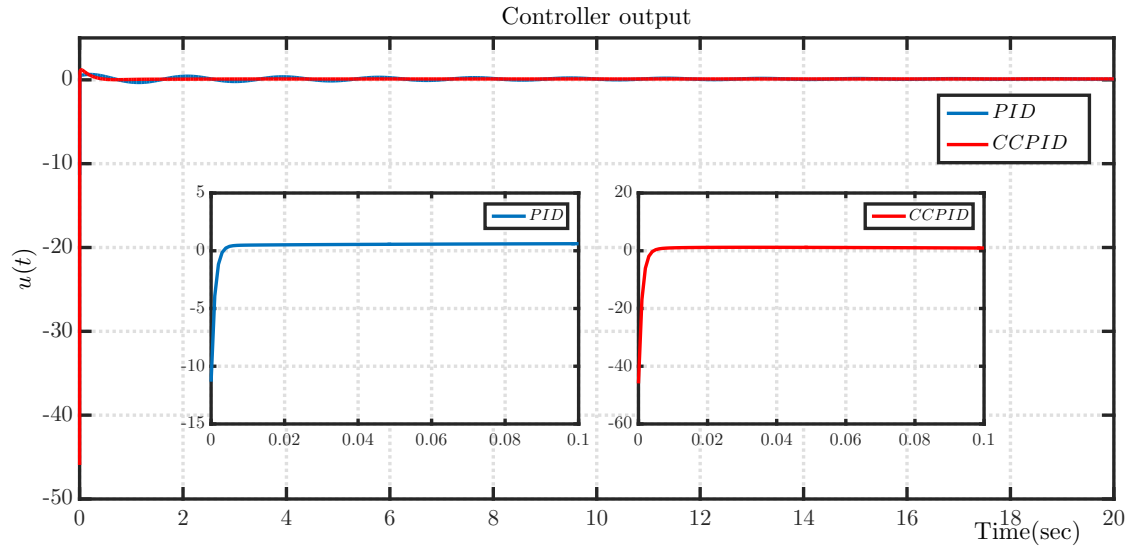

Figure 4.28: Controller output responses of case III with PID and $CCPID$

Table 4.3: Observations from $|S(j\omega)|$ and $|T(j\omega)|$ plots of real and complex valued IOCs

Case	Controller	ω^+ analysis	ω^- analysis
I	PI	$M_S = 1.6140; M_T = 1.0495;$ $GM \geq 8.3947dB; PM \geq 36.0932^\circ$ $\omega_{BW} = 1.0743\, rad/sec$	$M_S = 2.0510; M_T = 1.7045;$ $GM \geq 5.8072dB; PM \geq 28.2198^\circ$ $\omega_{BW} = 0.7923\, rad/sec$
	$CCPI$	$M_S = 1.3632; M_T = 1.1003;$ $GM \geq 11.4874dB; PM \geq 43.0332^\circ$ $\omega_{BW} = 0.8534\, rad/sec$	$M_S = 1.3073; M_T = 1.0961;$ $GM \geq 12.5771dB; PM \geq 44.9746^\circ$ $\omega_{BW} = 0.7599\, rad/sec$
II	PD	$M_S = 1.1717; M_T = 1.1088;$ $GM \geq 16.6798dB; PM \geq 50.5193^\circ$ $\omega_{BW} = 7.1400\, rad/sec$	$M_S = 2.5927; M_T = 2.8473;$ $GM \geq 4.2323dB; PM \geq 22.2378^\circ$ $\omega_{BW} = 3.5856\, rad/sec$
	$CCPD$	$M_S = 1.0620; M_T = 1.4243;$ $GM \geq 24.6792dB; PM \geq 56.1757^\circ$ $\omega_{BW} = 6.3149\, rad/sec$	$M_S = 1.0335; M_T = 1.2966;$ $GM \geq 29.7816dB; PM \geq 57.8659^\circ$ $\omega_{BW} = 6.5724\, rad/sec$
III	PI	$M_S = 1.1150; M_T = 1.1642;$ $GM \geq 19.7332dB; PM \geq 53.2873^\circ$ $\omega_{BW} = 6.6067\, rad/sec$	$M_S = 17.8246; M_T = 18.0907;$ $GM \geq 0.5015dB; PM \geq 3.2148^\circ$ $\omega_{BW} = 5.6490\, rad/sec$
	$CCPI$	$M_S = 1.0783; M_T = 1.3797;$ $GM \geq 22.7799dB; PM \geq 55.2515^\circ$ $\omega_{BW} = 7.4259\, rad/sec$	$M_S = 1.0626; M_T = 1.2537;$ $GM \geq 24.5907dB; PM \geq 56.1369^\circ$ $\omega_{BW} = 6.6383\, rad/sec$
	PD	$M_S = 3.0017; M_T = 2.5733;$ $GM \geq 3.5194dB; PM \geq 19.1775^\circ$ $\omega_{BW} = 1101.80\, rad/sec$	$M_S = 2.1354; M_T = 2.0664;$ $GM \geq 5.4868dB; PM \geq 27.0834^\circ$ $\omega_{BW} = 20.24\, rad/sec$
	$CCPD$	$M_S = 2.3614; M_T = 1.5776;$ $GM \geq 4.7838dB; PM \geq 24.4488^\circ$ $\omega_{BW} = 60.74\, rad/sec$	$M_S = 1.2244; M_T = 1.2281;$ $GM \geq 14.7393dB; PM \geq 48.2058^\circ$ $\omega_{BW} = 15.70\, rad/sec$
	PID	$M_S = 1.1592; M_T = 1.1456;$ $GM \geq 17.2433dB; PM \geq 51.1033^\circ$ $\omega_{BW} = 6.9302\, rad/sec$	$M_S = 14.3505; M_T = 14.5842;$ $GM \geq 0.6274dB; PM \geq 3.9934^\circ$ $\omega_{BW} = 5.7158\, rad/sec$
	$CCPID$	$M_S = 1.4670; M_T = 1.6017;$ $GM \geq 9.9424dB; PM \geq 39.8554^\circ$ $\omega_{BW} = 14.6506\, rad/sec$	$M_S = 1.1806; M_T = 1.1632;$ $GM \geq 16.3085dB; PM \geq 50.1142^\circ$ $\omega_{BW} = 7.1434\, rad/sec$

4.6.2 Case Study for CCFCOCs

To demonstrate the usage of CCFCOCs, case II defined in Table 4.1 is used. The following values are selected as design specifications and bounds for controller parameters: $\omega_{gc} = 5\,rad/sec$, $\phi_m = 60^\circ$, $K_{pr} \in [-10, 10]$, $K_{pi} \in [-10, 10]$, $K_{ir} \in [-10, 10]$, $K_{ii} \in [-10, 10]$, $K_{dr} \in [-10, 10]$, $K_{di} \in [-10, 10]$, $\alpha \in [-1, 1]$ and $\beta \in [-1, 1]$.

The fmincon() solver available in MATLAB [161] is used to solve the optimization problem repeatedly with sufficiently large number of randomly selected initial guesses. For each controller case, 2000 random initial guesses are taken and the corresponding converged values are found to be unique. The results of the proposed optimization problem are presented in Table 4.4 and these controllers are the only possible outcomes of the chosen case study. To show its superiority, these results are compared with the corresponding real coefficient FOCs obtained in chapter 3 for the same case study shown in Table 3.2 and are listed in Table 4.4.

Table 4.4: Tuning results of real and complex valued FOCs

Plant parameters	Controller	Controller parameters	Controller effort $(J = \int_0^\infty \lvert u(t)\rvert^2 dt)$
Case:II $K = 1, L = 0, a_0 = 3,$ $b_0 = 4, c_0 = 0.8, d_0 = 0.2,$ $c_1 = 0.5, d_1 = 0.3, \alpha_0 = 0,$ $\beta_0 = 0, \gamma_0 = 1.9, \delta_0 = 0.4,$ $\gamma_1 = 0.8, \delta_1 = 0.2,$	$CCPD^{\beta_r+j\beta_i}$	$K_{pr} = 0.4408; K_{pi} = -0.6003$ $K_{dr} = 1.1850; K_{2i} = -0.5314$ $\beta_r = 0.6019; \beta_i = 0.3347$	6.9185
	PD^{β}	$K_p = 1.5735; K_d = 0.2066$ $\beta = 1.0807$	148.104
	$CC[PD]^{\beta_r+j\beta_i}$	$K_{pr} = 0.2644; K_{pi} = -0.7629$ $K_{dr} = 0.2945; K_{di} = -0.6107$ $\beta_r = 0.5793; \beta_i = 0.4616$	47.6554
	$[PD]^{\beta}$	$K_p = 1.360; K_d = 0.1420;$ $\beta = 1.4269$	25676.274

Fig. 4.29 and Fig. 4.31 show the ω^+ and ω^- Bode magnitude response of case II with the listed controllers in the Table 4.4 respectively. Fig. 4.30 and Fig. 4.32 show the ω^+ and ω^- Bode phase response of case II with the listed controllers in the Table 4.4 respectively.

It is noted that magnitude and phase responses for plant with real valued FOCs satisfy the required specifications in ω^+ but not in ω^-. This is due to the unsymmetrical behaviour of the plant not getting compensated by the real valued FOCs having symmetrical behaviour. Hence, it necessitates to design a complex valued FOCs to satisfy the constraints simultaneously in both ω^+ and ω^-.

$|S(j\omega)|$ and $|T(j\omega)|$ plots for $CCPD^{\beta_r+j\beta_i}$ and PD^{β} for case II are shown in Fig. 4.33 and Fig. 4.34 respectively. Similarly, $|S(j\omega)|$ and $|T(j\omega)|$ plots for $CC[PD]^{\beta_r+j\beta_i}$

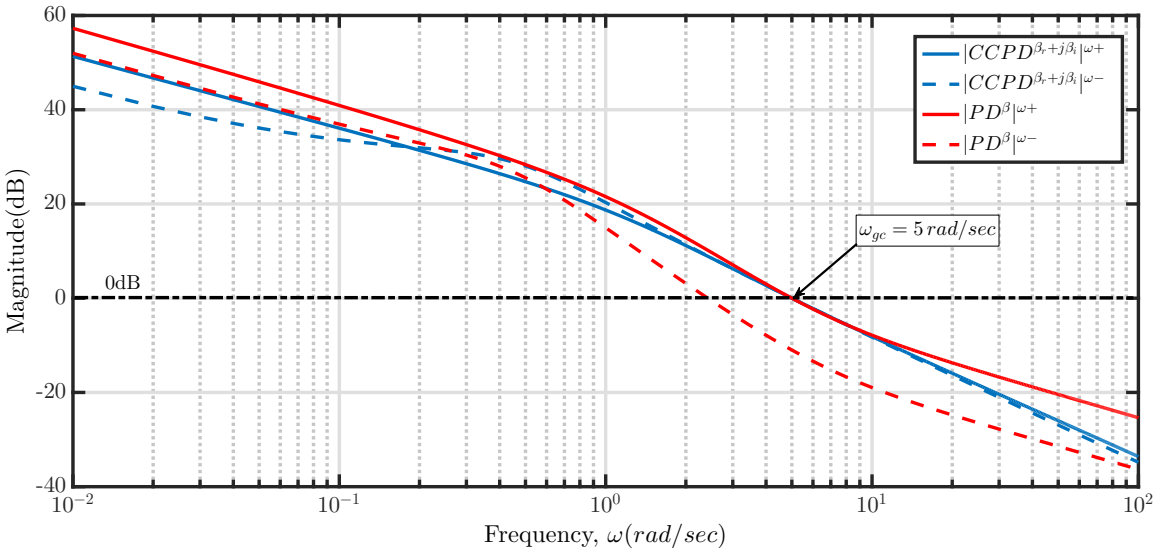

Figure 4.29: Open loop magnitude responses of case II with $CCPD^{\beta_r+j\beta_j}$ and PD^{β} controllers in ω^+ and ω^-

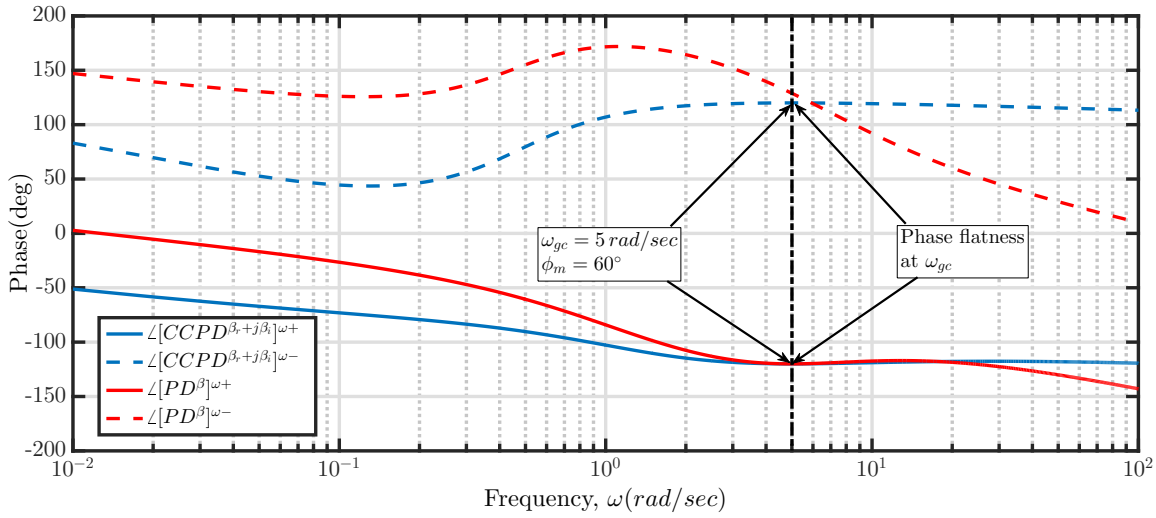

Figure 4.30: Open loop phase responses of case II with $CCPD^{\beta_r+j\beta_j}$ and PD^{β} controllers in ω^+ and ω^-

and $[PD]^{\beta}$ for case II are shown in Fig. 4.35 and Fig. 4.36 respectively.

M_S, M_T, Bandwidth (ω_{BW}) and guaranteed stability margins $(GM$ and $PM)$ are also obtained from these $|S(j\omega)|$ and $|T(j\omega)|$ plots. These values are computed for both $\omega+$ and $\omega-$ and are listed in Table 4.5.

To obtain the time response characteristics, ORA is extended for the approximation of $CCPD^{\beta_r+j\beta_i}$ and $CC[PD]^{\beta_r+j\beta_i}$. The real part of the closed loop unit step responses are shown in Fig. 4.37 for case II with $CCPD^{\beta_r+j\beta_i}$ and PD^{β} controllers. The real part of

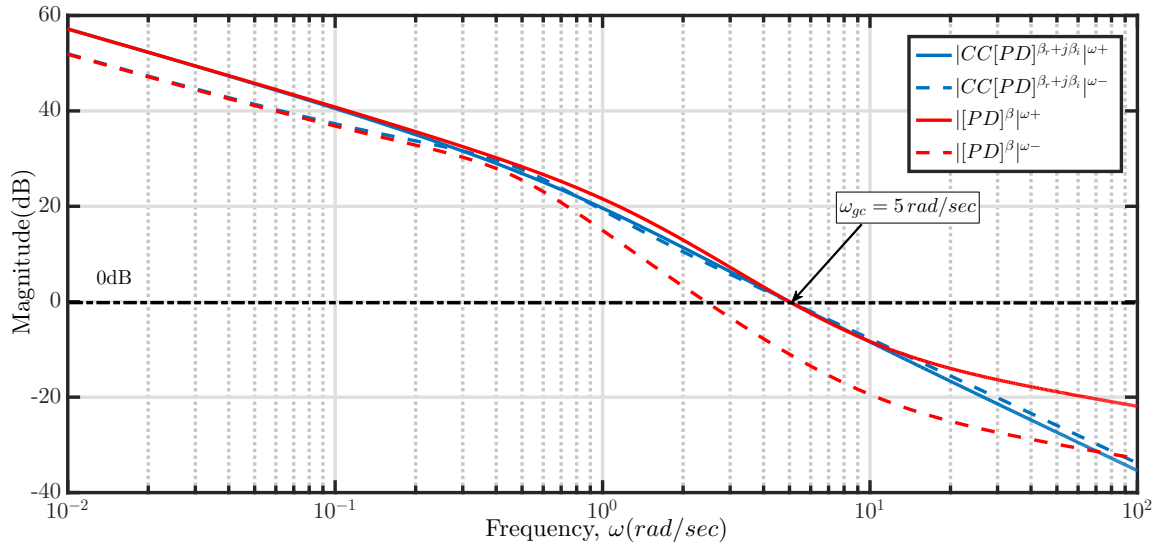

Figure 4.31: Open loop magnitude responses of case II with $CC[PD]^{\beta_r+j\beta_j}$ and $[PD]^{\beta}$ controllers in ω^+ and ω^-

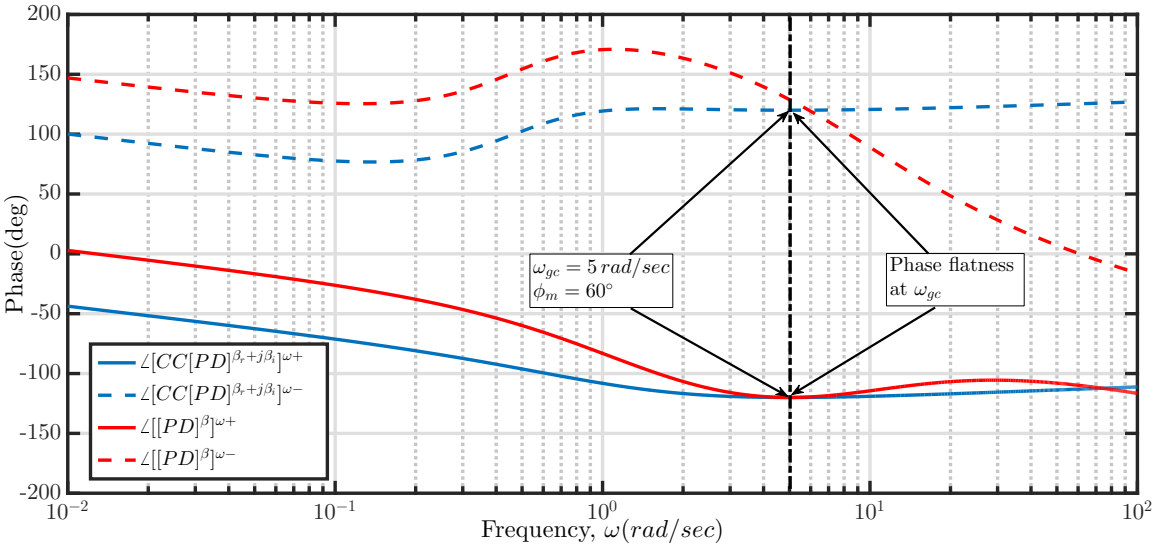

Figure 4.32: Open loop phase responses of case II with $CC[PD]^{\beta_r+j\beta_j}$ and $[PD]^{\beta}$ controllers in ω^+ and ω^-

the closed loop unit step responses are shown in Fig. 4.39 for case II with $CC[PD]^{\beta_r+j\beta_i}$ and $[PD]^{\beta}$ controllers.

The real part of the controller output responses are shown in Fig. 4.38 for case II with $CCPD^{\beta_r+j\beta_i}$ and PD^{β} controllers. The real part of the controller output responses are shown in Fig. 4.40 for case II with $CC[PD]^{\beta_r+j\beta_i}$ and $[PD]^{\beta}$ controllers.

For case II, it is observed that both M_S and M_T obtained for $CCPD^{\beta_r+j\beta_i}$ are lesser

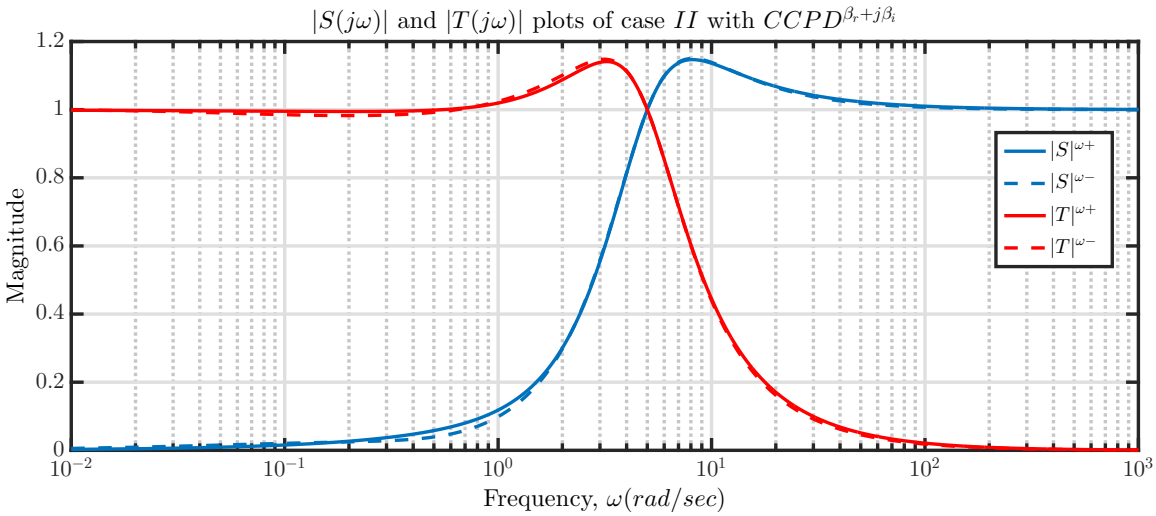

Figure 4.33: Sensitivity plots of case II with $CCPD^{\beta_r+j\beta_j}$ in ω^+ and ω^-

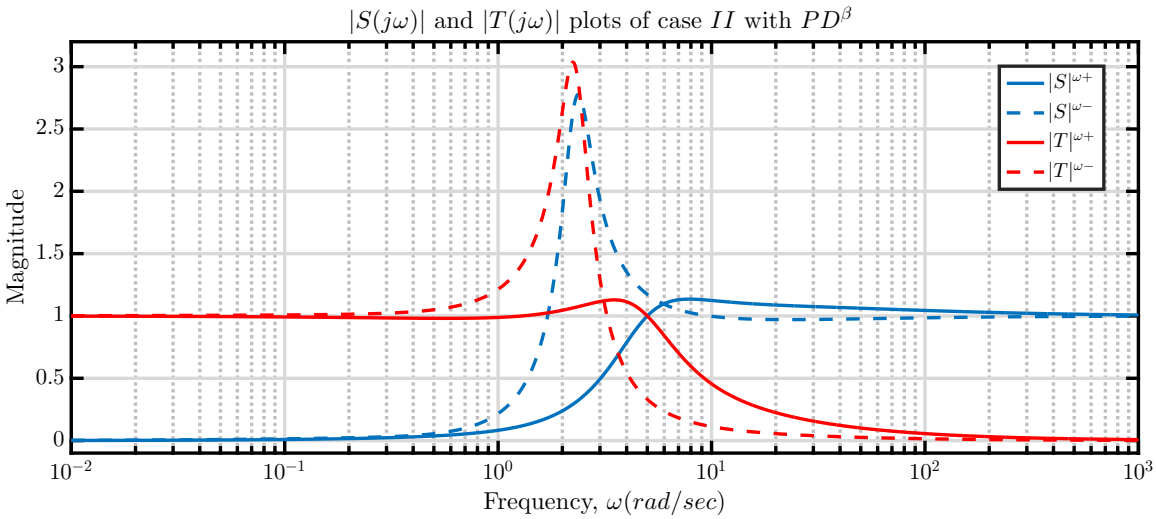

Figure 4.34: Sensitivity plots of case II with PD^{β} in ω^+ and ω^-

in comparison to PD^{β} from ω^+ and ω^- analysis. This assures increased GM and PM for $CCPD^{\beta_r+j\beta_i}$ which is seen as a reduced overshoot in Fig. 4.37. It is also observed that $CCPD^{\beta_r+j\beta_i}$ has larger ω_{BW} than PD^{β} which is reflected as lesser rise time in Fig. 4.39. Similar trend is also observed for $CC[PD]^{\beta_r+j\beta_i}$ in comparison to $[PD]^{\beta}$ of case II.

Controller effort is computed for case II with controllers as shown in Table 4.2. Since, tuning of real valued FOCs are performed by considering only ω^+ and whereas complex valued FOCs are tuned by considering both ω^+ and ω^-, the comparison of their controller efforts are not performed.

From the above analysis, it is observed that $CCPD^{\beta_r+j\beta_j}$ and $CC[PD]^{\beta_r+j\beta_j}$ simulta-

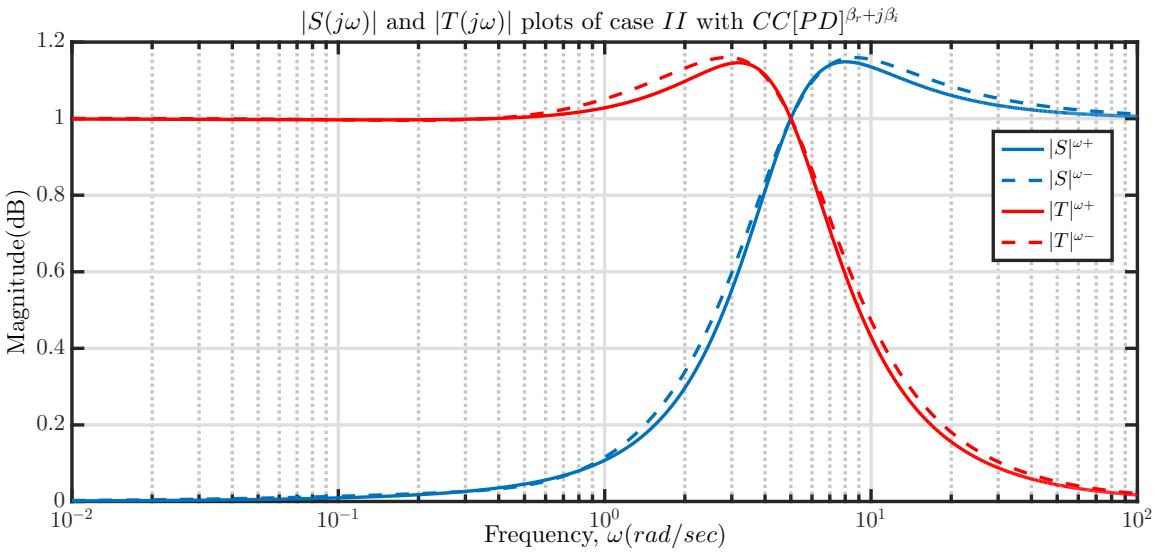

Figure 4.35: Sensitivity plots of case II with $CC[PD]^{\beta_r+j\beta_j}$ in ω^+ and ω^-

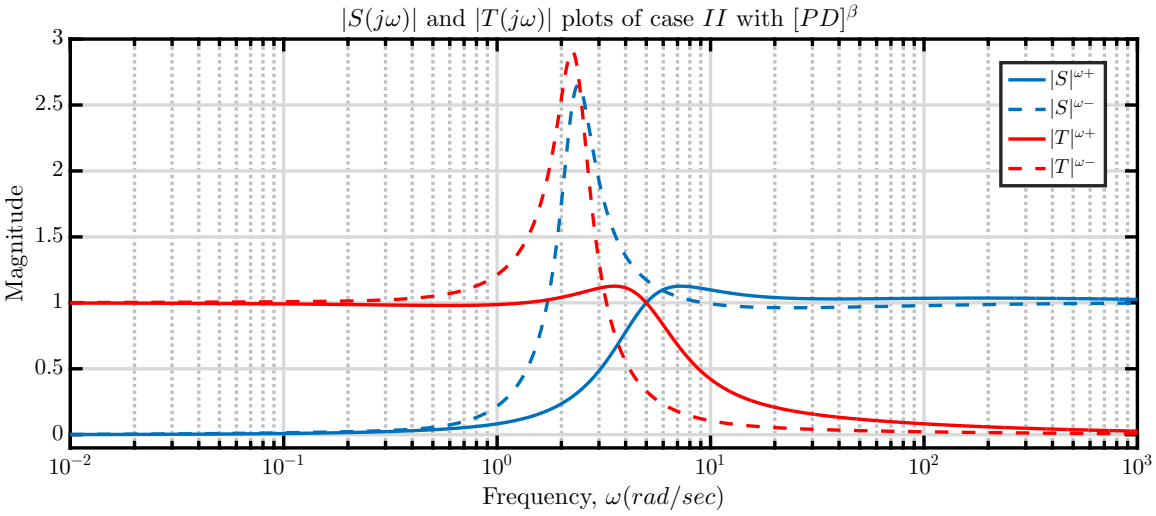

Figure 4.36: Sensitivity plots of case II with $[PD]^{\beta}$ in ω^+ and ω^-

neously satisfy the required specifications in ω^+ and ω^-. It also provides improved stability margins and better time response than real valued FOCs. Hence, only complex valued FOCs or complex valued IOCs have to be selected for complex valued plants.

Table 4.5: Observations from $|S(j\omega)|$ and $|T(j\omega)|$ plots of real and complex valued FOCs

Case	Controller	ω^+ analysis	ω^- analysis
II	$CCPD^{\beta_r+j\beta_i}$	$M_S = 1.1469; M_T = 1.1412;$ $GM \geq 17.8507dB; PM \geq 51.6931^\circ$ $\omega_{BW} = 7.0763\, rad/sec$	$M_S = 1.1502; M_T = 1.1480;$ $GM \geq 17.6845dB; PM \geq 51.5356^\circ$ $\omega_{BW} = 7.0684\, rad/sec$
	PD^{β}	$M_S = 1.1349; M_T = 1.1290;$ $GM \geq 18.4962dB; PM \geq 52.2778^\circ$ $\omega_{BW} = 6.9699\, rad/sec$	$M_S = 2.7770; M_T = 3.0362;$ $GM \geq 3.8778dB; PM \geq 20.7453^\circ$ $\omega_{BW} = 3.6345\, rad/sec$
	$CC[PD]^{\beta_r+j\beta_i}$	$M_S = 1.1485; M_T = 1.1460;$ $GM \geq 17.7667dB; PM \geq 51.6139^\circ$ $\omega_{BW} = 7.0183\, rad/sec$	$M_S = 1.1594; M_T = 1.1598;$ $GM \geq 17.2344dB; PM \geq 51.0943^\circ$ $\omega_{BW} = 7.2825\, rad/sec$
	$[PD]^{\beta}$	$M_S = 1.1261; M_T = 1.1264;$ $GM \geq 19.0147dB; PM \geq 52.7180^\circ$ $\omega_{BW} = 6.8180\, rad/sec$	$M_S = 2.6514; M_T = 2.9064;$ $GM \geq 4.1124dB; PM \geq 21.7394^\circ$ $\omega_{BW} = 3.6536\, rad/sec$

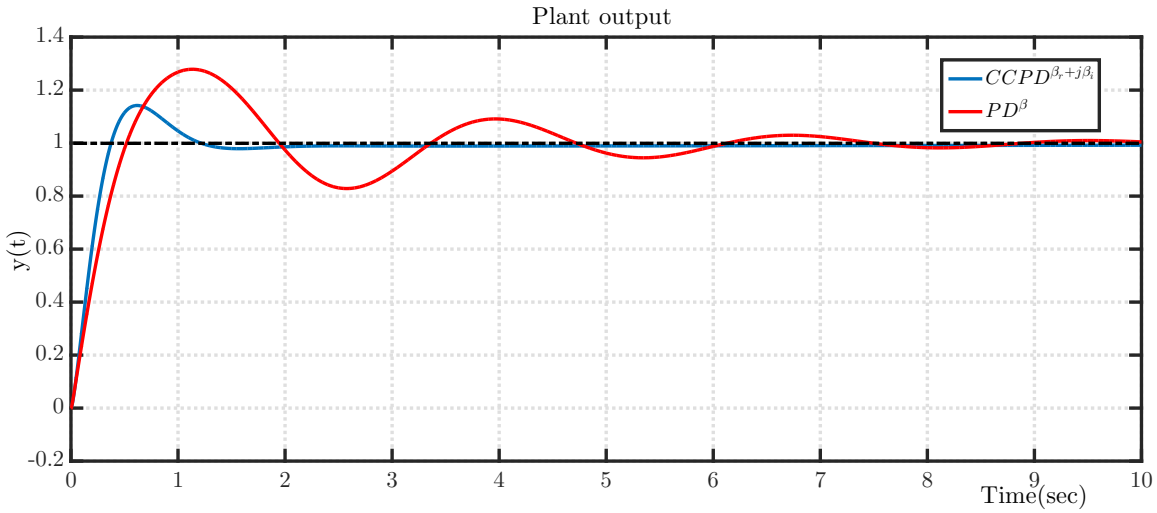

Figure 4.37: Plant output responses of case II with $CCPD^{\beta_r+j\beta_j}$ and PD^{β}

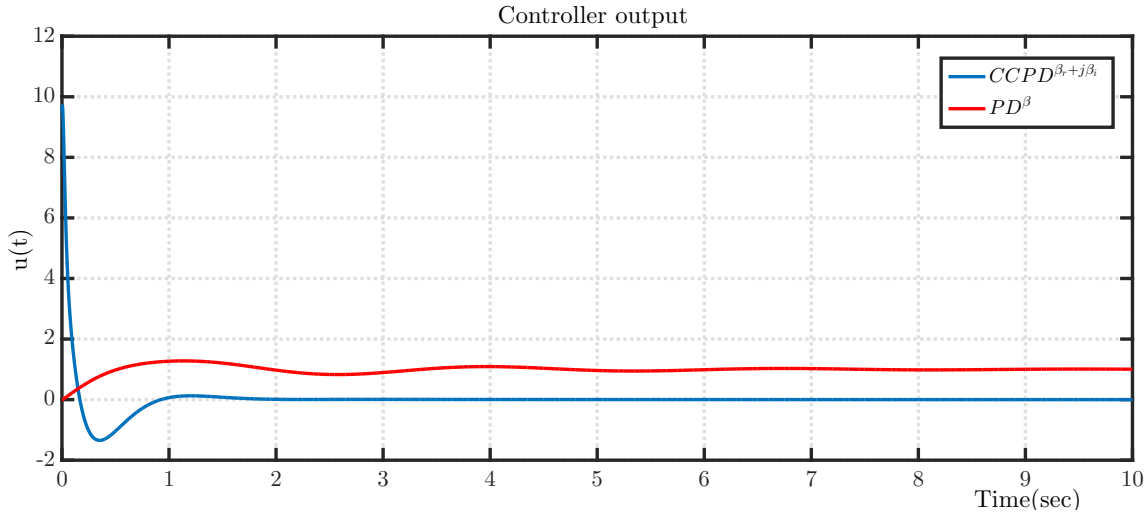

Figure 4.38: Controller output responses of case II with $CCPD^{\beta_r+j\beta_j}$ and PD^{β}

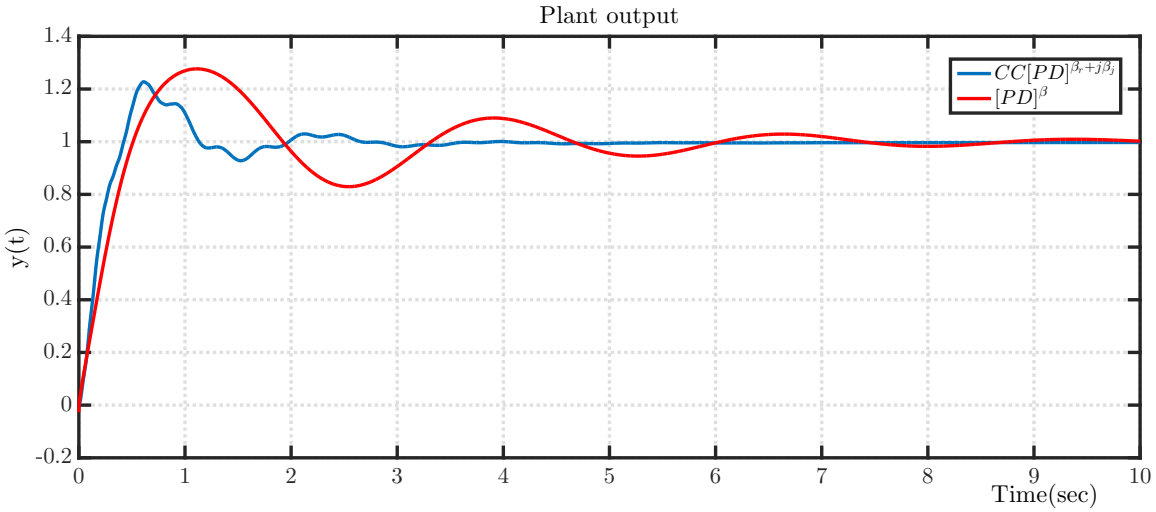

Figure 4.39: Plant output responses of case II with $CC[PD]^{\beta_r+j\beta_j}$ and $[PD]^{\beta}$

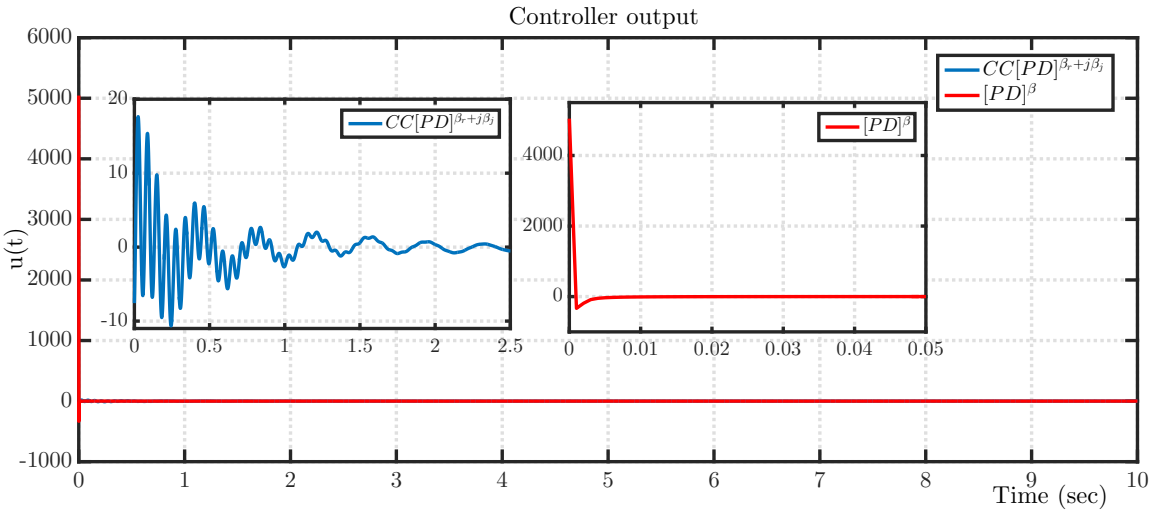

Figure 4.40: Controller output responses of case II with $CC[PD]^{\beta_r+j\beta_j}$ and $[PD]^{\beta}$

4.7 Summary

In this chapter, complex valued integer order PI/PD/PID controllers are proposed for the universal plant structure. The unified expressions of complex and real valued IOCs are derived for complex valued universal plant to meet the desired specifications. Three different complex valued case studies are chosen to validate the obtained complex and real valued IOCs. It is observed that only complex valued IOCs with plant had the ability to satisfy the constraints both in ω^+ and ω^-. Also, complex valued IOCs have better stability and robustness to parameter uncertainty than real valued IOCs which is observed from its sensitivity and complementary sensitivity analysis. Due to this, an improved frequency domain and equivalent time domain performance are achieved. Hence, complex valued IOCs are suggested for controlling complex valued plants. To show the superiority of fractional controllers, this work is further extended to tune the proposed CCFCOCs to satisfy the constraints both in ω^+ and ω^- through optimization technique.

Chapter 5

Limit Cycle Prediction and Suppression for System with Multiple Nonlinearities

5.1 Introduction

In engineering, system with nonlinearities (backlash, relay, saturation, etc.,) experiences an undesirable behaviour at steady state under closed loop operation. It is termed as limit cycle oscillation which is of constant magnitude and frequency. Describing Function (DF) analysis tool is used to study such systems under the assumption that linear part of the system provides very good low pass filtering effect [128]. DF is a first order harmonic approximation of the nonlinearities [164] and it is used to predict the limit cycle details either graphically or analytically. In this chapter, graphical approach techniques such as root locus and Nyquist plot are dealt to predict the limit cycle information for system with nonlinearity. Root locus and Nyquist plot are well established techniques to predict the limit cycle details for system with single separable nonlinearity [159]. In [143], Input Dependent Root Locus (IDRL) is proposed to predict the limit cycle for system with multiple nonlinearities but there is no literature existing in case of Nyquist plot for system with multiple nonlinearities. Hence, an Input Dependent Nyquist Plot (IDNP) is proposed in this chapter to predict the limit cycle for system with multiple nonlinearities. These predicted details are compared with IDRL and verified under the closed loop simulation. Controller design for these system with multiple nonlinearities using DF analysis is also not explored in the existing literature. Hence, an optimization problem is also proposed in this chapter to tune the integer order controllers (IOCs) and Fractional Order Controllers (FOCs) to suppress the limit cycle oscillation in addition to meet desired transient specifications.

At first, the existing DF method based limit cycle prediction using root locus and Nyquist plot for system with single nonlinearity are described in section 5.2. The extension

of these predicting methods to predict the limit cycle information for system with multiple nonlinearities are discussed in section 5.3. The general closed loop schematic representation of system with multiple nonlinearities is described in section 5.4. As a case study to validate the proposed IDNP, servo position control system is considered and described. To suppress this limit cycle, an optimization problem is proposed to obtain IOCs and FOCs in addition to meet the desired closed loop specifications. Section 5.5 discusses about the usage of the proposed IDNP to predict the limit cycle information for the servo system with the all the obtained controllers from the proposed optimization problem. Further in section 5.6, simulation is carried out to test the servo system under parameter uncertainty, disturbance and measurement noise conditions to observe the robustness of the designed controllers.

5.2 System with Single Nonlinearity

Closed loop schematic of linear system $G(s)$ in series with single separable nonlinearity ($N(X)$ is the DF of the memoried or non-memoried nonlinearity and X is the limit cycle magnitude) is shown in Fig. 5.1. Due to this nonlinearity, the closed loop system experiences an undesirable limit cycle oscillation at steady state. The prediction of this limit cycle details using the well established graphical approaches such as root locus and Nyquist plot techniques are explained in the below subsections.

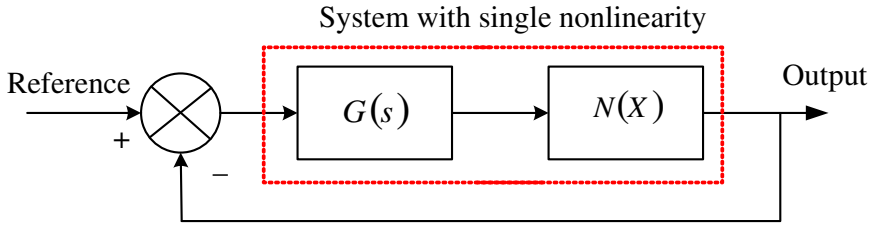

Figure 5.1: System with single nonlinearity

5.2.1 Limit Cycle Prediction using Root Locus

To have limit cycle oscillation at steady state, the closed loop poles of the root locus should occur at the imaginary axis [159]. For the block diagram shown in Fig. 5.1, the open loop transfer function (OLTF) is given as: $G(s)N(X)$. Since the OLTF is a function of X, the closed loop poles vary with different value of X. For such system, IDRL [143] is used to predict the limit cycle information.

To predict the limit cycle details using IDRL, the movement of the closed loop poles of this open loop transfer function for different values of X ranging from 0 to ∞ have to be observed. This pole movement forms a locus connecting all the operating points in the increasing direction of X and the number of locus drawn is equal to the number of closed loop poles. Limit cycle is ensured if there is an intersection between the locus drawn and the imaginary axis. Limit cycle is characterised by the value of X for which the locus crosses the imaginary axis as limit cycle magnitude X_0 and the crossing $j\omega$ value on the imaginary axis as limit cycle frequency ω_0. If there is a crossing, then one has to check the stability of the limit cycle by applying the perturbation technique at the crossing point.

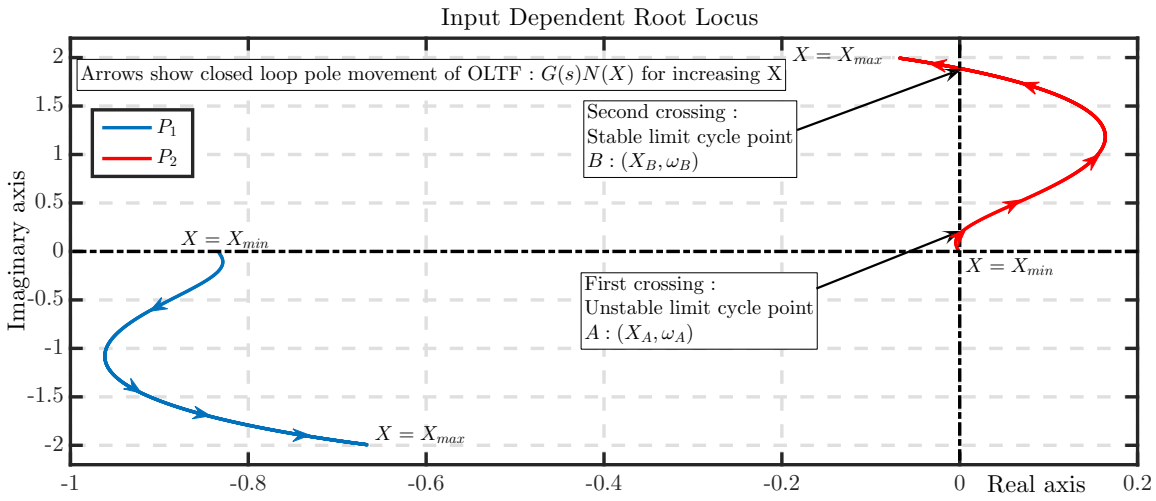

Figure 5.2: Limit cycle prediction using root locus

Let us consider a system with two numbers of closed loop poles which vary with the value of X. The movement of these poles in the increasing direction for a range of X : $[X_{min}$ to $X_{max}]$ as shown in Fig. 5.2. It is found that one of the loci $(P1)$ is completely in the left half of the s-plane and the other locus $(P2)$ crosses the imaginary axis at two points $A : (X_A, \omega_A)$ and $B : (X_B, \omega_B)$ which is responsible for the limit cycle oscillation. This crossing ensures the limit cycle existence and the stable limit cycle is found by using the perturbation technique at the points A and B.

On giving a small perturbation to X (say $X_A + \delta X_A$) at point A, it is observed that the pole moves from stable left half of s-plane to unstable right half of s-plane which in turn increases the limit cycle magnitude X. Here, the pole moves away from the crossing point A and hence, point A is an unstable limit cycle point. Similarly, on giving a small perturbation to X (say $X_B + \delta X_B$) at point B, it is observed that the pole moves from unstable right half of s-plane to stable left half of s-plane which in turn decreases the limit

cycle magnitude X. Here, the pole comes back again to the crossing point B and hence, point B is a stable limit cycle point.

Here, the limit cycle is characterised by the value of X_B as limit cycle magnitude X_0 and the corresponding $j\omega_2$ crossing value on the imaginary axis as limit cycle frequency ω_0.

5.2.2 Limit Cycle Prediction using Nyquist Plot

In case of linear systems to have limit cycle oscillation at steady state, the Nyquist plot of the linear system should pass through the critical point $(-1, j0)$ [128]. If the Nyquist plot of the linear system encloses the critical point $(-1, j0)$, then the system is unstable and if the Nyquist plot of the linear system is enclosed by the critical point $(-1, j0)$, then the system is stable.

But, in case of system shown in Fig. 5.1, the critical point is no longer $(-1, j0)$. Here, the critical point is $\frac{-1}{N(X)}$ which is obtained from the characteristic equation of the closed loop system [159]. The critical point can be on the negative real axis in case of nonlinearity without memory and can be in the third quadrant in case of nonlinearity with memory. Then, the condition for the limit cycle occurrence is:

$$G(s)\Big|_{s=j\omega_0} = -\frac{1}{N(X)}\Big|_{X=X_0} \tag{5.1}$$

From equation (5.1), it is obvious that the possibility of a limit cycle oscillation depends on the intersection of the Nyquist plot of $G(s)$ at particular frequency ω and $\frac{-1}{N(X)}$ locus at particular X [128], [159]. There can be single or multiple sets of (X, ω) are possible to ensure the intersection condition (5.1). This single or multiple crossing points indicate the presence of stable and unstable limit cycle points. Hence, to find the stable limit cycle point, one has to perform the stability analysis at the crossing points. To check the stability of the limit cycle, a small perturbation to X is applied at the crossing point. Due to perturbation, if the updated single critical point $\frac{-1}{N(X+\delta X)}$ encloses the Nyquist plot of $G(s)$, then the observed crossing point is a stable limit cycle with magnitude X and frequency ω. Otherwise, the observed crossing point is an unstable point. This limit cycle is characterized by the value of X on $\frac{-1}{N(X)}$ as limit cycle magnitude X_0 and the value of ω on $G(j\omega)$ as limit cycle frequency ω_0.

Let us consider the Fig. 5.3 showing the intersection of the Nyquist plot of $G(s)$ and the locus $\frac{-1}{N(X)}$ drawn for a range of X. It has two crossing points $A : (X_1, \omega_1)$ and $B : (X_2, \omega_2)$

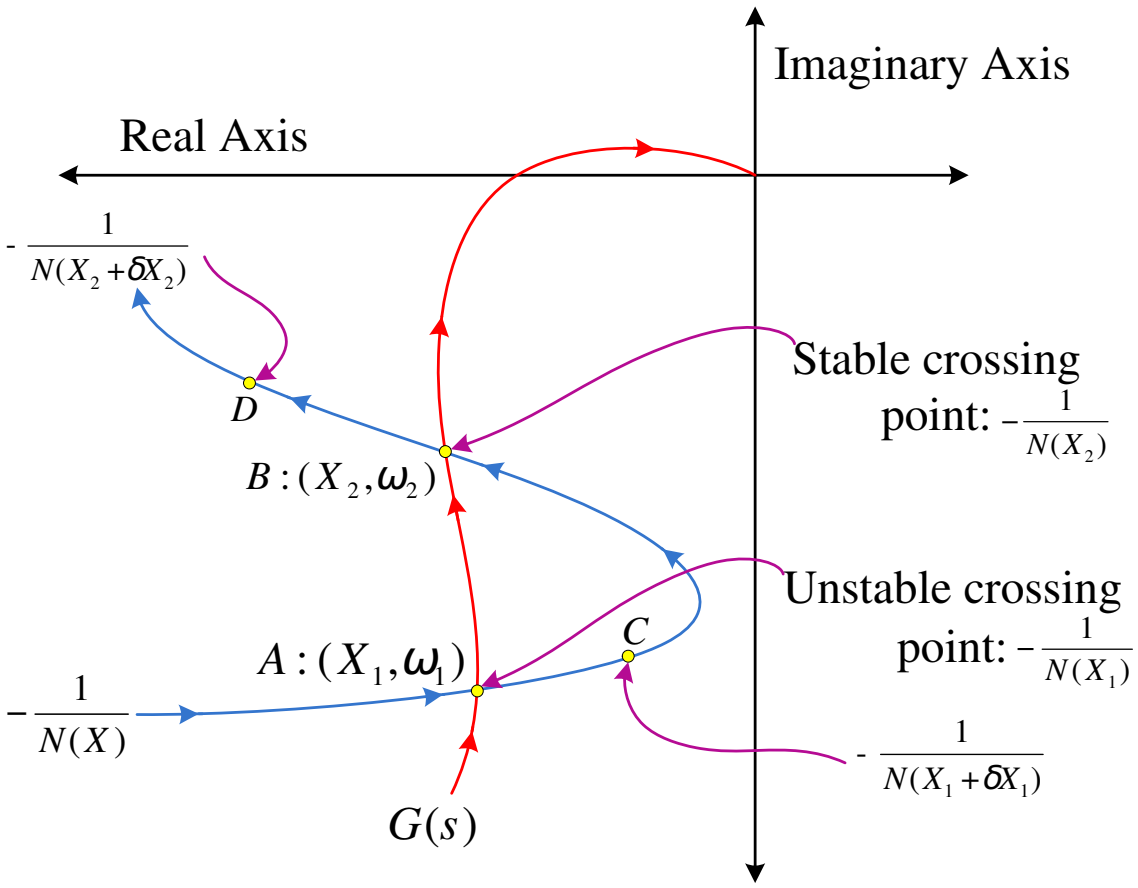

Figure 5.3: Limit cycle prediction using Nyquist plot

which satisfy the condition (5.1) ensuring limit cycle oscillation. The stable limit cycle is found by using the perturbation technique at the points A and B.

On giving a small perturbation to X (say $X_1 + \delta X_1$) at point A, it is observed that the updated critical point C : $\frac{-1}{N(X_1+\delta X_1)}$ is enclosed by the Nyquist plot $G(s)$. Hence, this point A is an unstable limit cycle point. Similarly, on giving a small perturbation to X (say $X_2 + \delta X_2$) at point B, it is observed that the updated critical point D : $\frac{-1}{N(X_2+\delta X_2)}$ is not enclosed by the Nyquist plot $G(s)$. Hence, this point B is a stable limit cycle point.

Here, the limit cycle is characterised by the value of X_2 as limit cycle magnitude X_0 and the value of ω_2 as limit cycle frequency ω_0.

5.3 System with Multiple Nonlinearities

In case of system with multiple nonlinearities, the position of the nonlinearities can be anywhere in the loop. In this work, linear system with feedback nonlinearity connected in

series with another nonlinearity is considered as system with multiple nonlinearities.

Linear system with feedback nonlinearity is represented as $G_1(s, X)$ and the series nonlinearity is represented by its DF $N(X)$ (where, X is the limit cycle magnitude). Its closed loop schematic is shown in Fig. 5.4.

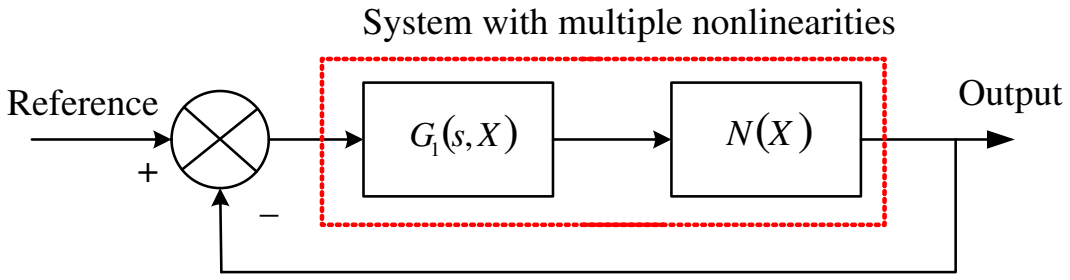

Figure 5.4: Representation of system with multiple nonlinearities

Generally, the limit cycle prediction for such systems are performed using root locus and Nyquist plot. In case of root locus, the characteristic equation obtained for the open loop system $G_1(s, X)N(X)$ and for the system $G(s)N(X)$ are functions of X only. Hence, the same approach explained in section 5.2.1 is adopted to predict the limit cycle details.

5.3.1 Limit Cycle Prediction using Proposed IDNP

Limit cycle prediction for the closed loop system shown in Fig. 5.4 is not possible with the existing Nyquist plot approach. It is because the linear part of the system $G_1(s, X)$ is a function of limit cycle magnitude X and hence the TF varies with each value of X. Due to the variation in TF, the Nyquist plot keeps varying and the crossing of the resultant Nyquist plot with the corresponding critical point $\frac{-1}{N(X)}$ is of interest to predict the limit cycle details. The crossing X of the critical point $\frac{-1}{N(X)}$ is characterised as limit cycle magnitude and the crossing frequency of the Nyquist plot of $G_1(s, X)$ for the same X is characterised as limit cycle frequency. To ensure the limit cycle occurrence, Nyquist plot of $G_1(s, X)$ is drawn for the selected value of X and it is examined whether the corresponding critical point $\frac{-1}{N(X)}$ lies on the Nyquist plot of $G_1(s, X)$. If the above condition is not met, choose different set of X and examine for the above condition. Once the possibility of limit cycle occurrence is ensured, then its stability needs to be checked by giving small perturbation to X at the crossing point. After giving a small perturbation to X (say $X+\delta X$), if the updated single critical point $\frac{-1}{N(X+\delta X)}$ is not enclosed by the corresponding updated Nyquist plot of $G_1(s, X + \delta X)$, then the observed crossing point gives a stable limit cycle with magnitude X and frequency ω. Otherwise, the observed crossing point is an unstable point.

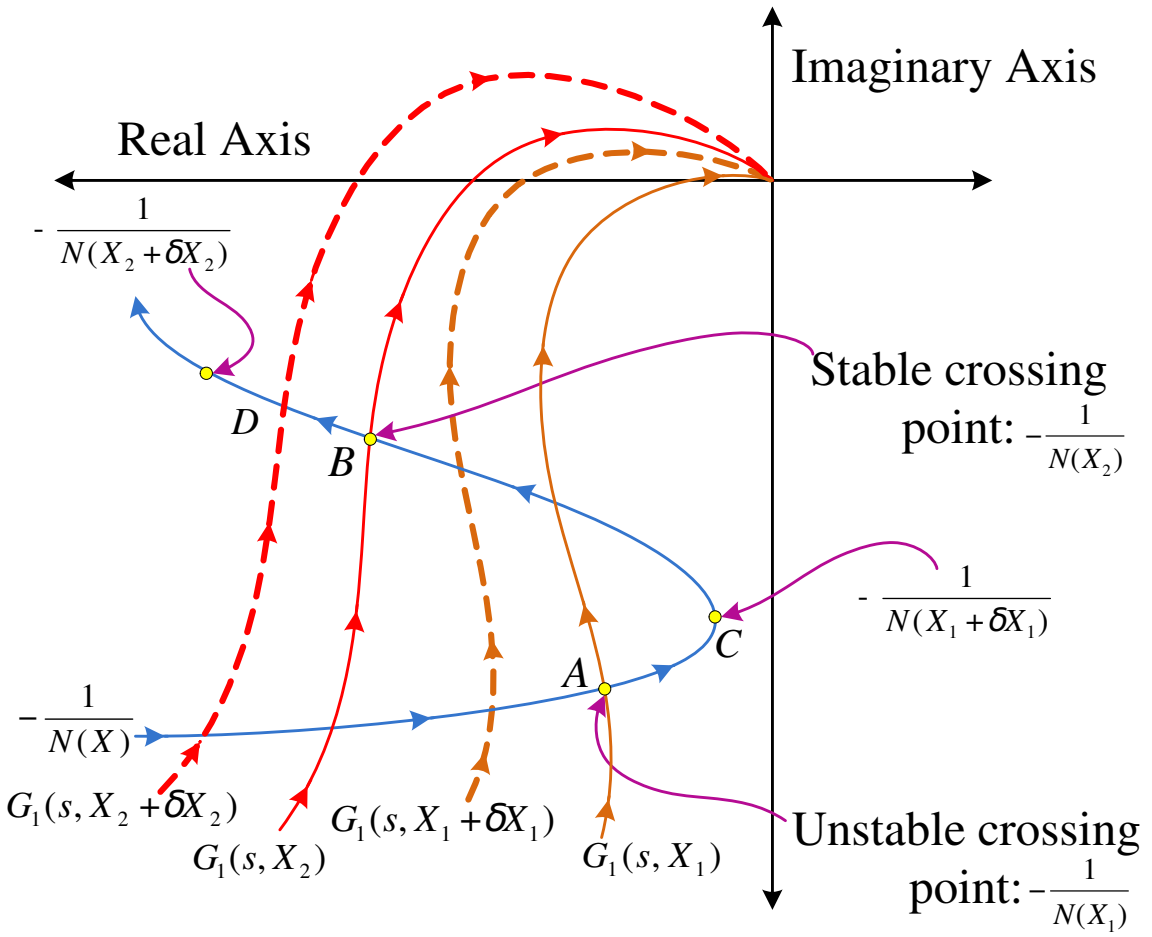

Figure 5.5: Stability analysis of $G_1(s, X)$ with $\frac{-1}{N(X)}$ using IDNP

The stability analysis of the observed limit cycle using IDNP is shown in the Fig. 5.5. Consider the Nyquist plot of $G_1(s, X_1)$ drawn for the selected value of X_1 and the corresponding single critical point $\frac{-1}{N(X_1)}$ lies on the Nyquist plot. This crossing is shown as A and to assess the stability a small perturbation is given to X_1 at this point A. After a small perturbation, the updated single critical point $\frac{-1}{N(X_1+\delta X_1)}$ lies at the point C. It is found that the corresponding updated Nyquist plot of $G_1(s, X_1 + \delta X_1)$ encloses the critical point cC. This shows that the observed crossing point A is an unstable limit cycle point. Similarly, the Nyquist plot of $G_1(s, X_2)$ is drawn for the selected value of X_2 and the corresponding single critical point $\frac{-1}{N(X_2)}$ lies on the Nyquist plot. This crossing is shown as B and a small perturbation is given to X_2 at this point B for checking the stability. By giving a small perturbation, the updated single critical point $\frac{-1}{N(X_2+\delta X_2)}$ lies at the point D. It is found that the corresponding updated Nyquist plot of $G_1(s, X_2 + \delta X_2)$ does not enclose the critical point D. This shows that the observed crossing point B is a stable limit cycle point.

5.4 Generalised Block Diagram Representation

The OLTF $G(s, X)$ is the representation of the system containing multiple nonlinearities. The closed loop control schematic of the system $G(s, X)$ with controller $C(s)$ is shown in Fig. 5.6.

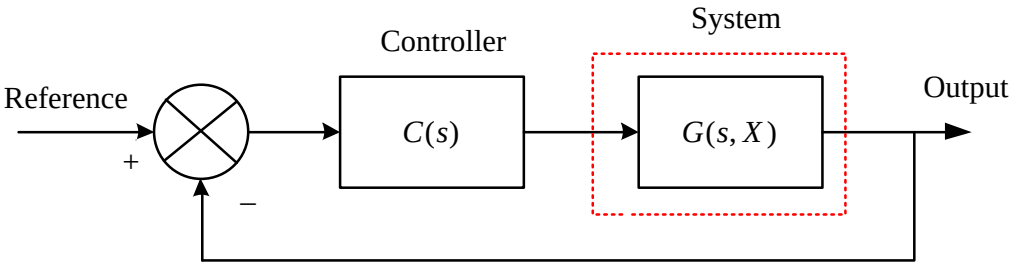

Figure 5.6: Closed loop control system representation

This system $G(s, X)$ experiences limit cycle oscillation at steady state due to the presence of multiple nonlinearities under closed loop operation. Prediction of this limit cycle details using graphical approaches (IDRL and proposed IDNP) and its suppression by implementing controller $C(s)$ are seen in this chapter.

5.4.1 System Description

A servo system with separable backlash and relay like nonlinearities is considered for controller design and limit cycle prediction as shown in Fig. 5.7. Due to these nonlinearities, system experiences limit cycle oscillation $x(t)$ at steady state and for analysis these nonlinearities are replaced by their equivalent describing functions $N_b(X)$ and $N_r(X_1)$ as follows [164]:

$$N_b(X) = \left(\frac{1}{\pi}\right)\left(\frac{\pi}{2} + \theta + 0.5\sin(2\theta) - j\cos^2\theta\right) \tag{5.2}$$

$$N_r(X_1) = \frac{4M}{\pi X_1} \tag{5.3}$$

$$\text{where, } \theta = \sin^{-1}\left[1 - \left(\frac{2H}{X}\right)\right]$$

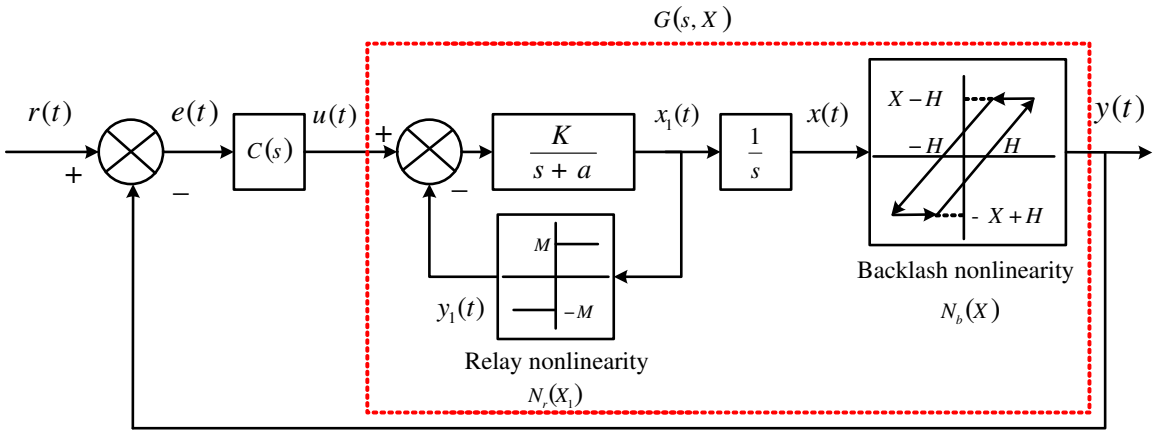

Figure 5.7: Closed loop schematic diagram of servo system with multiple nonlinearities

$$
\begin{aligned}
X &= \text{ peak value of the signal } x(t) \\
X_1 &= \text{ peak value of the signal } x_1(t) \\
&= X\omega \\
M &= \text{ saturation value of relay output} \\
H &= \text{ half of the backlash gap}
\end{aligned}
$$

Then, the open loop complex gain of the system shown in the Fig. 5.7 at steady state is given by:

$$C(s)G(s,X)\Big|_{s=j\omega} = \frac{C(s)KN_b(X)}{s(s+a+\frac{4M}{\pi X\omega})}\Big|_{s=j\omega} \tag{5.4}$$

5.4.2 Proposed Optimization Problem

The schematic diagram shown in Fig. 5.7 is further deduced to have a OLTF model of the form $C(s)G_1(s,X)$ in series with single nonlinearity $N_b(X)$ as shown in Fig. 5.8.

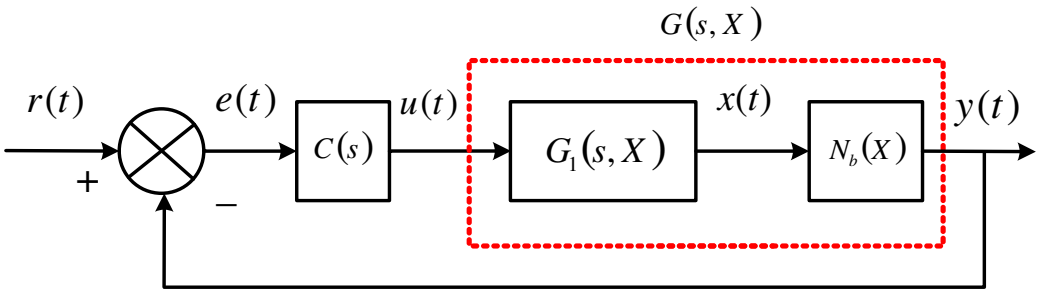

Figure 5.8: System model of the form $C(s)G_1(s,X)$ in series with nonlinearity $N_b(X)$

The main objective of the optimization problem is to minimize the controller output at steady state and it is systematized as a nonlinear constrained optimization problem :

$$\underset{\text{(Controller Parameters},X_0,\omega_0)}{\text{Minimize}} \left| X_0 N_b(X_0) C(j\omega_0) \right|$$

subject to:

1. Nyquist condition for limit cycle occurrence:

$$C(s)G_1(s,X)\Big|_{X=X_0,s=j\omega_0} = \frac{-1}{N_b(X)}\Big|_{X=X_0} \tag{5.5}$$

2. Loeb's condition for limit cycle stability [159]:

   The characteristic equation of the closed loop system shown in Fig. 5.8 is given by

$$U(X,\omega) + jV(X,\omega) = 1 + C(s)G_1(s,X)N_b(X) = 0$$

   Then, the stability condition is

$$\frac{\partial U}{\partial X}\frac{\partial V}{\partial \omega} - \frac{\partial U}{\partial \omega}\frac{\partial V}{\partial X}\Big|_{X_0,\omega_0} > 0 \tag{5.6}$$

3. Gain cross over frequency (ω_{gc}) specification:

$$|C(s)G(s)|_{s=j\omega_{gc}} = 1 \tag{5.7}$$

4. Phase margin (ϕ_m) specification:

$$\pi + \angle[C(s)G(s)]\Big|_{s=j\omega_{gc}} = \phi_m \tag{5.8}$$

5. Sensitivity $S(s)$: Robust output disturbance rejection performance,

$$|S(j\omega)|_{dB} = \left|\frac{1}{1+C(j\omega)G(j\omega)}\right|_{dB} < A, \forall\omega \leq \omega_l \tag{5.9}$$

6. Complementary sensitivity $T(s)$: Robust measurement noise rejection performance,

$$|T(j\omega)|_{dB} = \left|\frac{C(j\omega)G(j\omega)}{1+C(j\omega)G(j\omega)}\right|_{dB} < B, \forall\omega \geq \omega_h \tag{5.10}$$

7. Assured stability margins: M_S and M_T should be in the range of 1.2 to 2.0 and 1 to 1.5 respectively for a good measure of robustness [163]. Hence, the followings maximum limits are selected as constraints.

$$(i)\, M_S \leq 2 \tag{5.11}$$

$$(ii)\, M_T \leq 1.5 \tag{5.12}$$

where, $M_S = \underset{\omega}{max}|S(j\omega)|$; and $M_T = \underset{\omega}{max}|T(j\omega)|$. Then, the assured stability margins are:
$GM \geq \frac{M_S}{M_S-1}; PM \geq 2\sin^{-1}\left(\frac{1}{2M_S}\right)$

8. Relation on ω_0 and ω_{gc}:

$$\omega_0 < \omega_{gc} \tag{5.13}$$

Remark 5.1. *The alternating component of $x(t)$ at steady state is a sinusoidal signal of peak magnitude X_0 and frequency ω_0. This implies,*

$$x(t)|_{AC} = X_0\, sin(\omega_0 t)$$

Then the output of a backlash nonlinearity under first order harmonic approximation is given by

$$y(t)|_{AC} = |X_0 N_b(X_0)|\, sin(\omega_0 t + \angle[N_b(X_0)])$$

Then the controller output at steady state is given by

$$u(t)|_{AC} = |X_0 N_b(X_0) C(j\omega_0)|\, sin(\omega_0 t + \angle[N_b(X_0)] - \pi + \angle[C(j\omega_0)])$$

Hence, the optimization problem is proposed as minimization of $\left|X_0 N_b(X_0) C(j\omega_0)\right|$ at steady state with stability and robustness constraints to tune $C(s)$.

Remark 5.2. *The impact of nonlinearities are mostly seen at steady state. To nullify the effect of $N_b(X)$ in the feed forward path, its gain must be $1\angle 0^\circ$. This is possible only for $X = \infty$ and in turn $N_r(X_1)$ becomes 0. Hence, it is assumed that $N_b(X) = 1\angle 0^\circ$ and $N_r(X_1) = 0$ in equation* (5.4) *to have $C(s)G(s,X)$ as $C(s)G(s)$ in equations* (5.7)*,* (5.8)*,* (5.9) *and* (5.10)*.*

5.5 Results and Discussions

In this section, limit cycle details are predicted by graphical approaches such as IDRL and proposed IDNP. Further, these predicted results are compared with the optimization results and verified through closed loop simulations for the system with:

- PID controller: $C(s) = \left(K_p + \frac{K_i}{s} + K_d s\right)$
- $[PI]^\alpha$ controller defined in (2.49): $C(s) = \left(K_p + \frac{K_i}{s}\right)^\alpha$
- $[PD]^\beta$ controller defined in (2.53): $C(s) = (K_p + K_d s)^\beta$
- $PI^\alpha D^\beta$ controller defined in (2.55): $C(s) = \left(K_p + \frac{K_i}{s^\alpha} + K_d s^\beta\right)$

For illustration, the following values are selected as system parameters: $M = 0.1$, $H = 0.5$, $a = 0.7$ and $K = 5$. The following values are selected as design specifications and bounds for controller parameters: $\omega_{gc} = 5\,rad/sec$, $\phi_m = 60°$, $\omega_l = 0.01\,rad/sec$, $\omega_h = 50\,rad/sec$, $A = -20\,dB$, $B = -20\,dB$, $K_p \in [0, 10]$, $K_i \in [0, 10]$, $K_d \in [0, 10]$, $\alpha \in [0, 1]$, $\beta \in [0, 1]$, $X_0 \in [0.5001, 1]$, $\omega_0 \in [0.001, 4.99]$. The controller, which is the outcome of this proposed optimization for the selected value of ω_l and ω_h has to ensure the rejection of (i) the load disturbance signal less than the selected ω_l and (ii) the high frequency measurement noise signal greater than the selected ω_h.

5.5.1 Solutions to Constrained Optimization Problem

The parameters of the controllers are obtained from the proposed optimization problem for suppressing the limit cycle magnitude. In general, the proposed optimization problem in section 5.4.2 is non-convex in nature which is tedious to solve analytically. Hence, a numerical approach is chosen. However, due to the existence of local minima, it usually leads to the sub-optimal solutions. Therefore, it is mandatory to solve the optimization problem repeatedly with sufficiently large number of randomly selected initial guesses.

The fmincon() solver available in MATLAB [161] is used for this purpose which simulates Sequential quadratic programming algorithm. For each controller case, 2000 random initial guesses are taken and the corresponding converged values are found to be unique. The results of the proposed optimization problem are presented in Table 5.1.

It is found that PD, PD^β and $[PD]^\beta$ are the only unique controllers obtained for the selected PID, $PI^\alpha D^\beta$ and $[PD]^\beta$ controller structures respectively which meet the desired

Table 5.1: Optimization results

Selected controller structure	Obtained unique controller	Optimization results						
		Controller Parameters					Limit cycle details	
		Kp	Ki	Kd	α	β	Magnitude X_0	Frequency $\omega_0\, rad/sec$
PID	PD	3.1062	0.0000	0.7960	–	–	0.6800	2.3727
$PI^{\alpha}D^{\beta}$	PD^{β}	1.9640	0.0000	1.1027	0.0000	0.8221	0.5625	1.2204
$[PD]^{\beta}$	$[PD]^{\beta}$	2.8144	0.0000	1.8729	0.0000	0.7101	0.5576	1.1052

specifications. Other controllers such as PI, PI^{α} and $[PI]^{\alpha}$ do not exist for the proposed optimization problem.

5.5.2 Limit Cycle Prediction for Servo System using IDRL

To perform limit cycle prediction using IDRL, the obtained controllers have to be proper and integer order TF. The proper and integer form of obtained controllers are given as follows :

- PD controller : $PD = K_p + K_d s$. It is improper due to $K_d s$. It is made biproper by including a filter coefficient ($N = 1000$). Then the PD controller structure becomes:

$$\begin{aligned} PD &= K_p + \frac{K_d N s}{s + N} \\ &= 3.1062 + \frac{796s}{s + 1000} \\ &= \frac{799.1062s + 3106.2}{s + 1000} \end{aligned}$$

- For simulating the fractional order controllers (FOCs): $PD^{\beta} = K_p + K_d s^{\beta}$ and $[PD]^{\beta} = [K_p + K_d s]^{\beta}$, Oustaloup Recursive Approximation (ORA) [56] with order (N) 4 is used over a band of frequency [0.001 to $1000\, rad/sec$]. The approximated FOCs are biproper [165] and are as follows:

  - PD^{β} Controller:

$$
\begin{aligned}
PD^{\beta} &= K_p + \frac{K_d s^{\beta}}{10^{-3}s^{\beta}+1} \\
&= 1.9640 + \frac{1.1027 s^{0.8221}}{10^{-3}s^{0.8221}+1} \\
&= \frac{\begin{array}{r} 251.6s^9 + 8.041*10^4 s^8 + 4.725*10^6 s^7 + 6.447*10^7 s^6 \\ +2.449*10^8 s^5 + 2.907*10^8 s^4 + 9.808*10^7 s^3 \\ + 7.996*10^6 s^2 + 1.409*10^5 s + 445.5 \end{array}}{\begin{array}{r} s^9 + 931.5s^8 + 1.735*10^5 s^7 + 6.98*10^6 s^6 \\ +6.073*10^7 s^5 + 1.14*10^8 s^4 + 4.604*10^7 s^3 \\ + 3.976*10^6 s^2 + 7.126*10^4 s + 226.4 \end{array}}
\end{aligned}
$$

– $[PD]^{\beta}$ Controller:

$$
\begin{aligned}
[PD]^{\beta} &= \left[K_p + \frac{K_d s}{0.001s+1}\right]^{\beta} \\
&= \left[2.8144 + \frac{1.8729 s}{0.001s+1}\right]^{0.7101} \\
&= \frac{\begin{array}{r} 100.5s^9 + 1.78*10^4 s^8 + 7.151*10^5 s^7 + 9.791*10^6 s^6 \\ +6.247*10^7 s^5 + 2.178*10^8 s^4 + 4.431*10^8 s^3 \\ + 5.267*10^8 s^2 + 3.4*10^8 s + 9.221*10^7 \end{array}}{\begin{array}{r} s^9 + 421.1s^8 + 3.969*10^4 s^7 + 1.056*10^6 s^6 \\ +1.051*10^7 s^5 + 5.033*10^7 s^4 + 1.303*10^8 s^3 \\ + 1.88*10^8 s^2 + 1.424*10^8 s + 4.43*10^7 \end{array}}
\end{aligned}
$$

For the given case study, the closed loop characteristic equation of the system with designed controllers are functions of X and ω. Hence, the root locus approach explained in section 5.2.1 is adopted for predicting the limit cycle details.

Here, OLTF is given as: $G_1(s, X)N_b(X)$. To predict the limit cycle details, the movement of the closed loop poles of this open loop transfer function for the selected ω is drawn by ranging the values of X from 0 to ∞. This pole movement forms a locus connecting all the operating points in the increasing direction of X and the number of locus drawn is equal to the number of closed loop poles. Limit cycle is ensured if there is an intersection between the locus drawn and the imaginary axis. Limit cycle is characterised by the value of X for which the locus crosses the imaginary axis as limit cycle magnitude X_0. And the crossing $j\omega$ value on the imaginary axis matching with the selected ω is termed as limit cycle frequency ω_0. If there is a crossing, then one has to check the stability of the limit cycle by applying the perturbation technique at the crossing point.

The limit cycle prediction for servo system with the obtained controllers using IDRL is shown in Fig. 5.9, Fig. 5.10 and Fig. 5.11. Table 5.2 shows the predicted limit cycle details using IDRL. For simulating fractional order PD^{β} and $[PD]^{\beta}$ controllers, ORA [56] with order (N) 4 is used over a band of frequency [0.001 to $1000\,rad/sec$].

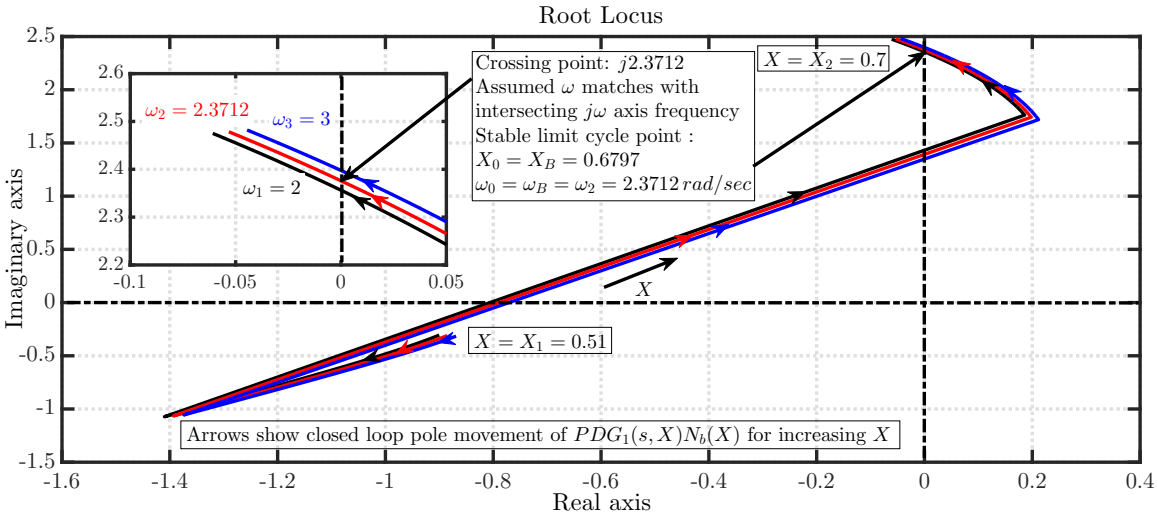

Figure 5.9: Intersection of family of IDRL of $PDG_1(s,X)N_b(X)$ with $j\omega$ axis

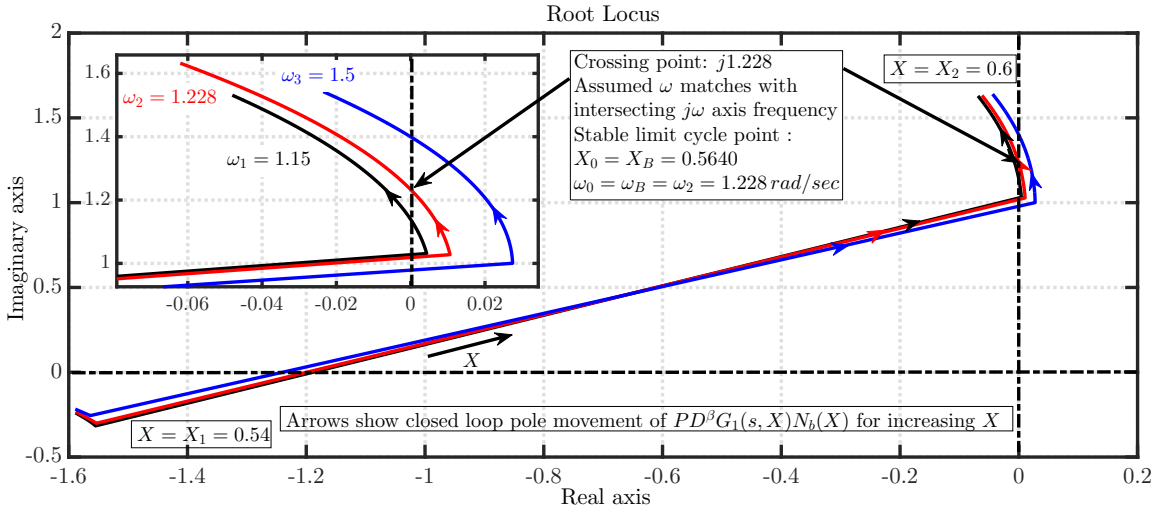

Figure 5.10: Intersection of family of IDRL of $PD^{\beta}G_1(s,X)N_b(X)$ with $j\omega$ axis

Table 5.2: Comparison of limit cycle details of system with obtained controllers using IDRL

System with	Limit cycle details	
	Magnitude, X_0	Frequency, $\omega_0\,rad/sec$
PD	0.6797	2.3712
PD^{β}	0.5640	1.2280
$[PD]^{\beta}$	0.5540	1.0390

It is observed that the predicted limit cycle magnitude for system with PD, PD^{β} and $[PD]^{\beta}$ controllers are closely matching with optimization results presented in Table 5.1. It

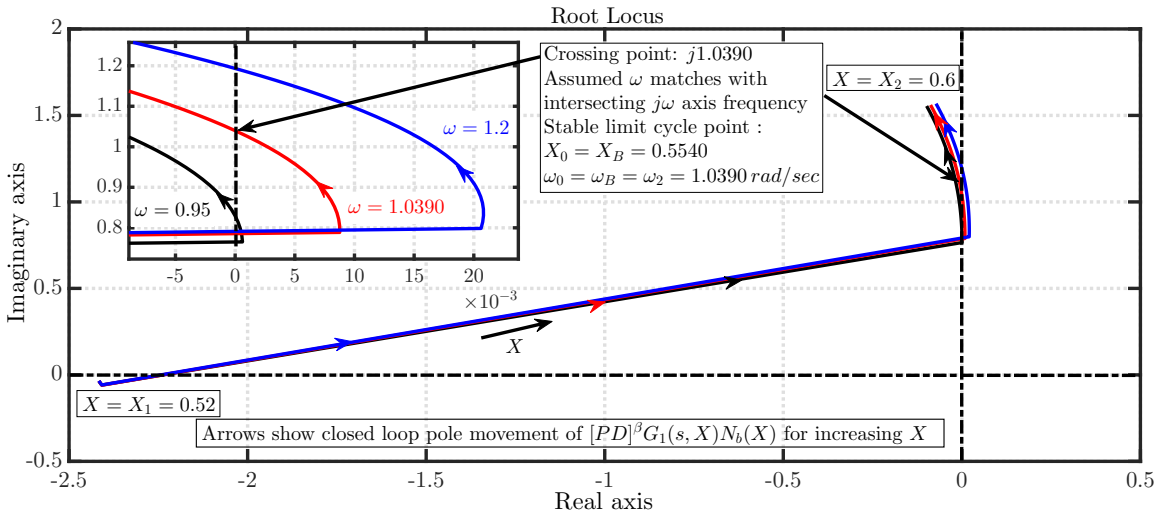

Figure 5.11: Intersection of family of IDRL of $[PD]^{\beta}G_1(s,X)N_b(X)$ with $j\omega$ axis

is also noted that the predicted limit cycle frequency obtained from PD, PD^{β} match with optimization results. However, a small deviation is found in the limit cycle frequency for system with $[PD]^{\beta}$ in comparison with optimization results.

5.5.3 Limit Cycle Prediction for Servo System using IDNP

Proposed IDNP is used to predict the limit cycle for the system with FOCs and IOCs. Let $C(s)$ be PD controller and the limit cycle condition (5.4) can be rewritten as:

$$PDG_1(s,X) = \frac{K(K_p + K_d s)}{s(s + a + \frac{4M}{\pi X \omega})}\bigg|_{X_0,\omega_0} = \frac{-1}{N_b(X)}\bigg|_{X_0} \tag{5.14}$$

For illustration, the selected set of (X,ω) are : X = [0.51545; 0.53; 0.55; 0.6799; 0.9] and ω =[0.454; 1.5; 2; 2.3729; 5]. From Fig. 5.12, it is found that crossing takes place for curves corresponding to two sets of (X,ω). First crossing takes place when (X_1,ω_1) : $(0.51545, 0.454)$. For an increase in X from this point, it is found that the Nyquist plot of $PDG_1(s, X_1 + \delta X_1)$ encloses the critical point $\frac{-1}{N_b(X_1+\delta X_1)}$ and hence the system produces an unstable limit cycle oscillation. Second crossing takes place when (X_4,ω_4) : $(0.6799, 2.3729)$. For an increase in X from this point, it is found that the critical point $\frac{-1}{N_b(X_4+\delta X_4)}$ is not enclosed by the Nyquist plot of $PDG_1(s, X_4 + \delta X_4)$ which produces stable limit cycle oscillation with magnitude $X_0 = X_4 = 0.6799$ and frequency $\omega_0 = \omega_4 = 2.3729\, rad/sec$. Similarly, the analysis can be done with PD^{β} and $[PD]^{\beta}$ with set of (X,ω) values.

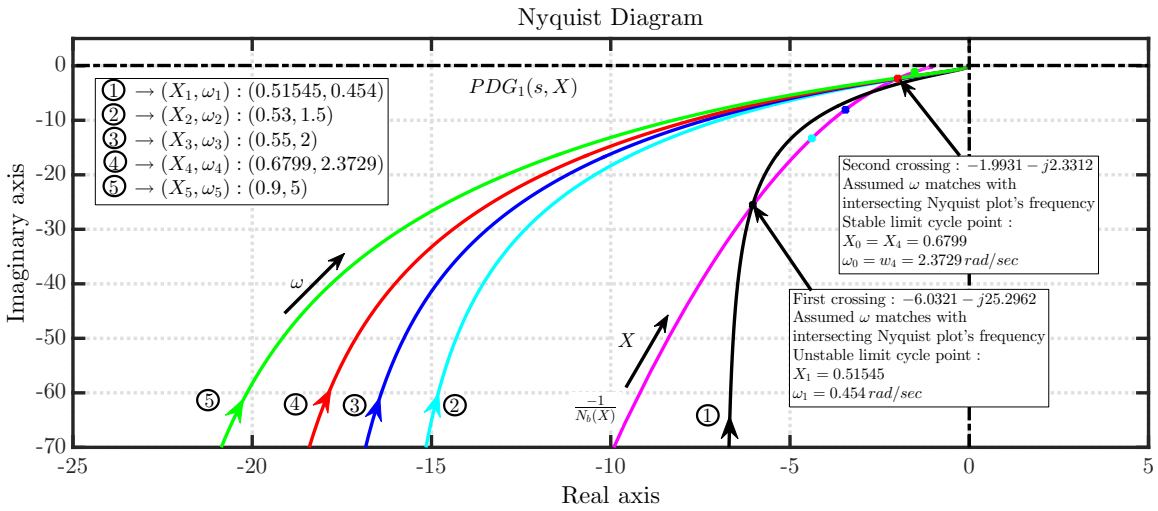

Figure 5.12: Intersection of family of IDNP of $PDG_1(s,X)$ with $\frac{-1}{N_b(X)}$

Fig. 5.13 shows the family of IDNP drawn for the system with PD^β (with Oustaloup approximation) controller. The selected set of (X,ω) are: X =[0.53 ; 0.5626 ; 0.8] and ω =[1.2; 1.2227; 2]. The observed stable limit cycle details are: $X_0 = X_2 = 0.5626$ and $\omega_0 = \omega_2 = 1.2227\,rad/sec$.

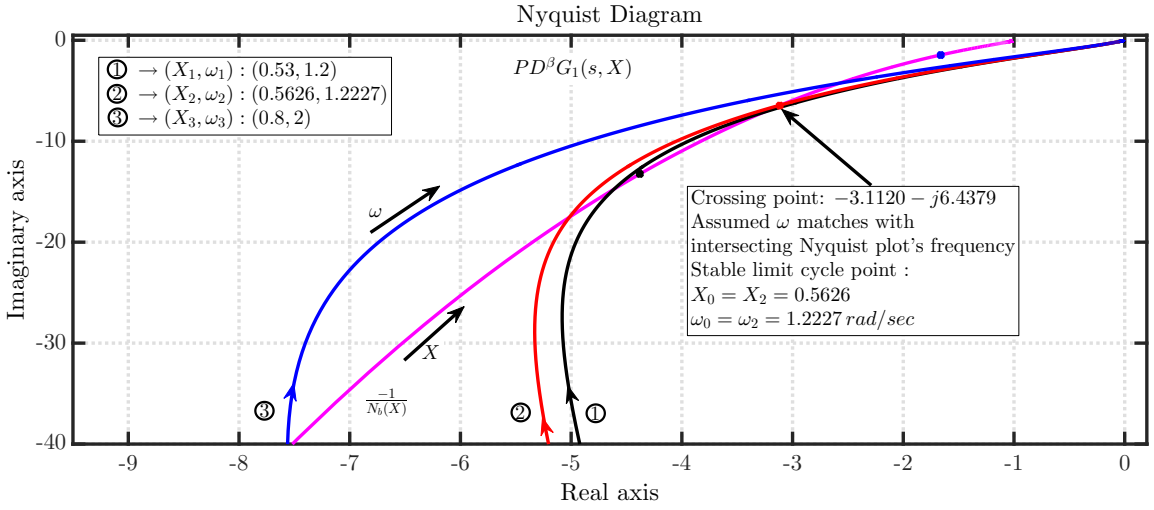

Figure 5.13: Intersection of family of IDNP of $PD^\beta G_1(s,X)$ (with Oustaloup approximation) with $\frac{-1}{N_b(X)}$

Further, simulation is carried out for PD^β by avoiding Oustaloup approximation. In order to predict the limit cycle details without any approximation of PD^β, it is realized as follows:

$$
\begin{aligned}
PD^{\beta}\Big|_{s=j\omega} &= K_p + K_d s^{\beta}\Big|_{s=j\omega} \\
&= K_p + K_d(j\omega)^{\beta} \\
&= K_p + K_d\omega^{\beta}(j)^{\beta} \\
&= K_p + K_d\omega^{\beta}\left[\cos\left(\frac{\pi}{2}\right) + j\sin\left(\frac{\pi}{2}\right)\right]^{\beta} \\
&= K_p + K_d\omega^{\beta}\left[\cos\left(\frac{\pi\beta}{2}\right) + j\sin\left(\frac{\pi\beta}{2}\right)\right] \\
&= \left[K_p + K_d\omega^{\beta}\cos\left(\frac{\pi\beta}{2}\right)\right] + j\left[K_d\omega^{\beta}\sin\left(\frac{\pi\beta}{2}\right)\right] \\
&= \left[K_p^2 + K_d^2\omega^{2\beta} + 2K_pK_d\omega^{\beta}\cos\left(\frac{\pi\beta}{2}\right)\right]^{\frac{1}{2}} \angle\left[tan^{-1}\left(\frac{K_d\omega^{\beta}\sin\left(\frac{\pi\beta}{2}\right)}{K_p + K_d\omega^{\beta}\cos\left(\frac{\pi\beta}{2}\right)}\right)\right] \\
PD^{\beta}\Big|_{s=j\omega} &= \left[K_p^2 + K_d^2\omega^{2\beta} + 2K_pK_d\omega^{\beta}\cos\left(\frac{\pi\beta}{2}\right)\right]^{\frac{1}{2}} e^{jtan^{-1}\left(\frac{K_d\omega^{\beta}\sin\left(\frac{\pi\beta}{2}\right)}{K_p + K_d\omega^{\beta}\cos\left(\frac{\pi\beta}{2}\right)}\right)} \qquad (5.15)
\end{aligned}
$$

Using (5.15), the family of IDNP drawn for the system with PD^{β} (without Oustaloup approximation) controller is shown in Fig. 5.14. The selected set of (X, ω) are: X =[0.53 ; 0.5623 ; 0.8] and ω =[1.2; 1.2182; 2]. The predicted limit cycle details are : $X_0 = X_2 = 0.5623$ and $\omega_0 = \omega_2 = 1.2182\, rad/sec$. From the results, it is observed that the predicted limit cycle details obtained with and without Oustaloup approximation for PD^{β} controller are close to the optimization results.

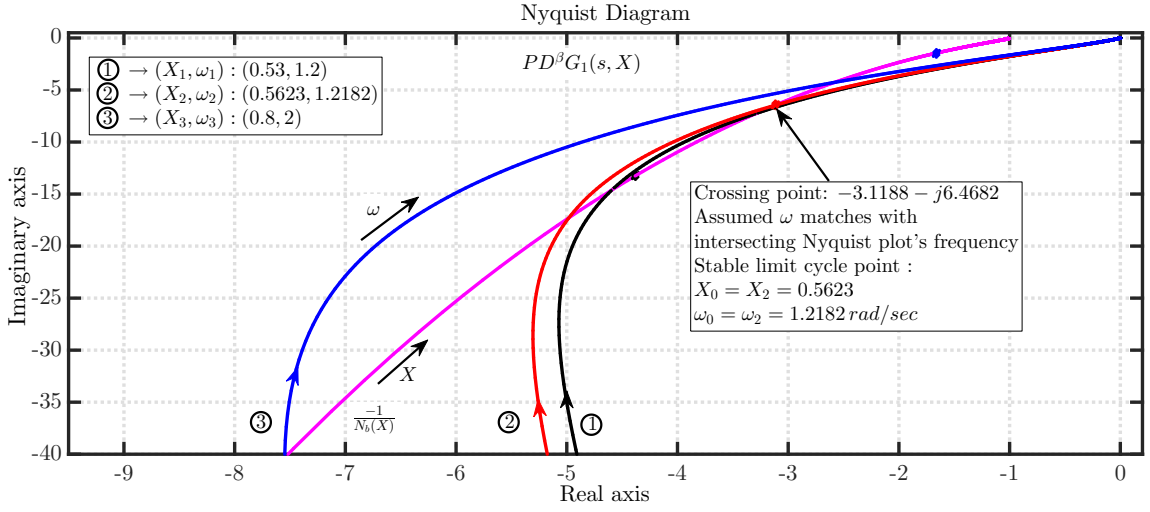

Figure 5.14: Intersection of family of IDNP of $PD^{\beta}G_1(s, X)$ (without Oustaloup approximation) with $\frac{-1}{N_b(X)}$

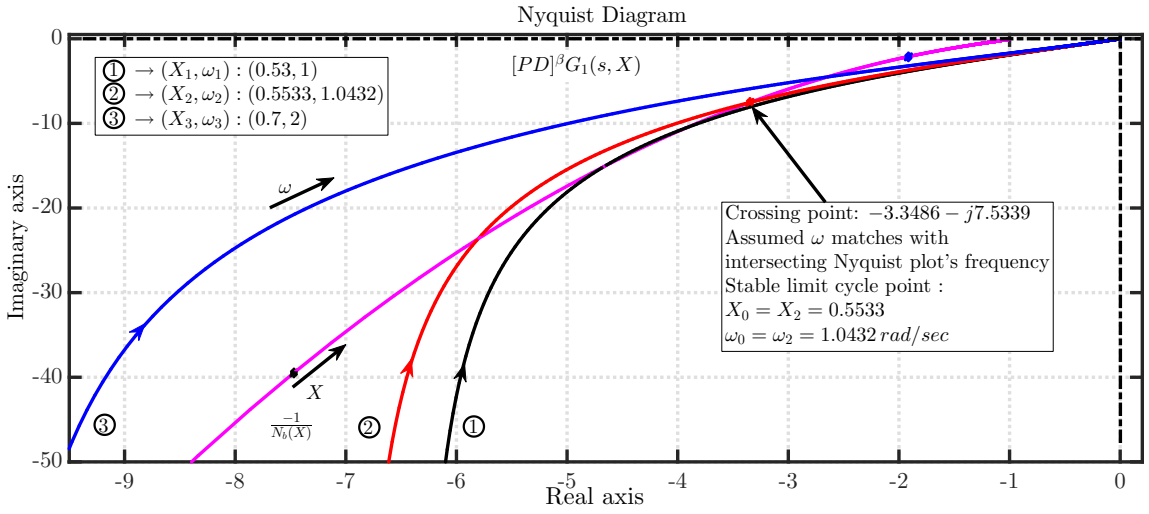

Figure 5.15: Intersection of family of IDNP of $[PD]^{\beta}G_1(s, X)$ (with Oustaloup approximation) with $\frac{-1}{N_b(X)}$

Fig. 5.15 shows the family of IDNP drawn for the system with $[PD]^{\beta}$ (with Oustaloup approximation) controller. The selected set of (X, ω) are : X =[0.53; 0.5533; 0.7] and ω =[1; 1.0432; 2]. The observed stable limit cycle details are: $X_0 = X_2 = 0.5533$ and $\omega_0 = \omega_2 = 1.0432\, rad/sec$. It is found that the predicted limit cycle magnitude matches with the optimization result, but the frequency deviates slightly which is similar to prediction using IDRL.

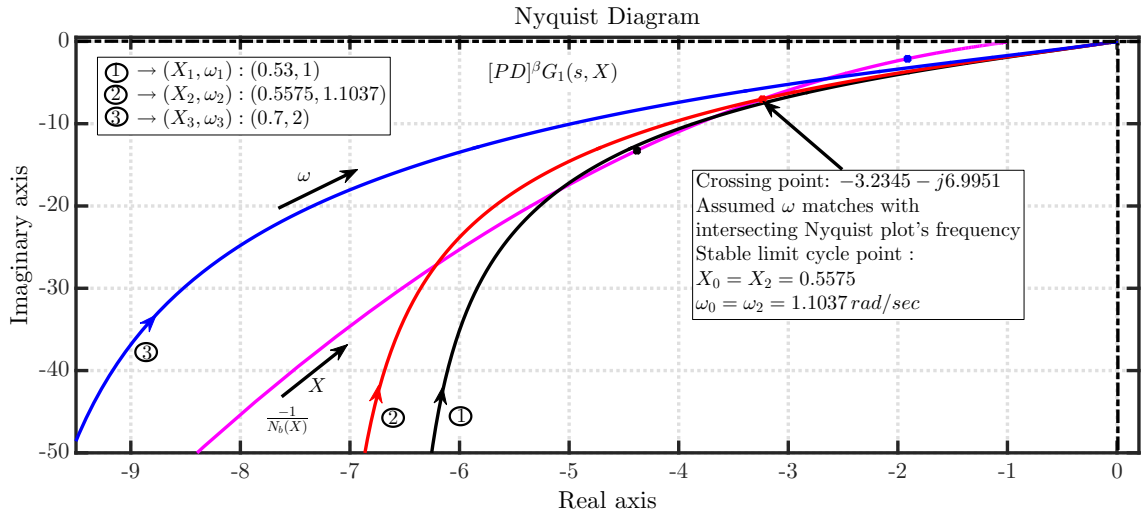

Figure 5.16: Intersection of family of IDNP of $[PD]^{\beta}G_1(s, X)$ (without Oustaloup approximation) with $\frac{-1}{N_b(X)}$

By avoiding Oustaloup approximation for $[PD]^{\beta}$, it is realized as follows :

$$
\begin{aligned}
[PD]^{\beta}\Big|_{s=j\omega} &= (K_p + K_d s)^{\beta}\Big|_{s=j\omega} \\
&= (K_p + jK_d\omega)^{\beta} \\
&= \left(\left[K_p^2 + K_d^2\omega^2\right]^{\frac{1}{2}} \angle\left[tan^{-1}\left(\frac{K_d\omega}{K_p}\right)\right]\right)^{\beta} \\
[PD]^{\beta}\Big|_{s=j\omega} &= \left[K_p^2 + K_d^2\omega^2\right]^{\frac{\beta}{2}} e^{\,j\beta tan^{-1}\left(\frac{K_d\omega}{K_p}\right)}
\end{aligned} \tag{5.16}
$$

Using (5.16), the family of IDNP drawn for the system with $[PD]^{\beta}$ (without Oustaloup approximation) controller is shown in Fig. 5.16. The selected set of (X, ω) are: X =[0.53; 0.5575; 0.7] and ω =[1; 1.1037; 2]. The observed limit cycle details are : $X_0 = X_2 = 0.5575$ and $\omega_0 = \omega_2 = 1.1037\,rad/sec$. These predicted limit cycle magnitude and frequency closely match with the optimization results.

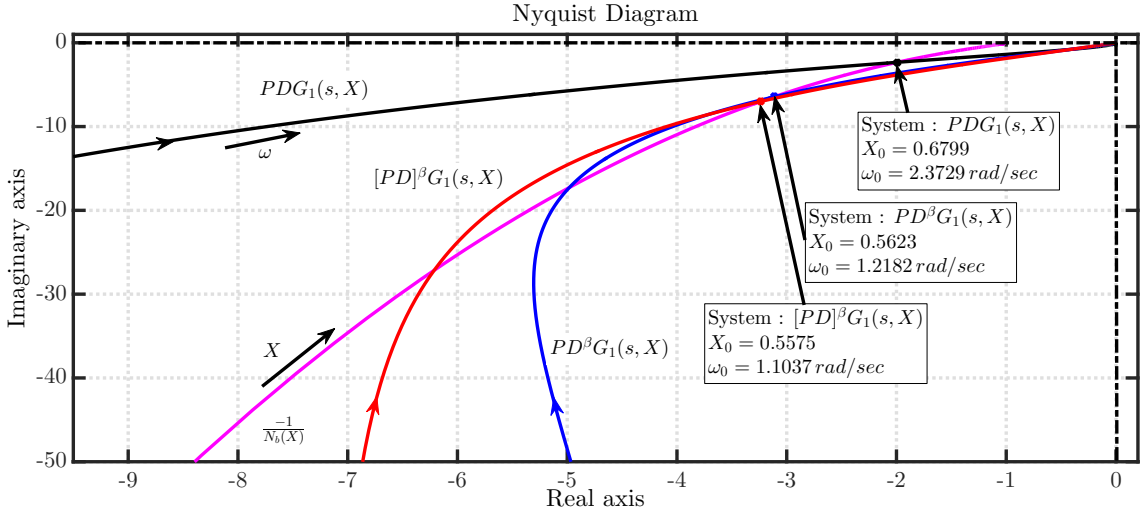

Figure 5.17: Intersection of family of IDNP of $C(s)G_1(s,X)$ for PD, PD^{β} and $[PD]^{\beta}$ with $\frac{-1}{N_b(X)}$

Fig. 5.17 shows the IDNP drawn for the system with PD, PD^{β} and $[PD]^{\beta}$ controllers. It is observed that $[PD]^{\beta}$ has highly suppressed the limit cycle magnitude when compared to other controllers.

5.5.4 Limit Cycle Verification Using Closed Loop Simulation

The closed loop simulation for the system shown in Fig. 5.7 is performed by constructing a SIMULINK patch-up to verify the limit cycle details.

The closed loop system considered in Fig. 5.7 is nonlinear and the effect of the nonlinearity is present both in transient and steady state. In order to validate the obtained controllers in the closed loop simulation, the effect of nonlinearity during transient has to be nullified [156] (i.e. $N_b(X) = 1\angle 0^\circ$ and $N_r(X_1) = 0$) which in turn satisfy the constraints (5.7), (5.8), (5.9) and (5.10) and hence, appropriate command input $r(t)$ should be selected. It is found that, beyond the step reference input $r(t) = 25u(t)$, the effect of nonlinearity during transient is highly suppressed and mimics the linear simulation response. This ensures the validation of these constraints during the course of optimization process.

In this work, closed loop simulation for the system shown in Fig. 5.7 is performed with step command input (magnitude $= 30$). During transient, the value of X and ω are 19 and $2.2065\,rad/sec$ respectively for the step input $r(t) = 30u(t)$. Hence, the value of $N_b(X) = 0.9933\angle -1.8821^\circ$ and $N_r(X_1) = 0.003036$ during transient. Since we designed the controller to meet the loop performance for $N(X) = 1\angle 0^\circ$ and $N_r(X1) = 0$, the transient responses for this reference with linear and nonlinear simulation match closely as can be seen from Fig. 5.18.

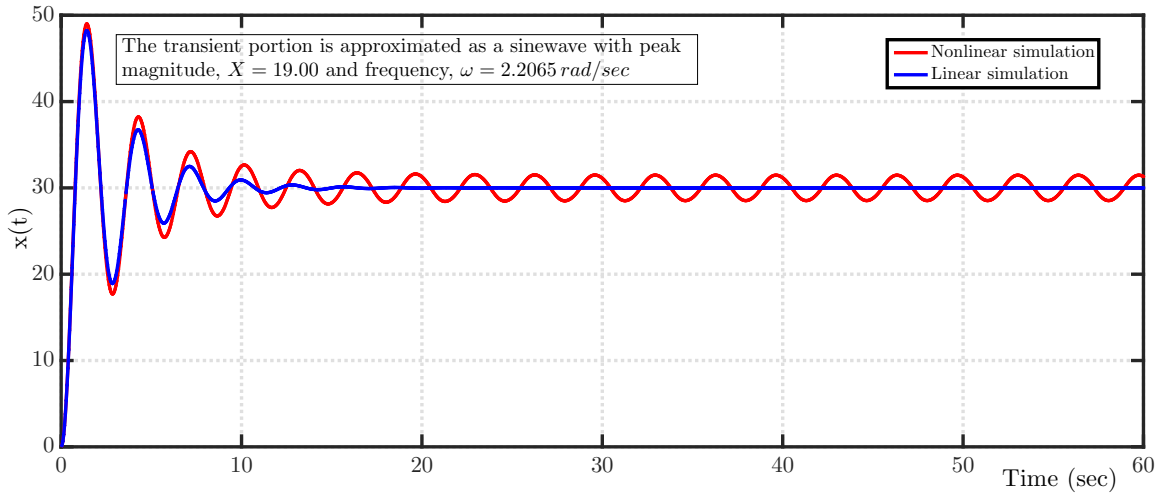

Figure 5.18: Linear and nonlinear simulation of servo system

It is found that the system with PD controller produces sustained oscillation magnitude $Y = X_0 - H = 0.1188$ at steady state with limit cycle magnitude $X_0 = 0.6188$ and frequency $\omega_0 = 1.9570\,rad/sec$. This limit cycle behaviour is completely eliminated for system with PD^β and $[PD]^\beta$ controllers as shown in the Fig. 5.19. The zoomed view of the plant output $y(t)$ during transient is shown in Fig. 5.20 and during steady state is shown in Fig. 5.21. It must be noted that Oustaloup approximation is considered for fractional-order term. The order of approximation is taken as 4 and is considered over the band of

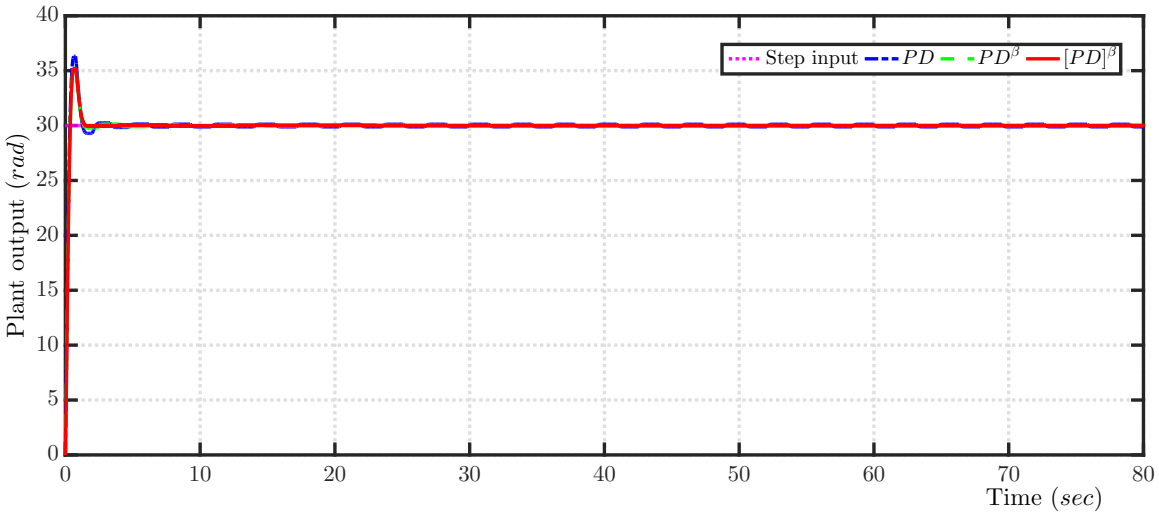

Figure 5.19: Closed loop response of system with PD, PD^{β}, $[PD]^{\beta}$ controllers

frequency $[0.001, 1000]\, rad/sec$. The respective controller output is shown in Fig. 5.22.

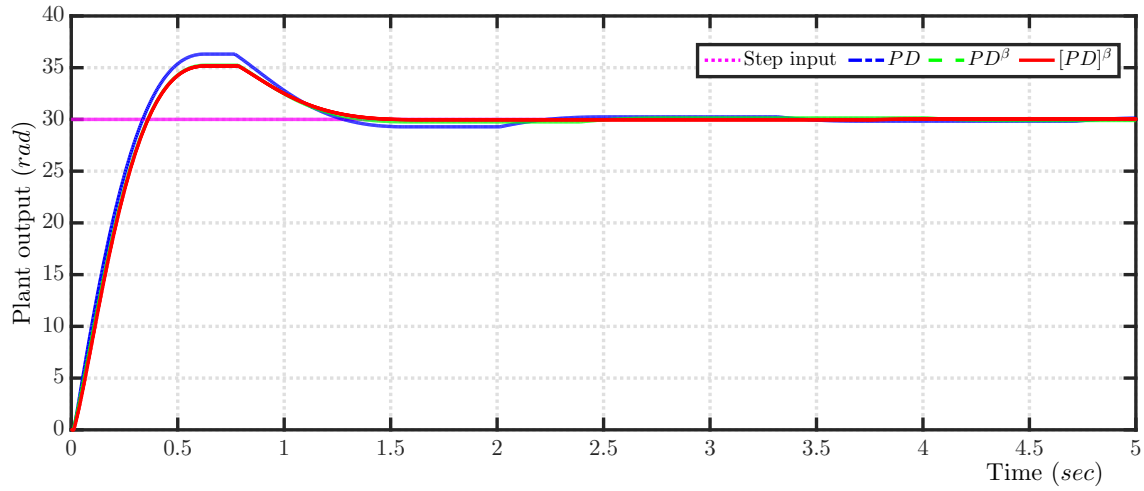

Figure 5.20: Zoomed view of Fig. 5.19 during transient

5.5.5 Limit Cycle Performance Comparison with Various Controllers

The predicted limit cycle details (X and ω) from IDRL, proposed IDNP and optimization results are shown in Table 5.3. It is found that the predicted limit cycle details for system with PD and PD^{β} controllers using graphical approaches matched with the optimization results. Whereas in the case of system with $[PD]^{\beta}$ controller, the predicted limit cycle magnitude using graphical approaches alone matched with the optimization results but not

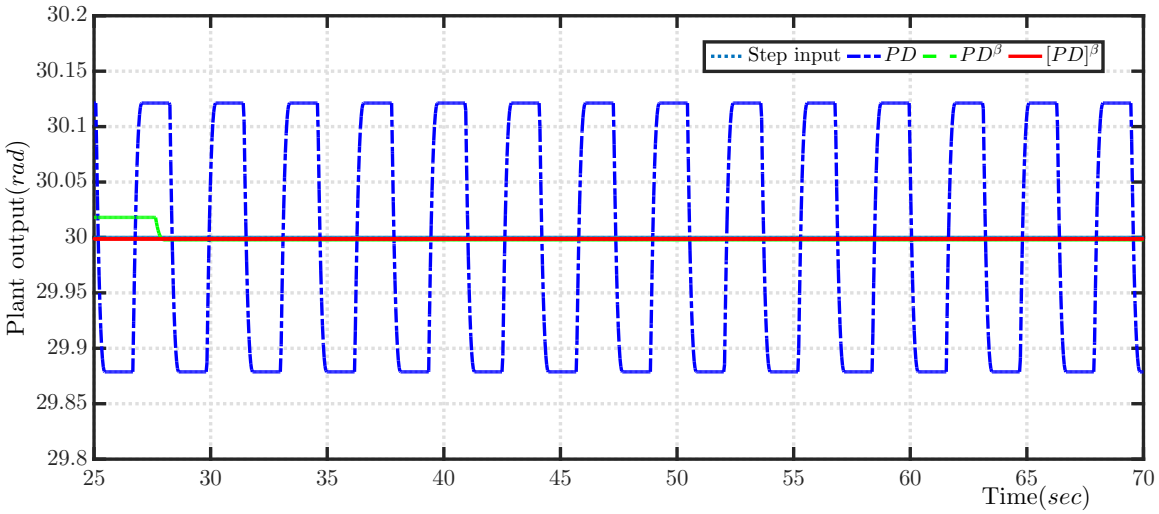

Figure 5.21: Zoomed view of Fig. 5.19 during steady state

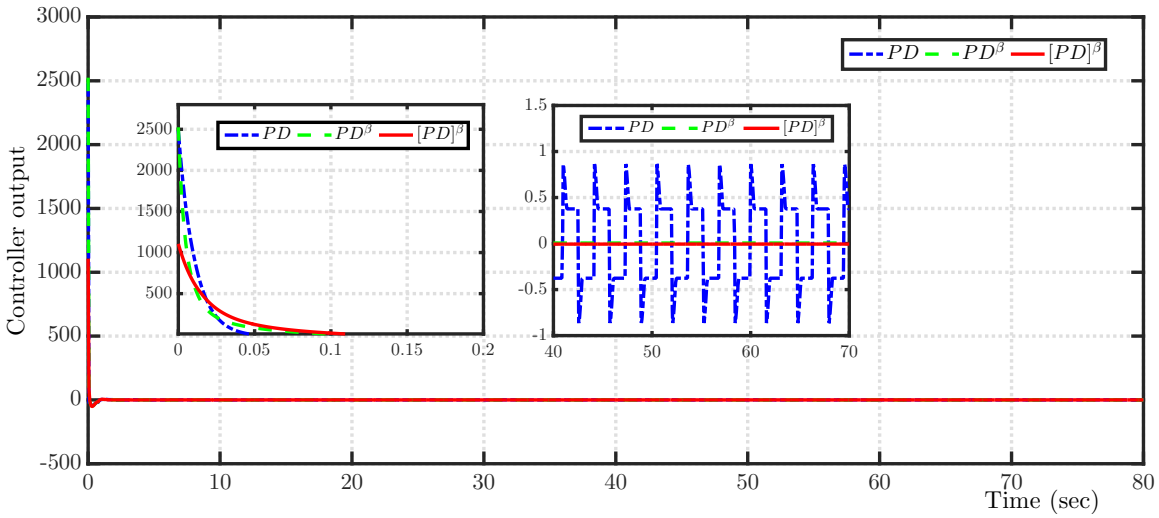

Figure 5.22: Controller response of system with PD, PD^{β}, $[PD]^{\beta}$ controllers

the limit cycle frequency. A small deviation was observed in the predicted limit cycle frequency using IDRL in comparison with IDNP and optimization results. It is due to the Oustaloup approximation of $[PD]^{\beta}$. This shows IDNP is superior to IDRL in the case of limit cycle prediction for system with $[PD]^{\beta}$ controller.

These predicted limit cycle details (X and ω) are validated through closed loop simulation. In case of system with PD controller, it is observed that the predicted values are not that close to the closed loop simulation values. This is due to the reduction in the low pass filtering effect [141] of the system with obtained unique PD controller through PID structure. Whereas in case of system with fractional controllers PD^{β} and $[PD]^{\beta}$,

Table 5.3: Comparison of limit cycle details

System with	Limit cycle details	Graphical approach			Optimization results	Closed loop simulation (actual values)		
		IDRL	IDNP (Proposed)			Limit cycle oscillation $x(t)$	Sustained oscillation $y(t)$	Controller effort $J = \int_0^\infty \|u(t)\|^2 dt$
			with Oustaloup	without Oustaloup				
PD	Magnitude X_0	0.6797	—	0.6799	0.6800	0.6188	0.1188	$3.321 * 10^4$
	Frequency $\omega_0\, rad/sec$	2.3712	—	2.3729	2.3727	1.9570	1.9570	
PD^β	Magnitude X_0	0.5640	0.5623	0.5623	0.5625	Limit cycle does not exist	Limit cycle does not exist	$2.171 * 10^4$
	Frequency $\omega_0\, rad/sec$	1.2280	1.2227	1.2182	1.2204			
$[PD]^\beta$	Magnitude X_0	0.5540	0.5533	0.5575	0.5576	Limit cycle does not exist	Limit cycle does not exist	$1.274 * 10^4$
	Frequency $\omega_0\, rad/sec$	1.0390	1.0432	1.1037	1.1052			

this undesirable limit cycle behaviour is completely eliminated at steady state. However, the proposed optimization and prediction methods depict the presence of limit cycle. The limit cycle existence is assured by optimization results and graphical approaches under the assumption that the closed loop system offers very good low pass filtering effect. In reality, system with the controllers PD^β and $[PD]^\beta$ have offered poor low pass filtering effect which makes limit cycle prediction through graphical approaches and optimization inaccurate. Further, it is observed that $[PD]^\beta$ requires lesser control effort than the other obtained controllers.

5.6 Robustness Verification

In this section, performance of the system with designed controllers are observed under parameter uncertainty, disturbance and noise conditions. The detailed sensitivity and complementary sensitivity analysis are also carried out for the selected case study.

5.6.1 Performance Study under Parameter Uncertainty

To study the performance of the system with various designed controllers under parameter uncertainty, $\pm 15\%$ variation is imposed for the system parameters a, K, M and H around its nominal value. Table 5.4 shows the transient specifications and limit cycle oscillation details of system with PD, PD^β and $[PD]^\beta$ controllers under $\pm 15\%$ variation of system parameters. It is observed that there is no significant variation in its transient specifications

and limit cycle details from the nominal value.

Table 5.4: Performance study under parameter variation

System with	Parameter variations				Transient specifications		Limit cycle details	
	a	K	M	H	ω_{gc} rad/sec	ϕ_m deg	Magnitude X_0	Frequency $\omega_0\, rad/sec$
PD	0.595	4.25	0.085	0.425	4.46	56.40	0.6210	1.8318
	0.70	5.00	0.100	0.500	5.00	60.00	0.6188	1.9570
	0.805	5.75	0.115	0.575	5.54	63.10	0.6159	2.0466
PD^{β}	0.595	4.25	0.085	0.425	4.45	57.80	Limit cycle doesn't exist	
	0.70	5.00	0.100	0.500	5.00	59.90		
	0.805	5.75	0.115	0.575	5.54	61.60		
$[PD]^{\beta}$	0.595	4.25	0.085	0.425	4.43	57.90	Limit cycle doesn't exist	
	0.70	5.00	0.100	0.500	4.99	59.60		
	0.805	5.75	0.115	0.575	5.54	60.90		

5.6.2 Performance Study under Disturbance

To analyse the performance of the system under plant output disturbance, a slow time varying signal shown in Fig. 5.23 of frequency $\omega = 0.01\, rad/sec$ is applied between $40^{th}-50^{th}\, sec$. Fig. 5.24 shows the output responses of the system under output disturbance condition and observed that all the designed controllers are capable to reject the effect of output disturbance. Fig. 5.25 shows the zoomed view of the system response $y(t)$.

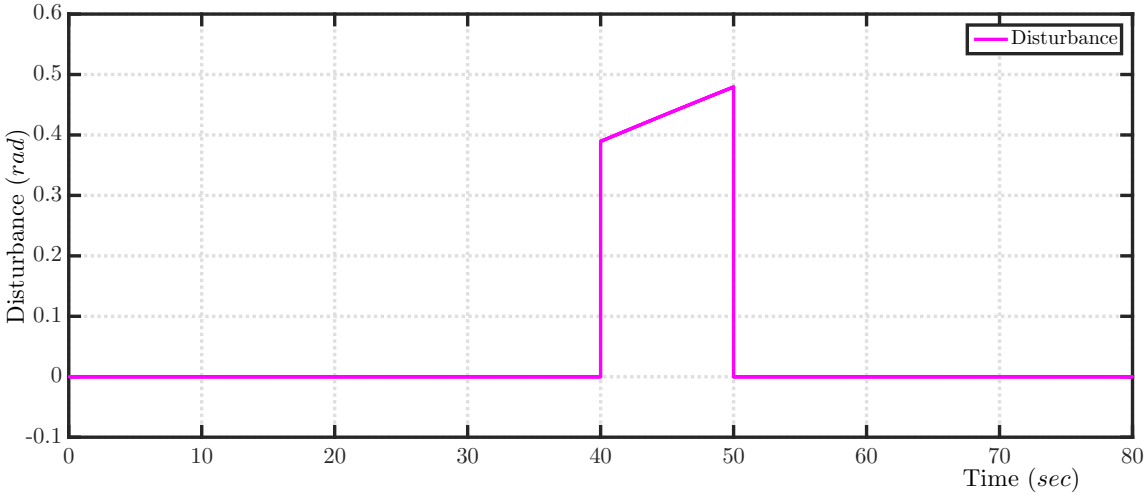

Figure 5.23: Low frequency disturbance signal

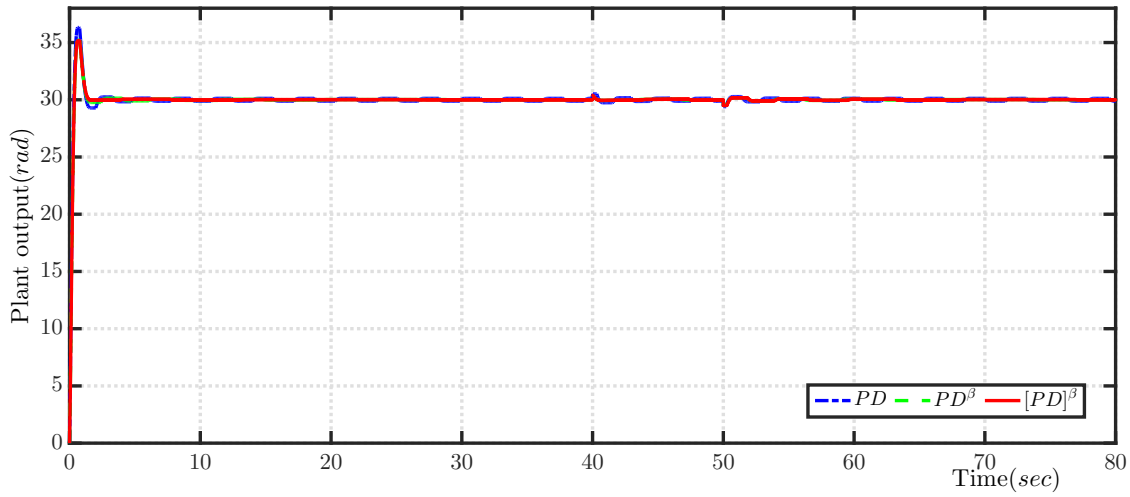

Figure 5.24: Closed loop system response

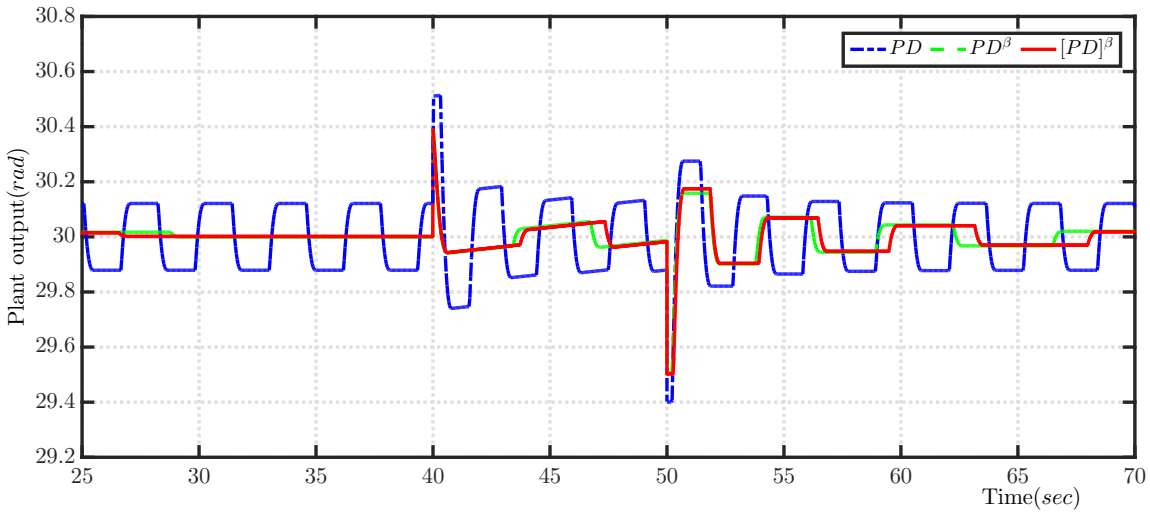

Figure 5.25: Zoomed view of Fig. 5.24 during disturbance

5.6.3 Performance Study under Noise

To analyse the effect of measurement noise in the closed loop system, a Gaussian noise signal shown in Fig. 5.26 of Mean $= 0$ and Standard Deviation $= 0.1$ is introduced between $40^{th} - 50^{th}$ sec. The output response of the system under noise with various controllers are shown in Fig. 5.27 and its zoomed response is shown in Fig. 5.28. It is seen from the response that the measurement noise is completely eliminated for all controllers.

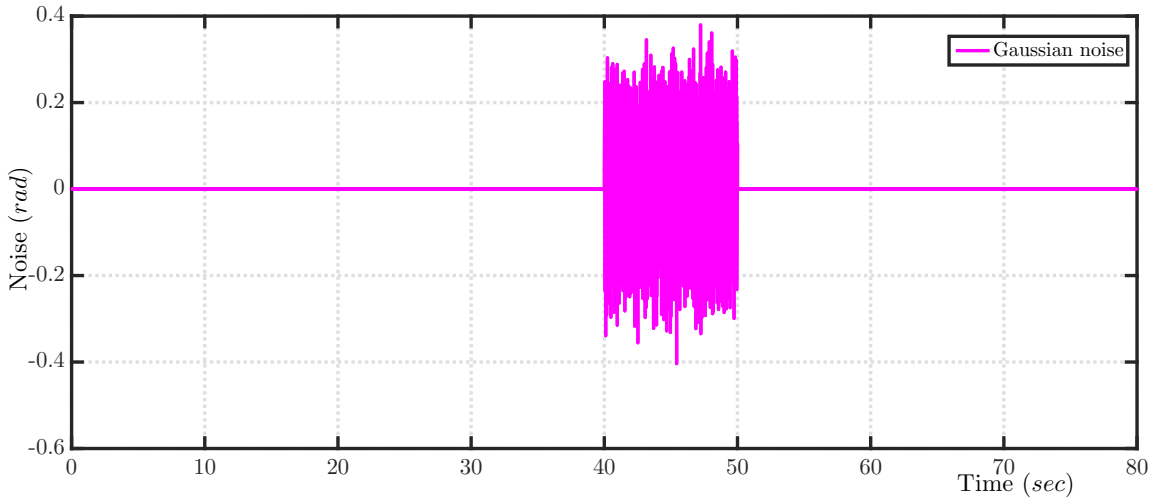

Figure 5.26: Measurement noise signal

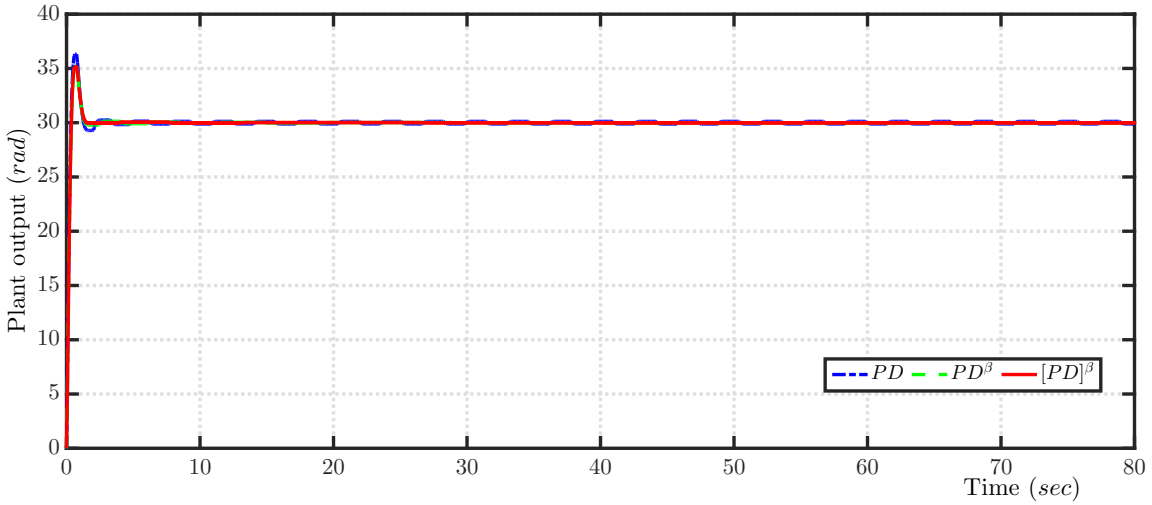

Figure 5.27: Closed loop system response

5.6.4 Sensitivity and Complementary Sensitivity Analysis

The robustness measures M_S, M_T, assured stability margins (GM and PM) and Bandwidth (ω_{BW}) are obtained from Fig. 5.29 for system with all controllers and are shown in Table 5.5. The obtained values are within the limits specified in the proposed optimization problem for tuning various controller parameters. Since, sensitivity and complementary sensitivity analysis are carried (i) with the negligence of nonlinearities during transient period and (ii) without carrying out the approximation of FOCs, the comparison of the obtained results with the actual closed loop simulation results are not attempted.

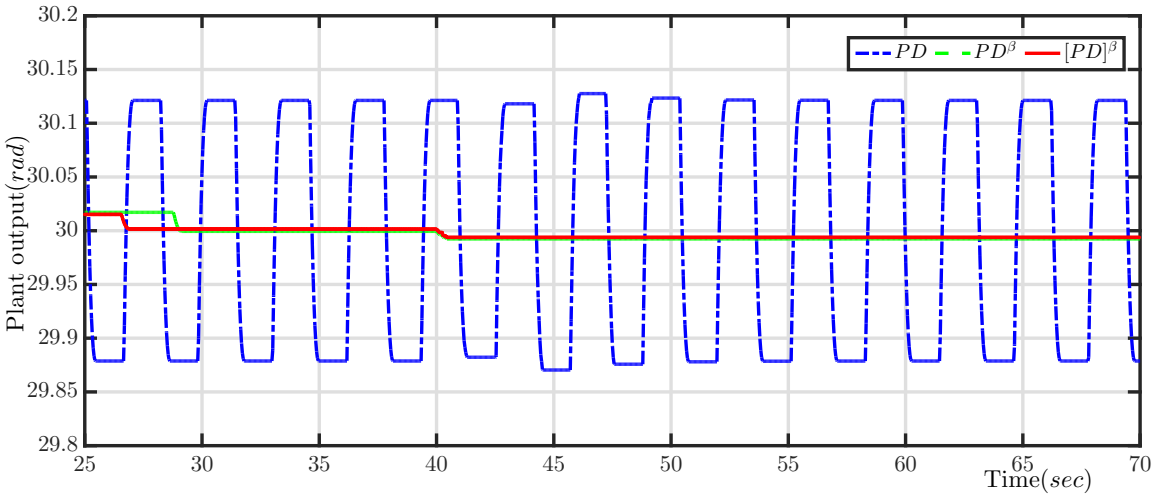

Figure 5.28: Zoomed view of Fig. 5.27

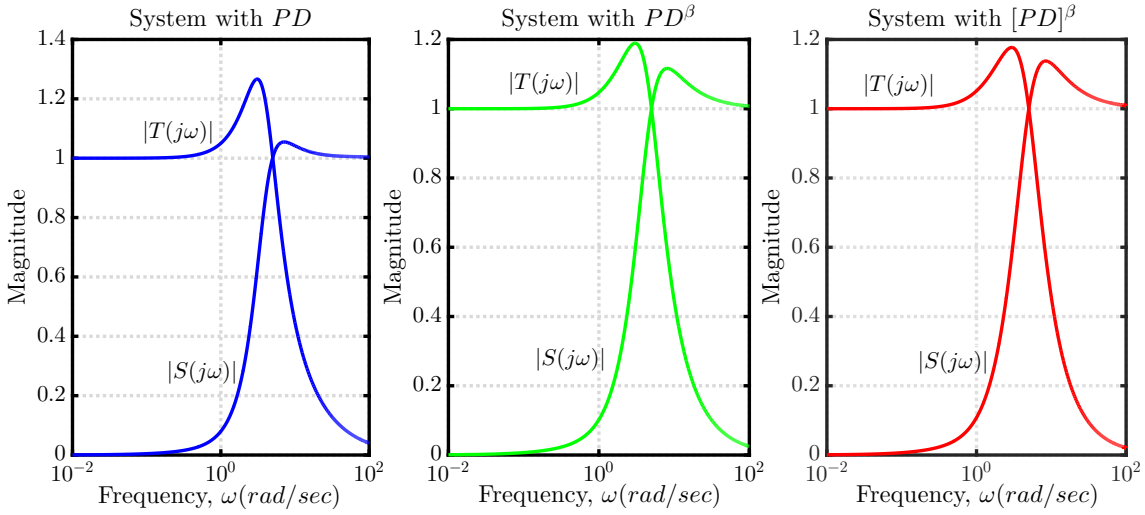

Figure 5.29: $|S(j\omega)|$ and $|T(j\omega)|$ plots of system with controllers

Table 5.5: Observations from $|S(j\omega)|$ and $|T(j\omega)|$ plots

System with	From $\|S(j\omega)\|$ plot	From $\|T(j\omega)\|$ plot
PD	$M_S = 1.0546$; $GM \geq 25.7171\,dB$; $PM \geq 56.6030°$	$M_T = 1.2665$; $\omega_{BW} = 6.8210$
PD^β	$M_S = 1.1163$; $GM \geq 19.6453\,dB$; $PM \geq 53.2201°$	$M_T = 1.1891$; $\omega_{BW} = 7.0117$
$[PD]^\beta$	$M_S = 1.1376$; $GM \geq 18.3449\,dB$; $PM \geq 52.1445°$	$M_T = 1.1768$; $\omega_{BW} = 7.1226$

5.7 Summary

In this chapter, an optimization problem is presented to tune the FOCs and IOC parameters to suppress the limit cycle magnitude by meeting the desired closed loop specifications for system with multiple nonlinearities. To predict the limit cycle for the system with the obtained unique controllers PD, PD^{β} and $[PD]^{\beta}$ controllers, an IDNP is developed. These predicted results are compared with optimization results, IDRL and are validated through closed loop simulation. It is also observed that the performance of the system with the designed controllers are robust towards system parameter uncertainty, disturbance and noise conditions.

Chapter 6

Conclusions and Future Scope

This research work deals with fractional controllers for complex valued systems and system with multiple nonlinearities.

The summary of this research work is as follows:

(i) A modified plant structure comprising complex coefficient plus fractional complex order plant with dead time model was proposed as a universal plant structure. A unified Fractional Order Controllers (FOCs) and Fractional Complex Order Controller (FCOC) parameter expressions were derived for the proposed plant structure to meet the Wang et al specifications. Simulations were carried out for two different plants to validate the obtained unified expressions.

(ii) Complex Coefficient Integer Order Controllers (CCIOCs) were proposed for the universal plant structure. The unified expressions of CCIOCs and real valued Integer Order Controllers (IOCs) were derived for complex valued universal plant to meet the desired specifications. Three different complex valued case studies were chosen to validate the obtained CCIOCs and real valued IOCs. It was observed that only CCIOCs with plant had the ability to satisfy the constraints both in positive frequency (ω^+) and negative frequency (ω^-). Also, CCIOCs had better stability and robustness to parameter uncertainty than real valued IOCs which was observed from its sensitivity and complementary sensitivity analysis. Due to this, an improved frequency domain and equivalent time domain performance were achieved. Hence, CCIOCs were suggested for controlling complex valued plants. To show the superiority of fractional controllers, tuning of complex coefficient fractional complex order controllers are proposed to satisfy the constraints both in ω^+ and ω^- through optimization technique. The proposed structure with unified controller expressions obtained in (i) and (ii) greatly reduce the effort of controller tuning for control engineering

practitioners.

(iii) Superiority of FOCs were investigated in achieving better limit cycle suppression in comparison with IOCs for system with multiple nonlinearities. Servo position control system with backlash and relay nonlinearities was chosen as a case study for system with multiple nonlinearities. An optimization problem was formulated to tune IOCs and FOCs in addition to meet desired closed loop specifications. It is observed that limit cycle got eliminated in the case of system with FOCs in comparison with IOCs. Further, Input Dependent Nyquist Plot (INDP) is also proposed to predict the limit cycle for system with multiple nonlinearities and results are compared with existing input dependent root locus, optimization results and are validated through closed loop simulation. This investigation made an effective use of Describing Function (DF) of the nonlinearity for design and analysis of control systems.

The future directions of the research work carried out in this thesis are as follows:

- The obtained unified expressions of IOCs, FOCs, CCIOCs and FCOC can be (i) exercised on real time systems having viscoelastic property (ii) extended to include stability constraints to tune controllers and (iii) incorporated in the existing MATLAB toolbox.

- Improving the accuracy of the limit cycle prediction by incorporating the higher order harmonic information of the loop through DF matrix approach [166] for system with multiple nonlinearities. Using the higher order harmonic information, a better controller can be designed. Another possible future work is to predict the limit cycle details for universal plant structure with multiple nonlinearities using IDNP. The other potential future directions are extending the proposed way of limit cycle prediction and suppression for multiple input multiple output systems with multiple nonlinearities.

Bibliography

[1] K. B. Oldham and J. Spanier, *The Fractional Calculus: theory and applications of differentiation and integration to arbitrary order*. New York: Academic Press, 1974, vol. 111.

[2] K. S. Miller and B. Ross, *An introduction to the fractional calculus and fractional differential equations*. New York: John Wiley & Sons, 1993.

[3] S. G. Samko, A. A.Kilbas, and O. I. Marichev, *Fractional integrals and derivatives: theory and applications*. Switzerland: Gordon and Breach Science Publishers, 1993.

[4] R. Gorenflo, *Fractional Calculus*. Vienna: Springer, 1997, pp. 277–290.

[5] P. L. Butzer and U. Westphal, *An introduction to fractional calculus*. World Scientific, 2000.

[6] P. J. Torvik and R. L. Bagley, "On the appearance of the fractional derivative in the behavior of real materials," *Journal of Applied Mechanics*, vol. 51, no. 2, pp. 294–298, 1984.

[7] A. A. Kilbas, H. M. Srivastava, and J. J. Trujillo, *Theory and applications of fractional differential equations*. Elsevier Science Limited, 2006, vol. 204.

[8] J. A. T. Machado, V. Kiryakova, and F. Mainardi, "Recent history of fractional calculus," *Communications in Nonlinear Science and Numerical Simulation*, vol. 16, no. 3, pp. 1140–1153, 2011.

[9] M. Caputo and F. Mainardi, "A new dissipation model based on memory mechanism," *Pure and Applied Geophysics*, vol. 91, no. 1, pp. 134–147, 1971.

[10] I. Podlubny, *An introduction to fractional derivatives, fractional differential equations, to methods of their solution and some of their applications*. San Diego: Academic Press, Inc., 1999, vol. 198.

[11] F. Mainardi, *Fractional calculus and waves in linear viscoelasticity: an introduction to mathematical models*. World Scientific, 2010.

[12] V. E. Tarasov, *Fractional Dynamics: Applications of Fractional Calculus to Dynamics of Particles, Fields and Media*. Springer, 2011.

[13] D. Baleanu, J. A. T. Machado, and A. C. J. Luo, *Fractional dynamics and control*. Springer, 2012.

[14] D. Cafagna, "Fractional calculus: A mathematical tool from the past for present engineers [past and present]," *IEEE Industrial Electronics Magazine*, vol. 1, no. 2, pp. 35–40, 2007.

[15] R. Herrmann, *Fractional calculus: An introduction for physicists*. World Scientific, 2011.

[16] M. D. Ortigueira, *Fractional calculus for scientists and engineers*. Springer, 2011, vol. 84.

[17] R. L. Bagley and P. J. Torvik, "A theoretical basis for the application of fractional calculus to viscoelasticity," *Journal of Rheology*, vol. 27, no. 3, pp. 201–210, 1983.

[18] R. C. Koeller, "Applications of fractional calculus to the theory of viscoelasticity," *Journal of Applied Mechanics*, vol. 51, no. 2, pp. 299–307, 1984.

[19] I. S. Jesus and J. A. T. Machado, "Development of fractional order capacitors based on electrolyte processes," *Nonlinear Dynamics*, vol. 56, no. 1-2, pp. 45–55, 2009.

[20] M. Axtell and M. E. Bise, "Fractional calculus application in control systems," in *proc. of IEEE National Aerospace and Electronics Conference*, 1990, pp. 563–566.

[21] B. M. Vinagre, , and Y. Q. Chen, "Fractional calculus applications in automatic control and robotics," in *proc. of IEEE Conference on Decision and Control*, 2002.

[22] B. M. Vinagre, C. A. Monje, and A. J. Calderón, "Fractional order systems and fractional order control actions," in *proc. of IEEE Conference on Decision and Control*, 2002, pp. 2550–2554.

[23] F. B. Tatom and B. Frank, "The relationship between fractional calculus and fractals," *Fractals*, vol. 3, no. 01, pp. 217–229, 1995.

[24] C. Alberto and F. Mainardi, *Fractals and fractional calculus in continuum mechanics*. Springer Verlag, 1997, vol. 378.

[25] W. Ahmad, R. Ei-Khazali, and A. S. Elwakil, "Fractional-order wien-bridge oscillator," *IET Electronics Letters*, vol. 37, no. 18, pp. 1110–1112, 2001.

[26] I. Petráš, "A note on the fractional-order chua's system," *Chaos, Solitons & Fractals*, vol. 38, no. 1, pp. 140–147, 2008.

[27] H. Schiessel, C. Friedrich, and A. Blumen, *Applications to problems in polymer physics and rheology*. World Scientific, 2000, vol. 376.

[28] R. Hilfer, P. L. Butzer, U. Westphal, J. Douglas, W. R. Schneider, G. Zaslavsky, T. Nonnemacher, A. Blumen, and B. West, *Applications of fractional calculus in physics*. World Scientific, 2000, vol. 5.

[29] R. L. Magin, *Fractional calculus in bioengineering*. Begell House Redding, 2006.

[30] R. L. Magin, "Fractional calculus models of complex dynamics in biological tissues," *Computers & Mathematics with Applications*, vol. 59, no. 5, pp. 1586–1593, 2010.

[31] N. Engheta, Nader, "On fractional calculus and fractional multipoles in electromagnetism," *IEEE Transactions on Antennas and Propagation*, vol. 44, no. 4, pp. 554–566, 1996.

[32] N. Engheia, "On the role of fractional calculus in electromagnetic theory," *IEEE Antennas and Propagation Magazine*, vol. 39, no. 4, pp. 35–46, 1997.

[33] K. B. Oldham, "Fractional differential equations in electrochemistry," *Advances in Engineering Software*, vol. 41, no. 1, pp. 9–12, 2010.

[34] M. D. Ortigueira and J. A. T. Machado, "Fractional calculus applications in signals and systems," *Signal Processing*, vol. 86, no. 10, pp. 2503–2504, 2006.

[35] B. Ross, "A brief history and exposition of the fundamental theory of fractional calculus," in *Fractional calculus and its applications*. Springer, 1975, pp. 1–36.

[36] V. S. Kiryakova, *Generalized fractional calculus and applications*. CRC Press, 1993.

[37] J. Sabatier, O. P. .Agrawal, and J. A. T. Machado, *Advances in fractional calculus*. Springer, 2007.

[38] D. Baleanu, Z. B. Güvenç, and J. A. T. Machado, *New trends in nanotechnology and fractional calculus applications*. Springer, 2010.

[39] S. Das, *Functional Fractional Calculus*. Berlin Heidelberg: Springer-Verlag, 2011.

[40] J. J. Distefano, A. R. Stubberud, and I. J. Williams, *Theory and problems of feedback and control systems*. New York: McGraw-Hill, 1967.

[41] Y. Q. Chen, "Ubiquitous fractional order controls," in *proc. of 2nd IFAC Workshop on Fractional Differentiation and Its Applications*, vol. 2, 2006.

[42] C. A. Monje, B. M. Vinagre, V. Feliu, and Y. Q. Chen, "Tuning and auto-tuning of fractional order controllers for industry applications," *Control Engineering Practice*, vol. 16, no. 7, pp. 798–812, 2008.

[43] C. A. Monje, Y. Q. Chen, B. M. Vinagre, D. Xue, and V. Feliu, *Fractional-order systems and controls: fundamentals and applications*. Springer, 2010.

[44] D. Valério and J. S. da Costa, *An introduction to fractional control*. London, UK: Institution of Engineering and Technology, 2013, vol. 91.

[45] D. P. M. D. Valério, "Fractional robust system control," Ph.D. dissertation, Universidade Técnica de Lisboa, 2005.

[46] R. Caponetto, *Fractional order systems: modeling and control applications*. World Scientific, 2010, vol. 72.

[47] Y. Chen and B. M. Vinagre, *Fractional-order systems and controls: fundamentals and applications*. Springer, 2010.

[48] I. Petráš, *Fractional-order nonlinear systems: modeling, analysis and simulation*. Springer, 2011.

[49] I. Petráš, Y. Q. Chen, and B. M. Vinagre, "A robust stability test procedure for a class of uncertain LTI fractional order systems," in *proc. of International Carpathian Control Conference (ICCC)*, may 2002, pp. 27–30.

[50] B. M. Vinagre, I. Podlubny, A. Hernandez, and V. Feliu, "Some approximations of fractional order operators used in control theory and applications," *Fractional calculus and applied analysis*, vol. 3, no. 3, pp. 231–248, 2000.

[51] I. Podlubny and I. Petráš and B. M. Vinagre and P. O'leary and L. Dorčák, "Analogue realizations of fractional-order controllers," *Nonlinear dynamics*, vol. 29, no. 1-4, pp. 281–296, 2002.

[52] G. Carlson and C. Halijak, "Approximation of fractional capacitors $(1/s)^{(1/n)}$ by a regular newton process," *IEEE Transactions on Circuit Theory*, vol. 11, no. 2, pp. 210–213, 1964.

[53] A. Charef, "Analogue realisation of fractional-order integrator, differentiator and fractional $PI^{\lambda}D^{\mu}$ controller," *IEE Proceedings - Control Theory and Applications*, vol. 153, no. 6, pp. 714–720, 2006.

[54] K. Matsuda and H. Fujii, "H(infinity) optimized wave-absorbing control - analytical and experimental results," *Journal of Guidance, Control, and Dynamics*, vol. 16, no. 6, pp. 1146–1153, 1993.

[55] S. D. Roy, "On the realization of a constant-argument immittance or fractional operator," *IEEE Transactions on Circuit Theory*, vol. 14, no. 3, pp. 264–274, 1967.

[56] A. Oustaloup, F. Levron, B. Mathieu, and F. M. Nanot, "Frequency-band complex noninteger differentiator: characterization and synthesis," *IEEE Transactions on Circuits and Systems I: Fundamental Theory and Applications*, vol. 47, no. 1, pp. 25–39, 2000.

[57] D. Xue, C. Zhao, and Y. Chen, "A modified approximation method of fractional order system," in *proc. of IEEE International Conference on Mechatronics and Automation*, 2006, pp. 1043–1048.

[58] D. Xue, Y. Q. Chen, and D. Atherton, *Linear Feedback Control - Analysis and Design with Matlab*. Philadelphia: SIAM Press, 2007, vol. 14, pp. 283–304.

[59] Y. Q. Chen and K. L. Moore, "Discretization schemes for fractional-order differentiators and integrators," *IEEE Transactions on Circuits and Systems I: Fundamental Theory and Applications,*, vol. 49, no. 3, pp. 363–367, 2002.

[60] Y. Chen, I. Petráš, and D. Xue, "Fractional order control - a tutorial," in *proc. of IEEE American Control Conference*, 2009, pp. 1397–1411.

[61] K. Diethelm, "An algorithm for the numerical solution of differential equations of fractional order," *Electronic transactions on numerical analysis*, vol. 5, no. 1, pp. 1–6, 1997.

[62] D. Heleschewitz and D. Matignon, "Diffusive realisations of fractional integrodifferential operators: structural analysis under approximation," 1998.

[63] R. S. Barbosa, J. A. T. Machado, and I. M. Ferreira, "PID controller tuning using fractional calculus concepts," *Fractional Calculus and Applied Analysis*, vol. 7, no. 2, pp. 119–134, 2004.

[64] M. S. Tavazoei, "From traditional to fractional PI control: a key for generalization," *IEEE Industrial Electronics Magazine*, vol. 6, no. 3, pp. 41–51, 2012.

[65] C. Yeroglu and N. Tan, "Note on fractional-order proportional–integral–differential controller design," *IET control theory & applications*, vol. 5, no. 17, pp. 1978–1989, 2011.

[66] I. Podlubny, "Fractional-order systems and $PI^{\lambda}D^{\mu}$-controllers," *IEEE Transactions on Automatic Control*, vol. 44, no. 1, pp. 208–214, 1999.

[67] C. A. Monje, *Design methods of fractional order controllers for industrial applications*, 2006.

[68] B. M. Vinagre, C. A. Monje, A. J. Calderón, and J. I. Suárez, "Fractional PID controllers for industry application. a brief introduction," *Journal of Vibration and Control*, vol. 13, no. 9-10, pp. 1419–1429, 2007.

[69] C. A. Monje, B. M. Vinagre, Y. Q.Chen, V. Feliu, P. Lanusse, and J. Sabatier, "Proposals for fractional $PI^{\lambda}D^{\mu}$ tuning," in *proc. of The First IFAC Symposium on Fractional Differentiation and its Applications (FDA)*, 2004, pp. 115–120.

[70] C. A. Monje, B. M. Vinagre, Y. Q. Chen, V. Feliu, P. Lanusse, and J. Sabatier, "Optimal tunings for fractional $PI^{\lambda}D^{\mu}$," *Fractional differentiation and its applications*, vol. 3, pp. 675–686, 2005.

[71] D. Valério and J. S. da Costa, "Tuning rules for fractional pid controllers," *IFAC Proceedings Volumes*, vol. 39, no. 11, pp. 28–33, 2006.

[72] C. Zhao, D. Xue, and Y. Q. Chen, "A fractional order PID tuning algorithm for a class of fractional order plants," in *proc. of IEEE International Conference on Mechatronics and Automation*, vol. 1, 2005, pp. 216–221.

[73] F. Padula and A. Visioli, "Tuning rules for optimal PID and fractional-order PID controllers," *Journal of Process Control*, vol. 21, no. 1, pp. 69–81, 2011.

[74] D. Xue, C. Zhao, and Y. Q. Chen, "Fractional order PID control of a DC-motor with elastic shaft: a case study," in *proc. of IEEE American control conference*, vol. 7, 2006, pp. 3182–3187.

[75] A. A. Kesarkar and N. Selvaganesan, "Investigation on superior performance by fractional controller for cart-servo laboratory set-up," *Advances in Electrical and Electronic Engineering*, vol. 12, no. 3, pp. 201–209, 2014.

[76] C. Wang, Y. Luo, and Y. Q. Chen, "An analytical design of fractional order proportional integral and [proportional integral] controllers for robust velocity servo," in *proc. of 4th IEEE Conference on Industrial Electronics and Applications*, May 2009, pp. 3448–3453.

[77] C. Wang, , and Y. Q. Chen, "Fractional order proportional integral (fopi) and [proportional integral] (fo[pi]) controller designs for first order plus time delay (foptd) systems," in *proc. of Chinese Control and Decision Conference*, June 2009, pp. 329–334.

[78] Y. Luo, Y. Q. Chen, C. Y. Wang, and Y. G. Pi, "Tuning fractional order proportional integral controllers for fractional order systems," *Journal of Process Control*, vol. 20, no. 7, pp. 823 – 831, 2010.

[79] Y. Q. Chen, H. Dou, B. M. Vinagre, and C. A. Monje, "A robust tuning method for fractional order PI controllers," in *proc. of Second IFAC Symposium on Fractional Derivatives and Applications*, 2006.

[80] H. S. Li and Y. Q. Chen, "A fractional order proportional and derivative (fopd) controller tuning algorithm," in *proc. of IEEE Chinese Control and Decision Conference*, July 2008, pp. 4059–4063.

[81] H. Li, Y. Luo, and Y. Q. Chen, "A fractional order proportional and derivative (fopd) motion controller: Tuning rule and experiments," *IEEE Transactions on Control Systems Technology*, vol. 18, no. 2, pp. 516–520, March 2010.

[82] Y. Luo, Y. Q. Chen, and Y. G. Pi, "Experimental study of fractional order proportional derivative controller synthesis for fractional order systems," *Mechatronics*, vol. 21, no. 1, pp. 204–214, 2011.

[83] Y. Luo and Y. Q. Chen, "Fractional-order [proportional derivative] controller for robust motion control: Tuning procedure and validation," in *proc. of IEEE American Control Conference*, June 2009, pp. 1412–1417.

[84] Y. Luo and Y. Q. Chen, "Fractional order [proportional derivative] controller for a class of fractional order systems," *Automatica*, vol. 45, no. 10, pp. 2446 – 2450, 2009.

[85] K. Khandani, A. A. Jalali, and M. R. Rahmani Mehdiabadi, "Robust complex order controller design for dc motors," in *proc. of 20th Iranian Conference on Electrical Engineering (ICEE2012)*, May 2012, pp. 900–903.

[86] Y. Q. Chen, C. H. Hu, and K. L. Moore, "Relay feedback tuning of robust PID controllers with iso-damping property," in *proc. of 42nd IEEE Conference on Decision and Control*, vol. 3. IEEE, 2003, pp. 2180–2185.

[87] A. Wallén, K. J. ÅRström, and T. Hägglund, "Loop-shaping design of PID controllers with constant Ti/Td ratio," *Asian Journal of Control*, vol. 4, no. 4, pp. 403–409, 2002.

[88] A. Koszewnik, T. Nartowicz, and E. Pawluszewicz, "Fractional order controller to control pump in festo mps ® pa compact workstation," in *proc. of 17th International Carpathian Control Conference (ICCC)*, 2016, pp. 364–367.

[89] T. Nartowicz, E. Pawluszewicz, and A. Mystkowski, "Robust fractional order controller for a linear active magnetic bearing system," in *proc. of 22nd International Conference on Methods and Models in Automation and Robotics (MMAR)*, Aug 2017, pp. 658–663.

[90] A. A. Kesarkar and N. Selvaganesan, "Tuning of robust PI^{α} / PD^{β} controller for generalized plant structure," in *proc. of IEEE International Conference on Recent Advancements in Electrical, Electronics and Control Engineering (IConRAEeCE)*, 2011, pp. 104–108.

[91] A. A. Kesarkar and N. Selvaganesan, "Design of fractional order robust controller for universal plant structure," in *proc. of Nirma University International Conference on Engineering*, Dec 2011, pp. 1–4.

[92] A. A. Kesarkar and N. Selvaganesan, "Novel tuning expressions for fractional order ($[PD]^{\beta}$ and $[PI]^{\alpha}$) controllers using a generalized plant structure," *Journal of Control Engineering and Applied Informatics*, vol. 17, no. 1, pp. 70–80, 2015.

[93] A. A. Kesarkar and N. Selvaganesan, "Investigating limit cycle performance and asymptotic bode behavior of fractional-order controllers," Ph.D. dissertation, Indian Institute of Space Science and Technology, 2015.

[94] M. P. de Barros and L. F. Lind, "On the splitting of a complex-coefficient polynomial," *IEE Proceedings G - Electronic Circuits and Systems*, vol. 133, no. 2, pp. 95–98, 1986.

[95] N. Bose and Y. Shi, "A simple general proof of kharitonov's generalized stability criterion," *IEEE Transactions on Circuits and Systems*, vol. 34, no. 10, pp. 1233–1237, 1987.

[96] S. Gataric and N. R. Garrigan, "Modeling and design of three-phase systems using complex transfer functions," in *proc. of 30th Annual IEEE Power Electronics Specialists Conference.Record. (Cat. No.99CH36321)*, 1999, pp. 691–697.

[97] L. Harnefors, "Modeling of three-phase dynamic systems using complex transfer functions and transfer matrices," *IEEE Transactions on Industrial Electronics*, vol. 54, no. 4, pp. 2239–2248, 2007.

[98] D. Henrion, J. Ježek, and M. Sebek, "Discrete-time symmetric polynomial equations with complex coefficients," *Kybernetika*, vol. 38, pp. 113–139, 2002.

[99] M. Hromcik, M. Sebek, and J. Ježek, "Complex polynomials in communications : motivation, algorithms, software," in *proc. of IEEE International Symposium on Computer Aided Control System Design*, 2002, pp. 291–296.

[100] E. Frank, "On the zeros of polynomials with complex coefficients," *Bulletin of the American Mathematical Society*, vol. 52, no. 2, pp. 144–157, 1946.

[101] S. Agashe, "A new general Routh-like algorithm to determine the number of rhp roots of a real or complex polynomial," *IEEE Transactions on Automatic Control*, vol. 30, no. 4, pp. 406–409, 1985.

[102] M. Benidir and B. Picinbono, "Extended table for eliminating the singularities in routh's array," *IEEE Transactions on Automatic Control*, vol. 35, no. 2, pp. 218–222, 1990.

[103] N. K. Bose, "Tests for Hurwitz and Schur properties of convex combination of complex polynomials," *IEEE Transactions on Circuits and Systems*, vol. 36, no. 9, pp. 1245–1247, 1989.

[104] S. S. Chen and J. S. H. Tsai, "A new tabular form for determining root distribution of a complex polynomial with respect to the imaginary axis," *IEEE Transactions on Automatic Control*, vol. 38, no. 10, pp. 1536–1541, 1993.

[105] M. Bodson and O. Kiselychnyk, "The complex Hurwitz test for the analysis of spontaneous self-excitation in induction generators," *IEEE Transactions on Automatic Control*, vol. 58, no. 2, pp. 449–454, 2013.

[106] N. Bose and Y. Shi, "Network realizability theory approach to stability of complex polynomials," *IEEE Transactions on Circuits and Systems*, vol. 34, no. 2, pp. 216–218, 1987.

[107] Y. Bistritz, "Stability criterion for continuous-time system polynomials with uncertain complex coefficients," *IEEE Transactions on Circuits and Systems*, vol. 35, no. 4, pp. 442–448, 1988.

[108] A. Katbab, F. Kraus, and E. I. Jury, "Some Schur-stability criteria for uncertain systems with complex coefficients," *IEEE Transactions on Circuits and Systems*, vol. 37, no. 9, pp. 1171–1176, 1990.

[109] J. Kogan, "Robust Hurwitz l_p stability of polynomials with complex coefficients," *IEEE Transactions on Automatic Control*, vol. 38, no. 8, pp. 1304–1308, 1993.

[110] W. C. Karl and G. C. Verghese, "A sufficient condition for the stability of interval matrix polynomials," *IEEE Transactions on Automatic Control*, vol. 38, no. 7, pp. 1139–1143, 1993.

[111] A. Dòria-Cerezo and M. Bodson, "Root locus rules for polynomials with complex coefficients," in *proc. of 21st Mediterranean Conference on Control and Automation*, 2013, pp. 663–670.

[112] S. Byun and C. Lee, "Pole assignment in rotating disk vibration control using complex modal state feedback," *Mechanical Systems and Signal Processing*, vol. 2, no. 3, pp. 225–241, 1988.

[113] Y. Ren, D. Su, and J. Fang, "Whirling modes stability criterion for a magnetically suspended flywheel rotor with significant gyroscopic effects and bending modes," *IEEE Transactions on Power Electronics*, vol. 28, no. 12, pp. 5890–5901, 2013.

[114] Y. Ren and J. Fang, "Complex-coefficient frequency domain stability analysis method for a class of cross-coupled antisymmetrical systems and its extension in MSR systems," *Mathematical Problems in Engineering*, vol. Article ID 765858, 2014.

[115] A. Dòria-Cerezo and M. Bodson, "Design of controllers for electrical power systems using a complex root locus method," *IEEE Transactions on Industrial Electronics*, vol. 63, no. 6, pp. 3706–3716, 2016.

[116] A. Dòria-Cerezo, M. Bodson, C. Batlle, and R. Ortega, "Study of the stability of a direct stator current controller for a doubly fed induction machine using the complex Hurwitz test," *IEEE Transactions on Control Systems Technology*, vol. 21, no. 6, pp. 2323–2331, 2013.

[117] X. Guo and J. M. Guerrero, "ABC-frame complex-coefficient filter and controller based current harmonic elimination strategy for three-phase grid connected inverter," *Journal of Modern Power Systems and Clean Energy*, vol. 4, no. 1, pp. 87–93, 2016.

[118] O. Troeng, B. Bernhardsson, and C. Rivetta, "Complex-coefficient systems in control," in *proc. of IEEE American Control Conference*, 2017, pp. 1721–1727.

[119] H. Yang, Y. Zhang, J. Liang, B. Xia, P. D. Walker, and N. Zhang, "Deadbeat control based on a multipurpose disturbance observer for permanent magnet synchronous motors," *IET Electric Power Applications*, vol. 12, no. 5, pp. 708–716, 2018.

[120] E. R. Love, "Fractional derivatives of imaginary order," *Journal of the London Mathematical Society*, vol. 2, no. 2, pp. 241–259, 1971.

[121] N. Makris, "Complex-parameter kelvin model for elastic foundations," *Earthquake engineering and structural dynamics*, vol. 23, no. 3, pp. 251–264, 1994.

[122] N. Makris and M. Constantinou, "Models of viscoelasticity with complex-order derivatives," *Journal of engineering mechanics*, vol. 119, no. 7, pp. 1453–1464, 1993.

[123] O. Cois, F. Levron, and A. Oustaloup, "Complex-fractional systems: Modal decomposition and stability condition," in *proc. of European Control Conference*, 2001, pp. 1484–1489.

[124] A. Guefrachi, S. Najar, M. Amairi, and M. Abdelkrim, "Frequency response of a fractional complex order transfer function," in *proc. of 13th International conference on Sciences and Techniques of Automatic control & computer engineering*, 2012, pp. 765–773.

[125] J. Laurila and S. Lahdelma, "Advanced fault diagnosis by means of complex order derivatives," *Insight-Non-Destructive Testing and Condition Monitoring*, vol. 56, no. 8, pp. 439–442, 2014.

[126] N. Abdolali, M. Yadollahzadeh, and D. Rahmat, "On fractional differential equation with complex order," *Progress in Fractional Differentiation and Applications*, vol. 1, no. 3, pp. 223–227, 2015.

[127] J. J. E. Slotine and W. Li, *Applied nonlinear control*. Prentice-Hall Englewood Cliffs, NJ, 1991, vol. 199, no. 1.

[128] M. Gopal, *Digital Control and State Variable Methods*. New Delhi: Tata McGraw-Hill, 2012.

[129] D. A. Gronner, "The describing function of backlash followed by a dead zone," *Transactions of the American Institute of Electrical Engineers, Part II: Applications and Industry*, vol. 77, no. 5, pp. 403–409, 1958.

[130] R. S. Barbosa and J. A. T. Machado, "Describing function analysis of systems with impacts and backlash," *Nonlinear Dynamics*, vol. 29, no. 1-4, pp. 235–250, 2002.

[131] F. B. Duarte and J. A. T. Machado, "Fractional describing function of systems with coulomb friction," *Nonlinear dynamics*, vol. 56, no. 4, pp. 381–387, 2009.

[132] F. B. Duarte and J. A. T. Machado, "Describing function of two masses with backlash," *Nonlinear Dynamics*, vol. 56, no. 4, pp. 409–413, 2009.

[133] F. B. Duarte and J. A. T. Machado, "Fractional describing function of systems with nonlinear friction," in *Intelligent Engineering Systems and Computational Cybernetics*. Springer, 2009, pp. 257–266.

[134] J. A. T. Machado, "Fractional order modelling of dynamic backlash," *Mechatronics*, vol. 23, no. 7, pp. 741–745, 2013.

[135] H. Jud, "Limit cycle determination for parallel linear and nonlinear elements," *IEEE Transactions on Automatic Control*, vol. 9, no. 2, pp. 183–184, 1964.

[136] A. Azenha and J. A. T. Machado, "On the describing function method and the prediction of limit cycles in nonlinear dynamical systems," *Systems Analysis Modelling Simulation*, vol. 33, no. 3, pp. 307–320, 1998.

[137] P. S. V. Nataraj and R. Kalla, "Computation of limit cycles for uncertain nonlinear fractional-order systems," *Physica Scripta*, vol. 2009, no. T136, p. 014021, 2009.

[138] C. Yeroglu and N. Tan, "Limit cycle prediction for fractional order systems with static nonlinearities," *IFAC Proceedings Volumes*, vol. 43, no. 11, pp. 144–149, 2010.

[139] D. P. Atherton, N. Tan, C.Yeroglu, G. Kavuran, and A. Yüce, "Limit cycles in nonlinear systems with fractional order plants," *Machines*, vol. 2, no. 3, pp. 176–201, 2014.

[140] R. S. Barbosa and J. A. T. Machado, "Limit cycle prediction of systems with fractional controllers and backlash," *Journal of Vibration and Control*, vol. 23, no. 4, pp. 587–603, 2015.

[141] M. Youhanaie and R. E. Reid, "Analysis of a system controlled by a relay with dead zone, hysteresis and integral feedback," in *proc. of IEEE American Control Conference*, 1982, pp. 660–665.

[142] E. A. Freeman, "Stability analysis of control systems having two non-linear elements with calculations for saturation and backlash," *Proceedings of the IEE - Part C : Monographs*, vol. 109, no. 16, pp. 665–675, 1962.

[143] R. Gran and M. Rimer, "Stability analysis of systems with multiple nonlinearities," *IEEE Transactions on Automatic Control*, vol. 10, no. 1, pp. 94–97, 1965.

[144] E. Davison and D. Constantinescu, "Application of the describing function technique in a single-loop feedback system with two nonlinearities," *IEEE Transactions on Automatic Control*, vol. 13, no. 2, pp. 168–170, 1968.

[145] E. Davison and D. Constantinescu, "A describing function technique for multiple nonlinearities in a single-loop feedback system," *IEEE Transactions on Automatic Control*, vol. 16, no. 1, pp. 56–60, 1971.

[146] D. K. Pantalone and D. M. Piegza, "Limit cycle analysis of hydroelectric systems," *IEEE Transactions on Power Apparatus and Systems*, vol. 100, no. 2, pp. 629–638, 1981.

[147] H. Miyagi and K. Yamashita, "Robust stability of luré systems with multiple nonlinearities," *IEEE Transactions on Automatic Control*, vol. 37, no. 6, pages = 883–886, year = 1992,.

[148] J. S. Yang, "Design of sampled-data control systems with one memoryless, time-invariant nonlinearity using QFT technique," in *proc. of American Control Conference*, 1992, pp. 915–916.

[149] F. Mougenet and H. V, "Limit cycle characterization, existence and quenching in the control of a high performance hydraulic actuator," in *proc. of IEEE International Conference on Robotics and Automation*, 1995, pp. 2218–2223.

[150] K. C. Hsu, W. Y. Wang, and P. Z. Lin, "Sliding mode control for uncertain nonlinear systems with multiple inputs containing sector nonlinearities and deadzones," *IEEE Transactions on Systems, Man, and Cybernetics, Part B (Cybernetics)*, vol. 34, no. 1, pp. 374–380, 2004.

[151] G. Kavuran and C. Yeroglu, "Sliding mode control for fractional order plants via limit cycle prediction," in *proc. of International Conference on Fractional Differentiation and Its Applications*, 2014, pp. 1–6.

[152] N. M. F. Oliveira, K. H. Kienitz, and E. A. Misawa, "An algebraic approach to the design of robust limit cycle controllers," in *proc. of American Control Conference*, vol. 3. IEEE, 2003, pp. 2419–2423.

[153] N. M. F. Oliveira, K. H. Kienitz, and E. A. Misawa, "A describing function approach to limit cycle controller design," in *proc. of American Control Conference*. IEEE, 2006, pp. 1511–1516.

[154] N. M. F. Oliveira, K. H. Kienitz, and E. A. Misawa, "A describing function approach to the design of robust limit-cycle controllers," *Nonlinear Dynamics*, vol. 67, no. 1, pp. 357–363, 2012.

[155] A. A. Kesarkar and N. Selvaganesan, "A novel framework to design and compare limit cycle minimizing controllers: demonstration with integer and fractional-order controllers," *Nonlinear Dynamics*, vol. 78, no. 4, pp. 2871–2882, 2014.

[156] A. A. Kesarkar, N. Selvaganesan, and H. Priyadarshan, "Novel controller design for plants with relay nonlinearity to reduce amplitude of sustained oscillations: Illustration with a fractional controller," *ISA Transactions*, vol. 57, pp. 295–300, 2015.

[157] P. Lanusse and A. Oustaloup, "Windup compensation system for fractional controller," *Proceedings of IFAC Workshop on Fractional Differentiation and its Applications*, July 2004.

[158] P. Lanusse and A. Oustaloup, *Anti-Windup System for 1st Generation Crone Controller*. Ubooks Edition, 2005, vol. 3.

[159] A. Gelb and W. E. Vander Velde, *Multiple-input describing functions and nonlinear system design*. New York, United States: McGraw-Hill Book Company, 1968.

[160] A. Loverro, "Fractional calculus: History, definitions and applications for the engineer," Department of Aerospace and Mechanical Engineering, University of Notre Dame, Tech. Rep., 2004.

[161] MATLAB, *version 7.10.0 (R2010a)*. Natick, Massachusetts: The MathWorks Inc., 2010.

[162] Y. Q. Chen and K. L. Moore, "Relay feedback tuning of robust pid controllers with iso-damping property," *IEEE Transactions on Systems, Man, and Cybernetics, Part B (Cybernetics)*, vol. 35, no. 1, pp. 23–31, 2005.

[163] K. J. Aström and R. M. Murray, *Feedback Systems: An Introduction for Scientists and Engineers*. Princeton, New Jersy: Princeton University Press, 2010.

[164] R. Sridhar, "A general method for deriving the describing functions for a certain class of nonlinearities," *IRE Transactions on Automatic Control*, vol. 5, no. 2, pp. 135–141, 1960.

[165] J. Sabatier, P. Lanusse, P. Melchior, and A. Oustaloup, *Fractional Order Differentiation and Robust Control Design*. London: Springer, 2015, vol. 77, pp. 63–105.

[166] A. I. Mees, "The describing function matrix," *IMA Journal of Applied Mathematics*, vol. 10, no. 1, pp. 49–67, 1972.

[167] D. Matignon, "Generalized fractional differential and difference equations: stability properties and modelling issues," in *proc. of the Mathematical Theory of Networks and Systems symposium (MTNS)*, 1998, pp. 503–506.

[168] H. Bateman and A. Erdelyi, *Higher Transcendental Functions, Vol. 3: Elliptic and Automorphic Functions, Lamé and Mathieu Functions*. New York: McGraw-Hill, 1955.

Appendix A

Some Important Properties in Fractional Calculus

A.1 Stability of Fractional Order Linear Time Invariant Systems

For the stability of class of fractional order Linear Time Invariant (LTI) systems having commensurate order $q \in (0, 1]$, the following theorem must be satisfied:

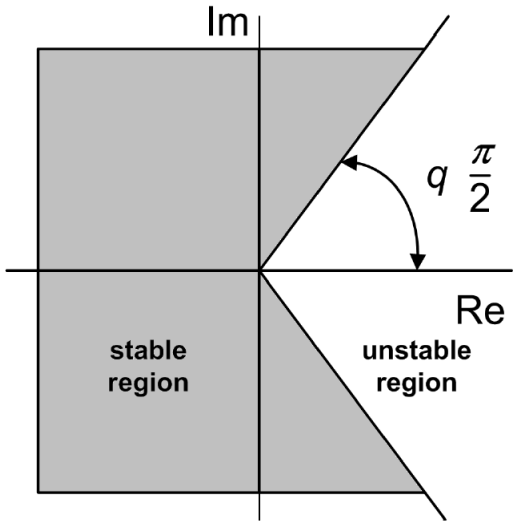

Figure A.1: Pictorial representation of Matignon's stability

Matignon's stability theorem [167]: *The fractional-order TF* $G(s) = \frac{Z(s)}{P(s)}$ *is stable if and only if the following condition is satisfied in s-plane (Pictorial representation has been*

shown in Fig. A.1):

$$|\angle(\sigma_i)| > q\frac{\pi}{2}, \forall \sigma_i \in \mathbb{C}, P(\sigma_i) = 0 \tag{A.1}$$

where, $\sigma := s^q$

For integer-order LTI systems, $q = 1$. Therefore, (A.1) becomes $|\angle(\sigma_i)| > \frac{\pi}{2}$, which means that all the roots of the characteristic polynomial must be located on the left half of the complex plane.

A.2 Analytical Solution of Fractional Order Differential Equations

In the solution of integer-order calculus equations, the exponential function e^z plays an important role. In case of fractional-order calculus equations, exponential function is replaced by the Mittag-Leffler function. The two-parameter Mittag-Leffler function is defined as follows [168]:

$$E_{\alpha,\beta}(z) = \sum_{k=0}^{\infty} \frac{z^k}{\Gamma(\alpha k + \beta)};\ (\alpha > 0, \beta > 0) \tag{A.2}$$

For $\beta = 1$, (A.2) results into the following one-parameter Mittag-Leffler function:

$$E_\alpha(z) := E_{\alpha,1}(z) = \sum_{k=0}^{\infty} \frac{z^k}{\Gamma(\alpha k + 1)} \tag{A.3}$$

It can be followed from (A.2) that:

$$E_{1,1}(z) = e^z, E_{2,1}(z) = cosh(\sqrt{z}), E_{1,2}(z) = \frac{e^z - 1}{z}, E_{2,2}(z) = \frac{sinh(\sqrt{z})}{\sqrt{z}}, \text{etc.} \tag{A.4}$$

The following Laplace transform identity holds true [39]:

$$\mathcal{L}\{t^{\alpha k+\beta-1} E^{(k)}_{\alpha,\beta}(at^\alpha)\} = \frac{s^{\alpha-\beta} k!}{(s^\alpha - a)^{k+1}} \tag{A.5}$$

where,

$$E^{(k)}_{\alpha,\beta} = \frac{d^{(k)}}{dt^{(k)}} E_{\alpha,\beta}$$

The property (A.5) is useful while obtaining the analytical solution of fractional order differential equation using Laplace transform method. The following example is considered for demonstration:

Example 2 Find solution of:

$$D_{RL}^{\frac{1}{2}} f(t) + a_1 f(t) = 0 \tag{A.6}$$

given that, $D_{RL}^{-\frac{1}{2}} f(0) = C$.

Solution: On taking the Laplace transform of (A.6) using (2.27), implies

$$s^{\frac{1}{2}} F(s) - D_{RL}^{-\frac{1}{2}} f(0) + a_1 F(s) = 0$$

Therefore,

$$F(s) = \frac{C}{s^{\frac{1}{2}} + a_1} \tag{A.7}$$

On taking inverse Laplace transform of (A.7) using (A.5), implies

$$f(t) = Ct^{-\frac{1}{2}} E_{\frac{1}{2},\frac{1}{2}}(-a_1\sqrt{(t)})$$

Appendix B

Unified Controller Tuning Expressions for Real Valued Integer Order Controllers

Real valued Integer Order Controllers (IOCs) such as $PI/PD/PID$ controller parameter expressions are obtained for the given $G(s)$ to meet the required specifications (4.1), (4.2) and (4.3) in ω^+ only.

B.1 Tuning Expressions for PI Controller

The PI controller structure is given as:

$$C(s) = K_p + \frac{K_i}{s} \tag{B.1}$$

Its positive frequency response (C_{ω^+}) is given by

$$C_{\omega^+} = K_p + \frac{K_i}{j\omega} \tag{B.2}$$

The magnitude and phase of C_{ω^+} at desired ω_{gc} are as follows:

$$|C^+_{\omega_{gc}}| = \sqrt{K_p^2 + \left(\frac{-K_i}{\omega_{gc}}\right)^2} \tag{B.3}$$

$$\angle C^+_{\omega_{gc}} = \tan^{-1}\left(\frac{-K_i}{K_p\omega_{gc}}\right) \tag{B.4}$$

Using (4.11) and (B.4), specification (4.2) becomes

$$\angle G^+_{\omega_{gc}} + \tan^{-1}\left(\frac{-K_i}{K_p\omega_{gc}}\right) + \pi = \phi_m$$

this implies,

$$K_i = -K_p \omega_{gc} \tan\left(A^+\right) \tag{B.5}$$

Using (4.10) and (B.3), specification (4.1) becomes

$$|G^+_{\omega_{gc}}| K_p \sqrt{1 + \left(\frac{-K_i}{K_p \omega_{gc}}\right)^2} = 1$$

this implies,

$$K_p = \frac{1}{|G^+_{\omega_{gc}}| \sqrt{1 + \tan^2 A^+}} \tag{B.6}$$

where, $A^+ = \phi_m - \pi - \angle G^+_{\omega_{gc}}$. Equations (B.5) and (B.6) are the controller parameters of PI which satisfy the specifications (4.1) and (4.2) in ω^+ only.

B.2 Tuning Expressions for PD Controller

The PD controller structure is given as:

$$C(s) = K_p + K_d s \tag{B.7}$$

Its positive frequency response (C_{ω^+}) is given by

$$C_{\omega^+} = K_p + jK_d\omega \tag{B.8}$$

The magnitude and phase of C_{ω^+} at desired ω_{gc} are as follows:

$$|C^+_{\omega_{gc}}| = \sqrt{K_p^2 + (K_d \omega_{gc})^2} \tag{B.9}$$

$$\angle C^+_{\omega_{gc}} = \tan^{-1}\left(\frac{K_d \omega_{gc}}{K_p}\right) \tag{B.10}$$

Using (4.11) and (B.10), specification (4.2) becomes

$$\angle G^+_{\omega_{gc}} + \tan^{-1}\left(\frac{K_d \omega_{gc}}{K_p}\right) + \pi = \phi_m$$

this implies,

$$K_d = \frac{K_p \tan A^+}{\omega_{gc}} \tag{B.11}$$

Using (4.10) and (B.9), specification (4.1) becomes

$$|G^+_{\omega_{gc}}|K_p\sqrt{1+\left(\frac{K_d\omega_{gc}}{K_p}\right)^2}=1$$

this implies,

$$K_p=\frac{1}{|G^+_{\omega_{gc}}|\sqrt{1+\tan^2 A^+}} \tag{B.12}$$

Equations (B.11) and (B.12) are the controller parameters of PD which satisfy the specifications (4.1) and (4.2) in ω^+ only.

B.3 Tuning Expressions for PID Controller

The PID controller structure is given as:

$$C(s)=K_p+\frac{K_i}{s}+K_d s \tag{B.13}$$

Its positive frequency response (C_{ω^+}) is given by

$$C_{\omega^+}=K_p+\frac{K_i}{j\omega}+jK_d\omega \tag{B.14}$$

The magnitude and phase of C_{ω^+} and slope of $\angle C_{\omega^+}$at desired ω_{gc} are as follows:

$$|C^+_{\omega_{gc}}|=\sqrt{K_p^2+\left(K_d\omega_{gc}-\frac{K_i}{\omega_{gc}}\right)^2} \tag{B.15}$$

$$\angle C^+_{\omega_{gc}}=\tan^{-1}\left(\frac{K_d\omega_{gc}-\frac{K_i}{\omega_{gc}}}{K_p}\right) \tag{B.16}$$

$$\left.\frac{d\angle C_{\omega^+}}{d\omega}\right|_{\omega=\omega_{gc}}=\frac{K_d+\frac{K_i}{\omega_{gc}^2}}{K_p\left[1+\left(\frac{K_d\omega_{gc}-\frac{K_i}{\omega_{gc}}}{K_p}\right)^2\right]} \tag{B.17}$$

Using (4.11) and (B.16), specification (4.2) becomes

$$\angle G^+_{\omega_{gc}}+\tan^{-1}\left(\frac{K_d\omega_{gc}-\frac{K_i}{\omega_{gc}}}{K_p}\right)+\pi=\phi_m$$

$$\frac{K_d\omega_{gc}-\frac{K_i}{\omega_{gc}}}{K_p}=\tan A^+$$

this implies,

$$K_d - \frac{K_i}{\omega_{gc}^2} = \frac{K_p \tan A^+}{\omega_{gc}} \tag{B.18}$$

Using (4.10) and (B.15), specification (4.1) becomes

$$|G^+_{\omega_{gc}}| K_p \sqrt{1 + \left(\frac{K_d \omega_{gc} - \frac{K_i}{\omega_{gc}}}{K_p} \right)^2} = 1$$

this implies,

$$K_p = \frac{1}{|G^+_{\omega_{gc}}| \sqrt{1 + \tan^2 A^+}} \tag{B.19}$$

Using (4.12) and (B.17), specification (4.3) becomes

$$\psi^+_{\omega gc} + \frac{K_d + \frac{K_i}{\omega_{gc}^2}}{K_p \left[1 + \left(\frac{K_d \omega_{gc} - \frac{K_i}{\omega_{gc}}}{K_p} \right)^2 \right]} = 0$$

this implies,

$$K_i = \frac{K_p \omega_{gc}}{2} \left(-\psi^+_{\omega_{gc}} \omega_{gc} (1 + \tan^2 A^+) - \tan A^+ \right) \tag{B.20}$$

Substituting (B.20) in (B.18), implies

$$K_d = \frac{K_p}{2\omega_{gc}} \left(\tan A^+ - \psi^+_{\omega_{gc}} \omega_{gc} (1 + \tan^2 A^+) \right) \tag{B.21}$$

Substituting (B.19) in (B.20) and (B.21), K_i and K_d are obtained respectively. Equations (B.19), (B.20) and (B.21) are the controller parameters of PID which satisfy the specifications (4.1), (4.2) and (4.3) in ω^+ only.

List of Publications

Papers in Refereed International Journals

1. **P. Sathishkumar** and N. Selvaganesan. *Fractional Controller Tuning Expressions for a Universal Plant Structure*, IEEE Control Systems Letters, IEEE, 2(3): 345-350, 2018.

2. **P. Sathishkumar** and N. Selvaganesan. *Input dependent Nyquist plot for limit cycle prediction and its suppression using fractional order controllers*, Transactions of the Institute of Measurement and Control, Sage Publications, 41(13): 3847-3860, 2019.

Papers in Proceedings of International Conferences

1. **P. Sathishkumar** and N. Selvaganesan. Fractional Controller Tuning Expressions for a Universal Plant Structure, *In Proceedings of* 57^{th} *IEEE Conference on Decision and Control*, Miami Beach, Florida, USA, 17-19 December, pp. 1-6, (2018).

2. **P. Sathishkumar** and N. Selvaganesan. Limit cycle prediction for Servo system with Multiple Nonlinearity using Input dependent Nyquist plot, *In Proceedings of TEQIP Sponsored International Conference on Contemporary Topics in Power Engineering and Aiding Technologies (ICCPEAT)*, Puducherry, India, 24-25 February, pp. 1-6, (2017).

Journal Papers (Revised / To be Submitted)

1. **P. Sathishkumar** and N. Selvaganesan. *Tuning of Complex Coefficient PI/PD/PID Controllers for a Universal Plant Structure*, International Journal of Control, Taylor and Francis. (Revised)

2. **P. Sathishkumar** and N. Selvaganesan. *Complex Coefficient Fractional Complex Order Controllers for a Universal Plant Structure*. (To be Submitted)